THE UNIVERSITY *of* EDINBURGH

Longitudinal Growth of Mammalian Bones: A Possible Role for Membrane Transporters in Mediating Chondrocyte Hypertrophy

Loqman Mohamad Yusof

PhD

The University of Edinburgh

2011

Declaration

I declare that all work included in this thesis is my own, except where otherwise stated. No part of this work has been, or will be, submitted for any other degree or professional qualification.

Loqman Mohamad Yusof

2011

School of Biomedical Sciences
College of Medicine and Veterinary Medicine
University of Edinburgh
George Square
Edinburgh
EH9 9XD

Abstract

Longitudinal Growth of Mammalian Bones: A Possible Role for Membrane Transporter in Mediating Chondrocyte Hypertrophy

Long bone lengthening occurs at the growth plate (GP) by well-regulated chondrocyte proliferation, hypertrophy and terminal matrix deposition. GP chondrocyte (GPC) hypertrophy has been implicated to be the main determinant of bone growth rate; however the mechanism is poorly understood. The work of this thesis examined some of the cellular process that drives the chondrocyte swelling or hypertrophy particularly in a mammalian post natal GPs using living *in situ* GPC and fixed GP tissues.

Confocal scanning microscopy (CLSM) was used to determine living *in situ* GPC volume and dimension changes in proliferative zone (PZ) through to hypertrophic zone (HZ) chondrocytes of different GPs of various bones. While PZ cells showed similar volumes and dimensions, HZ cells varied in different GPs, even within the same long bone but at opposite ends. However, the hypertrophic cell volume measured at a single post natal age (day 7) was independent of the corresponding bone length. This could reflect a complex interplay between local and systemic factors in different GPs, which occurs throughout the active phase of bone growth.

Maintaining GPC morphology was critical in studying GPC hypertrophy using fixed tissues. This work highlighted a problem caused by conventional fixative solutions, which caused up to 44% hypertrophic GPC shrinkage following GP fixation. This artifact appeared to be associated with the hyperosmotic nature of the fixatives used and could be abolished by adjusting the fixative osmolarity close to physiological level (280 mOsm), or could be significantly reduced by bisecting bone tissues prior to tissue fixation.

This thesis proposed roles for plasma membrane transporter(s) in mediating GPC hypertrophy. This hypothesis was tested by examining roles of sodium-

hydrogen exchanger (NHE) and anion exchanger (AE) in GPC hypertrophy using an *ex vivo* bone growth inhibition model. Inhibition of bone growth by inhibitors of NHE (EIPA) and AE (DIDS) respectively was shown to be dose-dependent. The histology of bones demonstrated that the late HZ width was significantly reduced in GPs treated with EIPA or DIDS. Although *in situ* GPC volumes in the PZ and HZ were not notably different in DIDS-treated GP, the cell volumes in both zones were significantly reduced by EIPA treatment. Fluorescence immunohistochemistry revealed distinctive cellular localisations of NHE1 and AE2 in the PZ and early HZ. These results suggest a possible role of AE in mediating GPC volume increase in PZ chondrocytes and those in the early stages of cell hypertrophy, whereas NHE could possibly maintain intracellular pH of GPC throughout all GP zones.

This thesis has characterized various changes in volume and dimensions of living *in situ* GPC from PZ through to HZ of different GPs of postnatal rats. This work emphasized the importance of fixative osmolarity in order to accurately preserve the normal volume/morphology of cells within tissues. Most importantly, this thesis confirmed a potential role of the plasma membrane transporters, AE and NHE in GPC hypertrophy of growing bones.

Acknowledgement

All praises to Allah Most High, Most Merciful, and Knower of the unseen and the evident, for His help and guidance that made me possible to accomplish this work.

I would firstly like to extend my deepest thanks and gratitude to all my supervisors, Dr Peter Bush, Prof Colin Farquharson and Dr Andrew Hall for their outstanding supervision throughout this work. The reading of their comments is itself a learning, and elevating process. Special thanks are due to my principal supervisor, Dr Andrew Hall for his exemplary supportive role, prompt feedbacks and thought provoking comments to all pieces of work submitted. Thank you for showing confidence in me and continuously encouraging me to pursue this project till end.

I also wish to thank the following people who gave me valuable advices and technical helps in various ways: Ms Lynn Alan (EUSA), Prof Michael Cousin, Dr Trudi Gillespie, Dr Vicky Tobin, Dr Kishan Sokhi, Peter McAuley, and other staffs of the Centre for Integrative Physiology, School of Biomedical Science; the Roslin Institutes, Royal (Dick) School of Veterinary Studies and the Faculty of Veterinary Medicine, Universiti Putra Malaysia.

I wish to extend a big thank you to all my friends, Malaysian community in Edinburgh, and to all those around me for making these past few years what they were.

My deepest thanks go to my beloved family for all their continuous support, especially to my mother for all her love, sacrifice and prayers that have been a never-ending source of inspiration. To my wife, a heartfelt thank you for her care, love and companionship throughout this demanding endeavor period. This experience has provided us a lifetime memories.

Finally, I gratefully acknowledge the Universiti Putra Malaysia for granting me the scholarship, and to the University of Edinburgh for the financial support.

This thesis is dedicated to mother and my late father
(May Allah bless both of them)

Table of Contents

List of Figures

List of Tables

Abbreviations

Ab	Antibody
AC	Articular surface
AE	Anion exchanger
Ag	Antigen
ANOVA	Analysis of variance
AR	Androgen receptor
ATP	Adenosine-5'-triphosphate
ADP	Adenosine diphosphate
hr(s)	Hour(s)
pH_i	Intracellular pH
BMP	Bone morphogenic protein
BSA	Bovine serum albumin
BT	Baseline threshold
CbfaI	Core binding factor A1
CLSM	Confocal laser scanning microscopy
CMFDA	5-chloromethylfluorescein diacetate
DIDS	4,4'-Diisothiocyano-2,2'-stilbenedisulfonic acid
DMSO	Dimethylsulfoxide
DNA	Deoxyribonucleic acid
DTDST	Diastrophic dysplasia sulphate transporter
E18	18-day-old fetus
EC_{50}	Half maximal effective concentration
ECM	Extracellular matrix
EDTA	Ethylenediaminetetraacetic acid
EGF	Epidermal growth factor
EIPA	5-ethylisopropyl amiloride
Em	Peak emission wavelength (nm)

Ex	Peak excitation wavelength (nm)
FIHC	Fluoroscence-immunohistochemistry
FITC	Fluorescein isothiocyanate
ER	Oestrogen receptor
FBS	Foetal bovine serum
FGF	Fibroblast growth factor
FGFR	Fibroblast growth factor receptor
FITC	Fluorescein isothiocyanate
G_1	G_1 phase of cell cycle
G_2	G_2 phase of cell cycle
GA	Glutaraldehyde
GC	Glucocorticoid
GH	Growth hormone
GHR	Growth hormone receptor
GHRH	Growth hormone-releasing hormone
GIT	Gastrointestinal tract
GP	Growth plate
GPOF	Growth plate-orienting factor
HIAR	Heat-induced antigen retrieval
HC	Hypertrophic cell
HZ	Hypertrophic cells zone
HZC	Hypertrophic zone cell
IGF	Insulin-like growth factor
IGF-I	Insulin-like growth factor-I
Ihh	Indian hedgehog
M	Molar
MB	Mineralised bone
MEM	Minimum Essential Medium
MSC	Mesenchymal stem cell
NA	Numerical apperture
NHE	Sodium-hydrogen exchanger

NKCC	Na-K-Cl cotransporter (NKCC SLC12A2)
P7	7-day-old post natal
P_i	Inorganic phosphate
PBS	Phosphate-buffered saline
PFA	Paraformaldehyde
pH_i	Intracellular pH
PTH	Parathyroid hormone
PTHrP	Parathyroid hormone related peptide
PZ	Proliferative zone
PZC	Proliferative zone cell
r^2	Coefficient of determination/ squared correlation coefficient
rER	Rough-surfaced endoplasmic reticulum
RHT	Ruthenium hexamine trichloride
RNA	Ribonucleic acid
ROI	Regions of interests
RT	Room temperature
RZ	Reserve or resting zone
S	Section
SD	Standard deviation
SEM	Standard error of the mean
SOC	Secondary ossification centre
T_3	3,5,3'-L-triiodothyonine
T_4	3,5,3',5'-L-tetraiodothyronine, thyroxine
TGF	Transforming growth factor
TGFβ2	Transfroming growth factor-beta 2
Tris	Tris(hydroxymethyl)aminomethane
VEGF	Vascular endothelial growth factor
3D	Three dimensional

Chapter 1

Introduction

Preface

How does bone grow longer?

Bone growth is generated by a process, which is composed of a finely balanced cycle of cartilage growth, matrix formation and cartilage calcification, which occurs during phase of skeletal development. This process takes place at regions of a specialised cartilage, the epiphyseal growth plate, involving the activities of chondrocytes. The predominant cell type in the growth plates of long bones undergo proliferation, enlargement, maturation and subsequently cell death during the process (Wilsman *et al.,* 1996b).

Chondrocyte enlargement or hypertrophy at the later stage of the cell's differentiation is of significant importance for longitudinal bone growth as it has been implicated as the main determinant of the rate of the bone elongation (Breur *et al.,* 1991; Wilsman *et al.,* 1996b). Hitherto, however, an understanding of the underlying mechanism(s) involved in the growth plate hypertrophy is still lacking. This knowledge is crucial in the research of some growth plate disorders and their subsequent treatment (Breur *et al.,* 1992; de Luca, 2006).

The present work explores the question what is/ are the mechanisms responsible for growth plate chondrocyte hypertrophy. This is achieved by examining living *in situ* and fixed growth plate chondrocytes and furthermore by studying the fundamental cellular process involved in chondrocyte enlargement.

1.1 Thesis Overview

This work comprises four main related study projects. The general aim and hypothesis of the work and the projects undertaken are described at the end of this chapter. The general methods employed to achieve them are described in chapter two, whereas the specific methods used in each project are given in the respective project results chapters:

- Characterization performed on *in situ* living chondrocyte hypertrophy in various growth plates of post natal rats are detailed in chapter three.
- Experiments examining the importance of fixative osmolarity for maintaining growth plate chondrocyte morphology in growth plate tissue preservation are given in chapter four.

- Results derived from sodium-hydrogen exchanger (NHE) and anion exchanger (AE) inhibition using *ex vivo* bone culture are presented in chapter five.
- The changes to NHE1 and AE2 expression levels with growth plate chondrocyte hypertrophy using the immunofluorescence technique is the subject of chapter six.
- Finally, the findings of chapter three to six are summarized and discussed in chapter seven.

The following section in this chapter is a synopsis of relevant background theory. It outlines: (i) introduction to skeletal bone development, (ii) introduction to epiphyseal growth plate, (iii) longitudinal bone growth, (iv) the clinical importance of bone growth and pertinent disorders, (v) relevant previous research findings ((a) growth plate cell hypertrophy and longitudinal bone growth (b) growth rate and differential growth, (c) regulatory volume transporters and chondrocyte enlargement) and (vi) experimental models used to study skeletal bone development.

1.2 Skeletal Bone Development

Embryonic bone formation occurs through two distinct processes. Intramembranous growth results in the formation of flat bones-such as the cranium, mandible, and scapula, whereas the process of endochondral growth (Figure 1.1) accounts for the formation of long bones-such as the tibia, femur and humerus, bones of the extremities, and those parts of the axial skeleton that bear weight, *e.g.* vertebrae (Farquharson, 2003; Clarke, 2008). Longitudinal and radial growth occurs during childhood and adolescence. In addition, bone modelling and remodelling occur constantly during life to help the bone to adapt to changing biomechanical forces, as well as to remove old, microdamaged bone and replace it with new, mechanically stronger bone (Clarke, 2008). Therefore, modelling and remodelling are two important biological mechanisms that determine the strength of the bone (Frost and Schonau, 2000).

In the main, bones grow in two directions: through a cartilage template to increase its length (longitudinal or endochondral growth), and through the

formation of new bone on the outer surfaces of existing bone to increase its width (appositional growth; Farquharson, 2003; Figure 1.2 and 1.3).

1.2.1 Intramembranous Bone Formation

During intramembranous bone formation, mesenchymal cells proliferate within a highly vascularised area of the embryonic connective tissue, forming early cell condensations within which cells differentiate directly into osteoblasts. These cells synthesize a woven bone matrix, while mesenchymal cells at the periphery continue to differentiate into osteoblasts. Blood vessels are incorporated between the woven bone trabeculae and form the hematopoietic bone marrow (Sims and Baron, 2000). Clearly, during the process there is no intervention of a cartilage precusor or concomitant resorption of cartilage and deposition of bone on a spicule (remnant of the cartilage resorption) of calcified matrix as occurs in endochondral bone formation (Ross and Reith, 1985).

1.2.2 Endochondral Bone Formation

Most bones develop through a process known as endochondral ossification, the initial stage of which is the formation of a cartilage anlage. During foetal development and postnatal growth, this anlage is gradually replaced by bone. Cartilage anlages are formed through condensation of mesenchymal cells, followed by their differentiation into chondrocytes and secretion of typical cartilage extracellular matrix components (Fig. 1.1). The cartilage anlage once formed is invaded first at its centre and later at each end by a mixture of cells that establish the primary and secondary (respectively) centres of ossification. These centres of ossification gradually encroach on the remaining cartilage, ultimately replacing it (except at the articular surfaces, where a thick cartilage layer forms the articular surfaces) by the time skeletal maturity is achieved. The importance of the cartilage model lies not only in its provision of a mechanically stable template or scaffold for bone formation, but also in its role as the source of longitudinal bone growth (Mackie *et al.,* 2008) by a finely balanced cycle of cartilage growth with matrix formation and calcification of cartilage (Gerber *et al.,* 1999).

As bones continue to develop, so-called secondary ossification centres are established (Fig. 1.1). In the long bones of the limb, the secondary centres of ossification are separated from the primary centre of ossification by a distinct

group of chondrocytes that continue to proliferate and responsible for the longitudinal growth. This cartilage is referred to as the growth plate, as it forms a distinct region of cells (plate) between the bone of the secondary ossification centre and the primary spongiosa (Kronenberg, 2003). In the adult bone, the metaphyseal and epiphyseal bone fuse to each other by the formation of boney bridges, leading to the growth plate closure (Mackie *et al.,* 2008).

1.2.3 Bone Modelling

Modelling is the process by which bones change their overall shape and size in response to physiological influences or mechanical forces, leading to gradual adjustment of the skeleton to the forces that it encounters by following Wolff's law[1]. Modelling enables long bones to increase in diameter, to change shape and develop a marrow cavity, to widen or change axis by removal or addition of bone to the appropriate surfaces. This process is achieved through bone formation by osteoblasts at some sites (*e.g.* periosteal apposition) and through bone destruction by osteoclasts at other sites (*e.g.* endosteal resorption; Fig. 1.3). However, during bone modelling, bone formation and resorption are not tightly coupled (Clarke, 2008). It is most active during childhood and adolescence, and continues throughout adult life, but is less frequent than remodelling in adults (Kobayashi *et al.,* 2003).

1.2.4 Bone Remodelling

Remodelling is the process by which bone is renewed to maintain bone strength and mineral homeostasis (bone turnover). Remodelling involves continuous removal of discrete packets of old bone, replacement of these packets with newly synthesized proteinaceous matrix, and subsequent mineralization of the matrix to form new bone. The remodelling process resorbs old bone and forms new bone to prevent accumulation of bone microdamage. Remodelling begins before birth and continues until death. The bone remodelling unit is composed of a tightly coupled group of osteoclasts and osteoblasts that sequentially carry out resorption of old

[1] A law (developed by Julius Wolf, 1836-1902) stating that bone adapts its external shape and internal structure in response to the mechanical forces it is required to support (Prendergast and Huiskes, 1995; Villemure and Stokes, 2009).

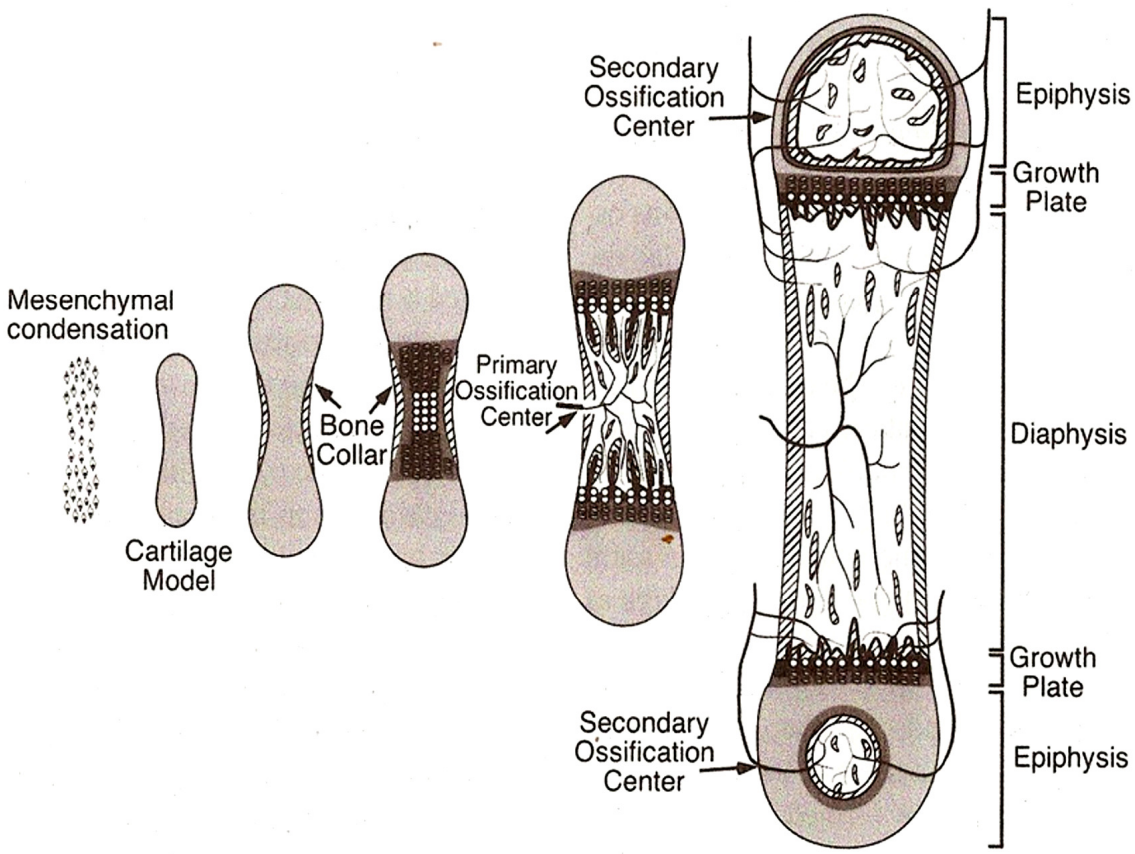

Figure 1.1 Endochondral bone development. Schematic diagram showing the initial stages of endochondral ossification. Bone development begins with mesenchymal condensation to form a cartilage model (anlage) of the bone to be formed. Following chondrocyte hypertrophy and matrix mineralization, osteoclast activity and vascularization result in formation of the primary and then secondary ossification centers. In mature adult bones, the growth plate is fully resorbed so that one marrow cavity extends the full length of the bone (after Sims and Baron, 2000**).**

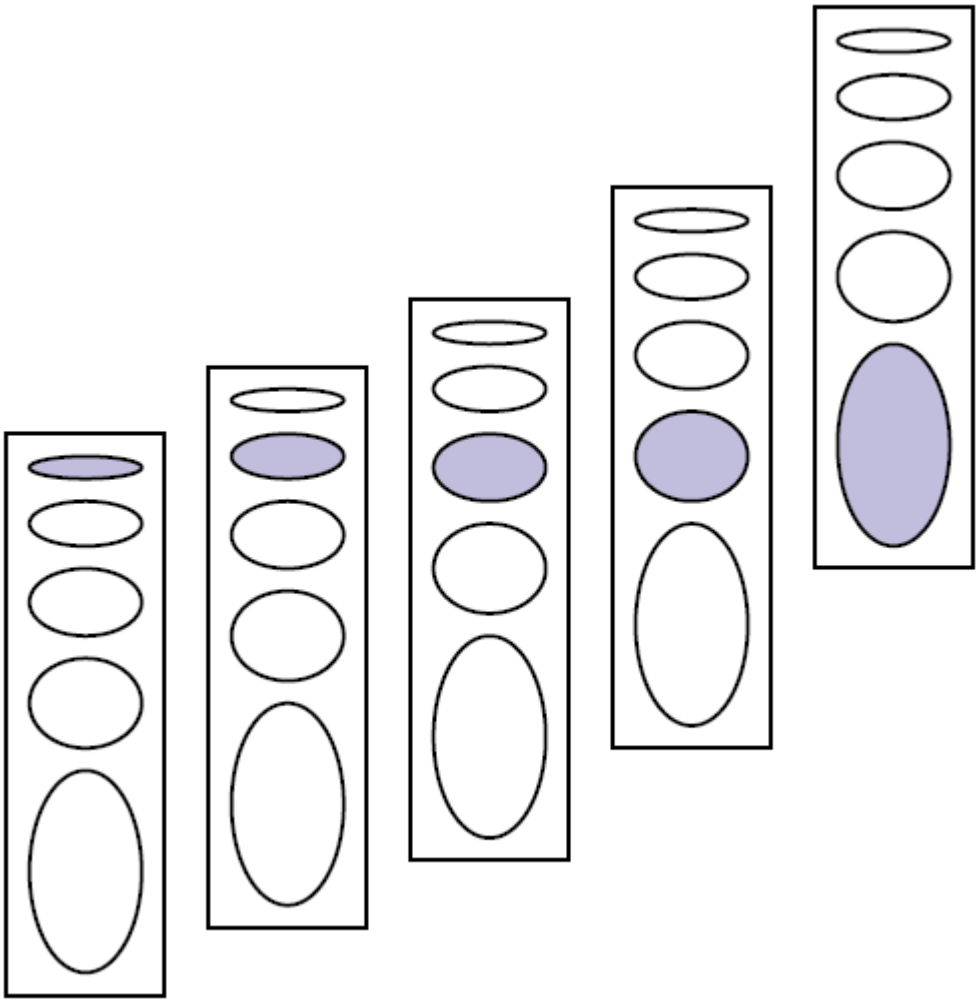

Figure 1.2 A diagrammatic representation of the mechanism of growth plate cell enlargement and longitudinal bone growth. An index cell (shaded) is pictured during longitudinal growth of the epiphyseal growth plate. As longitudinal growth proceeds, the index cell remains in a constant position while the growth plate undergoes its developmental changes. After Hochberg (2002).

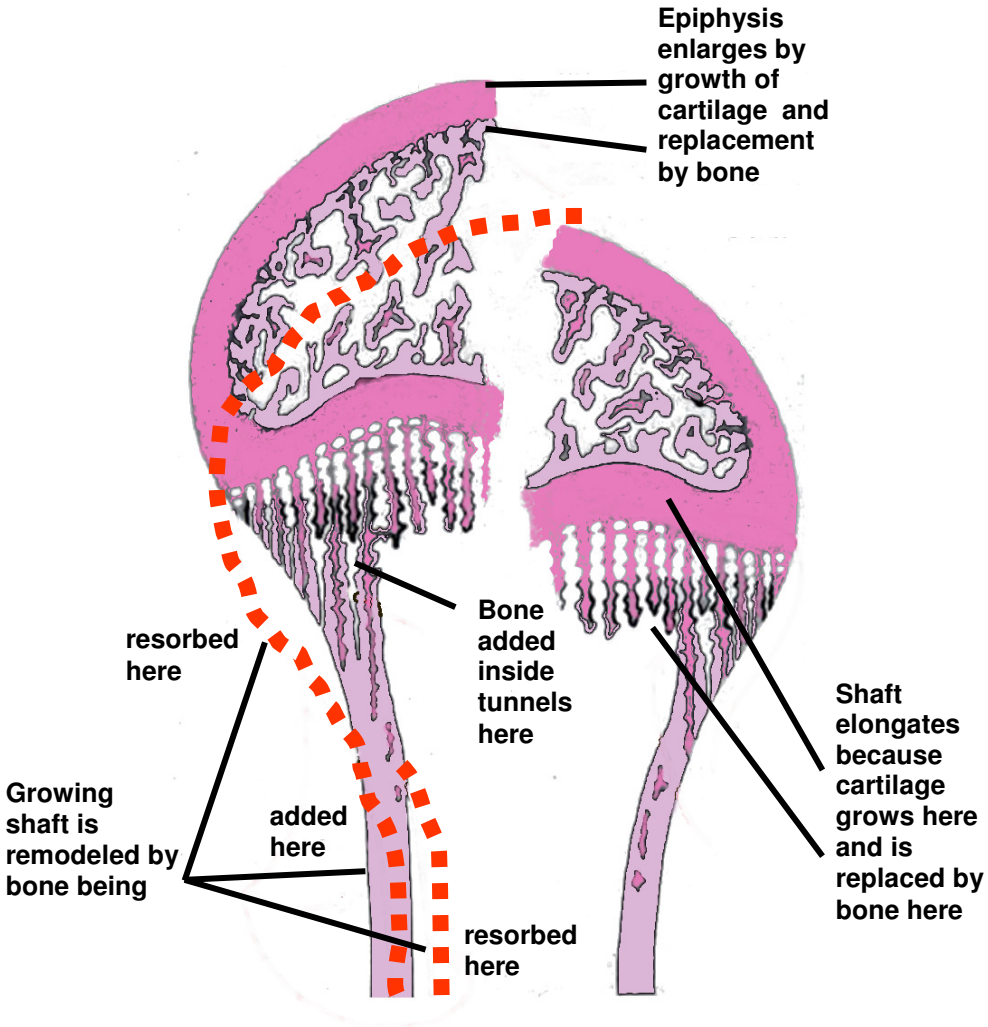

Figure 1.3 Bone growth, modelling and remodelling. Diagram showing surfaces on which bone is deposited and resorbed to account for the remodelling that takes place at the ends of growing long bones that have flared extremities. After Ham (1952).

bone and formation of new bone (Clarke, 2008). The remodelling cycle is composed of four sequential phases: i) activation, ii) bone resorption, iii) reversal, and finally iv) bone formation. Remodelling sites develop mostly in a random manner but are also targeted to areas that require repair through the actions of the osteocyte (Burr, 2002; Clarke, 2008). Both modelling and remodelling processes are induced by mechanical loads (Ehrlich and Lanyon, 2002), predominantly from muscle- and gravity-derived forces (Beck, 2009).

1.2.5 General Bone Classification and Basic Structure

The four general categories of bones are long bones, short bones, flat bones, and irregular bones. Long bones include the clavicles, humeri, radii, ulnae, metacarpals, femurs, tibiae, fibulae, metatarsals, and phalanges. Short bones include the carpal and tarsal bones; and sesamoid bones such as patellae. Flat bones include the skull, mandible, scapulae, sternum, and ribs. Irregular bones include the vertebrae, sacrum, coccyx, and hyoid bone (see Appendix 1 for overview diagram of these bones in a rat skeleton). Flat bones form by membranous bone formation, whereas long bones are formed by a combination of endochondral and membranous bone formation (Clarke, 2008).

The long bones are composed of a hollow shaft, or diaphysis; flared, cone-shaped metaphyses below the growth plates, and rounded epiphyses above the growth plates. The diaphysis is composed primarily of dense cortical bone, whereas the metaphysis and epiphysis are composed of trabecular meshwork bone surrounded by a relatively thin shell of dense cortical bone (Clarke, 2008). Bone tissue contains hydroxyapatite and various extracellular proteins, producing bone matrix (Vaughan, 1981; Marks *et al.,* 1988).

Osteoblasts develop from mesenchymal stem cells. Many stimulatory factors are known to activate osteoblast differentiation. Mature osteoblasts synthesize bone matrix and may further differentiate into osteocytes (Sims and Baron, 2000; Clarke, 2008). Osteocytes maintain structural bone integrity and allow bone to adapt to mechanical and chemical stimulus (Knothe Tate *et al.,* 2004). Osteoclasts are derived from haematopoietic stem cells. A number of transcription and growth factors have been identified to be essential for osteoclast differentiation and function (Crockett *et al.,* 2011). Finally, there is a complex

interaction between osteoblasts and osteoclasts. Bone resorption begins with attachment of osteoclasts to the bone surface. Following this, osteoclasts undergo specific morphological changes. The process of bone resorption starts by acid dissolution of hydroxyapatite. After that, osteoclasts start to breakdown the organic matrix by the production of proteases (Blair *et al.,* 2002; Crockett *et al.,* 2011).

1.3 The Growth Plate

The previous section has emphasised the central role of the growth plate in longitudinal bone growth. This section describes in greater detail the morphology and function of the growth cartilage.

1.3.1 General Morphology

At the macroscopic level the skeleton appears to be a static organ whereas in reality it is an extremely dynamic organ (Khosla *et al.,* 2008), and this is exemplified by the growth plate chondrocyte differentiation process (Figure 1.4). While often considered a simple structure, the growth plate, or physis, of an endochondral bone is a complex composite of cells that appears to vary from species to species and even among different bones within the same species. This variability is not well recognized, but is important for understanding specific diseases of bone growth in children, and the selection of appropriate animal models of such diseases (Ogden and Rosenberg, 1988). However, all growth plates have a common role in the endochondral ossification process as discussed earlier. The primary function of the growth plate is the longitudinal growth of bones although it also contributes significantly to circumferential expansion of the bone through the peripheral zone of Ranvier (Speer, 1982; Langenskiold, 1998). The growth plate can be divided into a series of anatomical zones that distinguish unique morphological and biochemical stages during the process of chondrocyte differentiation (Ballock and O'Keefe, 2003)(Fig. 1.5).

1.3.2 Growth Plate Chondrocyte

1.3.2.1 The Cell

Chondrocytes, the characteristic cell of cartilage tissue, are easily recognized histologically. They have a specific shape and orientation (Buckwalter *et al.,* 1985; Figure 1.5) embedded in the cavities of the extracellular matrix; the lacunae. The

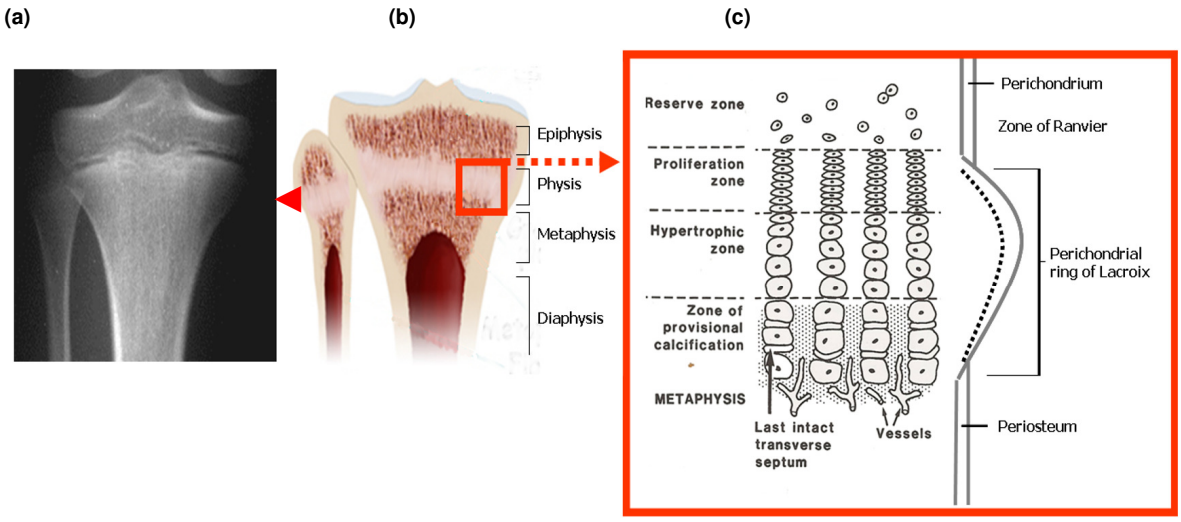

Figure 1.4 Different zones of the growth plate (physis). (a) X-ray film of the proximal tibia of a young male showing the growth plate location (arrow head), (b) schematic of bisected proximal tibial bone to show the gross appearance of a growth plate, (c) diagram of differentiating chondrocyte zones in the growth plate that are divided according to their morphology and function. From Revell (1986).

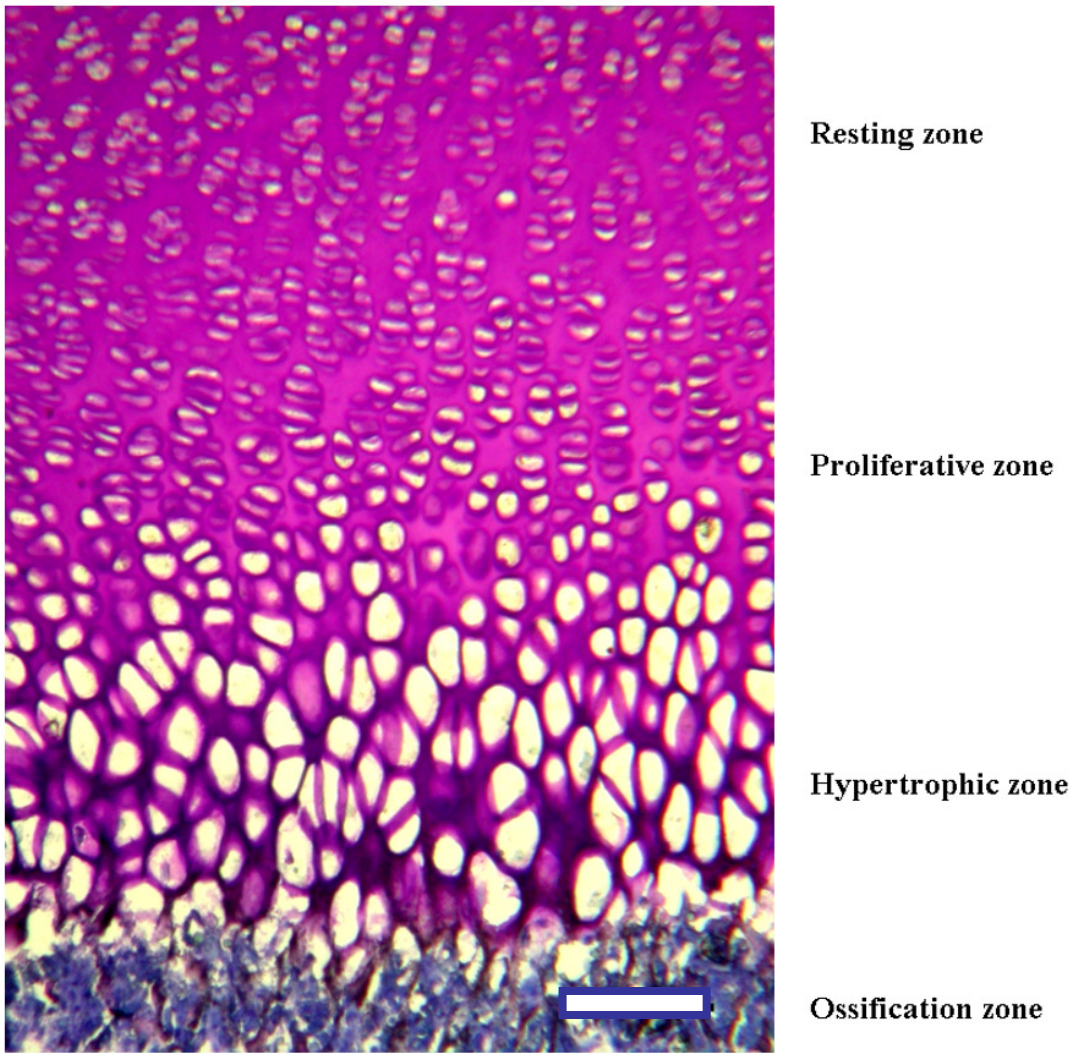

Figure 1.5 A histological section highlighting the different cellular zones of the growth plate. Light microscopic appearance of growth plate showing part of reserve, proliferative, hypertrophic and provisional calcification zones, together with adjacent metaphysis (Toluidine Blue staining). Bar = 60 µm. (The author's own diagram).

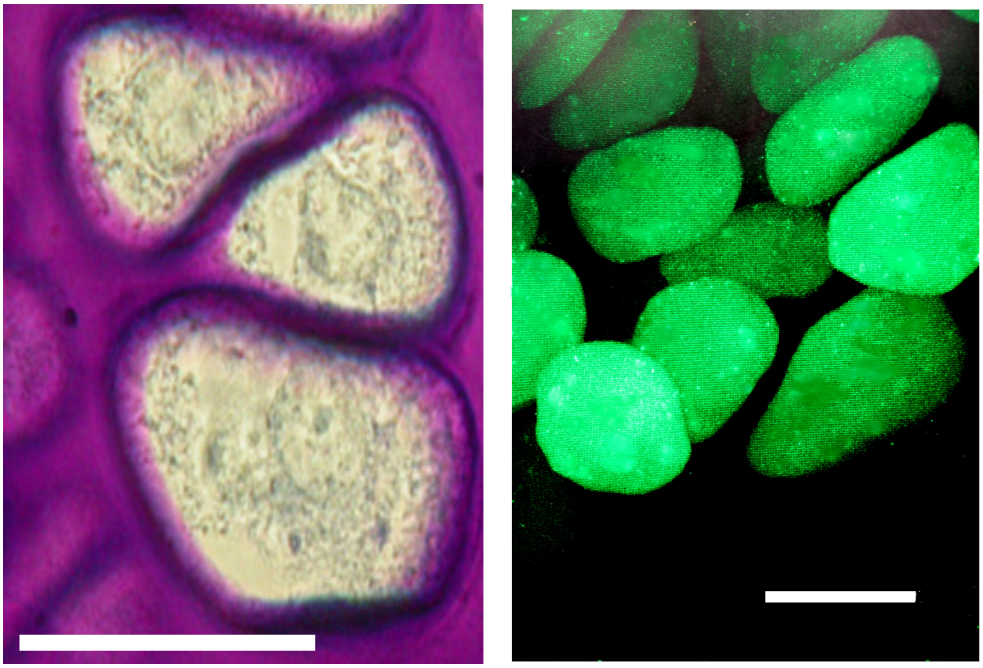

Figure 1.6 Microscopic image of hypertrophic growth plate chondrocytes. Left: A high power (2500x magnification) light microscopic view of hypertrophic chondrocytes from a proximal tibia of 7-day-old rat growth plate histological section fixed in 1.3% glutaraldehyde (GA) with 0.5% ruthenium hexamine trichloride (RHT) and stained with 0.1% Toluidine Blue O. Right: A projection of sequential confocal images of a rat growth plate showing fluorescently labeled (calcein) living *in situ* hypertrophic chondrocytes in proximal tibia. Bar=20 μm. (The author's own diagram).

lacunae are completely filled by chondrocytes with the cell membranes directly attached to the proteoglycan-rich pericellular matrix along the whole lacunae surface (Hunziker *et al,* 1983; Oi and Utsumi*,* 1980; Figure 1.8).

Identification of chondrocytes, in practice, often depends on recognizing their synthetic and secretory products such as collagen type II and the proteoglycan aggrecan. Typical chondrocytes are ovoid cells ranging in maximum diameter from 10 µm in articular cartilage to about 30 µm in other hyaline cartilage (Stockwell, 1978; Figure 1.6). With the electron microscope (ultrastructural level), the chondrocyte is seen to contain numerous profiles of rough-surfaced endoplasmic reticulum (rER), a large Golgi, secretory granules, vesicles, intermediate filaments, microtubules, and actin microfilaments, with the nucleus is eccentrically located. The large amount of rER and the extensive Golgi area indicative of a cell actively engaged in the production of cartilage matrix (Ross and Reith, 1985; Figures 1.7 & 1.8). Mitochondria are common in young cells but rarer in old cells (later in the maturation stage), and glycogen and lipid are common inclusions. The chondrocyte is unique in its ability to synthesize greater amounts of chondroitin sulphate proteoglycans and collagen than almost any other cell type (Vaughan, 1981). Chondrocytes also express a characteristic genetic program driven by SOX9 and other transcription factors (Kronenberg, 2003).

Two morphologically distinct types of chondrocytes coexisting in zones of proliferation and hypertrophy and are termed ‘light’ and ‘dark’ chondrocytes (Ahmed *et al.,* 2007). Light chondrocytes are usually oval or round cells with a few thin cytoplasmic processes extending into the surrounding matrix; the cytoplasm contains sparse endoplasmic reticulum and an inconspicuous Golgi region. Dark chondrocytes are of an irregular shape with numerous dense cytoplasmic processes and vesicles budding from the cell surface; the cytoplasm contains well developed endoplasmic reticulum and a prominent Golgi zone consisting of numerous vacuoles filled with fibrillar material (Ahmed *et al.,* 2007b).

1.3.2.2 Plasma Membrane and Membrane Transporters

The plasma membrane is a selectively permeable barrier between the cytoplasm and the extracellular environment (Figures 1.9 & 1.10). Its permeability properties ensure that essential molecules such as glucose, amino acids, and lipids readily

enter the cell, metabolic intermediates remain in the cell, and waste compounds leave the cell. The selective permeability of the plasma membrane, together with the roles of intracellular buffers and membrane transporters allows the cell to maintain a constant internal environment (Lodish *et al.,* 1995).

A plasma membrane which is composed of a phospholipid alone is only slightly permeable to water (*e.g.* through aquaporin water channels; Verkman and Mitra, 2000) and is essentially impermeable to most water-soluble molecules, such as glucose, nucleosides, and amino acids, and to ions such as hydrogen, sodium, calcium, and potassium (Figure 1.10). Proteins spanning the phospholipid bilayer are required to transport such molecules and ions across all cellular membranes. Because different cell types have different requirements for these low-molecular-weight compounds, the plasma membrane of each cell type contains a specific set of transport proteins that allow only certain ions or molecules to cross, as does the membrane surrounding each type of subcellular organelle. Figure 1.11 illustrates three major types of membrane transport proteins (Lodish *et al.,* 1995).

1.3.2.3 Chondron

Chondrocytes encapsulate themselves in basket-like networks of fine fibrils of elaborate structure, each termed a chondron. These may be isolated intact and are found to contain one or several chondrocytes. Chondrons appear to be compression-resistant, meshwork that dampens mechanical, osmotic and physico-chemical changes induced by dynamic loading. Their long axes are oriented parallel to the lines of force operating *in situ* (Muir, 1995). Immunolocalisation experiments show that chondrons contain several constituents, including types II, VI, and IX collagens (Muir, 1995).

1.3.3 Chondrocyte Differentiation Zones

The growth plate can be divided into various zones according to their morphology and function (Figures 1.4 & 1.5). Immediately next to the secondary ossification centre is the RZ (reserve zone), and adjacent to this are the proliferation and then the hypertrophic zones. The zone of growth is concerned with both longitudinal and diametric (latitudinal) expansion of a bone. It is the area where cellular addition and mitosis occur (Ogden and Rosenberg, 1988). The hypertrophic zone is

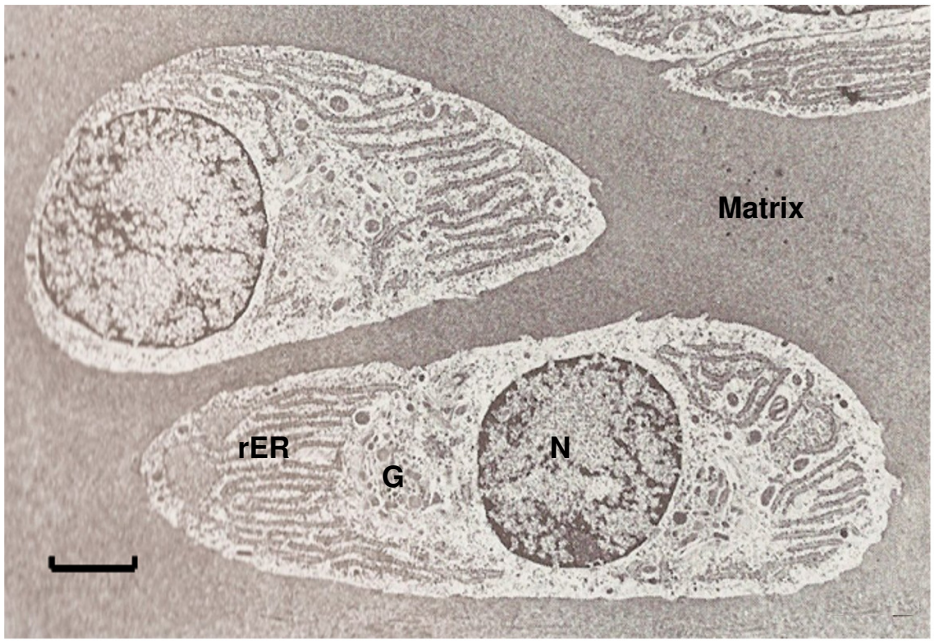

Figure 1.7 Ultra microscopic image of proliferative chondrocytes. Electron micrograph of proliferative chondrocytes from rat growth plate cartilage (35-day-old; proximal tibia). Tissue was processed by high pressure freezing, freeze substitution, and low temperature embedding. Bar = 2µm. N, nucleus; G, Golgi; rER, rough-surfaced endoplasmic reticulum. From Hunziker, (1992a).

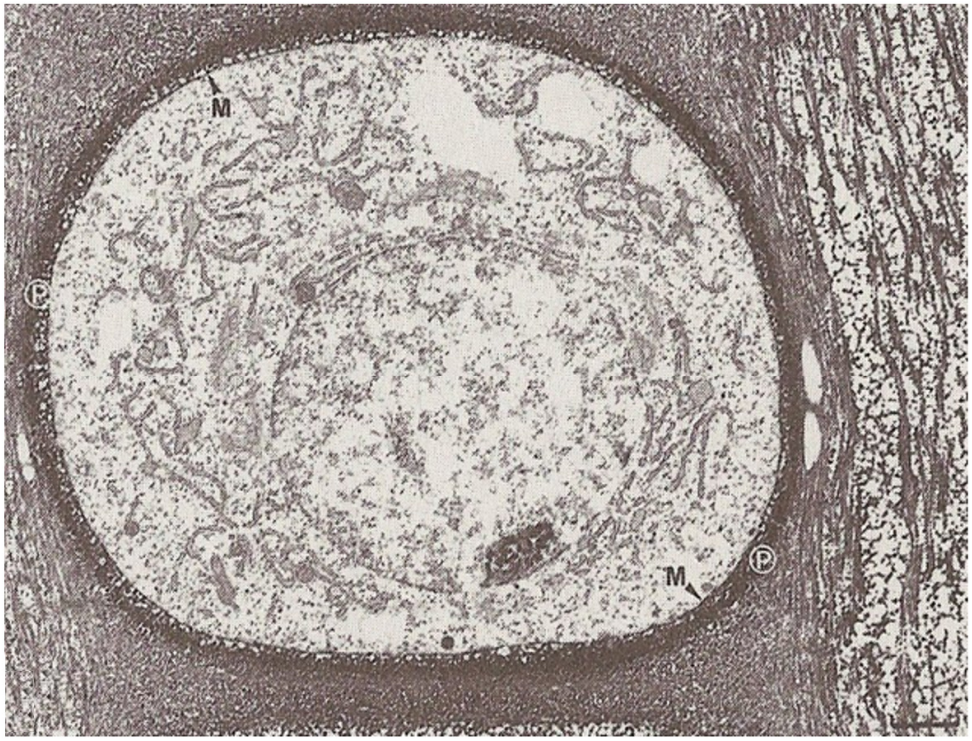

Figure 1.8 Ultra microscopic image of a hypertrophic chondrocyte. Electron micrograph of a hypertrophic chondrocyte after standard RHT fixation. The cell membrane (M) is intact and attached to the pericellular matrix (P) along the whole surface. No lacunar space visible between the cell membrane surface and the pericellular wall, which will be evident in case of artefactual shrinkage of the chondrocyte due to poor cell fixation. Bar = 2µm. After Hunziker *et al. (*1983).

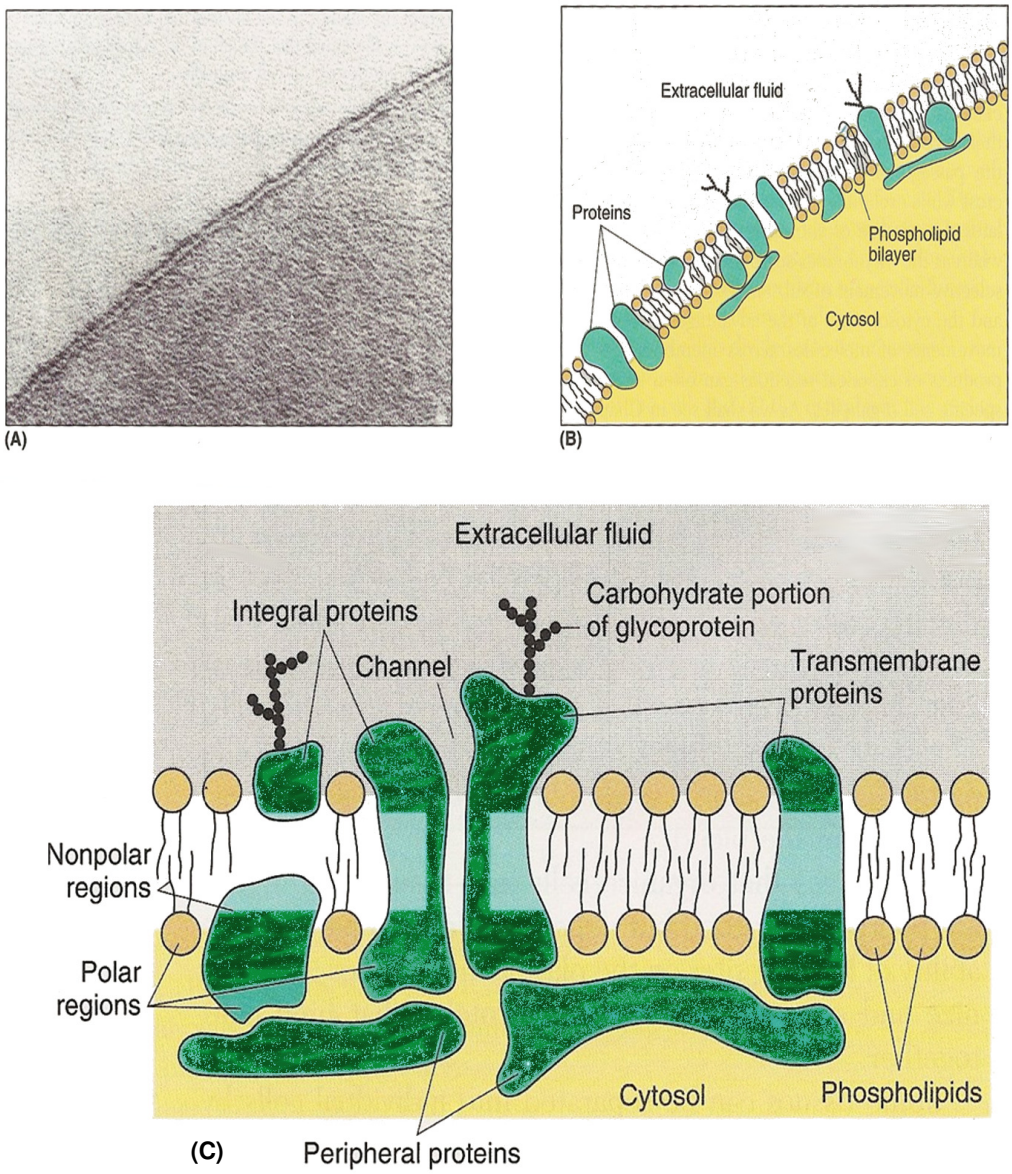

Figure 1.9 Cell membrane structure. (A) Electron micrograph of a human red-cell plasma membrane. Cell membranes are 6 to 10 nm thick, too thin to be seen without the aid of an electron microscope. In an electron micrograph a membrane appears as 'railroad track' appearance at the cell surface - two dark lines separated by a light interspace. The dark lines correspond to the polar regions of the proteins and lipids, whereas the light interspace corresponds to the nonpolar regions of these molecules. (B) Arrangement of the proteins and lipids in the membrane. (C) Arrangement of integral and peripheral membrane proteins in association with a bimolecular layer of phospholipids. Dark-green areas indicate the polar regions of integral membrane proteins. After Vander *et al.* (1994).

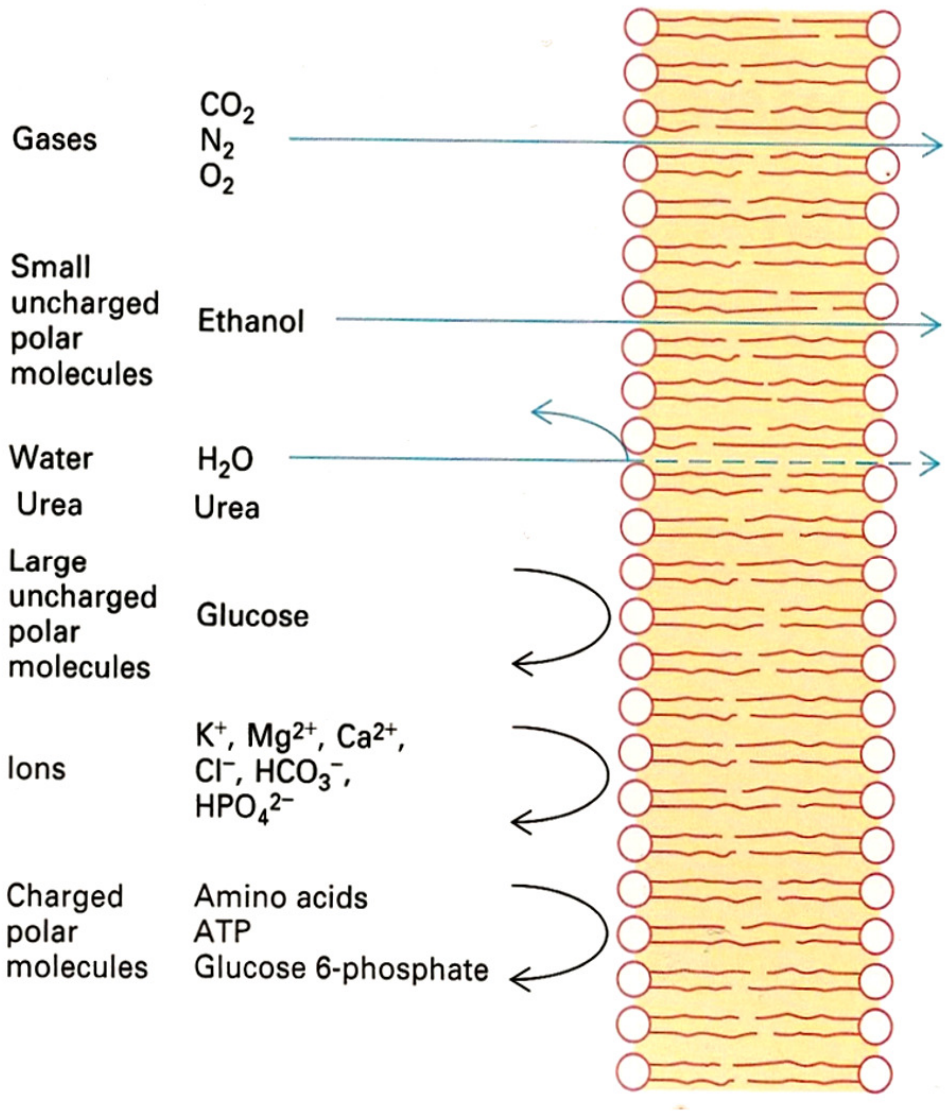

Figure 1.10 Plasma membrane phospholipid bilayer permeability. A pure phospholipid bilayer is permeable to small hydrophobic molecules and small uncharged polar molecules. It is slightly permeable to water and impermeable to ions and to large uncharged polar molecules. When a small phospholipid bilayer separates two aqueous compartments, membrane permeability can be easily determined by adding a small amount of radioactive materials to one compartment and measuring its rate of appearance in the other compartment. After Lodish *et al.* (1995).

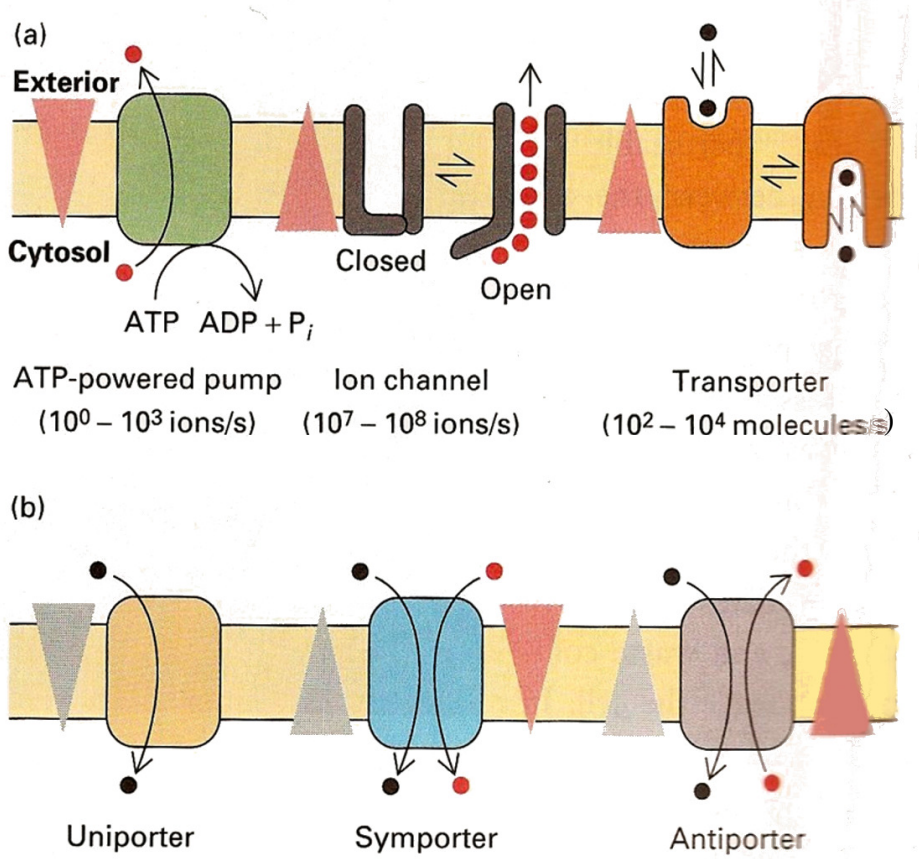

Figure 1.11 Membrane transport proteins. Schematic diagrams illustrating action of membrane transport proteins. (a) The three major types of transport proteins. Pumps utilize the energy of hydrolysis of a phosphoanhyride bond in ATP to power movement of specific ions (red circles) against their electrochemical gradient. (Gradients are indicated by triangles with the tip pointing towards lower concentration and/ or electrical potentials). Channels catalyze movement of specific ions (or water) down their electrochemical gradient. Transporters, which fall into three groups, facilitate movement of specific small molecules, such as glucose and amino acids (black circles) or of ions, such as Na^+ and H^+. (b) The three groups of transporters. Uniporters (also shown in part [a]) transport a single type of molecule down its concentration gradient. The movement of one molecule against its concentration gradient (black circles), driven by movement of one or more ions down an electrochemical gradient (red circles) is catalyzed by symporters and antiporters. These cotransport proteins differ in the relative direction of movement of the transported molecule and cotransported ion. After Lodish *et al.* (1995).

sometimes subdivided into zones of maturation and provisional calcification (Revell, 1986). The easy identification of cells at each maturational stage in this lineage cascade makes the study of chondrocyte cell biology *in vivo* much easier than, say, that for osteoblasts or osteoclasts (Loveridge, 1999).

1.3.3.1 Reserve Zone

An alternative name given to the reserve zone is the 'resting zone', even though the cells at this level are not resting (Revell, 1986). They are spherical in shape and are present singly or in pairs. They are separated by more extracellular matrix than in other zones, and contain glycogen, more lipid and less alkaline, acid phosphatase and other enzymes than in the other zones (Kuhlman, 1960**;** Brighton *et al.,* 1973). The chondrocytes show little or no proliferative activity, and the function of the RZ has not been clearly defined. Although commonly accepted that it serves as precursors for the flat proliferating columnar chondrocytes (Kronenberg, 2003), there was no direct evidence to support the idea that it provides a source of chondrocytes for the rest of the growth plate (Revell, 1986). However, growth plate organ culture studies showed recruitment of cells from the RZ to the proliferating zone under stimulation of certain hormone, *e.g.* thyroid hormone (1.4.2.1.2). In addition, a more recent study suggested that RZ cartilage makes important contributions to endochondral bone formation at the growth plate: i) contains stem-like cells that give rise to clones of proliferative chondrocytes, ii) produces a growth plate-orienting factor (GPOF), a morphogen that directs the alignment of the proliferative clones into columns parallel to the long axis of the bone, and iii) may also produce a morphogen that inhibits terminal differentiation of nearby proliferative zone chondrocytes and thus may be partially responsible for the organization of the growth plate into distinct zones of proliferation and hypertrophy (Abad *et al.,* 2002).

The RZ cells are intimately associated with the epiphyseal blood vessels that supply this region. These small arterioles and capillaries may also be instrumental in providing undifferentiated cells from the perivascular regions that are subsequently added to the pool of RZ chondrocytes. Additional cells are also elaborated peripherally through a specialized area of the perichondrium, the zone of Ranvier (Ogden and Rosenberg, 1988).

With age, the growth plate undergoes programmed senescence, where longitudinal bone growth slows down and eventually stops. This process has been associated with the decrease in RZ chondrocytes proliferative capacity due to the loss of cell DNA methylation. This event could serve as a fundamental biological mechanism that determines the overall adult size of the organism (Nilsson *et al.,* 2005).

1.3.3.2 Proliferation Zone

The proliferative zone contains flattened cells arranged in longitudinal columns (Figures 1.4 & 1.5). The cells contain glycogen and have been shown by electron microscopy to have large amounts of endoplasmic reticulum which increases 3-fold from the beginning to the bottom of this zone (Brighton *et al.,* 1973; Fig. 1.7). Autoradiographic studies of tritiated thymidine incorporation have shown that the cartilage cells in the proliferative zone are the only ones that divide (Kember 1960). It is the topmost cell of each column which acts as the source of those lower down. Proliferation of cartilage cells is responsible for the increase in bone length but the cartilage columns themselves do not increase in length, being converted at their metaphyseal ends into bone (Revell, 1986) at the same rate as new cell production. In this zone of growth active cell division occurs principally in a longitudinal direction and leads to cell column formation (Ogden and Rosenberg, 1988).

1.3.3.3 Hypertrophic Zone

The next functional area is the zone of cartilage formation. Following proliferation, chondrocytes pass through a transition stage in which they are known as 'prehypertrophic' chondrocytes (Mackie *et al.,* 2008). These cells then undergo hypertrophy, a reflection of their increased metabolic activity (Ogden and Rosenberg, 1988), increasing their volume dramatically, at the same time remodeling old, and secreting new extracellular matrix, which eventually becomes mineralized (Mackie *et al.,* 2008).

The flattened chondrocytes on the metaphyseal side of the cartilage columns are changed into large spherical cells in the hypertrophic zone (Figure 1.8). The cells increase in size by twofold to seventyfold within this zone (Farnum *et. al.,* 2008) in different growth plates, and lower down the cells lose the

intracytoplasmic glycogen which is present in the upper half of the hypertrophic zone (Brighton *et al.,* 1969). There is a twofold to fivefold increase in the mean cellular surface area of rough endoplasmic reticulum, the Golgi membranes, and the mean cellular mitochondrial volume, which reflects a high metabolic activity of hypertrophic cells (Hunziker *et al.,* 1987b).

The hypertrophic chondrocyte, simply through its increase in size, is the principal engine of bone growth, and is also a master regulatory cell. Hypertrophic chondrocytes direct the mineralization of their surrounding matrix, attract blood vessels through the production of factors such notably vascular endothelial growth factor (VEGF), and attract chondroclasts (closely related or identical to osteoclasts, which are cells of the macrophage lineage that digest matrix) and direct adjacent perichondrial cells to become osteoblasts, which secrete a characteristic matrix and form the bone collar (Kronenberg, 2003).

The last part of this zone is involved with cartilage transformation. The cartilaginous matrix (chondroid) is sufficiently calcified to allow vascular invasion by the metaphyseal sinusoidal loops. These vessels invade the hypertrophic cell columns by a breakdown of the transverse septa and provide cellular components for initial bone formation from the perivascular tissue. The osteoblasts elaborate osteoid matrix directly on the preformed longitudinal chondroid septa. This tissue is mineralized and forms the primary spongiosa (Ogden and Rosenberg; 1988)

There is also progressively increasing vacuolation of the cells which is extensive at the bottom of the zone, where there is fragmentation of the cell membranes and of the nuclear envelope (Brighton 1978). Electron microscopy has demonstrated the presence of electron-dense granules in the mitochondria of growth plate chondrocytes, and these granules have been shown to contain calcium and phosphorus by X-ray spectroscopy (Sutfin *et al.,* 1971). Chondrocytes at this level contain higher concentrations of lysosomal enzymes than at any other chondrocytes in the growth plate, which suggests that probably bring about degradation of of proteoglycans (Revell, 1986).

The initial calcification which takes place in the growth plate occurs only in the longitudinal septa of the matrix. The septum becomes calcified by the growth and confluence of crystals in the bottom of the hypertrophic zone, hence is frequently called ‘the zone of provisional calcification’. Matrix vesicles are small

membrane limited extracellular structures distinguishable at the ultra structural level and produced by the chondrocytes. They occur in greatest concentration in the hypertrophic zone (Anderson 1969) and are considered to play a central role in the process of mineralization.

1.3.3.4 Chondrocyte Death

The fate of terminally differentiated hypertrophic chondrocyte is unclear. It is accepted however, that in order to compensate for the rapid chondrocyte proliferation and hypertrophy rates, the differentiated chondrocyte must be removed to maintain the steady-state thickness of the growth plate (Farquharson, 2003). In growing rats it has been calculated that eight hypertrophic chondrocytes (including their associated matrices) are eliminated from each column of cells every day (Hunziker *et al.,* 1987b).

Hypertrophic chondrocytes then die, and as they do so, the transverse septa of cartilage matrix surrounding them are broken down, leaving vertical septa largely intact and allowing entry of the invading cells of the ossification front: blood vessels, osteoclasts (multinucleate bone-resorbing cells), and precursors of osteoblasts (bone-forming cells) and bone marrow cells (Mackie *et al.,* 2008). The cartilage matrix left behind provides a scaffold for osteoblasts that invade the cartilage template along with blood vessels and lay down a true bone matrix within the primary spongiosa (Ogden and Rosenberg; 1988; Kronenberg, 2003).

The process by which hypertrophic chondrocytes die is currently the subject of debate. Many authors have described these cells as dying by apoptosis (as reviewed by Gibson, 1998; Adams & Shapiro, 2002), the programmed cell death that plays an important role in physiological cell removal, in particular during foetal development (Aigner, 2002). Apoptosis is characterized by distinctive morphological features, including intense condensation of chromatin into geometric shapes, and fragmentation of the nucleus and cytoplasm into membrane-bound apoptotic bodies (Kerr *et al.,* 1972). Many of the papers describing apoptosis of hypertrophic chondrocytes have done so on the basis of detection of DNA strand breaks or other molecular features known to be associated with apoptosis, rather than on the basis of the definitive morphology (Adams & Shapiro, 2002; Gibson, 1998). On the basis of early ultrastructural studies and recent observations,

however, in a number of publications it has been argued strongly that the process by which hypertrophic chondrocytes die is morphologically distinct from apoptosis (Roach and Clarke, 1999, 2000; Colnot *et al.,* 2001; Roach *et al.,* 2004). Roach *et al*. (2004) proposed the term 'chondroptosis' to refer the non-classical apoptosis of chondrocyte, which results in ultimate self-destruction of the cell without the requirement of phagocytosis - therefore may be more advantageous for chondrocytes that are isolated within their lacunae.

Shapiro *et al* (2005) have put forward the hypothesis that hypertrophic chondrocytes die by autophagic cell death. Ahmed *et al*. (2007) have demonstrated that light and dark hypertrophic chondrocytes die by cell type-specific (non-apoptotic) processes. Light cells appear to disintegrate within their cell membrane, whereas dark cells undergo progressive extrusion of cytoplasm into the extracellular space; for both cell types, nuclear condensation is late and irregular (Mackie *et al.,* 2008).

1.3.4 Extracellular Matrix

Chondrocytes secrete an extracellular matrix that is composed mainly of collagen types II, IX and XI, with type X collagen specific to the hypertrophic zone. Non-collagenous proteins also exist and include proteoglycans such as aggrecan and perlecan; cartilage oligomeric matrix protein (matrilins-1) and matrilins-3 (Aszodi *et al.,* 2000; White and Wallis, 2001).

Although the matrix of articular, structural (such as nasal and costal cartilage), and growth plate cartilage appears histologically similar, the function of these different types of cartilage is quite dissimilar. Physeal cartilage serves a structural function as well as being responsible for bone growth through the process of endochondral ossification. Generally all types of cartilage matrix are comprised of approximately 50% water and 25% each proteoglycan and collagen (Sussman, 1998). However, matrix of hyaline cartilage that serves as the epiphyseal growth plate, or presents at the articular bone surface shows high degree of hydration, where 60-78 percent of the net weight is water (Ross and Reith, 1985). The proteoglycan of cartilage exists as large aggregates that form a gel with water and gives cartilage its unique physical consistency. Proteoglycans exert a swelling pressure that is constantly restrained by the collagen network in which

they are entrapped (Muir, 1978). Most of the collagen is organised in a network of fibrils that provides additional structural stability to the cartilaginous matrix (van der Rest and Garrone, 1991; Figure.1.12).

Type II collagen is the major structural collagen in cartilage and comprises 80% and 90% of the collagen therein. This collagen is distributed evenly throughout cartilage as collagen fibrils. Type IX collagen is an unusual disulphide-linked collagen that has a proteoglycan-like domain and it is speculated that it may play a role in collagen-proteoglycan interactions (Sussman, 1998). Type X collagen appears to be unique to cartilage just prior to ossification and is found in the growth plate, foetal preosseus cartilage and fracture callus (Sussman, 1998). This distribution indicates that it has a significant role in the process of endochondral ossification. Grant *et al.* (1985) have demonstrated that this collagen is not synthesised in structural cartilage, and in the growth plate is only synthesised in significant quantities in the hypertrophic zones. Type XI collagen is a constituent of all cartilage fibrils and has been isolated and characterized by its unique solubility characteristics (Mendler *et al.,* 1989).

All of the matrix components of the growth plate including the collagens are synthesised by chondrocytes therein, and all chondrocytes are capable of synthesising any or all to these collagen types as well as the proteoglycans (Sussman, 1998).

What is the role of the extracellular matrix? Most certainly, the ability of chondrocytes to enlarge requires changes to occur in the composition and organization of the surrounding matrix. Matrix changes in the hypertrophic cell zone that have been investigated as possible mechanisms to promote and control an increase in cellular volume include the removal of calcium, increased degradation of proteoglycans, increased activity of collagenase, and decreased collagen content (Campo, 1988; Dean *et al.,* 1992).

As chondrocytes increase in volume, the cell enlargement has to be constrained or otherwise regulated. Without such active regulation the initially flattened chondrocytes of the proliferative zone would become spherically shaped chondrocytes, and in normal growth plates, this is not the case. In normal animals, vertical hypertrophic chondrocyte expansion is at least five times that of horizontal expansion, leading to the conclusion that one of the roles of the cartilaginous

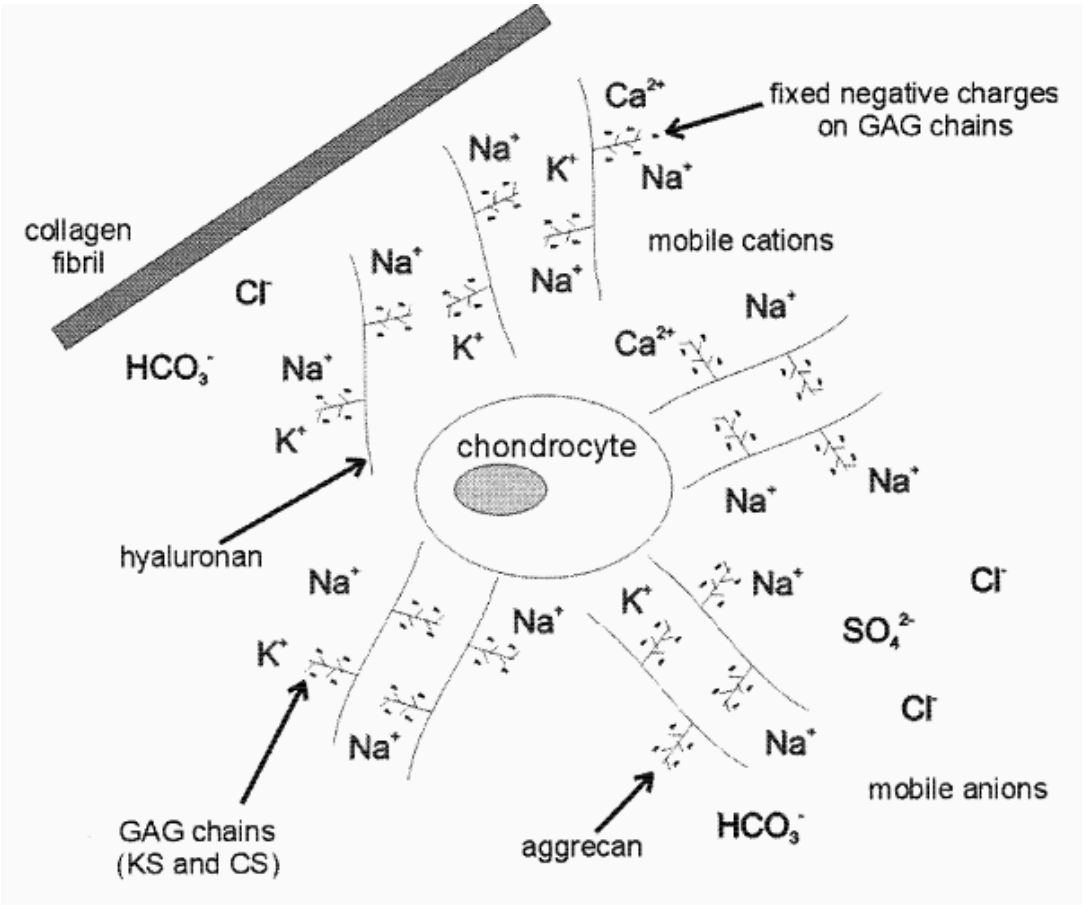

Figure 1.12 The extracellular environment of chondrocytes. The high numbers of fixed negative charges on the keratan sulphate (KS) and chondroitin sulphate (CS) of glycosaminoglycan (GAG) chains attracts mobile cations and leaves out mobile anions from the extracellular matrix of articular chondrocytes. After Wilkins *et al.* (2000).

matrix is to constrain the increase in cellular volume, directing expansion of the vertical diameters at the expense of the horizontal diameters (Breur *et al.,* 1992).

In addition, the extracellular matrix also has a significant impact on chondrocyte differentiation within the growth plate. For example, proteoglycans play an essential role in the binding and presentation of important signalling molecules such as fibroblast growth factor (FGFs) and Indian hedgehog (Ihh) to their receptors (White and Wallis, 2001).

1.3.5 Ossification Groove and Perichondrial Ring

The details of the structure of the growth plate given above are reasonably well recognised. The peripheral structures in this region are less so. The periphery of the growth plates is encircled by a wedge-shape groove of cells termed the ossification groove of Ranvier and a band of fibrous tissue and bone known as the perichondrial ring (Figure 1.4).

The ossification groove contains oval cells, which are considered to pass from the groove into the cartilage at the level of the RZ. It is thought that the function of the groove is to contribute chondrocytes to the growth plate for its increased diameter (Tonna 1961) by chondroblast precursors via appositional chondrogenesis (Shapiro *et al.* 1977).

The perichondrial ring is a dense fibrous band encircling the growth plate at the level of the bone-cartilage junction. It is continuous at one end with the group of fibroblasts and collagen fibres of the ossification groove and at the other end with the periosteum and metaphyseal subperiosteal bone. The perichondrial ring provides a mechanical support for the otherwise weak bone-cartilage junction of the growth plate (Shapiro *et al.* 1977)

1.3.6 Chondro-osseous Junction and Metaphysis

The metaphysis begins immediately distal to the last intact transverse septa at the bottom of the cartilage cell columns. The upper part of the metaphysis immediately adjacent to the growth plate shows the presence of small vessels invading the calcified cartilage. Plum and oval-shaped active osteoblasts are present in the upper part of this region and within a few cells show evidence of forming bone within and upon the calcified cartilage. The area of vascularised calcified cartilage is

sometimes termed the primary spongiosum while the area in which there is bone formed on the cartilage template is the secondary spongiosum (Revell, 1986).

The initially formed woven bone of this region is replaced by lamellar bone in the process of internal remodelling. Osteoclasts/ chondroclasts are present within the metaphysis, resorbing both calcified cartilage and the lamellar bone in the remodelling process. They are also present at the perisoteal surface of the metaphysis, where they are responsible for the external remodelling which results in the narrowing of the bone at the diaphyseal region (Revell, 1986). The differentiating osteoblasts use the remnants of cartilage matrix after removal by osteoclasts as a scaffold for the deposition of bone matrix (Mackie *et al.,* 2008).

1.4 Longitudinal Bone Growth

1.4.1 The Longitudinal Growth Process

The mechanisms of long bone growth are similar across many animal species. They are, however, major variations in the growth rate between similar bones of different species, bones of an individual animal and the two growing regions (growth plates) of the same bone (Farquharson, 2003).

Endochondral ossification of the embryonic cartilaginous model of most bones contributes to longitudinal growth (Mackie *et al.,* 2008). Bone lengthening, particularly rapid during foetal life, is driven primarily by the rate of production of hypertrophic chondrocytes from these proliferating chondrocytes (Kronenberg, 2003).

During this process, the epiphyseal growth plate undergoes morphogenesis. A region of resting chondrocytes differentiates into a zone of proliferating chondrocytes that then hypertrophies and finally undergoes cell death, while being replaced by bone. The net result is lengthening of the bone, while the thickness of the growth plate remains relatively constant. Such a sequence of events relies on the precise coupling of chondrogenesis (cartilage production) with osteogenesis (bone formation). During this process, blood vessel invasion from the metaphysis coincides with mineralization of the extracellular matrix (ECM), apoptosis of hypertrophic chondrocytes, ECM degradation and bone formation (Gerber *et al.,* 1999; Blair et *al.,* 2002). The sequential changes in chondrocyte dynamics are tightly regulated by both systemic factors and locally (autocrine/ paracrine)

secreted factors, which act on receptors to affect intracellular signalling and activation of chondrocyte-selective transcription factors (Mackie *et al.,* 2008).

1.4.2 The Regulatory Process

Longitudinal growth of long bones depends on the precise coordination, both temporally and spatially, of a multitude of processes (Roach *et al.,* 2003). Overall longitudinal bone growth is governed by a complex network of endocrine signals, including growth hormone (GH), insulin-like growth factor I (IGF-I), glucocorticoid (GC), thyroid hormone, sex steroids, vitamin D, and leptin. Many of these signals regulate growth plate function, both by acting locally on growth plate chondrocytes and also indirectly by modulating other endocrine signals in the network. Some of the local effects of hormones are mediated by changes in paracrine factors that control chondrocyte proliferation and differentiation. Many human skeletal growth disorders are caused by abnormalities in the endocrine regulation of the growth plate (Nilsson *et al.,* 2005).

1.4.2.1 Systemic (Hormonal) Regulation

The major systemic hormones that regulate longitudinal bone growth during childhood are GH and IGF-I, thyroid hormone (T_3 and T_4), and GC, whereas during puberty the sex steroids (androgens and oestrogens) contribute a great deal to this process (van der Eerden *et al.,* 2003).

1.4.2.1.1 GH-IGF-I System

There are two possible mechanisms that explain the dependent functions between GH and IGF-I axis on bone growth. First, GH stimulates growth at the epiphysis by systemically derived liver IGF-I, and second, besides that GH acts on RZ precursors of the GP to stimulate the differentiation of chondrocytes and then amplifies local IGF-I synthesis, which, in turn, induces the clonal expansion of chondrocyte columns and hypertrophy in an autocrine/ paracrine manner (Ahmed and Farquharson, 2010).

The relative contributions of GH and IGF-I to pre- and postnatal bone growth have been examined through growth analysis of various transgenic mouse lines (Baker *et al*., 1993; Lupu *et al.* 2001). Before birth, IGF-I and -II are believed

to be the key regulators of growth, and largely independent of GH (Woods *et al.,* 1996). After birth, GH is an important modulator of longitudinal bone growth and appears, together with IGF-I, the central player of the hypothalamus-pituitary-growth plate axis. GH secretion from the pituitary is tightly controlled by the activity of GHRH (stimulator) and somatostatin (inhibitor), which are released by the hypothalamus (van der Eerden *et al.,* 2003).

In brief, IGF-I signalling is considered to be GH independent at prenatal age, whereas IGF-I is partly or fully GH dependent for post natal bone growth. However, the possibility of GH and IGF-I have both independent and common functions (Lupu *et al.* 2001, Wu *et al.* 2009) could not be ruled out and this was especially predominant in the GP chondrocytes (Lupu *et al.* 2001).

Prepubertal growth is primarily regulated by GH and IGF-I, with important contributions from GC and thyroid hormone (Siebler *et al.,* 2001).

1.4.2.1.2 Thyroid Hormone

Besides GH, T_3 and, to a lesser extent, its precursor T_4 are crucial for normal bone maturation (Stevens and Williams, 1999). Both congenital hypothyroidism and T_3 deficiency are associated with severe growth retardation in rodents and humans. Hyperthyroidism causes an increased growth velocity in children but also leads to premature growth plate fusion and short stature (van der Eerden *et al.,* 2003).

T_3 functions to stimulate the recruitment of cells to the proliferating zone from the germinal (reserve) zone and facilitate the differentiation of growth plate chondrocytes in embryonic avian cartilage organ culture, and in rat mandibular condyle and femur organ cultures (Burch and Wyk, 1987; Wakita *et al.,* 1998)**.** Recent data have confirmed that T_4 induces the expression of both type II and X collagen, the activity of the differentiation marker alkaline phosphatase, and chondrocyte hypertrophy (Okubo and Reddi, 2003). Besides influencing GH secretion, thyroid hormones have been shown to interact with the GH-IGF-I pathway at the level of the growth plate. In short, thyroid hormones act through chondrocytes bearing thyroid hormone receptors to modulate growth plate proliferation, differentiation, and vascular invasion. Part of these effects appear to be mediated by modulating local GH and/or IGF-I actions (van der Eerden *et al.,* 2003).

1.4.2.1.3. Glucocorticoids

Various clinical conditions, such as juvenile rheumatoid arthritis, chronic asthma, and post renal transplantation, require prolonged GC therapy, leading among other phenomena to decreased bone volume and growth retardation. Dexamethasone, a synthetic GC inhibits chondrocyte proliferation and matrix synthesis, suggesting that GC is a potent negative regulator of chondrogenesis (van der Eerden *et al.,* 2003).

A few studies have localized the GC receptor (GR) in rat bone cells, including chondrocytes (van der Eerden *et al.,* 2003), and in human growth plates, especially in hypertrophic chondrocytes, suggesting direct effects of GC on the growth plate (Abu *et al.,* 2000). GR was demonstrated in the proliferating and hypertrophic zone of rat growth plates, and treatment with high doses of corticosterone in rats resulted in a reduced growth plate width in long bones, concomitant with growth retardation (Siverstrini *et al.,* 2000). These findings are most likely explained by reduced chondrocyte proliferation, in combination with increased apoptosis in terminal hypertrophic chondrocytes (Chrysis *et al.,* 2003). GC has also been shown to suppress growth by impairing the IGF system. GC treatment significantly decreased the number of growth plate chondrocytes expressing IGF-I, which could contribute to the GC-induced growth retardation (Smink *et al.,* 2003).

GC is also capable of modulating (local) thyroid hormone levels (Miura *et al.,* 2002). Apparently, GC causes growth retardation, not only through direct effects via the GR but also by interference with other growth-modulating pathways.

1.4.2.1.4 Oestrogens

It has long been established that sex steroids are important for longitudinal growth, especially during puberty (van der Eerden *et al.,* 2003). Previous studied have led to the assumption that in both males and females, oestrogen is the main determinant for the puberty-associated phenomena related to longitudinal growth and bone quality (Juul, 2001). Oestrogen is also the principal driver of growth plate closure in both genders (Weise *et al.,* 2001). Disruptive mutations of the genes for the ER in males and females have been shown to cause the delay in the GP fusion (Smith *et al.,* 1994; Carani *et al.,* 1997). The presence of ER in prepubertal children

re-emphasises the essential role of oestrogen in skeletal maturation process (Egerbacher *et al.,* 2002). In addition, immunofluorescent study showed the ER was detected in matured GP age in species that shows GP fusion at puberty such as rabbits, and absent in rats whose GP remain open at maturity (Kennedy *et al.,* 1999).

1.4.2.1.5. Androgens

The androgen receptor (AR) has been localized to hypertrophic chondrocytes of the human tibiae (Abu *et al.,* 1997). AR mRNA and protein were also expressed in the tibial growth plate of the rat (van der Eerden *et al.,* 2002). The differences in subcellular AR expression between males and females around sexual maturation suggests a role for testosterone in establishing sex differences in longitudinal growth during sexual maturation, which account for some skeletal differences between males and females (van der Eerden *et al.,* 2003).

1.4.2.1.6. Vitamin D

In growing mammals, vitamin D deficiency produces a constellation of skeletal abnormalities known as rickets, a classic metabolic bone disease of humans and animals (Dittmer and Thompson, 2010). The width of the hypertrophic zone of the growth plate is increased and mineralization is defective in mice lacking the vitamin D receptor. In these mice there is decreased apoptosis of hypertrophic chondrocytes at the metaphyseal ends of the columns and delayed invasion by blood vessels and bone cells (Donohue and Demay, 2002)

The growth plate effects of vitamin D may be mediated primarily through the vitamin D receptor expressed in intestinal epithelial cells, leading to increased calcium and phosphate absorption from the intestinal lumen. Vitamin D metabolites, however, may also act directly on the growth plate. 24R,25-dihydroxycholecalciferol ($24,25(OH)_2D_3$) injected directly into rachitic chick growth plates resulted in healing (Lidor *et al.,* 1987). *In vitro*, the 24,25-dihydroxyvitamin D_3 stimulates differentiation but decreases proliferation in RZ cells, while 1,25-dihydroxyvitamin D_3 ($1,25(OH)_2D_3$) decreases proliferation in reserve and proliferative zones (Boyan *et al.,* 2002).

1.4.2.1.7. Leptin

Leptin, a protein secreted primarily by white adipose tissue, regulates food intake and body weight. Because circulating leptin levels are increased in obesity, it has been hypothesized that leptin might contribute to the robust linear growth that occurs in obese children, despite low GH levels (Vignolo *et al.,* 1988).

Consistent with this hypothesis, leptin deficiency in mice impairs longitudinal bone growth, while treatment of these mice with leptin injections increased the rate of bone growth (Steppan *et al.,* 2000). In organ cultures of mandibular condyle, a model of endochondral ossification, chondrocytes were found to contain specifiic binding sites for leptin (Maor *et al.,* 2002), and leptin, at high concentrations, was found to stimulate chondrocyte proliferation and differentiation as well as IGF-I-receptor expression. The presence of the leptin receptor was also reported in primary cultures of rabbit chondrocytes (Nakajima *et al.,* 2003). Taken together, these lines of evidence suggest that leptin may have a direct effect on chondrocytes in addition to its indirect effects, exerted through its ability to regulate appetite, energy metabolism, and endocrine systems.

The systemic regulators of longitudinal bone growth are summarized in Figure 1.13.

1.4.2.2 Local Regulation

The most important locally acting growth factors influencing longitudinal growth are Indian hedgehog (Ihh), parathyroid hormone-related peptide (PTHrP), Fibroblast growth factors (FGFs), bone morphogenetic proteins (BMPs), and vascular endothelial growth factor (VEGF)(van der Eerden *et al.,* 2003). The summary of the local regulators of longitudinal bone growth are shown in Figure 1.14. IGF-I as described above acts in a systemic manner through synthesis in the liver under GH stimulation. However, IGF-I also has local effects on most tissues including the growth plate and bone growth (Isgaard *et al.,* 1986; Mushtaq *et al.,* 2004; Stratikopoulos *et al.,* 2008).

1.4.2.2.1 Indian Hedgehog

Ihh belongs to the family of hedgehog proteins, which are morphogens that play crucial roles in embryonic patterning and development. Ihh is expressed by

prehypertrophic chondrocytes of chicken and mouse foetal long bones (Vortkamp *et al.,* 1998). Ihh has been recognized as a regulator of the pace of chondrocyte differentiation. Ihh acts as a coordinator of endochondral ossification, regulating chondrocyte proliferation and differentiation and osteoblast differentiation, and coupling chondrogenesis to osteogenesis (Karp *et al.,* 2000). Chondrocyte proliferation is maintained via the Ihh/PTHrP feedback loop (see section 1.4.2.2.2 below) and any interference with this loop results in stunted patterns of bone growth (Wallis, 1996).

1.4.2.2.2 PTH-related Peptide

PTHrP pharmacological actions are closely similar to those of parathyroid (PTH). PTH and PTHrP bind to the same receptor (PTH/PTHrP-R), however a second receptor has been identified that binds only PTH (Segre *et al.,* 1997). The crucial role of PTHrP and the PTH/PTHrP receptor in embryonic bone formation and longitudinal growth was recognized in a number of studies (van der Eerdeen *et al.*, 2003). PTHrP is expressed abundantly in the embryonic periarticular perichondrium in mouse (Karperien *et al.,* 1996). Its receptor at that stage is detected in late proliferating and early hypertrophic chondrocytes (Karperien *et al.,* 1994).

The natural functions of PTHrP are best illustrated by PTHrP(-/-) mutant mice. These mice die at birth, and they manifest abnormalities in their endochondral bone development that all can be attributed to accelerated bone differentiation. In these growth plates, the zone of proliferating cells is markedly reduced, the onset of cell hypertrophy, matrix mineralization, and chondrocyte apoptosis is more advanced compared with wild–type mice. This observation suggests that PTH/PTHrP-R mediates the actions of PTHrP during chondrocyte differentiation and PTH/PTHrP receptor must respond to more than just foetal PTHrP during early development (Segre *et al.,* 1997).

PTHrP together with Ihh form a feedback loop that regulates the pace of cartilage differentiation (Figure 1.14). During bone growth, chondrocytes differentiate from proliferating chondrocytes through an intermediate prehypertrophic cell type to become hypertrophic chondrocytes. Prehypertrophic chondrocytes express both PTH/PTHrP-R and Ihh. PTH/PTHrP-R is expressed in

cells just before the onset of Ihh expression. A target of the secreted Ihh signal is the perichondrium, which responds by directly or indirectly increasing expression of PTHrP in the periarticular perichondrium. PTHrP then signals through the PTH/PTHrP receptor in the prehypertrophic cells and prevents differentiation to the prehypertrophic phenotype. When the prehypertrophic chondrocytes have fully differentiated into hypertrophic cells, Ihh expression ceases. The reduction in Ihh expression attenuates the negative feedback loop and allows new cells to initiate the differentiation pathway. The level of Ihh produced by the prehypertrophic chondrocytes, therefore, reflects the number of cells committed to the hypertrophic pathway, providing a mechanism for regulating the rate of chondrocyte hypertrophy (Segre *et al.,* 1997).

1.4.2.2.3 Fibroblast Growth Factors

The family of FGFs constitutes at least 22 members that interact with at least four receptors (FGFR) and are major regulators of embryonic bone development (Ornitz and Itoh, 2001; Ornitz and Marie, 2002). Unique expression patterns of FGFRs have been identified in the growth plate. Both FGF-1 and -2 as well as FGF receptors, FGFR-1, -2, and -3, are expressed in chondrocytes (Jingushi *et al.,* 1995; Leach *et al.,* 1997; Hamada *et al.,* 1999)**.**

FGFR3 is expressed in the epiphyseal growth plate and is most highly expressed by proliferating and prehypertrophic chondrocyte. This expression pattern suggests a direct role for FGFR3 in regulating chondrocyte proliferation and possibly differentiation. In contrast, FGFR1 is prominently expressed in hypertrophic chondrocytes (Delezoide *et al.,* 1998), suggesting a role for FGFR1 in maintaining the hypertrophic phenotype of these cells (cell survival), in regulating the production of unique extracellular matrix products of hypertrophic chondrocytes, or in signaling their eventual apoptotic death (Ornitz, 2000).

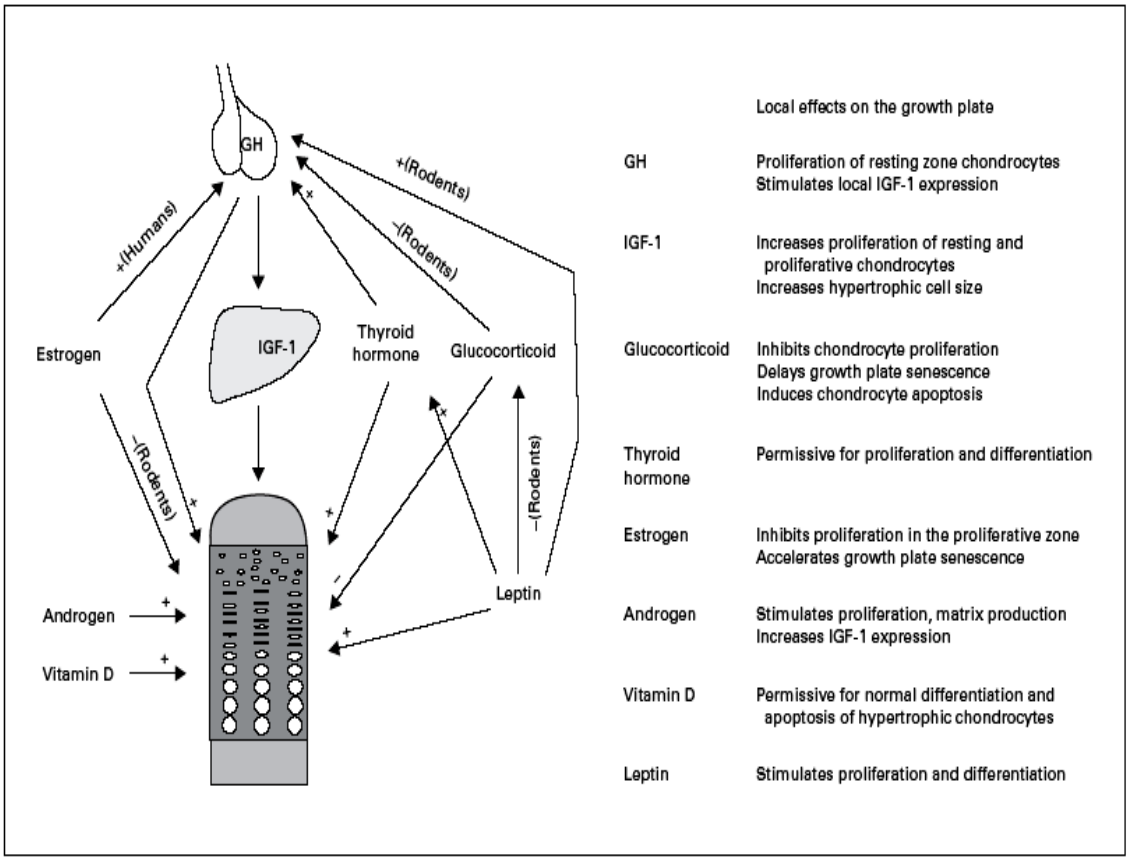

Figure 1.13 The endocrine signals that regulates longitudinal bone growth. Arrows indicate direct action on the growth plate and indirect action by modulating other endocrine signals. + = Stimulatory effect; – = inhibitory effect. After Nilsson *et al.* (2005).

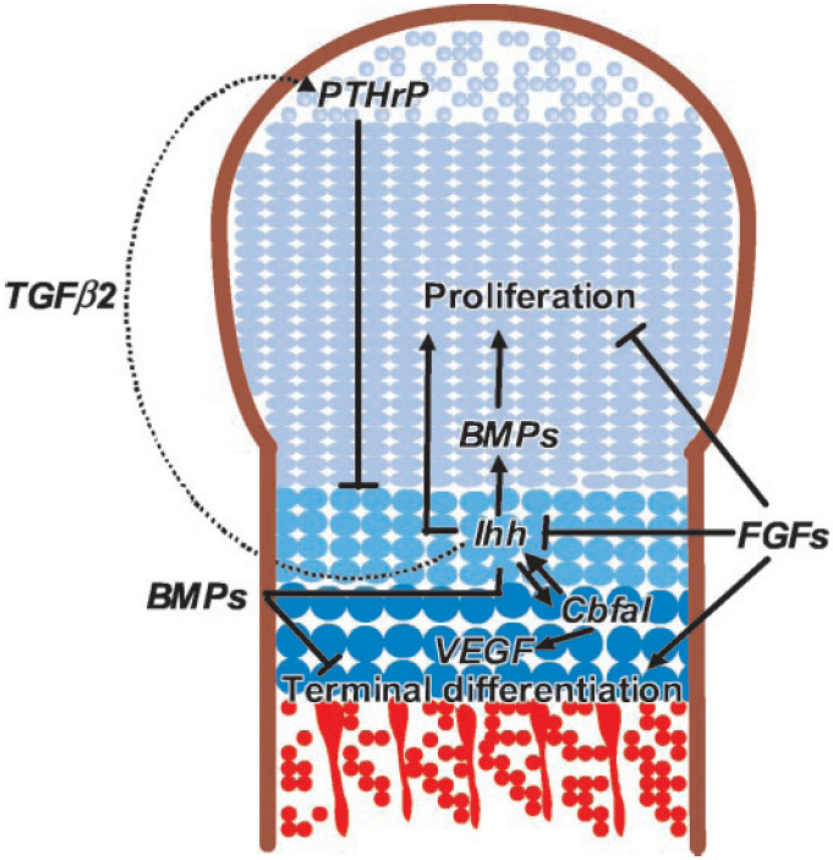

Figure 1.14 The local regulation of longitudinal bone growth. Interaction of Ihh, PTHrP, BMP, and FGF signaling in modulating chondrocyte proliferation and differentiation during prenatal endochondral bone formation. Ihh is expressed by chondrocytes making the transition from a proliferating into a hypertrophic phenotype. Expression of Ihh at this stage is up-regulated by BMPs but inhibited by FGFs. Ihh activates adjacent chondrocytes and diffuses toward the lateral perichondrium, where it can bind to its receptor patched. Via an as yet unknown mechanism, PTHrP production is stimulated in the periarticular perichondrium. Then, PTHrP diffuses toward the prehypertrophic zone, which expresses high levels of PTH/PTHrP receptors and inhibits the differentiation of proliferating chondrocytes to cells capable of synthesizing Ihh. Besides modulating chondrocyte differentiation, Ihh also stimulates chondrocyte proliferation, both directly and indirectly (through BMP signaling). FGFs are able to inhibit chondrocyte proliferation independently of the two stimulatory pathways. BMP signaling inhibits terminal differentiation of chondrocytes, a process that FGFs can promote. The balance between BMP and FGF signaling seems to be crucial in regulating proliferation, Ihh expression, and terminal differentiation of chondrocytes. After van der Eerdeen *et al.* (2003).

1.4.2.2.4 Bone Morphogenetic Proteins/ Transforming Growth Factor

The family of BMPs is comprised of at least 15 members, which are all part of the TGF superfamily. BMPs were originally identified as stimulators of bone formation but are now recognized as important regulators of growth, differentiation, and morphogenesis during embryology (Reddi, 2001). Within the developing limb cartilage elements, BMP2, -4, and -7 have been detected in the perichondrium, whereas BMP6 was found in prehypertrophic and hypertrophic chondrocytes (Lyons *et al.,* 1989; Lyons *et al.,* 1990; Jones *et al*., 1991; Macias *et al.,* 1997; Haaijman *et al.,* 1999; Grimsrud *et al.,* 1999). In addition, BMP7 was detected in chick sternal prehypertrophic and murine metatarsal proliferating chondrocytes (Haaijman *et al.,* 1999; Grimsrud *et al.,* 1999).

1.4.2.2.5 Vascular Endothelial Growth Factor

VEGF is a chemoattractant for endothelial cells and is one of the most important growth factors for endothelial cells (Ferrara and Davis-Smyth, 1997). Hypertrophic chondrocytes in the epiphyseal growth plate express VEGF. VEGF is an essential coordinator of chondrocyte death, chondroclast function, extracellular matrix remodelling, angiogenesis and bone formation at the growth plate (Gerber *et al.,* 1999).

1.4.2.3 Systemic and Paracrine Regulatory Interactions

There is an increasing body of evidence suggesting interactions between endocrine and local factors within the growth plate to control bone growth. Receptors for GH, T_3/T_4, GC, oestrogens, and androgens have all been localised to growth plates in various species, indicating that most hormones can have direct effects on processes in the growth plate after birth. These actions maybe either direct or act via the expression of locally acting growth factors, such as Ihh, PTHrP, BMPs, FGFs, and VEGF (van der Eerden *et al.,* 2003).

1.5 Clinical importance of Growth Plate: Longitudinal Bone Growth Disorders

From the review above it is clear that longitudinal bone growth is dependent upon normal growth plate function and endochondral ossification; regulated by a complex interaction of molecular signals acting systemically as well as locally

within the growth plate. This network is often dysregulated during chronic illnesses and this results in impaired chondrogenesis and, in turn, growth failure (De Luca, 2006).

Mutations in the genes are involved in the regulation of various stages of the chondrocyte proliferation and differentiation process have also been implicated in human growth plate disorders, resulting in skeletal dysplasias and short stature. For example, mutations involving most of the ECM encoding genes have been shown to cause heritable disorders of skeletal morphology and growth, a family disorders called "chondrodysplasias" (Aszodi *et al.,* 2000). In addition, abnormalities of collagen have been demonstrated to be responsible for aberrations of growth in certain hereditary chondrodystrophies, and it is likely that many, if not all, of these heritable disorders will ultimately be described on the basis of their underlying biochemical defect (Sussman, 1998). To date, there are over three hundred well defined disorders of skeletal growth and development. Achondroplasia and osteogenesis imperfecta are among the most common skeletal dysplasias, while others are less common (Phornphutkul and Gruppuso, 2009).

Primary growth arrest can also be caused by direct physical injury to the epiphyseal growth plate such as physeal fracture, deleterious effects of chemotherapy, certain types of infection (particularly meningococcal septicaemia), neurological disease, burns, juvenile chronic arthritis, uraemia, intoxication (vitamins A, C, D and heavy metals) as well as endocrine disease and malnutrition (Bush *et al* 2008a).

Skeletal problems within the livestock industry also have a great potential impact on both welfare and economic issues (Loveridge, 1999). In particular, poultry production (meat type and egg laying birds) has a long association with skeletal problems which pose a major animal welfare issue (Fleming *et al.,* 2006) and represent a substantial direct cost to the poultry industry (Bennett *et al.,* 1999) due to economic loss from culling, death or carcass condemnations and downgrading at slaughter (Riddell, 1980; Robinson *et al.,* 1992; Thorp, 1994). In the US alone, skeletal deformities cost the broiler industry an estimated $120 million per year (Cook, 2000).

Whatever the aetiological inputs that brings about these skeletal growth disorders, the ultimate effect on the activity of the growth plate and structural

integrity must be controlled by the component cells and the signals which they receive. Hence, a better understanding of chondrocytes and their mechanisms of growth regulation will help to determine the causes of disease or malfunction of the growth plate (Bush *et al.,* 2008a). However, our understanding of the cell biology of the growth plate, its regulation under normal conditions, and how these can be influenced in clinical practice is still at an elementary stage (Bush *et al.,* 2008a).

In order to understand pathophysiology changes of the aforementioned growth plate disorders, the knowledge of normal growth plate cellular mechanism(s) essential for longitudinal bone growth is needed. In particular, a focus on new insights into the normal process which underpin the cell enlargement of growth-plate chondrocytes, will allow us to develop a more biologically oriented approach to address problems associated with growth plate disorders and the control of endochondral ossification in the future.

1.6 Growth Plate Chondrocyte Hypertrophy and Longitudinal Bone Growth

Growth can be defined as hypertrophy or hyperplasia at the tissue or cellular level (Goss, 1978). Cell hypertrophy usually refers to an increase in cell size and volume associated with an increase in organelles (Buckwalter *et al.,* 1986). Hyperplasia refers to an increased number of a certain type of cells in a given organ or tissue than is ordinarily observed (Ouyang *et al.,* 2011). Both cellular mechanisms are active in the growth plate (Van Sickle, 1985). A study of the growth plate of the rat proximal tibia showed the volume of the growth plate chondrocyte (GPC) increased up to 10-fold from proliferative (~1790μm^3) to hypertrophic zone (~17400μm^3) (Hunziker *et al.,* 1987b).

The rate of longitudinal bone growth is controlled at several levels. Namely the number of proliferative and hypertrophic zone cells, the rate of division of proliferative chondrocytes, chondrocyte ECM synthesis, the rate of volume increase of the hypertrophic zone cells and the final volume attained by these cells (Thorngren and Hansson, 1973; Hunziker, 1994; Wilsman *et al.* 1996b). In the proximal tibial growth plate of a 4-week old rat, 9% of growth was contributed by proliferation, 32% by matrix synthesis, and 59% by chondrocyte enlargement (Wilsman *et al.* 1996b; Figure 1.15). The cell volume increases at the later stage of

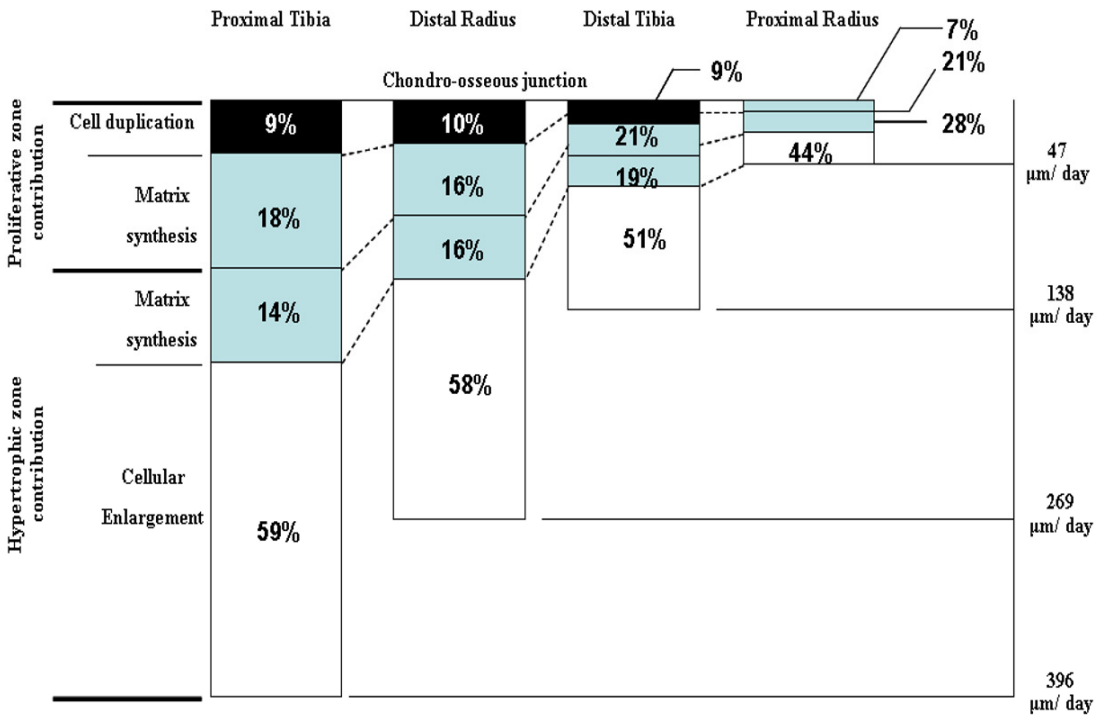

Figure 1.15 Differential growth by growth plates. Relative contributions to daily total elongation at the chondro-osseous junction are shown by longitudinal growth rate of the proximal and distal of radial and tibial growth plates of 28-day-old rats. The elongation fractions contributed by the hypertrophic and proliferative zones of the growth plates, via cell duplication, matrix synthesis and cell enlargement are also shown. After Wilsman *et al.* (1996b).

GPC differentiation has also been shown to be the main determinant of the rate of bone elongation in proximal and distal radial and tibia growth plates of rat and swine (Breur *et al.,* 1991).

1.7. Regulatory Volume Transporters and Chondrocyte Enlargement

The role of membrane transporters is indispensable in virtually all cellular functions of normal and pathological processes. Their roles, amongst others, involve acid-base homeostasis, ionic conductance, pH and cell volume regulation, cell growth and proliferation, intestinal absorption, cell death, and gene expression (Mahnensmith and Aronson; 1985; Seifter and Aronson, 1986; Yannoukakos *et al.,* 1994; Orlowski and Grinstein, 1997; Khaled *et al.,* 1999; de Congilani *et al.,* 2001; Alrefai *et al*., 2001; Nakamura, *et al.,* 2005; Zachos, *et al,* 2005; Bernardo *et al.,* 2006; Malo and Fliegel, 2006).

Cell volume regulation is one of the most fundamental homeostatic mechanisms and essential for normal cellular function. At the same time, however, many physiological mechanisms are associated with regulatory changes in cell size (Stuzin and Hoffmann, 2006). The necessity to rapidly regulate volume after shrinkage or swelling is obvious in cells from lower organisms, which are continually exposed to osmotic stress. Yet, in mammals, where osmolarity of the internal milieu is carefully regulated, cells also exhibit rapid volume regulatory responses (O'Neill, 1999).

Volume-regulatory pathways in mammalian cells are not merely a vestige that has no significant physiological role. Mammalian cells are still subject to volume changes, despite a relatively constant osmolarity. Furthermore, even if cell volume were not threatened, mechanisms are still needed to alter cell volume, such as during hypertrophy and atrophy, apoptosis, and differentiation. Thus mammalian cells clearly require volume-regulatory mechanisms, despite their relatively isosmotic existence. Although the principal volume regulatory transporters have been identified and characterized, their activation by changes in cell volume is poorly understood and their physiological role is largely unexplored (O'Neill, 1999).

To avoid excessive alterations to cell volume, cells have developed and utilize a multitude of volume regulatory mechanisms including transport across the cell membrane and metabolism. These mechanisms are triggered by minute

alterations of cell volume. They not only serve to readjust cell volume but profoundly modify a wide variety of cellular functions. Thus cell volume is an integral element within the cellular machinery regulating cellular performance (Lang *et al.,* 1998).

The cells ability to extrude Cl^- (coupled with extrusion of Na^+ by the Na^+-K^+ pump) appears to be the principal mechanism that maintains steady-state cell volume. However, additional mechanisms required by cells to correct acute deviations in their volume are termed regulatory volume increase (RVI) and regulatory volume decrease (RVD) adaptations and occur through activation of specific transporters in the plasma membrane that mediate net fluxes of osmotically active ions and molecules and therefore water (O'Neill, 1999).

Clearly, cell volume regulation is under a tight and dynamic control and abnormal cell volume regulation will ultimately lead to severe cellular dysfunction, including alterations in cell proliferation and cell death (Stuzin and Hoffmann, 2006). Figure 1.16 provides an overview of various membrane transporters involved in cell volume regulation.

Articular and growth plate chondrocytes share at least one feature in common. They lie isolated and embedded within a matrix, which has no capillary blood supply and the cells are nourished by dissolved substances diffusing through the intercellular substance (cartilage matrix) that surrounds them (Vaughan, 1981; Wilkins *et al.,* 2000; Serrat *et al.,* 2009). Therefore, chondrocytes, must possess effective membrane transport systems to counter this limitation and other related shortcomings caused by their remoteness from the vasculature. Cellular volume, pH and $[Ca^{2+}]$ control are three parameters which are highly relevant in the context of the extracellular environment experienced by these cells (Wilkins *et al.,* 2000). Cell volume regulatory function in articular chondrocyte is particularly important because they are constantly experiencing changes in their osmotic environment at least in two circumstances (Hall *et al.,* 1996a): (a) during static loading, when fluid expression raises the hydrostatic pressure of the interstitial fluid (Urban, 1994) and (b) in the initial stages of osteoarthrosis, when tissue swelling is the first detectable change of the disease process (Stockwell, 1991). Therefore the cellular volume homeostasis via cell membrane transport systems is fundamental to the maintenance of the articular cartilage integrity in general.

Regulatory transport systems involved in the articular chondrocyte cellular volume control have been reviewed by Hall *et al.* (1996a) and Wilkins *et al.* (2000). Volume regulatory functions of chondrocytes have been demonstrated and measured in living porcine articular chondrocytes explants (Errington and Hall, 1995; Errington et al., 1997) using confocal microscopy. A study on freshly isolated bovine articular chondrocytes suggested that the cells possess volume regulatory capacity (Hall, 1995), and despite the rigid nature of cartilage, *in situ* articular chondrocytes were osmotically sensitive within the extracellular matrix. In addition, the chondrocytes also possess a variety K^+ transport pathways sensitive to cell volume that are similar to those found in other cell types (Hall *et al.,* 1996b). The RVD capacity has been shown in *in situ* bovine articular chondrocytes and the RVD function remained intact in the isolated cells (Bush and Hall, 2001a; Hall and Bush, 2001). The main pathway involved in RVD in chondrocytes appears to be a volume-activated 'osmolyte' channel, which has some of the characteristics of similar channels in other cell types (Hall *et al.,* 1996a; Figure 1.16).

The RVI function was also shown in both the isolated and *in situ* bovine articular chondrocytes (Bush and Hall, 2001b), but in only limited capacity with a possible role of the cytoskeletal integrity in regulating the RVI activity, which appears to be mediated principally by the Na^+-K^+-$2Cl^-$ cotransporter (Kerrigan *et al.,* 2006). In short, the Na^+/K^+ pump and Na^+-K^+-$2Cl^-$ cotransporter are specific transporters which play a key role in articular chondrocyte ion transport and hence in the regulation of intracellular ionic/osmotic composition (Hall *et al.,* 1996a,b).

In the growth plate, chondrocyte volume increase is a crucial event during endochondral ossification and bone lengthening (Wilsman *et al.,* 1996). Morphometric analyses of electron micrographs on adult mice tibial GPs showed that GPC enlargement process was primarily the swelling of the cytoplasm and nucleus although the synthesis of organelles also contributes to the cell enlargement (Buckwalter *et al.,* 1986). The increase in the chondrocyte volume was reasonably achieved by transportation of fluid following active solute movement across the plasma membrane into the intracellular space (Hunziker *et al.,* 1987b).

However, based on searches of the relevant topics documented in current literatures hitherto, our knowledge of the growth plate cellular volume regulatory

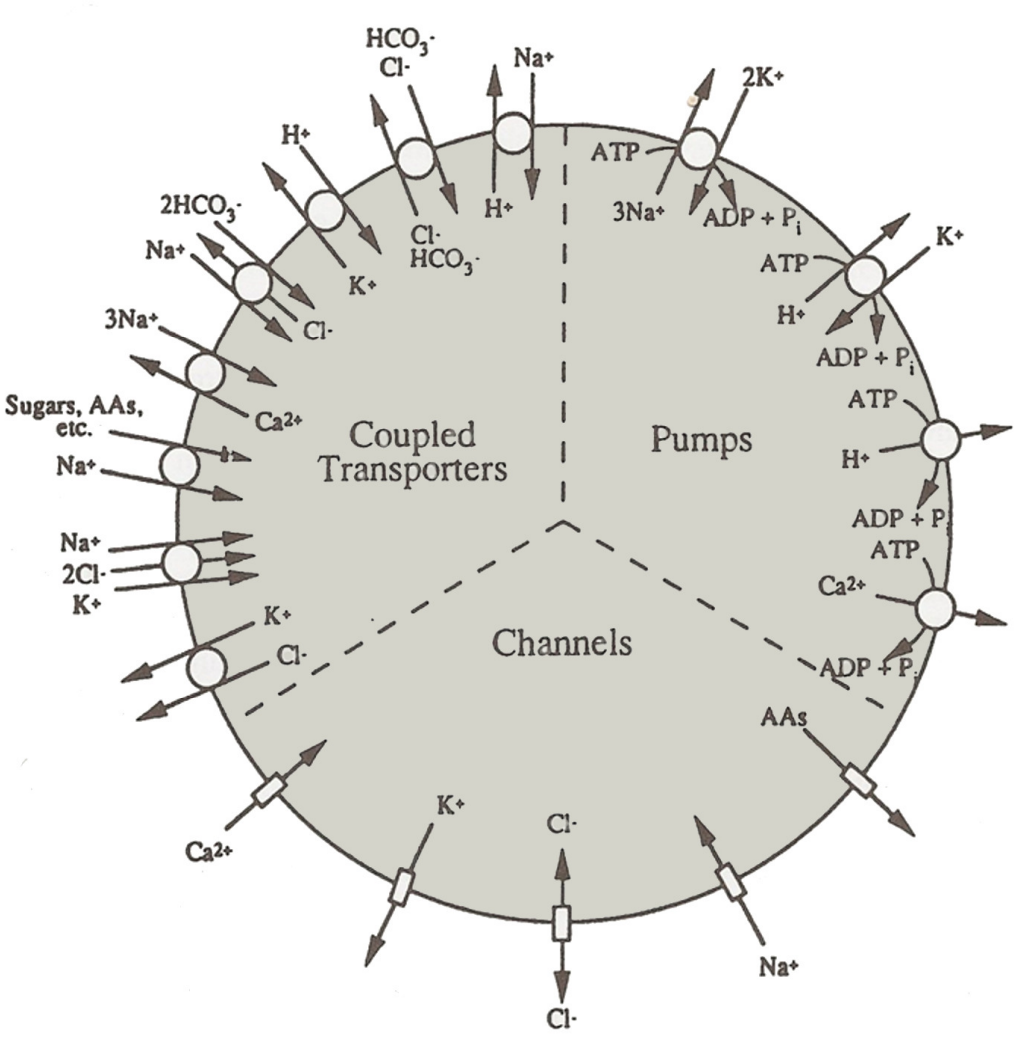

Figure 1.16 Transporters involved in cell volume regulation. The arrows show the usual direction of net flow, but many of the transporters (Na, K, 2Cl cotransporter; K-Cl cotransporter; K channels) operate in either direction depending on the electrochemical potential gradients of the relevant species. After Sachs, (1996).

transporters is meagre. Transport of metabolites and regulation of pH_i also remain largely uncharacterized for the growth plate chondrocyte.

Contrary to RVI volume recovery after cell shrinkage that returns a cell to its original volume, the growth plate chondrocytes require a coordinated and continual volume increase as they progress from proliferative chondrocyte (PZC) to terminal hypertrophic chondrocyte (HZC) phenotypes. Increased activity of membrane transporters may be able to drive the persistent cell enlargement (Bush *et al.,* 2010). In addition, the membrane transporters which normally prevent cell swelling are essentially suppressed; otherwise the increase in volume will be compromised (Bush *et al.,* 2006a).

An increase in the cell volume can be explained by classical "hypertrophy" (see section 1.6) and/or by "swelling" mechanisms (Bush *et al.,* 2008a, b; Buckwalter *et al.,* 1986). A study by Buckwalter *et al.* (1986) suggested that hypertrophic chondrocyte formation was primarily caused by swelling mechanism. Cell swelling involves cytoplasmic and nuclear enlargement via accumulation of fluid in the cell (Buckwalter *et al.,* 1986). However, an osmotic sensitivity study showed no difference between the osmotic sensitivity of PZC and HZC, suggesting a ''hypertrophic'' rather than ''swelling'' mechanism being responsible for cell volume increase (Bush *et al.,* 2008b). In other words, the total volume increase is not predominantly brought about by swelling but instead by an increase in non-osmotically active cellular ''dry matter''. This suggests that cell volume increase by hypertrophy has a greater role in cell enlargement than swelling, and is a main mechanism responsible for growth plate chondrocyte volume increase and hence bone elongation (Bush *et al.,* 2008a, b).

However, hypertrophy demands an increased movement of osmotically inactive structures (*e.g*., amino acids, simple sugars, *etc.*) into the cell but before the amino acids are synthesised into proteins they must act as osmolytes and exert a transient swelling pressure. Therefore, transport of the components may cause a transient osmotic gradient inducing cell swelling, which may be important in the last stages of cell differentiation. Thus we cannot rule out that cell swelling acts as the driving force for cell volume increase that is followed by cell consolidation through the production of ''dry matter'' (Bush *et al.,* 2008a, b).

Interestingly, both mechanisms of cell volume increase require an increase in the activity of plasma membrane transporters given that there has to be a net intracellular accumulation of osmolytes for swelling or hypertrophy to occur. Indeed, a study analysing mRNA showed that a number of candidate transporter required for swelling and hypertrophy mediated mechanisms of cell volume increase were more highly expressed in hypertrophic chondrocytes than in those found in the proliferative zone (Wang *et al.,* 2004). Figure 1.17 shows a schematic model outlining a possible role for membrane transporters in mediating the growth-plate chondrocyte volume increase.

1.8 Growth Rate and Differential Bone Growth

Differential growth is the phenomenon whereby each growth plate at different ages in an individual's life, may elongate at different rates by a factor of 3 to 7. Even the same phenomenon can be observed in the two growth plates at opposite ends of the same bone (Wilsman *et al.,* 1996b, 2008). For example, proximal and distal growth plates in both radius and tibia of the rat foetus elongated at similar rates; however, at 28 days of age, bone elongation due to proximal and distal growth plates in both bones was markedly different (Wilsman *et al.,* 2008).

A study by Wilsman *et al.* (1996b) using a set of eight independent variables suggested that differential growth was best depicted as a complex interplay among cellular division, matrix synthesis, and cellular enlargement during hypertrophy (Figure 1.15). This study confirmed the importance of cellular hypertrophy during elongation and the locally mediated regulatory systems controlling growth-plate activity.

Differential growth is primarily associated with differences in hypertrophic cell volume manifested when growth deceleration occurs (Figure 1.18). This study also illustrates that differential growth is superimposed on systemic regulators that affect all growth plates simultaneously. The most dramatic illustration of this is the sharp decline in growth velocity in all four growth plates that occurs perinatally (Wilsman *et al.,* 2008).

As has been discussed earlier, volume increase and cellular shape changes during hypertrophy may be regulated at the level of individual growth plates and that both are significant in understanding differential growth of long bones.

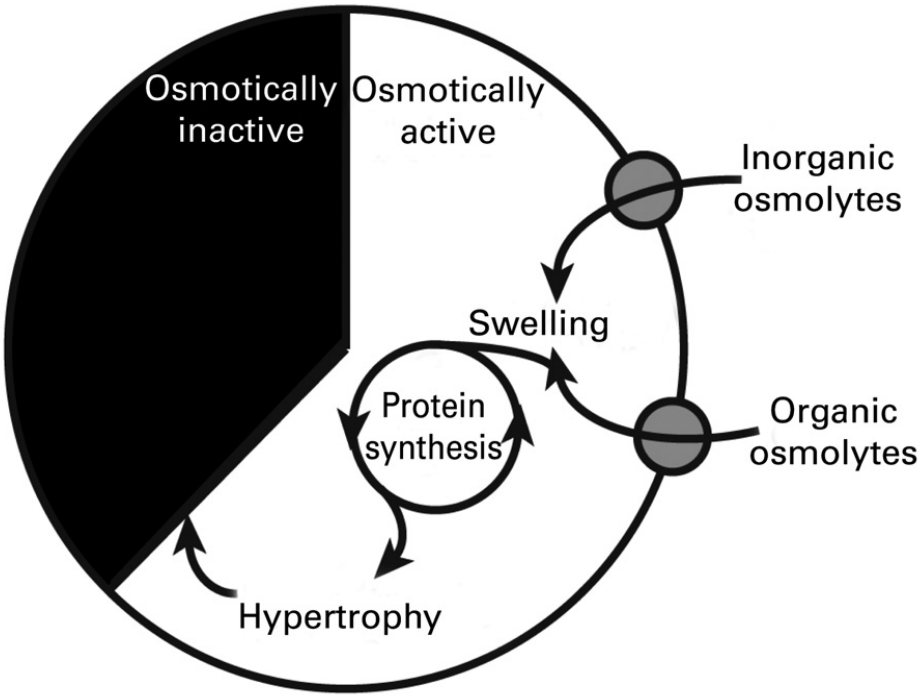

Figure 1.17 Diagram of a model to describe chondrocyte enlargement in the growth plate, encompassing both classical hypertrophy and swelling. If a cell is considered to be composed of osmotically-inactive (black) and osmotically-active (white) fractions, for 'dry' cell matter (*i.e.* proteins) and fluid respectively, then the proportion of chondrocyte enlargement due to hypertrophy and swelling can be represented. The intracellular accumulation of both organic (*e.g.* amino acids and simple sugars) and inorganic (*e.g.* K^+, Na^+, and Cl^-) osmolytes through membrane-transport proteins will create an osmotic gradient which water is obliged to follow thereby driving cell swelling. Accumulated amino acids can then be used in the synthesis of protein, contributing to the total 'dry' cell matter, and increasing cell volume by hypertrophy. From Bush *et al.* (2008a).

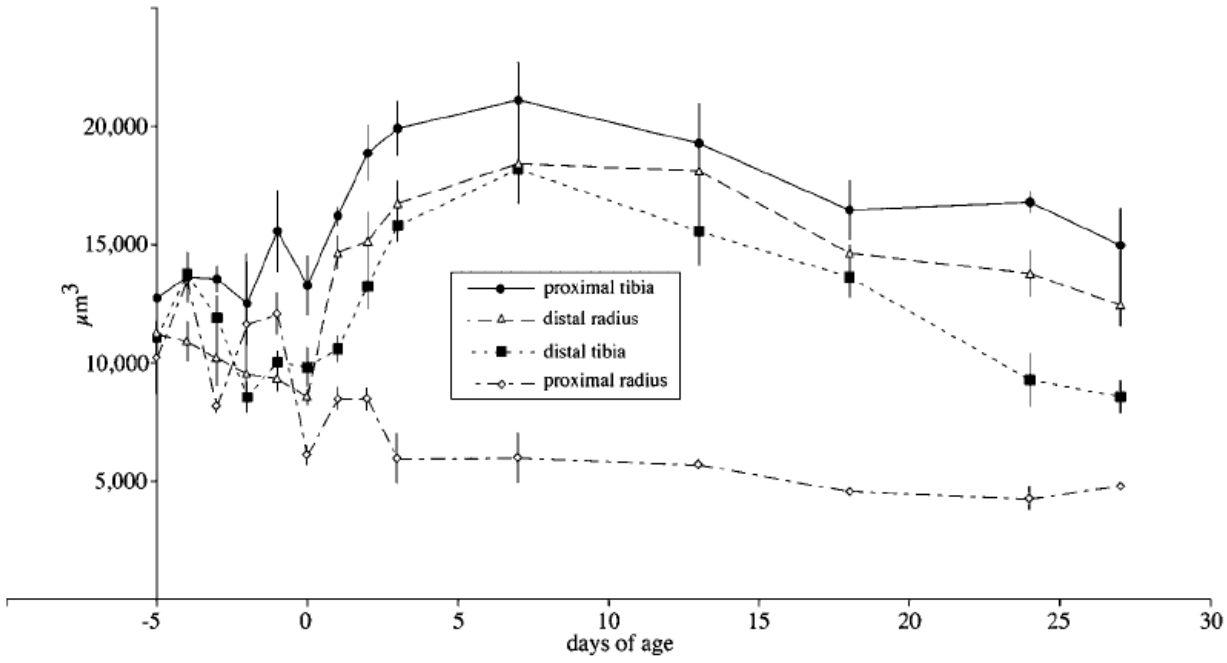

Figure 1.18 Changes in hypertrophic chondrocyte volumes and growth velocity over a course of study period. The changing pattern in cellular volumes of the postnatal adolescent period of Long-Evans rat pups, parallels changes in growth velocity during the same period in four different growth plates (the proximal and distal radial and the proximal and distal tibial). After Wilsman *et al.* (2008).

Wilsman *et al.* (1996a) demonstrated that chondrocytes in the proliferating zone of different growth plates have significantly different cell cycle times that regulated primarily through different G_1 phase duration. This study suggests that, in addition to systemic controls of chondrocyte proliferation, local controls may modulate rates of proliferation of individual growth plates and thus may be another locally mediated regulator of differential growth.

When considering bone growth rate as the variable of interest in differential growth, at any one time in any one growth plate, regulation of the kinetics of proliferation and regulation of the kinetics of hypertrophy occur simultaneously. Regulations of either the kinetics of proliferation or hypertrophy or both determine the final growth rate. It is also useful to consider the differential role of locally produced factors that to influence growth plate chondrocytes in regulating cell production, hypertrophic chondrocyte volume, cell shape, and integrating these cellular activities across these regulatory gates (Wilsman *et al.,* 2008).

1.9 Models for the Study of Bone Growth and Skeletal Development

Techniques used to study bone growth, development and modelling in children, adolescents and adults are restricted to non-invasive methods (Pedersen, 1982; Salle *et al.,* 2002; Bailey *et al* 2003; Kjar, 1974; Guadalupe-Grau, 2009; Yamamah *et al*., 2010). These techniques include fetal growth measurement using ultrasound, skeletal maturity evaluation using X-ray, and cross-sectional investigation including sports participation and dual-energy x-ray absorptiometry (DXA) measurement. However, the study of endochondral ossification and bone remodelling requires the use of appropriate experimental models as outlined below.

1.9.1 *In Vivo* Model

In vivo bone research has the potential to gain insight into growth and development, systemic response to varied cytokines, growth factors, and fracture repair of bone (Davies *et al.,* 2006). No *in vitro* cell culture system is able to produce loading that simulates the *in vivo* situation and currently very few *ex vivo* systems are able to approach such physiological loading (Pearce *et al.,* 2007). However, there are a few disadvantages of using this experimental model. Models

of this kind are expensive, requiring large numbers of animals, and it can be difficult to obtain discrete data due to systemic influences (Smith *et al.,* 2010). There is also inter-species, inter-site and inter-individual variability. Therefore caution is required when extrapolating data obtained from one model to other models and to the situation *in vivo* (Davies *et al.,* 2006).

1.9.1.1 Embryo

The foetal animal model has been used to study the morphology of normal and abnormal bone development in different species such as chick (Sawad *et al*., 2009), rodent (Efting *et al.,* 2004), ovine (Barbera *et al.,* 1995) and bovine (Kan and Cruess, 1987).

1.9.1.2 Postnatal

Post natal animal model are widely used in a number of studies using various animal species such as chicken (Glimcher *et al.,* 1980; Kocamis *et al.,* 1999), rabbit (Rivas & Shapiro, 2002), rat, bat (Farnum *et. al.,* 2008) and deer antler (Kierdorf *et al*. 2009). They were used to cover a broad scope of studies, which included collagen chemistry of healing bone, growth performance with administration of growth hormone, histological events in long bone formation, growth plate chondrocyte performance in longitudinal bone growth and mammalian tissue regeneration.

1.9.1.3 Genetic Manipulation: Transgenic and knock-out animals

Although various animals are used to investigate human skeletal biology, the mouse stands out because has been documented with a good understanding of molecular manipulation. Manipulation of the mouse genome has become an extremely powerful tool to define molecular mechanisms responsible for the morphogenesis and growth of the vertebrate skeleton (Horton, 2003).

Two strategies are used to change mouse genes namely transgenesis (injection of functional DNA pieces into single-cell embryos, that are expressed during subsequent embryonic development and postnatal life; Palmiter and Brinster, 1985) and targeted mutagenesis or gene targeting (introducing direct changes in endogenous genes of the mouse genome at the chromosomal locus; Cheah and Behringer, 2001). Mice with both alleles at a gene locus that are inactivated are referred to as knockout mice (Horton, 2003). For example

progesterone and GHR knock out mice have been used to study the effects of these ligands on bone growth and turnover (Sims *et al.,* 2000; Rickard *et al.,* 2008).

1.9.1.4 Other *In Vivo* Experimental Models

1.9.1.4.1 Models of Induced Bone Formation

Although there are dissimilarities between human and avian bone development (Leach and Gay, 1987), the avian model has been valuable in understanding human skeletal defects. For example, chickens were the primary model used to define nutrients necessary for normal long-bone growth (Cook, 2000). Ectopic bone formation has been studied by subcutaneous implantation of bone cells impregnated construct *in vivo* (Mai *et al*., 2006). Bone and cartilage formation in intraperitoneal diffusion chamber transplants have been used to test the osteogenic potential of both non-human and human cell sources (Johnson *et al.,* 1988; Krebsbach *et al.* 1999).

The effects of mechanical loading on bone formation have been studied using nonsurgical methods in mouse (Lee *et al.,* 2002; Gross *et al.,* 2002) and rat (Torrence *et al.,* 1994; Turner and Forwood, 1994; Hsieh and Turner, 2001; Ertem *et al.,* 2008). Other studies involved non-union bone treatment canine model (Heckman *et al.,* 1991) and calvarial bone formation model in mouse (Izbicka *et al.,* 1997).

1.9.1.4.2 Models of Longitudinal Bone Growth

Surgical and non-surgical approaches are used in animal model. Rodents are most commonly used (Buckwalter *et al.,* 1985; Wilsman *et al.,* 1996a & b, 2008). Rabbits are used as an alternative animal model to rodents (Wilson-Macdonald *et al.,* 1990) since the age of growth plate closure in rodents *e.g.* rats is longer than human in relation to their lifespan (Martin *et al.,* 2003). Whereas in humans an obvious growth spurt occurs during puberty and GP fusion at the end of it, rodents do not clearly demonstrate these phenomena during sexual maturation (van der Eerden *et al.,* 2003; Vico and Vanacker, 2010). The effects of mechanical loading on bone growth has been studied using surgical intervention methods in chicken (Rubin and Lanyon, 1984), calf, sheep, rabbit and rats (Stokes *et al.,* 1996, 2002, 2007; Stokes, 2002).

1.9.1.4.3 Models of Growth Plate Nutrient Transport

Serrat *et al.* (2009) used *in vivo* multiphoton imaging technique to quantitatively measure solute transport in tibial growth plates of mice. These analytical methods are a substantial advancement over traditional approaches to bone and cartilage imaging and important for elucidating the role of nutrient transport in natural and experimental models of growth plate dysfunction, particularly chondrodysplasias with known defects in components and structure of the ECM.

1.9.2 *In Vitro* System

As discussed earlier, the use of *in vivo* systems are to study mechanisms of bone growth in any detail are compromised by the complexity of the regulatory networks that operate in the whole animal. In addition these systems are subjected to various levels of factors such as loading over the bone or cartilage, growth rate and ageing which complicate interpretation. For this reason, the *in vitro* model systems are widely used and copious literature has documented work studies using these methods. The advantage of using *in vitro* models is that experimental replicates can be virtually identical, making statistical analysis and quantification easier. In addition, a great number of molecular and biochemical tools are currently available for these systems (Davies *et al.,* 2006).

In vitro bone research has three main branches: i) Cell culture – the growth of isolated cells no longer organised into complex tissues as *in vivo*. Cells are harvested from tissue either mechanically or through enzyme digestion and propagated in a cell suspension or attached to a surface as a monolayer. ii) Tissue culture – the maintenance of tissue fragments, not necessarily preserving tissue architecture. iii) Organ culture – the maintenance or growth of tissue, or organs (in whole or in part), which may allow differentiation and preservation of architecture and function (Davies *et al.,* 2006). Different examples of the various *in vitro* systems used are outlined below.

1.9.2.1 Primary Cells

Cells have been isolated from chick growth plates (Farquharson *et al.,* 1995) and bovine metacarpal epiphysis (Hutchison *et al.,* 2007), and can be fractionated into distinct populations (PZC and HZC) by means of Ficoll or Percoll density gradients (Trippel *et al.,* 1980; Warner *et al.,* 1983; Oberbauer and Peng, 1995). Percoll density gradient techniques have been used widely to examine growth plate

chondrocytes of varying maturation (Carey & Xia Liu, 1995; Farquharson *et al.,* 1999, 2000, 2001; Min *et al.,* 2002). Monolayer and suspension cultures of primary chondrocytes have been prepared from 21 day old rat tibia growth plate (Robson *et al.,* 2000), equine articular cartilage (Wilkins *et al.,* 2003; Ahmed *et al.,* 2007), rabbit and mouse chostochondral cartilage (Kato and Gospodarowicz, 1985; Yamakawa *et al.,* 2008; Fukai *et al.,* 2010), and bovine articular cartilage (Hall *et al.,* 1996b; Hall, 1999; Bush and Hall, 2001a, b; Simpkin *et al.,* 2007). Other sources of chondrocytes include those from the tip of xiphoid process of postnatal (11d) or adult (250 g body weight) rats, and 12 and 17-day chick embryo (Schmid and Conrad, 1982; Ishizaki *et al.,* 1994). Ichinose *et al.* (2005) used MSCs from human bone marrow as an *in vitro* differentiation model to study chondrogenesis. Human articular chondrocytes are also now available commercially (Akagi *et al.,* 2009).

There are some drawbacks in using isolated cells. This technique cannot reproduce the chondrocyte *in situ* environment and the environment of culture media into which cells are liberated during digestion is arguably unphysiological (Hall *et al.,* 1996a). The primary cell isolation process involves laborious digestion steps (Wilkins *et al.,* 2000). Harsh enzymatic digestion (Glade *et al.,* 1991) which the cells are subjected to was reported to destroy cell membrane proteins (Glant and Mikecz, 1986). There is also evidence that some chondrocyte parameters, such as regulatory volume responses, reset to match the environment of the isolation medium (Hall, 1995; Bush *et al.,* 2001a). The chondrocyte phenotype is also unstable and may undergo subsequent phenotypic drift and dedifferentiation following their isolation, which could be due to dissociation of cells from their three dimensional geometry and their propagation on a two dimensional substrate (Benya and Shaffer, 1982; Davies *et al.,* 2006).

1.9.2.2 Cell Line

Clearly, cultures of primary chondrocytes for studying chondrocyte cellular physiology are notoriously difficult to handle. An alternative is the use of chondrocytic cell lines: human chondrocyte-like cell line, HCS-2/8 (Takigawa *et al.,* 1989; Saas *et al.,* 2004; Chagin *et al.,* 2006) and C-20yA4 (Browning and Wilkins, 2004), TC6 derived from articular cartilage (Mataga *et al.,* 1996) or MCC-2, -5, -35 from costal cartilage of transgenic mice (Akagi *et al.,* 2009), and

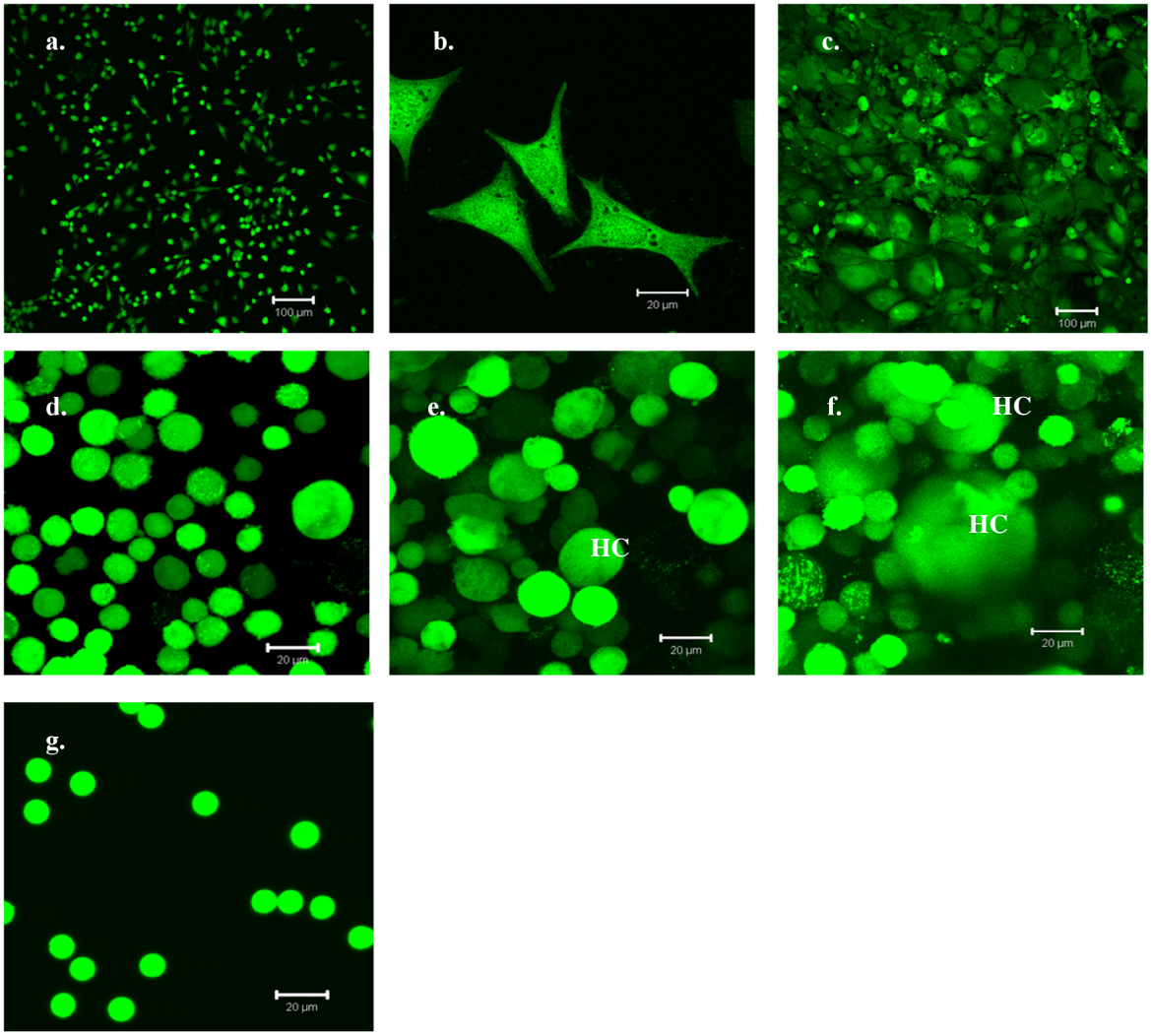

Figure 1.19 Chondrocyte-like murine ATDC5 cell line. Intact monolayer cells (a, b, c) and cell suspensions (d, e, f) stained with CMFDA (5 µg/ml) are shown. Cell suspensions were made from monolayer cells through trypsinization using 0.05% (v/v) Trypsin-EDTA solution. CLSM (Zeiss Axiovert-inverted microscopy for panel a and c; and upright Zeiss Axioskop LSM 510 for panel b, d, e, f and g) was used to acquire the fluorescence images. Increase in size of a number of cells was observed from day 0 to day 42 post confluence. Cells were visualized using a Plan-Neofluar x10/0.3NA lens (Zeiss Axiovert) or Achroplan x63/0.95 NA ceramic water-dipping lens (Zeiss Axioskop) at day 0 (a, b, and d); day 42 (c and f); and day 21 (e) post confluence. g. Fluoresbrite®YG Microparticles 10 µm (Polyscience, Inc.), fluorescent latex spheres, are shown for size comparison. Bar=20 µm (panel b, d, e, f, and g) and 100 µm (panel a and b). HC =hypertrophic cell.

ATDC5 from murine teratocarcinoma stem cells (Atsumi *et al.,* 1990; Shukunami *et al.,* 1997; Musthtaq *et al.,* 2002; MacRae *et al.,* 2006a, b; Takayama and Mizumachi, 2010; Figure 1.19).

Although cell lines offer an easily available, plentiful and reproducible source of chondrocytes, they have a number of disadvantages over primary cells. Immortalized chondrocyte cell lines appear to proliferate greatly and show less expression of genes of matrix synthesis and turnover (Saas *et al.,* 2004), thus their properties reflect only an approximation of the true chondrocytes.

Despite all these limitations, a combination of studies using *in situ* chondrocytes in cartilage explants (section 1.9.4.3), isolated primary chondrocytes and cultured cell lines has provided valuable fundamental information about chondrocyte properties and function (Wilkins *et al.,* 2000).

1.9.2.3 *In Situ* Cells in Tissue Explants

The visualisation of living cells within their ECM has been revolutionised by advances in confocal laser scanning microscopy. Many studies have been performed using living *in situ* chondrocytes model. In this technique the cartilage explants are freshly obtained and the chondrocytes left intact within the cartilage matrix for examination (Errington and Hall, 1995; Errington *et al.,* 1997; Bush *et al*, 2001a, b, 2005a, b, 2006a, 2007; Kerrigan *et al.,* 2006, 2008; Amin *et al.,* 2009; Amini *et al.,* 2010).

Using these models, the survivability and three- or four-dimensional morphological changes of cartilage *in situ* could be quantified at both tissue and cellular levels when the cartilage explants were subjected to various conditions such extracellular medium osmotic perturbation, Ca^{2+} treatment, and mechanical loading (Bush *et al*, 2001a, b, 2005a, b, 2006a, 2007; Kerrigan *et al.,* 2006, 2008; Amini *et al.,* 2010). This approach offers the possibility of obtaining new insights into the fundamental process of cellular regulatory capacity for example, without the perturbations arising from cell isolation.

1.9.2.4 Tissue or Organ Culture (*Ex Vivo*)

Ex vivo models have significant advantages, as the cells and tissue are able to be cultured in the same spatial arrangement as would be found in the *in vivo* situation, while systemic influences, which often hinder *in vivo* work, are removed (Smith *et*

al., 2010). The regulation of limb growth, and the signals involved in chondrocyte proliferation, maturation, and hypertrophy can be studied using these model systems (Di Nino *et al.,* 2002). Organ cultures taken from embryos of certain ages can be used for evaluating the local effect of various agents simultaneously, in a system where cellular interactions are intact (Chen and Klein, 1978; Chagin *et al.,* 2006). A role of a membrane transporter in GPC volume increase, and catch up bone growth of post dexamethasone treatment have been demonstrated using post natal rat bone culture (Bush *et al.,* 2010; Chagin *et al.,* 2010). The use of metatarsals from 18-day-old embryonic mice is well established and used in a number of studies (Mushtaq *et al.,* 2004; MacRae *et al.,* 2006a, b). Bovine cartilage tissue culture was used to study proteoglycans metabolism under influence of transforming growth factor β (Morales and Roberts, 1988).

A novel *ex vivo* mechanically loading culture system for 3D cancellous bone tissue has been developed to overcome some of the limitations discussed above for both cell culture and organ culture. The loading and media diffusion is believed to be more physiological than current organ culture techniques (Davies *et al.,* 2006). However this technique is limited to culture preparation of trabecular bone explants.

In spite of being widely used, there are number of limitations of the tissue and organ culture systems. Biochemical and molecular techniques in organ cultures are limited because the multi-cellular population makes determination of specific biochemical pathways attributed to a specific cell difficult. Organ cultures have a short lifespan, as they often undergo central necrosis due to vascular occlusion and rate-limiting mass transfer. The loss of the vascular system has implications in limiting the size of organ sample that can be harvested, since cells in culture depend upon diffusion of nutrients and metabolites as well as for the removal of waste (Davies *et al.,* 2006).

The above sections have given an overview of the relevant background literature reviews related to the scope of this work. The thesis aim/ hypothesis and the outline of the relevant projects undertaken are discussed below.

1.10 The Aim of Study and General Hypothesis

The general aim of this thesis was to investigate the following hypothesis: *Plasma membrane transporter(s) have a role in growth plate chondrocytes enlargement*

that contributes significantly to the rate of longitudinal bone growth. In order to test this hypothesis, four main projects were undertaken:

(1) Characterization of *in situ* living chondrocyte hypertrophy in various growth plates of post natal rats and their contribution to the bone length

(2) Investigation of the effect of fixative osmolarity in maintaining morphology of growth plate chondrocytes when using conventional fixative solutions

(3) Examination of the role of sodium–hydrogen and anion exchangers in longitudinal bone growth

(4) Study on changes to sodium/ hydrogen (NHE1) and anion exchanger (AE2) expression levels with growth plate chondrocyte hypertrophy.

Chapter 2

General
Materials and Methods

2.1 Materials

2.1.1 Equipments

(see Appendix 2)

2.1.2 Biochemicals and Solutions

Unless otherwise stated, all biochemicals and solutions were purchased from Sigma-Aldrich, Poole, U.K.

Buffer Solutions

Phosphate buffered saline (PBS)

A 200 ml PBS solution was prepared by dissolving a 5g PBS tablet (Invitrogen, U.K.) with 200 ml of distilled water. This buffer contains 10 mM phosphate, 150 mM sodium chloride, pH 7.3 to 7.5.

Sodium cacodylate (pH 7.4)

Prepared by diluting sodium cacodylate trihydrate powder (assay, approx. 98%) in distilled water; and the pH was corrected to 7.4 by addition of HCl.

Tris-EDTA-T80 HIAR buffer

10 mM Tris Base; 1 mM ethylenediaminetetraacetic acid (EDTA); 0.05% Tween 80, pH 9.0 was prepared as 1L stock solution by adding 1.21g Tris Base and 0.37 g of EDTA in 1L distilled water. The solution pH was adjusted to 9.0 with hydrogen chloride (HCl) before 0.5 ml of Tween 80 being mixed into the solution.

Bone Rudiment Culture Media

Dissection media (290-305 mOsm)

PBS solutions with:

7.5% (v/v) alpha modified essential medium (Invitrogen Ltd., Paisley, UK)

2% (w/v) bovine serum albumin V.

Standard culture media (postnatal rats)

α-MEM supplemented with:

1 mM Na_2 glycerol bi-phosphate

0.2% (w/v) bovine serum albumin (BSA), Fraction V

5mg.ml^{-1} L-ascorbic acid

1% (v/v) Pens/Strep (for a final concentration of 100 I.U./ ml penicillin and 100 µg/ ml streptomycin).

Standard culture media (embryonic mice) (Mushtaq *et al.,* 2004).

α-MEM supplemented with:

1 mM Na_2 glycerol bi-phosphate

0.2% (w/v) BSA, Fraction V,

0.05 mg.ml^{-1} L-ascorbic acid phosphate

0.05 mg.ml^{-1} gentamicin

1.25µg.ml^{-1} fungizone (amphotericin B)

Growth Plate Fixatives

1.3% (v/v) glutaraldehyde with 0.5% w/v ruthenium hexamine trichloride (RHT)

4% (w/v) paraformaldehyde (PFA), prepared from PFA powder (assay, 95%) in 0.01M phosphate buffer (pH 7.4).

Histological Slide Mounting Medium

FluoroSave™ (Calbiochem, Nottingham, U.K.)

Di-N-Butyl Phthalate in Xylen (DPX)

Histological Staining

0.1% (w/v) toluidine blue O in PBS buffer (pH 5.5)

Hematoxylin and Eosin (as described by Drury and Wallington, 1980)

Fluorescent Dyes

Vital cytoplasmic dyes

Chloromethylfluorescein diacetate (CMFDA, CellTracker™ Green) and calcein AM were both purchased from Invitrogen, Paisley, U.K. were prepared in dimethyl sulphoxide (DMSO) as 1 mM-stock and used at 5µM in tissue medium.

Nucleic acid stain

Propidium iodide (PI) was prepared as an aqueous 1 mM-stock solution and used at 5μM in tissue medium.

Pharmacological Agents

AE inhibitor solution

4,4-diidothiocyano-2,2-stilbenedisulfonate (DIDS) was prepared fresh as a 0.1M stock solution in 0.1 M potassium bicarbonate.

NHE inhibitor solution

5-(N-Ethyl-N-isopropyl) amiloride (EIPA) was prepared as a 120 mM stock solution in DMSO.

2.1.3 Animals and Growth Plate Preparation

Growth plates were obtained from 7- day-old Sprague-Dawley rat pups (7-day-old; P7) and 18-day-old fetal (E18) Swiss mice were dissected fresh and prepared for immediate image scanning, or further processed for later use in histology and immunohistochemistry. The bones with intact GP were dissected and temporarily placed in dissection medium. The P7 rats were humanely killed for other experiments following U.K. The post natal 7-day-old rat bones were chosen since at this age the bone mineralisation was found minimum and the histological section preparation could be performed by avoiding the possible immuno-comprimising bone decalcification step. Home Office guidelines, whereas the experimental protocol for E18 mice was approved by Roslin Institute's Animal Users Committee and the maintenance of the animals was in accordance to Home Office guidelines for the care and use of laboratory animals.

2.2 Tissue Culture (*Ex vivo*) Technique

2.2.1 Seven-day-old Post Natal Rat Metatarsals

Metatarsal rudiments mainly from the middle three with intact growth plate cartilage were dissected and temporarily placed in bone dissection media. The overall length of the metatarsal rudiments was measured before being cultured individually in 1 ml standard culture media supplemented with different

concentrations of treatment drugs. The vehicle-alone control was prepared by adding the standard culture media with the vehicle without their corresponding drugs. All the bone rudiments were maintained at 37^{o} C (CO_2 5%: air 95%; pH 7.4) for 24 hrs, before the second bone length measurement was taken.

2.2.2 Eighteen-day-old Embryonic Mouse Metatarsals

Middle three metatarsals were aseptically dissected under dissecting microscope (Figure 5.2B). All the bones were pooled together before being cultured individually in each well of a 24-multi-well plate. At least six bone rudiments were assigned to each treatment groups. Each culture well contained 300 µl of a standard culture medium with the different treatments, and placed at 37^{o} C in a humidified atmosphere of 95% air / 5% CO_2 for up to 11 days. In all experiments, the medium was changed every second/third day.

2.3 Tissue Processing

2.3.1 GP Fixation

Bones were fixed in 4% (v/v) paraformaldehyde (PFA) overnight, and stored at 4^{o}C in PBS in preparation of microscopy or 2% glutaraldehyde (GA) with 0.7% Ruthenium Hexammine Trichloride (RHT), where appropriate.

2.3.2 GP Histological Preparation

The bones were fixed overnight before being dehydrated through a graded series of ethanol solutions. After the dehydration, the bones were embedded in paraffin wax using a standard procedure (Kiernan, 1999) and cut into longitudinal 10 µm serial sections using a microtome (Reichert-Jung Microtome 2050 Supercut, Arnsberg, Germany). The sections were then mounted on poly-l-lysine-coated microscope slides (Polysine^{TM}, VWR International, Leicestershire, UK) and dried overnight.

2.3.3 Histological Staining

2.3.3.1 Toluidine Blue O

After de-paraffinisation with xylene and rehydration with a series of ethanol solutions (100%, 90%, 75%), the sections were stained with 0.1% toluidine blue O in PBS (pH 5.5; 30secs at room temperature) using the technique adapted from

Bancroft and Cook, 1994. The section slides were then rinsed briefly in distilled water and allowed to air dry prior to mounting in FluoroSave™ with cover slips.

2.3.3.1 Hematoxylin and Eosin

Hematoxylin and eosin procedure used was as described by Drury and Wallington (1980). Briefly, the dewaxed and rehydrated slides as previously described (2.3.3.1) were immersed in haematoxylin for 2-5 mins, washed with running tap water for 5 mins, immersed in eosin for 2 mins then washed again in running tap water for 5 minutes. Afterward, the sections were dehydrated in 70%, 95%, and two changes of 100% ethanol (60 seconds in each change). Then the slides were cleared in xylene before being mounted with DPX mountant.

2.3.4 Fluorescent Staining

2.3.4.1 Living *In Situ* Growth Plate Chondrocytes

Bones were washed, sagitally bisected (see Figure 4.6(A)) and then exposed to fluorescent dyes *e.g*. CMFDA or calcein AM (5 µM), and/ or PI (5 µM) for 30-60 mins at 37^{o} C. CMFDA or calcein was used to label the viable cells as they are permeable to intact live cell membrane and produces a membrane-impermeant fluorescent product once reacted with intracellular esterase that stains the cytoplasm of viable cells green. On the other hand, PI is only capable of crossing plasma membrane of dying/ dead cells and stains the nuclei of the dead cells red (Gatti *et al.*, 1998; Amin *et al.,* 2008).

2.3.4.2 Fluorescent Immunohistochemistry

Fluorescent immunohistochemstry (FIHC) was performed after pretreatment procedures being applied to the GP histological sections. Each GP section per histological slide was marked by a small hydrophobic circle drawn around the tissue sections using a PAP pen (Liquid Blocker, Daido Sangyo, Tokyo) to keep the Ab pooled in a small droplet and avoid any mixture between the Ab or serum applied in adjacent sections. One of the 3-4 sections per slide was designated to be a negative control while the other 2-3 underwent normal staining. Non-specific Ag

sites were blocked using goat serum (1:5 dilution) on all sections at RT. Goat serum was replaced after 30 mins by specific 1^{o} antibodies under investigation. Optimal dilution of the 1^{o} Ab, the concentration that gives the optimal specific staining with the least amount of background staining (Renshaw, 2007) was determined by titration test using series of different titres of the 1^{o} Ab. For the negative control section, the primary Ab was omitted and replaced with the serum from the species that the secondary antibody was generated. Slides were then incubated overnight at 4° C (or for 2 hrs at 37° C) in a humidity chamber. Afterwards, slides were washed 3 times with PBS for 5 mins each before being incubated with a FITC (fluorescein isothiocyanate)-tagged 2^{o} Ab at 37° C for 1hr. Sections were again washed 3 times with PBS for 5 mins each. Then, cover slips were mounted using FluorSave™ and left to dry for 3 hrs at 4°C in tinfoil wrap prior to imaging using a CLSM.

2.4 Cell Imaging

2.4.1 Histological imaging

Images of P7 rat growth plates were taken using the transmitted light detector of an upright confocal laser scanning microscope fitted with a x10 dry objective lens. For E18 mouse metatarsals, the bone histological sections were examined under a Leica DMR microscope which connected to a Leica DFC 490 digital camera. Image acquisition was performed with the Leica application suite (LAS, Peterborough, U.K.) software in conjunction with the use of the microscope and digital camera.

2.4.2 Confocal Laser Scanning Microscopy

An upright Zeiss Axioskop LSM 510 CLSM (Carl Zeiss Ltd., Welwyn Garden City, Herts., U.K.) was used to acquire fluorescent images of *in situ* GPC. Cells were visualized using a Plan-Neofluar x10 dry objective (numerical aperture (NA) = 0.3) for low power overviews and an Achroplan x63 ceramic water-dipping lens (NA=0.95) for high power views. Intracellular calcein (Exc/Em = 495/ 517 nm) or CMFDA (Exc/Em = 488/ 517 nm) was excited using an Argon laser (488 nm) and emitted fluorescence detected using a 500-550 nm band pass filter; whereas nucleic acids bound PI (Exc/Em = 536/ 617 nm) was excited using a He-Ne laser (543 nm)

and emitted fluorescence detected using a 560 nm long pass filter. The confocal detection pinhole was set at 1.00 Airy Unit. Laser power and detector sensitivity were adjusted to provide optimum image quality. The scanning speed was typically 0.6Hz with 2 frame integration of a 512x512 pixel image, with serial 1µm z-step optical sections (see Bush & Hall, 2001a & b; Bush *et al*., 2007 for further details).

2.5 Data Handling and Analysis

2.5.1 Proliferative and Hypertrophic *G*rowth Plate Zones Definition

Projections of adjacent high magnification image stacks were 'stitched' together to produce a montage encompassing the GP from proliferative to hypertrophic zones (Figure 3.1A). To determine the beginning and terminal point of the GP, GPC zones must be first clearly defined. We used several subjective criteria based on the cell size and organization as previously described by other groups. Briefly, chondrocytes within the PZ (between the reserve and HZ) appeared to be ellipsoidal and arranged with at least 3 cells per group (Buckwalter *et al.,* 1985). The cells in the HZ (between zone of proliferation and calcification) were larger and rounded in shape defined by the cell height being one-half than the cell's width (Farnum and Wilsman, 1986).

Whilst great care was taken to be consistent, there was inevitable variation in the angle of bone bisection, and GP from differing positions are of different length. Consequently the position of cell within GPs has to be normalized for comparisons to be made. The high power GP image montages were divided into eight equidistant sections (S1 to S8) from the proximal edge of the proliferative (S1) to the distal edge of the hypertrophic zone (S8) (Figure 3.1B). This could be performed in all GPs in the present study in spite of various GP lengths. Eight sections gave sufficient sensitivity to allow changes in chondrocytic cell parameters to be detected along the GP zones (Breur *et al.,* 1994) and at the same time permit a statistically adequate number of cells to be measured within each section. Therefore comparative analysis on the cellular parameters could be made between corresponding sections from different GP sections (Bush *et al.,* 2008b).

2.5.2 *In situ* Growth Plate Cell Volume and Surface Area Measurement

Volume analysis was performed using high performance 3D imaging software (Volocity®, Improvision, Coventry, U.K.) on scanned CLSM images using the calibrated cell volume method as previously described (Bush and Hall, 2001a). Briefly, cells and beads were individually selected as regions of interests (ROIs), and a 40% baseline threshold (BT) of the fluorescent intensity from the three-dimensional cell image was determined before the volume was calculated. This BT value was found to return accurate object volumes over a wide range of calibration beads used (Bush and Hall, 2001a).

2.6 Statistical Analysis

Data were expressed as means ± S.E.M. obtained from a minimum of 3 bones from separate animals (n) and (N) GPC cells at each condition with the data shown as (n[N]). Statistical significance between two groups was evaluated using two-tailed Student's unpaired *t*-tests, with the *P* value considered significant when $P<0.05$. The statistical significance of differences between treatments was ascertained using a one way and two way ANOVA for repeated measures, followed by a *post hoc* multiple comparisons analysis of pairwise differences between treatments using the Holm-Sidak method. Linear and non-linear relationships ware determined using Regression Wizard analytical application of SigmaPlot® (11.0). All other statistical tests were also performed using SigmaPlot® (11.0) statistical software (Systat Software Inc., GmbH, Germany).

Chapter 3

Investigation of *In situ* Living Chondrocyte Hypertrophy in Various Growth Plates of Post Natal Rats and Their Contribution to the Bone Length

3.1 Introduction

All growth plates exhibit a cascade of cell differentiation from the proliferative through to the hypertrophic zones. Different bones grow at different rates and ultimately achieve different lengths (Wilsman *et al.,* 2008). The growth plate chondrocyte (GPC) volume increase at the later stage of GPC differentiation has been shown to be the main determinant of the rate of bone elongation in proximal and distal radial and tibia growth plates of hooded rat and Yucatan swine (Breur *et al.,* 1991). In a previous study on proximal tibia of rat growth plates, the volume of the GPC has been shown to increase up to 10-fold from proliferative (~1790 μm^3) to hypertrophic zone (~17400 μm^3) (Hunziker *et al.,* 1987b). However, as different growth plates elongated at different rates at a given time point (Wilsman *et al.,* 2008), it was not clear whether the increase in cell volume and rate of longitudinal growth contribute to the final bone length. A comparison of the same bones from the laboratory mouse (*Mus musculus*) and big brown bat (*Eptesicus fuscus*) suggested longer bone length was correlated with and early attainment of final hypertrophic cell volume (Farnum *et al.,* 2008).

In order to understand further this differential growth phenomenon, the present study examined the profile of *in situ* living GPC volume increase in different growth plates from one animal species at one age (7-day-old Sprague Dawley rats) using CLSM. The present study examined the contribution of GP hypertrophic cell volume as the main differential GP variable determining the overall length of the corresponding growth plates and bones. Chondrocyte performance and kinetic studies have previously been undertaken using a stereological approach on fixed GP tissues (Buckwalter *et al.,* 1985; Hunziker *et al.,* 1987b; Breur *et al.,* 1991; Kuhn *et al.,* 1996; Noonan *et al.,* 1998; Wilsman *et al.,* 1996b; Wilsman *et al.,* 2008). A stereologically approach requires an optimal chemical fixation as the cell's morphology is prone to alter during the fixation process (Hunziker *et al.,* 1983; see Chapter 4). The present study utilized living, unfixed, *in situ* chondrocytes which were minimally perturbed and therefore were as close as possible to their natural physiological morphology. The use of CLSM offers an alternative way of visualizing and studying living, *in situ* GP cells

through calibrated, quantitative measurement of cell volume and dimensions whilst excluding any preceding fixation steps.

This study also expanded on previous work by examining GPs of long, short and flat bones, incorporating both load and non-load bearing bones. Thereby examining if different bone shapes (in particular the bone length) or load bearing function has any effect on GPC differentiation and hypertrophic cell size. Earlier studies have also shown the important contribution of the chondrocytic shape change especially in the direction of bone growth to bone lengthening growth (Farnum *et al.,* 2008). While the Farnum *et al.* (2008) study looked at the GPC shape changes in the digital bone GP of the laboratory mouse and big brown bat using stereological approaches, this present study measured the same parameters on *in situ* living GP cells of two different long bones (tibia and radius) of the same species (P7 laboratory rat). The quantitative and physiological understanding of how bone growth is regulated in response to mechanical loading is still lacking (Villemure and Stokes, 2009). However a few studies have reported significant effects of mechanical loading on endochondral bone growth at the tissue and cellular level when growth plates were subjected to compressive and distractive mechanical force (Stokes *et al.,* 2002; Stokes *et al.,* 2007 Cancel *et al.,* 2009; Amini *et al.,* 2010). Therefore, it is important to know how load bearing under normal physiological condition alters chondrocyte differentiation and hypertrophy and contributes, if any, to the longitudinal bone growth.

It is well recognized that there is a positive association between the GPC hypertrophy and the rate of longitudinal bone growth (Breur *et al.,* 1991; Kuhn *et al.,* 1996; Wilsman *et al.,* 1996b). In this study this observation has been extended by examining the link between the GPC hypertrophy and final bone length. In previous studies the rate of longitudinal bone growth was determined by the measurement of new bone formation in a single GP within 24 hrs by the use of fluorescing labeling agent such as oxytetracycline or calcein (Hunziker *et al.,* 1987b; Kuhn *et al.,* 1996; Wilsman *et al.,* 2008). Although informative, this experimental approach might not truly represent the total bone growth rate considering there are possible cumulative contributions of new bone formations

from two GPs of opposite cartilaginous ends of a same bone to make up the overall bone length increase. Therefore, in the present study the relationship between the GPC hypertrophy with longitudinal bone growth with reference to the final length of the respective bone has been examined.

In view of the possible dynamic regulation and control of cell volume increase that is present in the GP throughout the period of active longitudinal bone growth, it is likely that that the contribution of the GP hypertrophic cell volume to the overall length of the corresponding bone could not be directly exhibited at a single moment in time during bone lengthening. Therefore in the present study, this hypothesis was tested by measuring the *in situ* chondrocyte hypertrophy in different living growth plates of rats at a single time point (7-day-old) and examining the relationship between the chondrocyte hypertrophy and the corresponding final bone lengths at this given post natal age.

3.2 Materials and Methods

3.2.1 Animals and Growth Plate Preparation

Twenty-one Sprague-Dawley rats (7-day-old; P7) were prepared as described previously (2.1.3). Tibiae, radii, femora, humeri, metatarsi, metacarpi, pelvic ilia and rib bones were dissected and temporarily placed in dissection medium (293 mOsm). At least three bones with intact GP were obtained from three (n=3) different animals.

Bones were categorized based on gross morphology (Bannister *et al.,* 1995; Lever and Heinemann, 1980) namely: long bones (humerus, femur, tibia and radius), cuboid or short bones (metacarpus and metatarsus); and flat bones (pelvic ilium and rib). The long and cuboid bones were weight-bearing, whereas the flat bones were non-weight bearing (this was based mainly on observation in the older animals which are more physically active). The GPs studied were the proximal and distal of femur and tibia, proximal humerus and radius, distal metatarsus and metacarpus, pelvic iliac crest and rib cartilage beginning from the costochondral junction.

For the imaging of *in situ* living growth plate chondrocytes, surrounding soft tissue was carefully dissected away before the bones were cut sagittally to reveal the growth plate (Appendix (A)). Bone dissection was performed using a fresh scalpel blade (No.11) to minimize cell death by blunt injury (Huntley *et al.,* 2005). After bisection the bones were immediately incubated in calcein AM (5μM in dissection medium) at 37^{o} C for 30 min. The bones were then attached to the base of a 35x10 mm sterile tissue culture dish (Cellstar®, Greiner Bio One, U.K.) using cyanoacrylate super glue (Loctite®, Cheshire) at a point distant to that being imaged with the cut surface of the growth plate facing upwards. At all times, tissue was kept under dissection medium to prevent dehydration. CLSM imaging was performed within 6 hrs of the animal being sacrificed.

3.2.2 Confocal Laser Scanning Microscopy

An upright Zeiss Axioskop LSM 510 (Carl Zeiss Ltd., Welwyn Garden City, Herts., U.K.) CLSM was used to acquire fluorescent images of *in situ* GPC using the protocol that has been described previously (2.4.2). A series of adjacent high power image stacks were obtained from the osteochondral junction to the early proliferative zone cells at the cartilagenous end.

3.2.3 Determination of Proliferative and Hypertrophic Growth Plate Zones

Projections of adjacent high magnification image stacks were 'stitched' together to produce a montage encompassing the GP from proliferative to hypertrophic zones (Figure 3.1A). The proliferative and hypertrophic GP zones were determined using subjective criteria that have been described earlier (2.5.1).

3.2.4 *In Situ* Cell Count, Density, Volume, Surface Area, and Cell Dimensions Measurement

Three dimensional volume images were observed using high performance 3D imaging software (Volocity®) on CLSM image stacks. Cell numbers were counted by eye from each GP zone. Only whole cells which were entirely within the 3D image volume were counted and used to determine cell density.

FIGURE 3.1

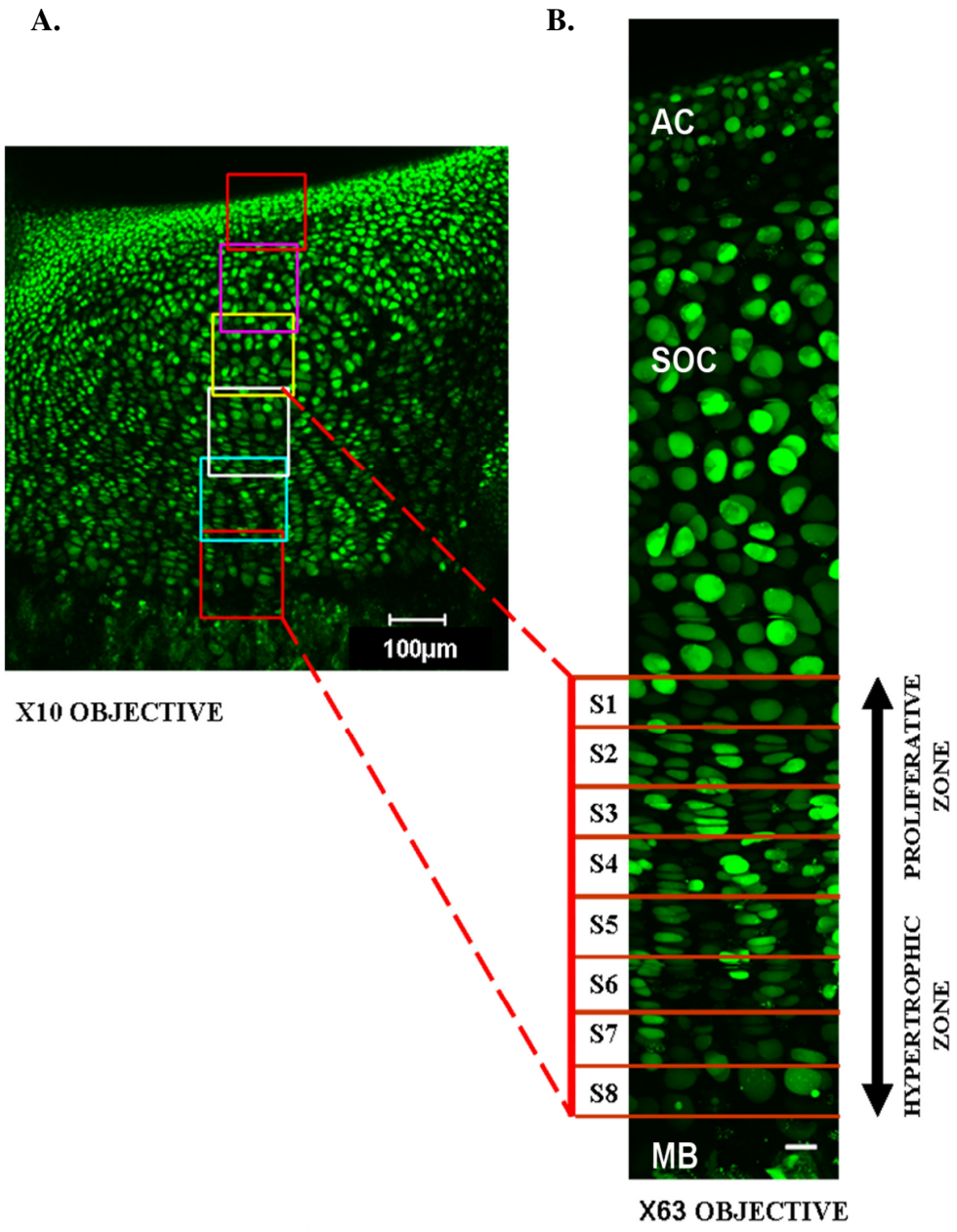
A.
B.
AC
SOC
100µm
X10 OBJECTIVE
S1
S2
S3
S4
S5
S6
S7
S8
MB
PROLIFERATIVE ZONE
HYPERTROPHIC ZONE
X63 OBJECTIVE

FIGURE 3.1

C.

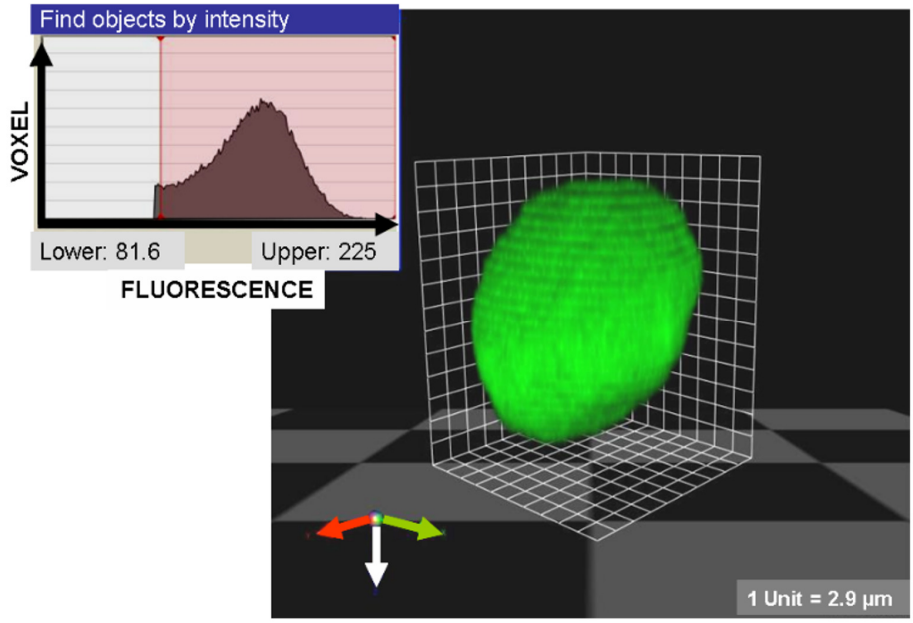
Find objects by intensity
VOXEL
Lower: 81.6
Upper: 225
FLUORESCENCE
1 Unit = 2.9 µm

D.

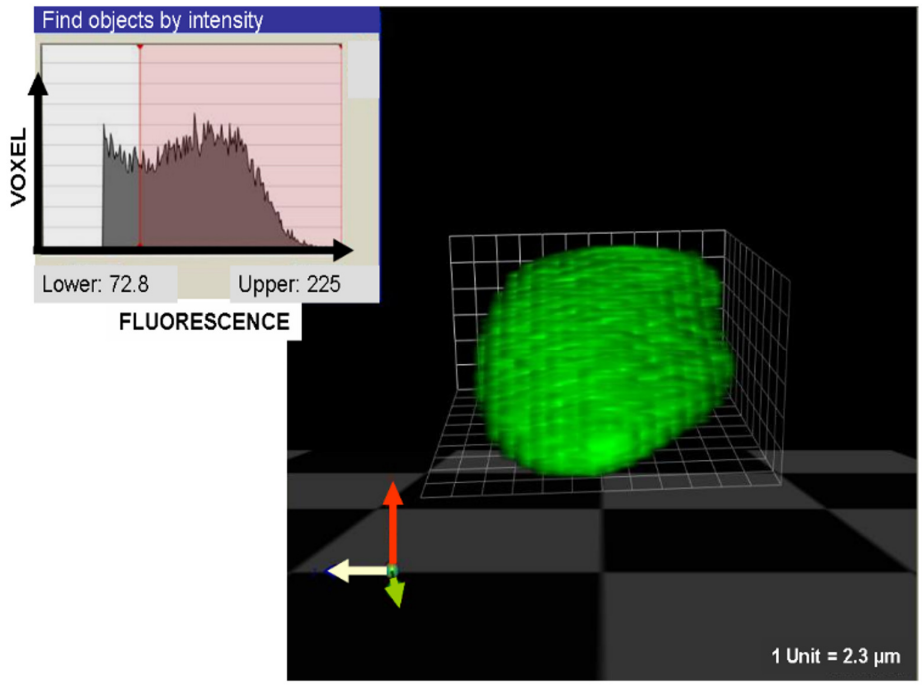
Find objects by intensity
VOXEL
Lower: 72.8
Upper: 225
FLUORESCENCE
1 Unit = 2.3 µm

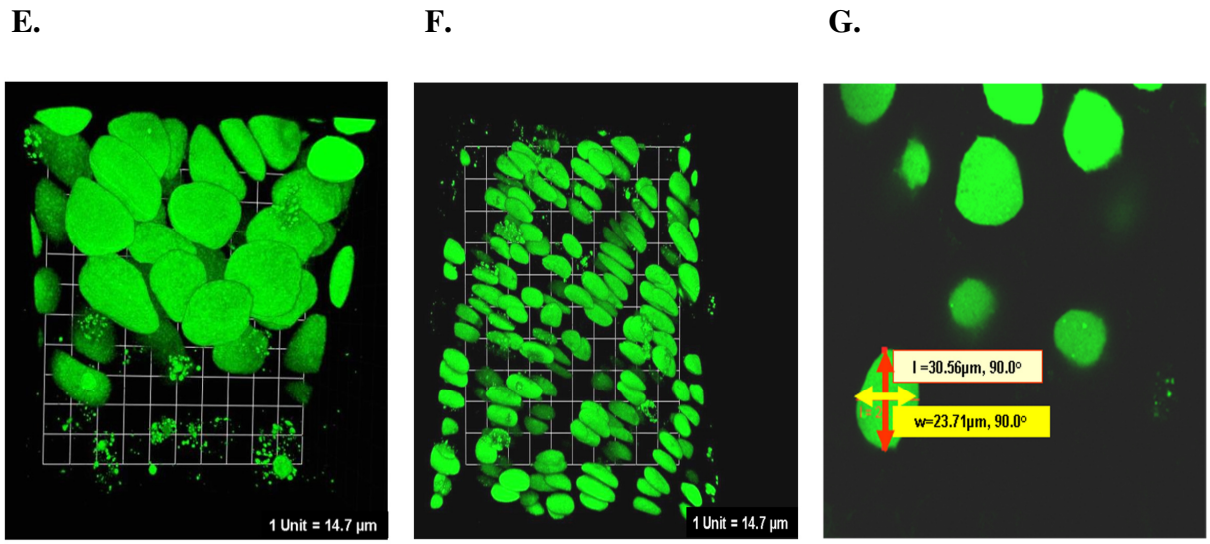

Figure 3.1 Overview of *in situ* living rat GPC as observed using CLSM and the evaluation of the GPC dimensional parameters. (**A**) Growth plate of P7 rat as observed under x10 objective dry lens of a confocal microscope. Series of regions of interest (ROI; series of square area) were identified and observed further under high power lens (x63 water-dipping lens, figure **B**). (**B**) The collated series of higher power magnification images provides a whole length high magnification view of the GP. (**C**) The constructed 3D cell image of a hypertrophic GPC and (**D**) proliferative GPC using Volocity® software which allows the measurement of the cell volume (see Materials and Methods). The inset of figure C and D shows the range of fluorescence intensity of a single chondrocyte cell image after the threshold correction, as a function of the voxels (three-dimensional pixel) of the cell image. Constructed 3D images of *in situ* chondrocytes (*e.g.* proliferative (**E**) and hypertrophic (**F**) GP zone cells) could be viewed from various angles and planes using 3D opacity mode (interactive rendered 3D image visualization mode) of the software for general evaluation of the cell shape and orientation. Measurement of the cell length, width and depth was determined using LSM Image Browser (**G**). AC, articular cartilage; SOC, secondary ossification centre; MB, mineralised bone. Bar scale in (B) = 20 µm.

The quantification of *in situ* chondrocytes volume and surface area was as described in General Materials and Methods (2.5.2). The cell dimensions were measured using LSM image browser (Zeiss LSM Image Browser Software, Carl Zeiss Microlmaging GmbH, Germany) (Figure 3.1G). Cell length and width dimensions were determined by inspecting individual optical sections. The greatest length (measured along the axis of longitudinal bone growth) and width (perpendicular to the length in the same place as the bisected bone cut surface) were measured. Cell depth was measured through adjacent optical sections, perpendicular to both length and width (Bush *et al.,* 2007).

3.2.5 Growth Plate and Bone Length Measurement

Growth plate length was determined based on the length of the GP as seen on the 'stitched' high-magnified GP images obtained from CLSM imaging as explained above. The GP beginning and terminal points were determined using a method that has been described in 2.5.1. The bone length was measured directly by eye using a rule graduated to 0.5 mm on the cleanly dissected whole bone tissue. Measurements were performed on each bone from at least three different animals.

3.3 Results

3.3.1 *In Situ* Living GPC as Observed Using CLSM

To visualize GP zones from different GPs this section describes the appearance of *in situ* living GPC as observed in various GPs. The length and width of the growth plates could conveniently be observed under a lower power magnification using x10 objective (Figure 3.1A). Using this live (*i.e.* unfixed) cell fluorescent labeling technique, an increase in the size of GPC from proliferative zone (PZ) to hypertrophic zone (HZ) was visualized in all growth plates (Figure 3.2A-E). Rib growth plates demonstrated the longest growth plate (Figure 3.2B). At day 7 postnatal, the secondary ossification centre could be clearly observed at the centre of the proximal radius bone cartilage where the GP differentiation cascade started immediately distal to the ossification centre (Figure 3.2C). The pelvic iliac crest GP showed variable length from the distal osteochondral junction to the proximal

edge of the GP because of its curved-shape which was atypical compared to the other GPs studied (Figure 3.2E).

Using higher power magnification, more detailed information of the shape and volume of individual living GPC *in situ* could be identified. To obtain the detailed morphology of *in situ* GPC the full length of the GP tissue (Figure 3.2F-L), a series of high magnification images (x63 objective) were collated and 'stitched' together before being divided into eight equidistant sections (Figure 3.1B, see Materials & Methods). Besides providing useful information of the *in situ* arrangement and orientation of the GPC along the GP differentiation cascade, this method also allowed any trends in the dimensions of cell to be studied along the GP. The classical ellipsoidal appearance of PZ cells and the rounded shaped of the larger HZ cells as seen in fixed GP tissue (Buckwalter *et al.,* 1986; Farnum and Wilsman, 1986) were observed in live *in situ* GPC. There was a clear variation in the arrangement of the GPCs along the GP among different GPs. For instance the organization of the GPC and a number of cells grouped together in columns particularly at the early stage of differentiation was most noticeable in the distal metacarpus GP (Figure 3.2L) compared to the other GPs.

Using Volocity®, the 3-dimensional image of individual GPC or groups of *in situ* living GPC could be constructed (Figures 3.1C and D). The insets show the fluorescent intensity recorded from the cell as a function of the image voxels after 40% baseline threshold adjustment to give more accurate volume measurement of the cell (see Materials and Methods). Figure 3.1E and 1F demonstrated the detailed shape and arrangement of GPC in HZ and PZ respectively and their orientation with the surroundings cells. Having acquired 3D images from the CLSM with the LSM browser software it was possible to determine cellular length, depth and width measurements of individual GPC (Figure 3.1G and Table 3.2). The result highlights the variability of GPC shape and orientation along the GP in different bones as the cells increase in size from PZ to HZ in all GPs.

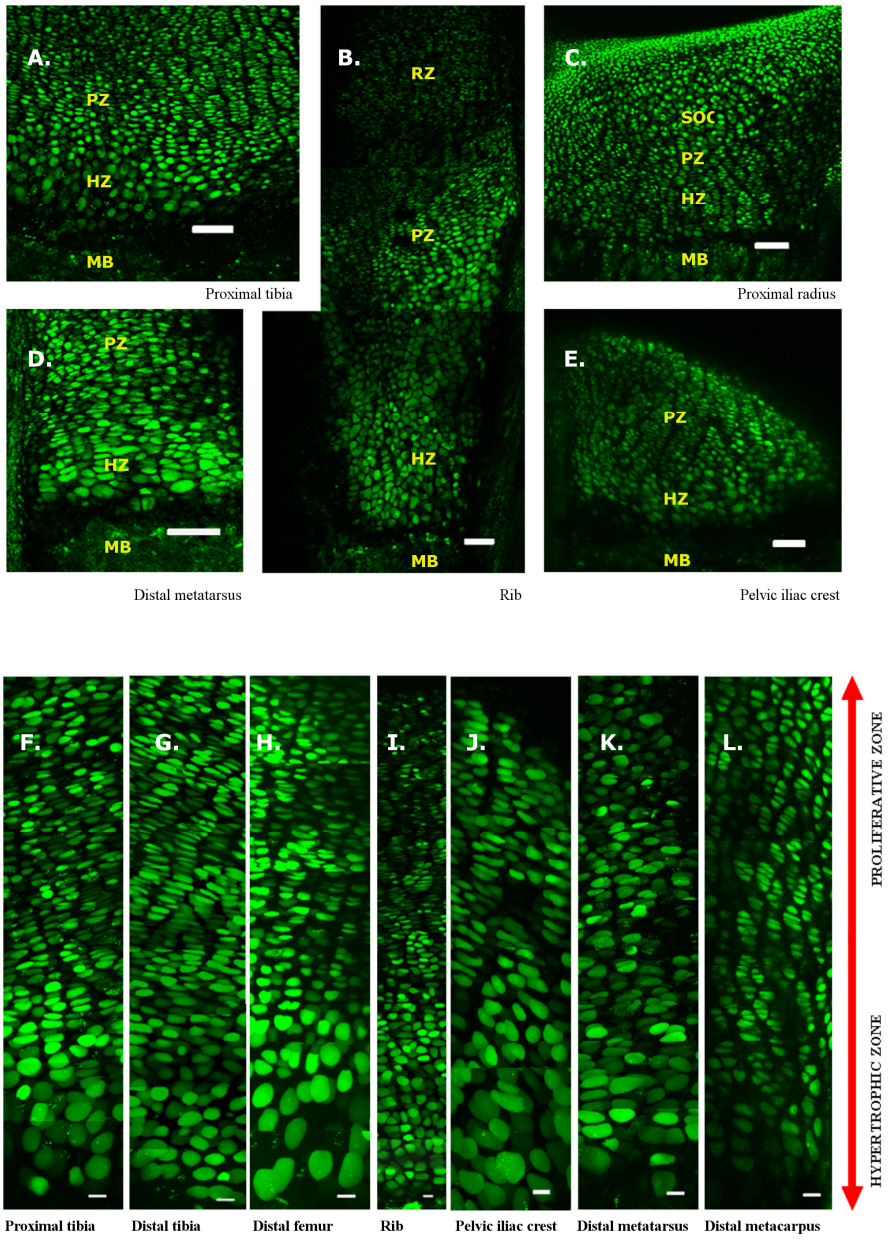

Figure 3.2 Comparative morphology of living *in situ* chondrocytes within different growth plates. Projected images (reconstructed three-dimensional images) of GP sections and chondrocytes from various living growth plates of 7-day-old rat pup as observed *in situ.* Panels **A, B, C, D & E** show low power views of GP (x10 objective lens) from proximal tibia, rib, proximal radius, metatarsus and pelvic iliac crest respectively. Bar = 100 µm for all panels. The lower panels demonstrate the higher power magnification views (x63 water-dipping objective) of the GP from proliferative to hypertrophic zones (**F.** proximal tibia, **G.** distal tibia, **H.** distal femur, **I.** rib, **J.** pelvic iliac crest, **K.** distal metatarsus and **L.** distal metacarpus). RZ, resting zone; PF, proliferative zone; HZ, hypertrophic zone; SOC, secondary ossification centre ; MB, mineralized bone. Bar = 20 µm.

3.3.2 Profile of Chondrocyte Volume Increase along GP Sections (Proliferative to Hypertrophic Zones) In GPC of Various Bones

Given the variation in the gross appearance of the GPC along the various GPs, the change in the GPC size by determining the profile of the GPC volume increase along the GP was then quantified. Figures 3.1, 3.4 and 3.5 demonstrate the variation in GPC volume increase along the GP sections in different GP, plotted from the proliferative through the hypertrophic zones (GP section 1 (S1) to GP section 8 (S8)).

(i) Long bones. For the GPC volume of the distal and proximal tibia, there was a dramatic increase of GPC volume from S4 to S7 and S4 to S8 respectively (Figure 3.3A and B). For distal tibia, the volume of HZ cells (S7-S8) was significantly higher than the volume of GPC at S1-S5 ($P<0.05$). For proximal tibia the volume of HZ cells (S8) was significantly higher than the volume of GP cells in S1-S6 (unpaired Student's *t*-test; $P<0.05$) and for S7 the GPC volume was significantly higher than in S1-S3 for the distal tibia GP ($P<0.05$). One way analysis of variance analysis (ANOVA) performed on the GPC volume data along the GP sections showed a significant volume increase ($P<0.001$) along the sections of both GPs. It was also noted that in distal tibia GP, the GPC surface area per volume generally decreased as the GPC volume increased along the PZ to HZ GP sections (S3-S7). For proximal radius, the volume increase from S1 to S8 was less remarkable. The GPC volume in the early PZ (S1-S3) was not significantly different although it appeared slightly higher than in the mid sections of the GP (S4-S5; Figure 3.3C). However, the HZ cell volume (in S8) was significantly higher than the GPC in S3-S6 (unpaired Student's t-test; $P<0.05$). There was a significant overall volume trend along the proximal radius GP (one way ANOVA; $P<0.001$). For femur, the distal and proximal GP showed obvious GPC volume increase from S5-S8 (Figure 3.4A and B) and the GPC volume increase was significant along the GP (one way ANOVA; $P<0.001$ and $P=0.012$ respectively). The similar increase of GPC volume

FIGURE 3.3

A. DISTAL TIBIA

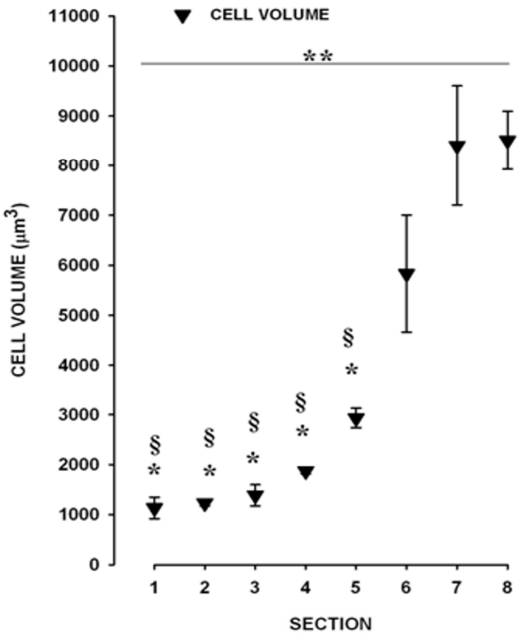

C. PROXIMAL RADIUS

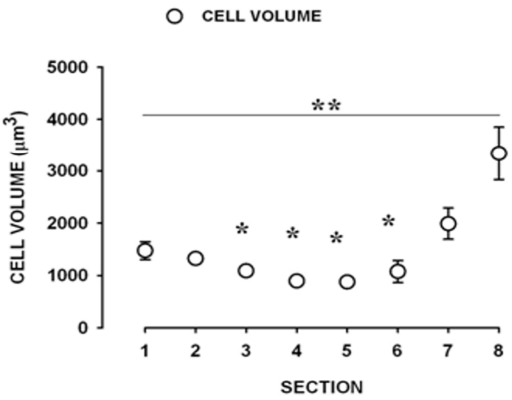

B. PROXIMAL TIBIA

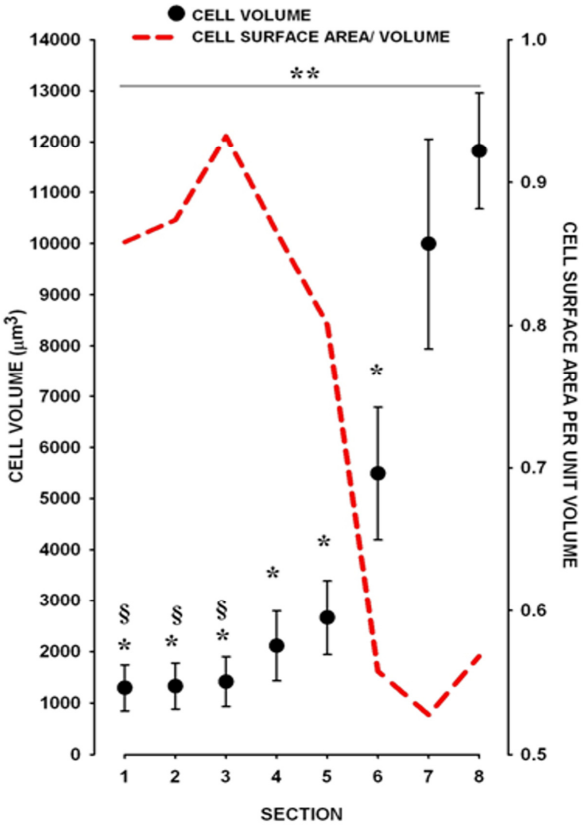

Figure 3.3 GPC volume change from the proliferative to hypertrophic zones of three long bone growth plates (proximal & distal tibia, and proximal radius). The profile of the GPC volume changes along the proliferative and hypertrophic zones in (**A**) distal tibia, (**B**) proximal tibia and (**C**) proximal radius of P7 rats. Each showed a different profile in GPC volume increase. In panel **B** the change in the volume changes along the GP was plotted together with the change in the surface area per unit volume (broken line) that demonstrates the decrease in the surface area-volume ratio as the cell volume increased. (Data are given as means ± S.E.M; from 3 different animals with in total of 146, 177, and 249 cells measured from distal tibial, proximal tibial and proximal radial GP respectively). *Significant difference from the cell volume at S8; §significant difference from the cell volume at S7 (unpaired Student's *t*-test, $P<0.05$); **one way ANOVA, $P<0.05$.

was also observed in proximal humerus GP (one way ANOVA; $P=0.007$; Figure 3.4C). *(ii) Short bones.* Distal metacarpal and metatarsal GP appeared to show a GPC volume increase from S5-S8 (Figure 3.5A). A one way ANOVA test showed significant GPC volume changes along the GP section in both GPs ($P<0.01$).

(iii) Flat bones. The pelvic iliac crest GP showed a significant GPC volume increase from S1 to S8 (one way ANOVA; $P=0.006$), and was particularly notable from S6-S8 (Figure 3.5B). For the rib, the increase of the GPC volume took place from S1 to S4; followed by a more dramatic change from S4-S8. The HZ cell (S7-8) volume was significantly higher than the GPC volume at S1-S4 (unpaired Student's *t*-test; $P<0.05$) and the trend along the GP sections were significant when tested with one way ANOVA ($P<0.001$).

The variety of GPC volume increase profiles in different bones could suggest the possibility of a different rate of cell hypertrophy along the length of the GP. To examine this, the ratio of the GPC volume changes along different GP zones (the slope value of GPC volume versus GP sections plot) was determined. Since the linear relationship between the GPC volume and GP sections among different GPs was found to have a wide range in the coefficient of determination value ($r^2=0.333$ to 0.872), the data plots were converted to semi- logarithmic plot to give better fit of the data to the linear relationship plot ($r^2=0.872$ to 0.993), hence make them more comparable. Since apparent GPC volume increase started to be observed from S4 to S8 in all GPs (Figure 3.3, 3.4, and 3.5), only GPC volume along these sections were studied. Log_{10}-transformed GPC volume data along S4-

FIGURE 3.4

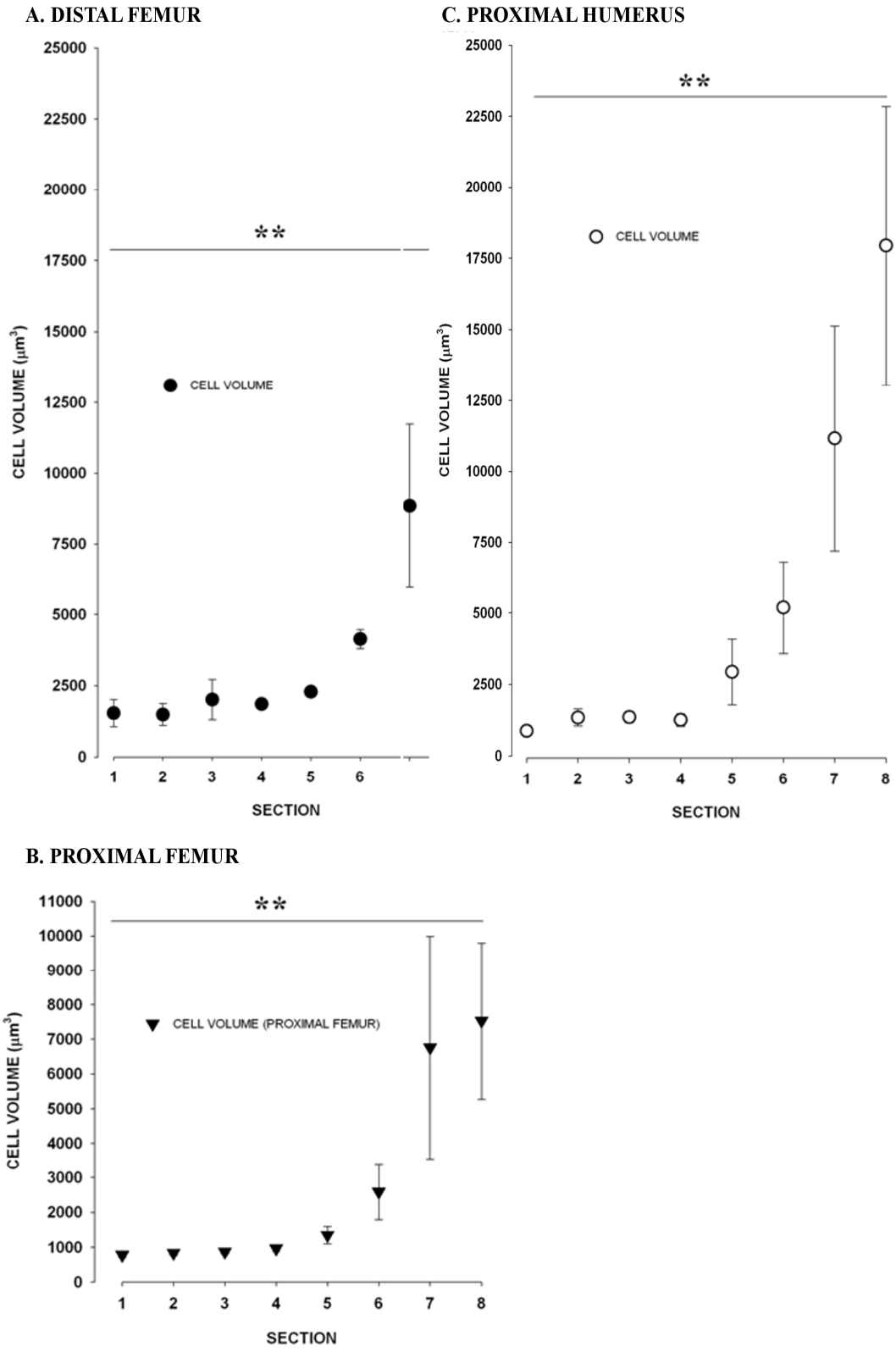
A. DISTAL FEMUR
C. PROXIMAL HUMERUS
B. PROXIMAL FEMUR
CELL VOLUME (µm³)
SECTION
CELL VOLUME
CELL VOLUME (PROXIMAL FEMUR)
**

Figure 3.4 GPC volume increase from the proliferative to hypertrophic zones of three long bone GPs (proximal humerus and proximal & distal femur). The profile of the GPC volume changes along the proliferative and hypertrophic zones in (**A**) distal femur, (**B**) proximal femur and (**C**) proximal humerus (Data are given as means ± S.E.M; from 3[76], 3[72], and 3[80] of distal femoral, proximal femoral and humeral GP respectively). *Significant difference from the cell volume at S8; §significant difference from the cell volume at S7 (unpaired Student's *t*-test, $P<0.05$); **one way ANOVA, $P<0.05$.

S8 in all GPs showed linear relationship when tested with linear regression test (coefficient of determination, r^2 = 0.70 to 0.99). The following semi-logarithmic plot slope values were presented as means ± SEM. Distal femur GP showed the highest slope (0.283 ± 0.014). This was followed by proximal femur, proximal humerus, distal metacarpus and proximal tibia (0.248 ± 0.032, 0.223 ± 0.022, 0.210 ± 0.024 and 0.207 ± 0.024 respectively). Pelvis ilium, distal tibia and distal metatarsal each showed slope value of 0.199 ± 0.039, 0.177 ± 0.029 and 0.158 ± 0.027 respectively. Proximal radius and rib GP each showed the lowest slope value (0.150 ± 0.033 and 0.105 ± 0.039 respectively). Regression test analysis performed on the slope value data with the HZ cell volume of the corresponding GPs (Table 3.1) suggests there was a good contribution of the plot slope value to the HZ cell volume (r^2=0.569; data not shown). The results in this section show it is possible to measure the volume of *in situ* living GPC along the GP using the method described earlier. Overall, the results suggested that the GPC volume profile along the GP sections did not relate to the type of bone or GP location, and the different HZ cell volume produced was contributed to some extent by the ratio of the GPC volume changes along different GP zones.

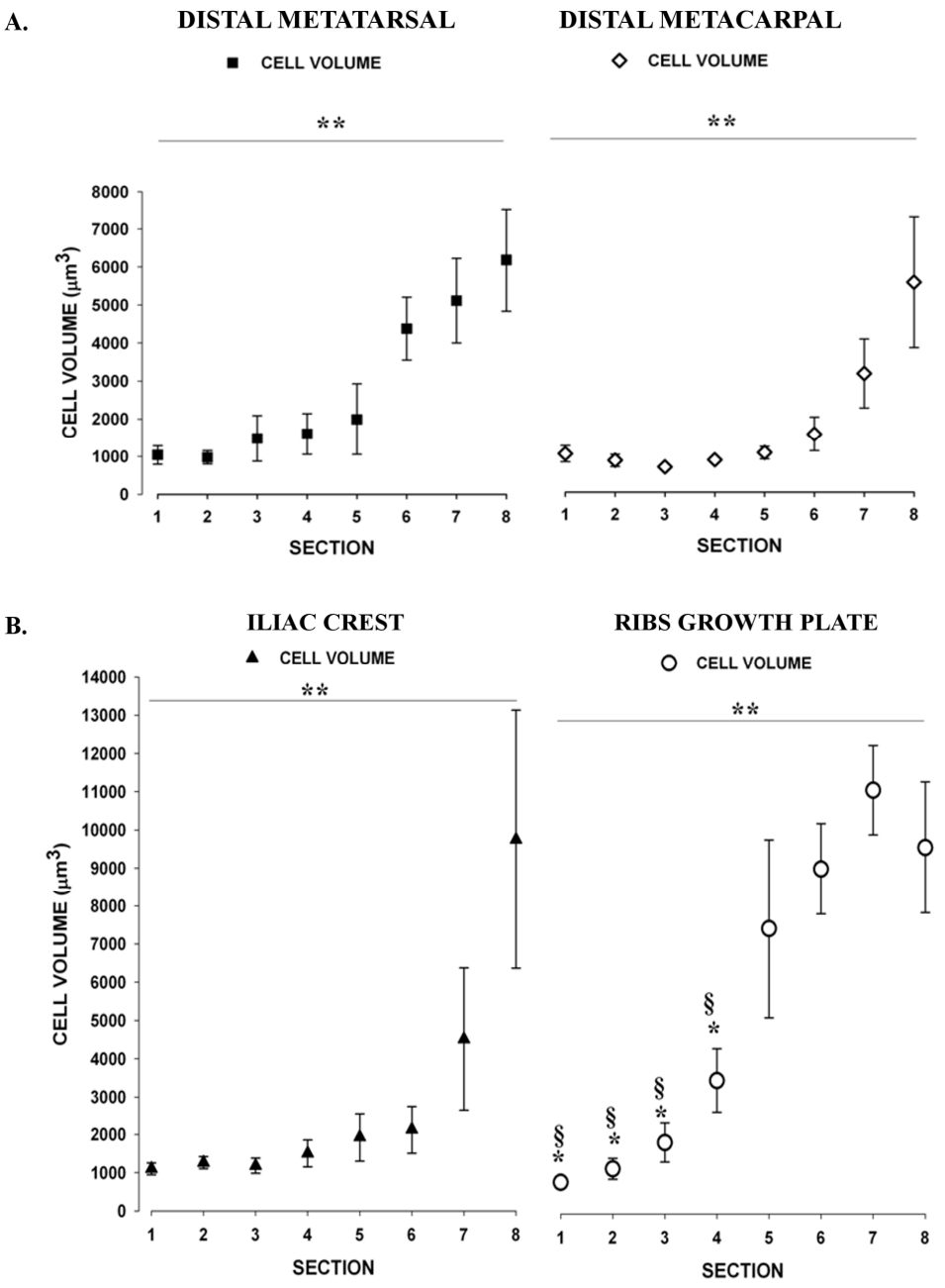

Figure 3.5 GPC volume increase from proliferative to hypertrophic zones of short bone and flat bone GPs. Profile of GPC volume changes along the GP in (**A**) distal metatarsal and metacarpal (short bones), (**B**) pelvic iliac crest and rib (flat bone) GP. The data are given as means ± S.E.M; from 3[120], 3[109], 3[146], and 3[281] for distal metatarsal, distal metacarpal, pelvic iliac crest and rib bone GP respectively). *Significant difference from the cell volume at S8; §significant difference from the cell volume at S7 (unpaired Student's *t*-test, $P<0.05$); **one way ANOVA, $P<0.05$.

FIGURE 3.6

A. DISTAL FEMUR

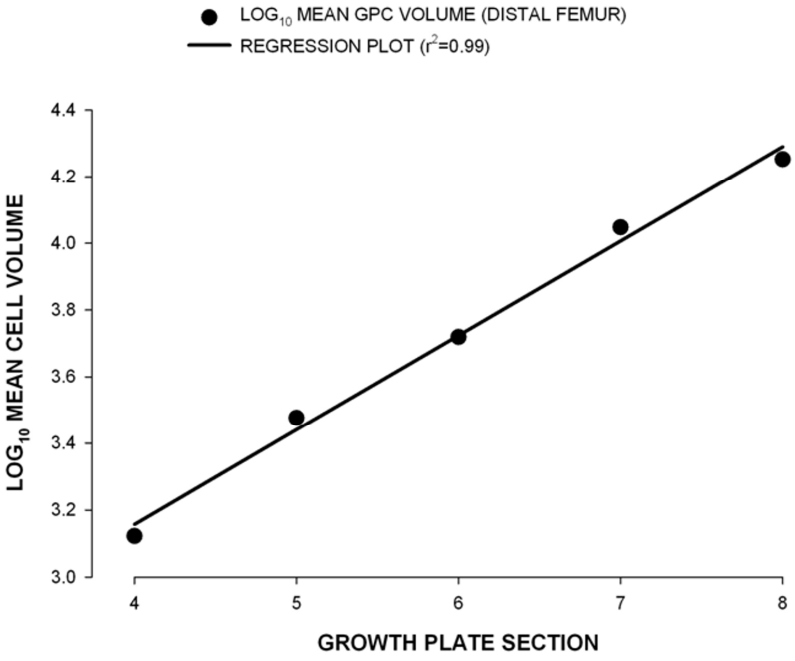

B. PROXIMAL TIBIA

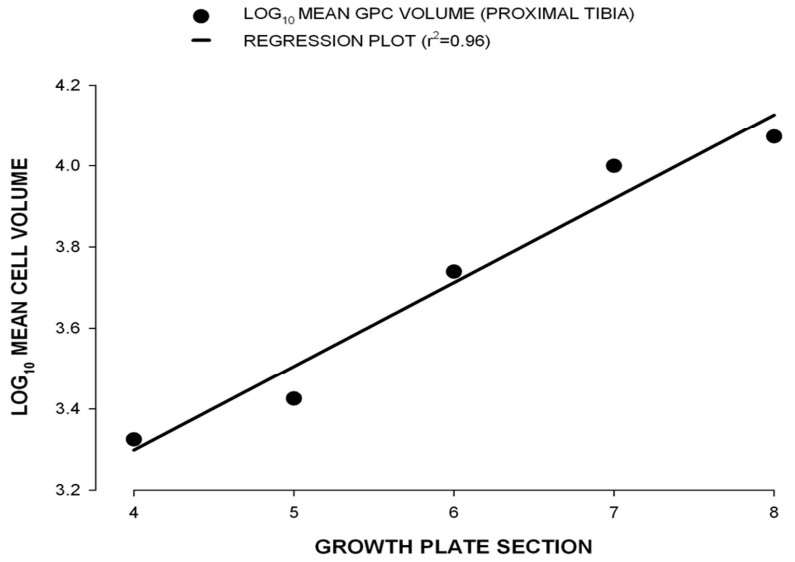

C. PROXIMAL RADIUS

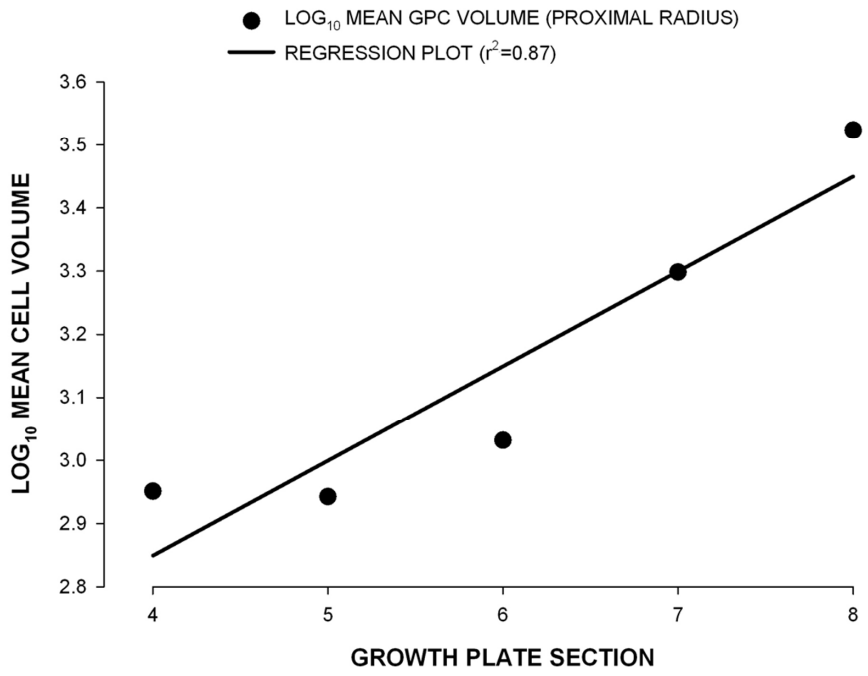

Figure 3.6. Semilogarithmic plot that shows log_{10}-transformed GPC volume data along S4-S8. The linear relationship between the GPC volume and GP sections among different growth plates was determined using linear regression test: (**A**) distal femur, (**B**) proximal tibia and (**C**) proximal radius. (Data are given as means ± S.E.M).

3.3.3 Hypertrophic GPC Volume Increase in Different GPs

In order to determine the absolute GPC volume increase and total cell swelling from PZ to HZ, the GPC volume at the beginning and end of the GPC differentiation cascade (S1-S2 and S8) among the GPs of the long, short and flat bones was compared (Table 3.1).

(i) Long bones. Among the long bones, distal femur GP showed the largest final HZ cell volume (17909 ± 4874 μm^3 (3[9])). This was a 1772 ± 543 % higher volume compared to PZ cells (1179 ± 195 μm^3 (3[18])), of the same GP. The proximal GP of the same long bone showed an increase of 846 ± 287 % cell volume from the PZ cells (808 ± 287 μm^3 (3[18])) to HZ cells (7533 ± 2264 μm^3 (3[9])). The distal tibia GP showed 655 ± 68 % higher cell volumes for PZ cells (1184 ± 81μm^3 (3[42])) in comparison to HZ cells (8510 ± 586 μm^3 (3[11])). On the other hand, the proximal tibia showed 1114 ± 488 % increase in volume from the PZ cells (1372 ± 463 μm^3 (3[62])) to HZ cells (11817 ± 1139 μm^3 (3[17])). Proximal humerus GPC volume in PZ increased from 1517 ± 428 μm^3 (3[124]) to 12284 ± 4585 μm^3 (3[7]) of HZ cells which was 849 ± 474% % increase. Proximal radius GP showed the smallest GPC volume change from PZ (1399 ± 92 μm^3 (3[57])) to HZ (3342 ± 508 μm^3 (3[9])) by showing only 134 ± 25 % cell swelling.

(ii) Short and flat bones. For the short bones, the metacarpal GP had 466 ± 137% volume increase from the PZ cell (811 ± 164 μm^3 (3[22])) to HZ cell (4850 ± 1504 μm^3 (3[14])). The metatarsal GP had 727 ± 259 % volume increase from the PZ cell (1008 ± 192 μm^3 (3[32])) to HZ cell (6187 ± 1348 μm^3 (3[10])). It was noted

Table 3.1

Bone	Growth plate		Mean volume of PZ cells (S1-S2; μm^3; of n[N])	Mean volume of HZ cells (S8; μm^3; of n[N])	GPC swelling (%; n=3)	Slope of Semi-logarithmic plot (S4-S8)
Long bone	i.	Proximal tibia	1372 ± 463 * (3[62])	11817 ± 1139 (3[17])	1114 ± 488	0.207 ± 0.024
	ii.	Distal tibia	1184 ± 81* (3[42])	8510 ± 586 (3[11])	655 ± 68	0.177 ± 0.029
	iii.	Proximal femur	808 ± 287* (3[18])	7533 ± 2264 (3[9])	846 ± 287	0.248 ± 0.032
	iv.	Distal femur	1179 ± 195* (3[18])	17909 ± 4874 (3[6])	1772 ± 543	0.283 ± 0.014
	v.	Proximal humerus	1517 ± 428 (3[124])	12284 ± 4585 (3[7])	849 ± 475	0.223 ± 0.022
	vi.	Proximal radius	1399 ± 92* (3[57])	3342 ± 508[¥, #] (3[9])	134 ± 25**	0.150 ± 0.033

Short/ cuboidal bone	i.	Distal metacarpus	811 ± 164 (3[22])	4850 ± 1504[¥] (3[14])	466 ± 137	0.210 ± 0.024
	ii.	Distal metatarsus	1008 ± 192* (3[32])	6187 ± 1348[¥] (3[10])	727 ± 259	0.158 ± 0.027
Flat bone	i.	Rib	1007 ± 212* (3[52])	9625 ± 1719 (3[32])	844 ± 242	0.105 ± 0.039
	ii.	Pelvic iliac crest	1182 ± 155 (3[34])	9750 ± 3380 (3[19])	855 ± 341	0.199 ± 0.039

Table 3.1 Chondrocyte growth plate volume increase from PZ to HZ in different bones and locations. The mean volume of GPC in the PZ (S1-S2) and HZ (S8) zones of GPs are shown. The GPC swelling (%) is shown as the percent increase of volume from the PZ cell volume. Data are given as (n[N]) are presented as means ± S.E.M. *Significantly different from the corresponding GP HZ cell; **significant difference from distal femur GPC swelling; [¥]significant difference from proximal tibia GP HZ cells; [#]significant difference from distal femur HZ cells (unpaired Student's *t*-test, $P<0.05$).

that the non-weight bearing GP such as proximal femur (greater trochanteric GP), rib and pelvic ilium GP showed consistently higher GPC swelling (about 8-fold increase in all the GPs). However the highest GPC swelling was observed in long bones (*e.g.* distal femur and proximal tibia GP).

There was no significant difference in PZ cell volume between all different GPs (unpaired Student's *t*-test; $P>0.05$). Generally, the mean PZ cell volume in all GPs was within a range of 808 to 1517 μm^3 (1101 ± 451 μm^3 (SD)).

However, there was a range of final volumes of HZ cells among different GPs. For instance the proximal tibia GP HZ cell volume was significantly different

from the proximal radius, distal metacarpus and distal metatarsus GPs (P<0.05); but was not significantly different from the rest of GPs studied (Table 3.1). In general, the highest HZ cell volumes (>11,000 μm^3) were observed in long bone GPs such as proximal tibia, distal femur and proximal humerus. However, another long bone GP, namely the proximal radius showed the lowest HZ cell volume. Flat bone GPs showed slightly higher HZ cell volumes compared to the short bones although the difference was not significant (P>0.05).

The HZ cell volume in almost all GPs were significantly higher than their corresponding PZ cell volume (P<0.05; Table 3.1). The exceptions were for distal metacarpus and pelvic ilium GP, which the HZ cell volume were not significantly different than the PZ cell volume although appeared higher (P<0.05). The relatively higher HZ cell volume was particularly evident for proximal and distal tibia GP (P<0.001 and P=0.001 respectively). Yet, there was no significant difference in the GPC swelling from PZ to HZ among different GPs (P>0.05) except the GPC swelling in proximal radius GP and distal femur GP, which was significantly different (P<0.05). The data in this section demonstrate while the GPC shared almost the same cell volume at the start of the GPC differentiation (*i.e.* PZ), the final volume reached at the end of the GP differentiation cascade varied markedly among different GPs and even from GPs of opposite cartilaginous end of the same bone.

3.3.4 Dimensional Changes of Chondrocytes along the Growth Plate of Two Different Bones

Given the variation in the final GPC volume among different GPs, the changes in GPC dimensions and properties of two different long bones was then compared. Figure 3.7 and 3.8 demonstrate the chondrocytic properties and dimension parameters (cell surface area, cell length, width and depth) and cell properties (*i.e.* cell density) between proximal tibia and proximal radius along the GP. These two bones were used as they are both long load-bearing bones but with different length and HZ cell volume (Table 3.1).

PROXIMAL TIBIA

A.

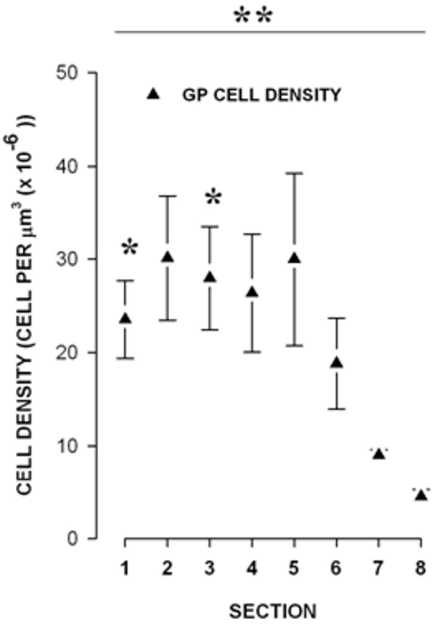

B.

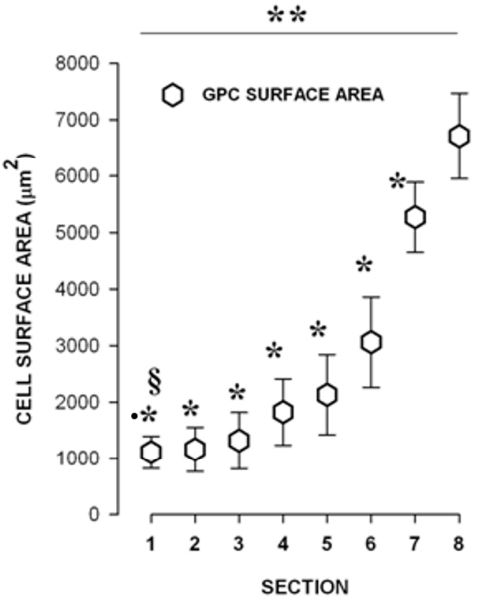

PROXIMAL RADIUS

C.

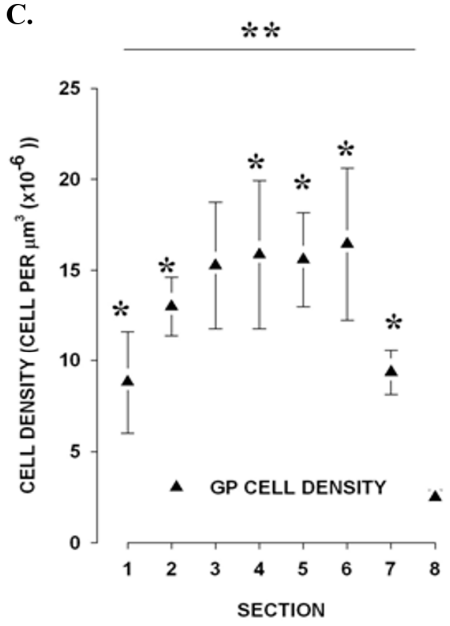

D.

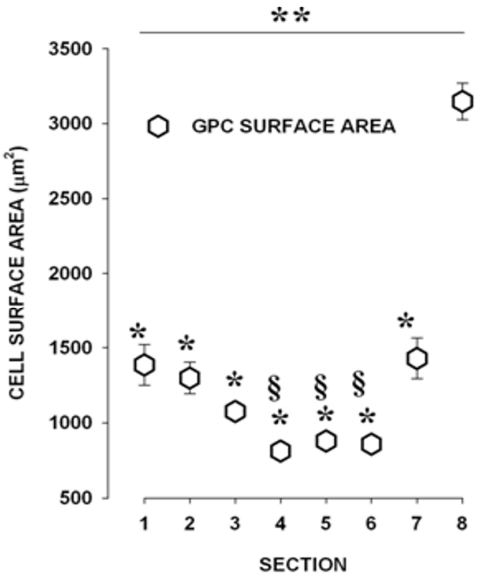

Figure 3.7 Comparative trends in the change of cell density and cell surface area between proximal tibia and radius GPC along growth plate sections. Data are given as means ± S.E.M; from 3[223] and 3[143] for proximal tibia and proximal radius GP respectively). *Significant difference from the cell volume at S8; §significant difference from the cell volume at S7 (unpaired Student's *t*-test, $P<0.05$); **one way ANOVA, $P<0.05$.

Figure 3.7A and C show the changes in cell density, and Figure 3.7B and D show the changes in cell surface area in both GPs. There was initially a slight increase in the density of cells (S1-S5) and then constant decrease (S5-S8) along the GP zones in proximal tibia GP (Figure 3.7A). The GPC density in S8 was significantly lower from the density in S1 and S3 (unpaired Student's *t*-test; $P<0.05$). One-way ANOVA analysis showed a decreasing trend in the volume along the GP ($P=0.027$). For proximal radius GP, the cell density initially increased from S1-S3, almost reached a plateau from S3-S6, and then declined abruptly from S6-S8. However there was no significant difference in cell density within the S1-S7 (unpaired Student's *t*-test; $P>0.05$) although the cell density was significantly reduced in S8 compared to the density in S1-S2 and S4-S7 ($P<0.05$). The overall GPC density decrease along the proximal radius GP was only just significant (one-way ANOVA; $P=0.043$; Figure 3.7C). Generally the proximal GP showed higher cell density compared to the proximal radius GP in each corresponding GP sections. The highest difference was observed at the S1 (~3-fold difference).

There was a significant progressive increase in GPC surface area from PZ to HZ in proximal tibia GP (one-way ANOVA; $P<0.001$; Figure 3.7B). However, the GPC surface area of the proximal radius gradually decreased from S1-S6, before a sudden increase at S6-S8 (Figure 3.7D). The GPC surface area trend along the GP was also statistically significant ($P<0.001$). It was noted that the cell surface area over S6 to S8 in proximal radius was much smaller compared to the cell surface area over the same GP sections in proximal tibia GP (~2 to 3-fold smaller). In both GPs the final GPC surface area in S8 was significantly higher in comparison to the cell surface area in the other sections (unpaired Student's *t*-test; $P<0.05$).

Growth plate	Growth plate cell zone	Surface area (μm^2; of n[N])	Surface area/ volume (μm)	Cell density (cell/ 10^6 μm^3)	Cell length (μm; of n[N])	Cell width (μm; of n[N])	Cell depth (μm; of n[N])
Proximal tibia	PZ (S1-S2)	1136 ± 260* 3[62]	1.0	27 ± 5*, #	11 ± 2* 3[45]	17 ± 2* 3[45]	20 ± 2* 3[45]
	HZ (S8)	6714 ± 758¥ 3[17]	0.6	4 ± 1	32 ± 2¥ 3[17]	29 ± 1¥ 3[17]	35 ± 1¥ 3[17]
Proximal radius	PZ (S1-S2)	1347 ±11* 3[55]	0.96	11 ± 2*	10 ± 1* 3[45]	11 ± 1* 3[45]	22 ± 4 3[45]
	HZ (S8)	3148 ± 121 3[9]	0.88	2 ± 1	19 ± 1 3[9]	22 ± 1 3[9]	24 ± 1 3[9]

Table 3.2 A comparison between the dimensions of chondrocytes in PZ and HZ cells as measured in two different P7 rat long bones. This table shows the mean volume of various chondrocytic performance parameters in the PZ and HZ zones of proximal tibial and radial GPs. Data are given as (n[N]) are presented as means ± S.E.M. *Significantly different from the corresponding HZ cells; **significantly different from distal femur GPC swelling; ¥significantly different from HZ of proximal radius GP; #significantly different from PZ of proximal radius GP (unpaired Student's *t*-test, $P<0.05$).

Table 3.2 presents the absolute value of the cell surface area, cell surface area-volume ratio and cell density from PZ (S1-S2) and HZ (S8) cells in proximal tibia and radius GP. The GPC surface area in PZ of both GPs was significantly higher than in the HZ (unpaired Student's *t*-test; $P=0.002$ and $P<0.001$ respectively). Similarly, the GPC density in PZ of both GPs was significantly higher than in the HZ (unpaired Student's *t*-test; $P=0.011$ and $P=0.016$ respectively). It was also shown that the GPC density in PZ of proximal tibia was significantly higher than in PZ of the radius GP (unpaired Student's *t*-test; $P=0.041$). However the GPC density in the HZ between both GPs was not significantly different ($P=0.230$). This result shows significant increase in the cell surface area and conversely decreased in the cell density towards the later stage of GP differentiation in both GPs.

Figure 3.8 shows the trends in cell shape changes along the GP sections in proximal tibia and radius. Cell dimensions were measured based on the cell length, width and depth as described in the Materials and Methods. Proximal tibia GP demonstrated clear GPC shape changes in all the three dimensional parameters as the PZ cells transformed to HZ cells along the GP sections (Figure 3.8A, B and C). One-way ANOVA test showed significant trends in the shape changes along the GP ($P<0.001$, $P=0.002$ and $P<0.001$ for cell length, width and depth measurements respectively). However, the increase in cell length for proximal radius GP only appeared to begin from S6-S8 (Figure 3.8D). The final cell length at S8 was significantly higher than in other sections (S1-S7) while cell length in S7 was significantly higher than in S3-S5 (unpaired Student's *t*-test; $P<0.05$). Similar trends could be seen for the cell width changes (Figure 3.8E). The GPC width in S8 was significantly higher than in S1-S6 (unpaired Student's *t*-test; $P<0.05$; one-way ANOVA; $P<0.001$). For the proximal radius GPC depth (Figure 3.8F) there was no significant difference in the cell depth observed along the GP.

Comparison of the absolute value of the dimensions of the cells (length, width and depth) between the PZ (S1-S2) and HZ (S8) cells is given in Table 3.2. The GPC of proximal tibia GP showed significant increases in its length, width and depth as it reached the HZ from the PZ ($P=0.002$, $P=0.006$ and $P=0.003$

PROXIMAL TIBIA

A. **B.** **C.**

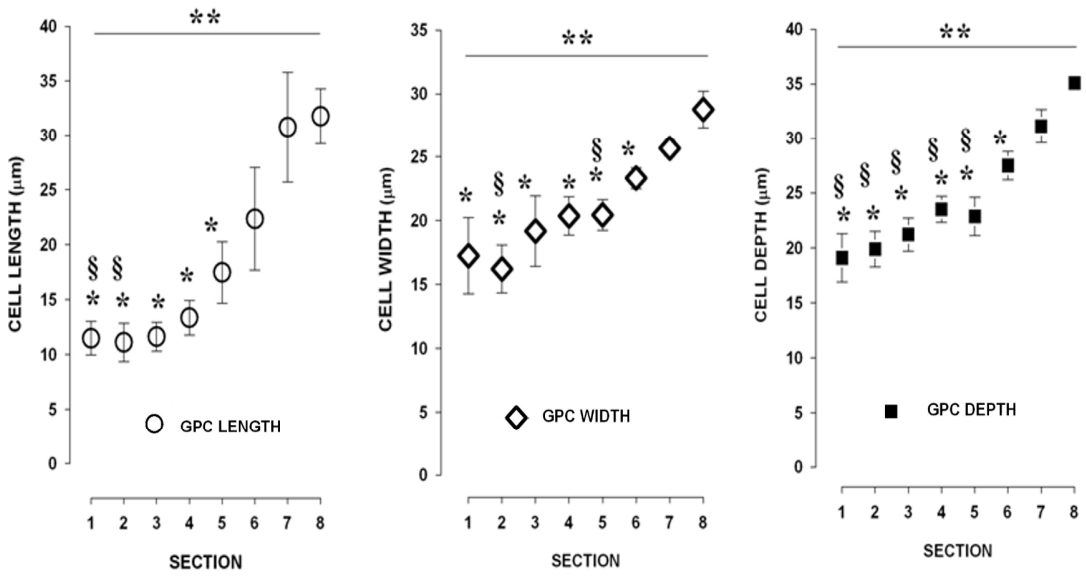

PROXIMAL RADIUS

D. **E.** **F.**

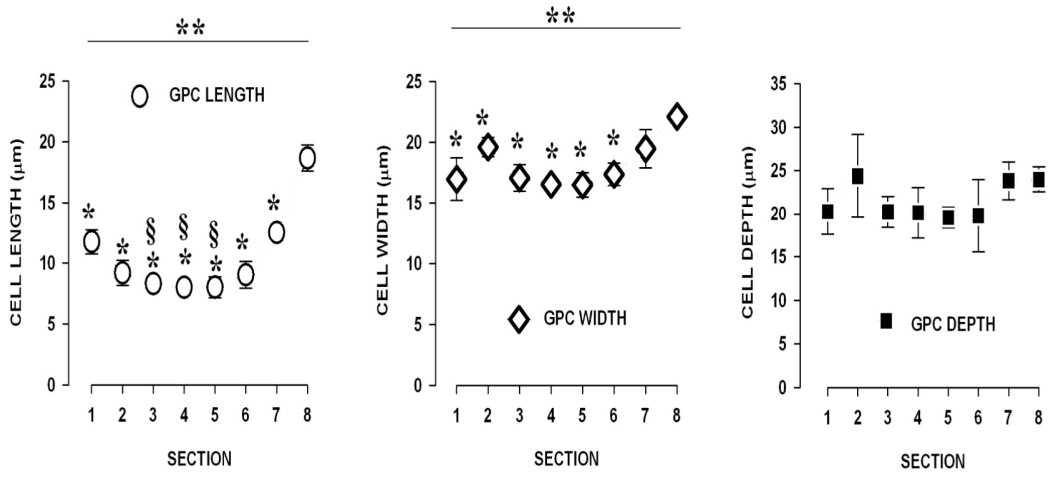

Figure 3.8 Comparison of changes in cell dimension between proximal tibia and radius GPC along GP sections. This graph demonstrates there was gradual increase in dimensions of GPC from PZ to HZ in proximal tibia GP. Data are given as means ± S.E.M; from 3[223] and 3[143] for proximal tibia and proximal radius GP respectively). *Significant difference from the cell volume at S8; §significant difference from the cell volume at S7 (unpaired Student's *t*-test, $P<0.05$); **one way ANOVA, $P<0.05$.

respectively; unpaired Student's *t*-test from 3 animals and in total 223 cells measured from both PZ or HZ). The HZ cell length, width and depth increased by 2.9, 1.70 and 1.75-fold from the PZ cells. For proximal radius GP, although the cell shape appeared to show changes in all directions as PZ cells were transformed to HZ cells, only the cell length and width increased significantly ($P=0.003$ and $P=0.001$ respectively (3[143])). The HZ cell length, width and depth increased by 1.8, 2.0 and 1.1-fold from the PZC. It was also found that the final HZ cell length, width and depth in proximal tibia GP were significantly higher than in proximal radius GP ($P=0.004$, P=0.008 and $P=0.001$ respectively). On the other hand, there was no significant difference in PZ cell shape and size between both GPs. The results in this section generally associated the increase in the final GP HZ cell volume and surface area with the increase in the cell length, width or depth. The HZ cells in the longer bones were also found to show preferentially higher increase in the cell length than in cell width and depth.

3.3.5 Relationship of GPC Volume Increase, HZ Cell Volume, Growth Plate Length and the Total Bone Length

After taking into consideration all the above results, the relationship between the chondrocytic parameters and GP and total bone length which is a result of accumulative chondrocyte performance was then investigated.

In Figure 3.9A, two GP chondrocytic parameters namely GPC volume increase and hypertrophic GPC volume were plotted against bone length of the corresponding bone (of P7 rats). GPC volume increase was shown as a % difference in volume between the PZ (S1-S2) and HZ (S8) cells (see Table 3.1). To examine any relationship between the chondrocytic parameters and the length of the various bones, linear regressions were plotted through data points that

FIGURE 3.9

A.

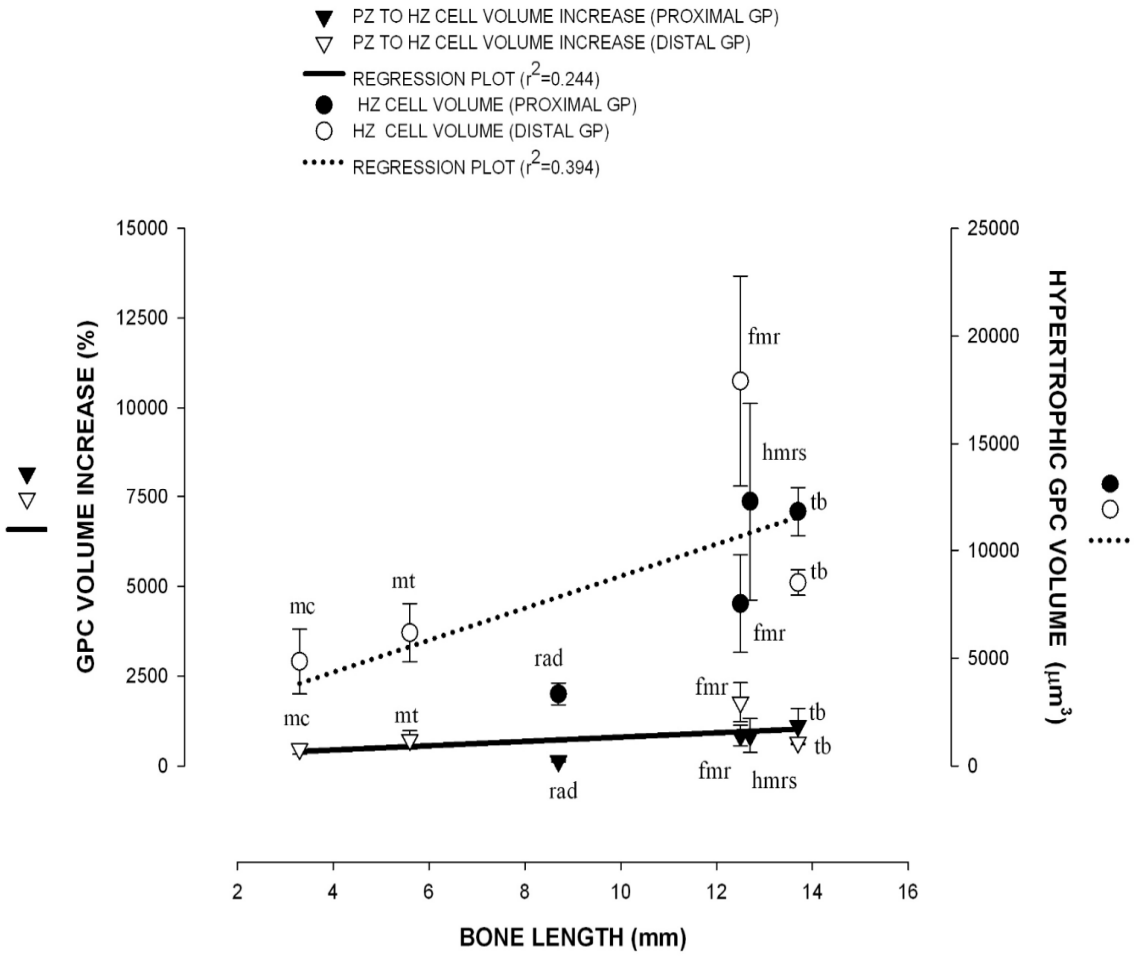
PZ TO HZ CELL VOLUME INCREASE (PROXIMAL GP)
PZ TO HZ CELL VOLUME INCREASE (DISTAL GP)
REGRESSION PLOT (r^2=0.244)
HZ CELL VOLUME (PROXIMAL GP)
HZ CELL VOLUME (DISTAL GP)
REGRESSION PLOT (r^2=0.394)
GPC VOLUME INCREASE (%)
HYPERTROPHIC GPC VOLUME (μm³)
BONE LENGTH (mm)
15000
12500
10000
7500
5000
2500
0
25000
20000
15000
10000
5000
0
2
4
6
8
10
12
14
16
mc
mt
rad
fmr
hmrs
tb

FIGURE 3.9

B.

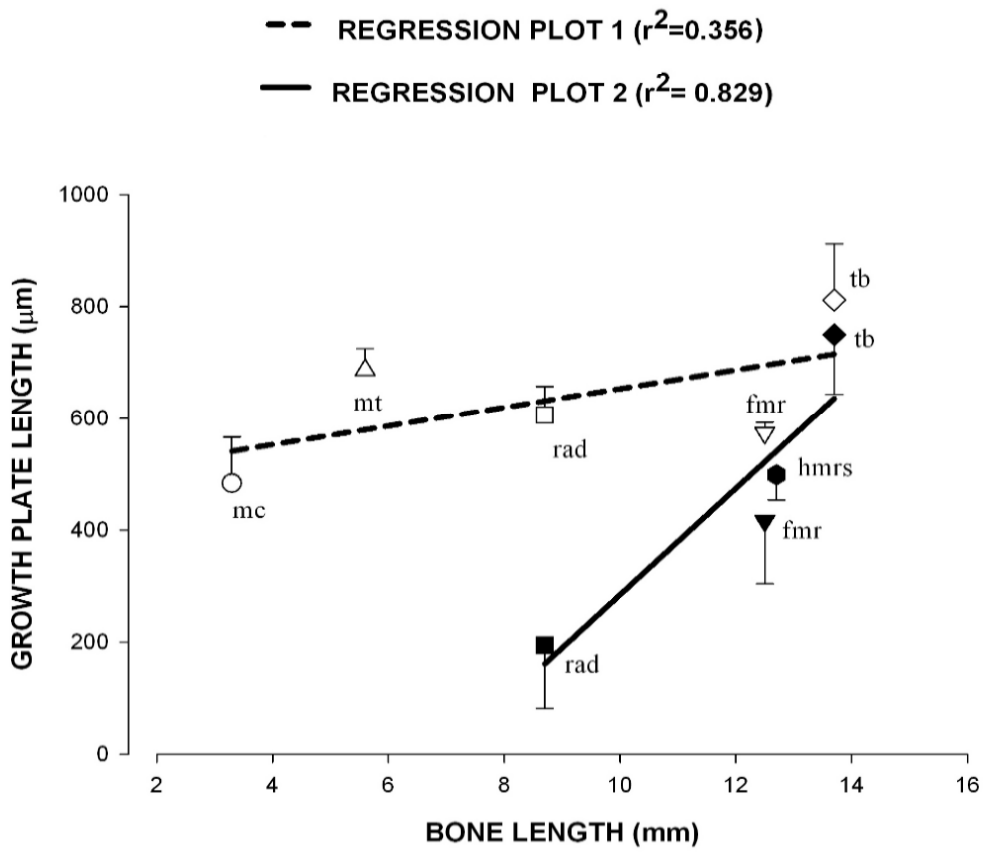
REGRESSION PLOT 1 (r^2=0.356)
REGRESSION PLOT 2 (r^2= 0.829)
GROWTH PLATE LENGTH (μm)
BONE LENGTH (mm)
1000
800
600
400
200
0
2
4
6
8
10
12
14
16
mc
mt
rad
tb
tb
fmr
hmrs
fmr
rad

FIGURE 3.9

C.

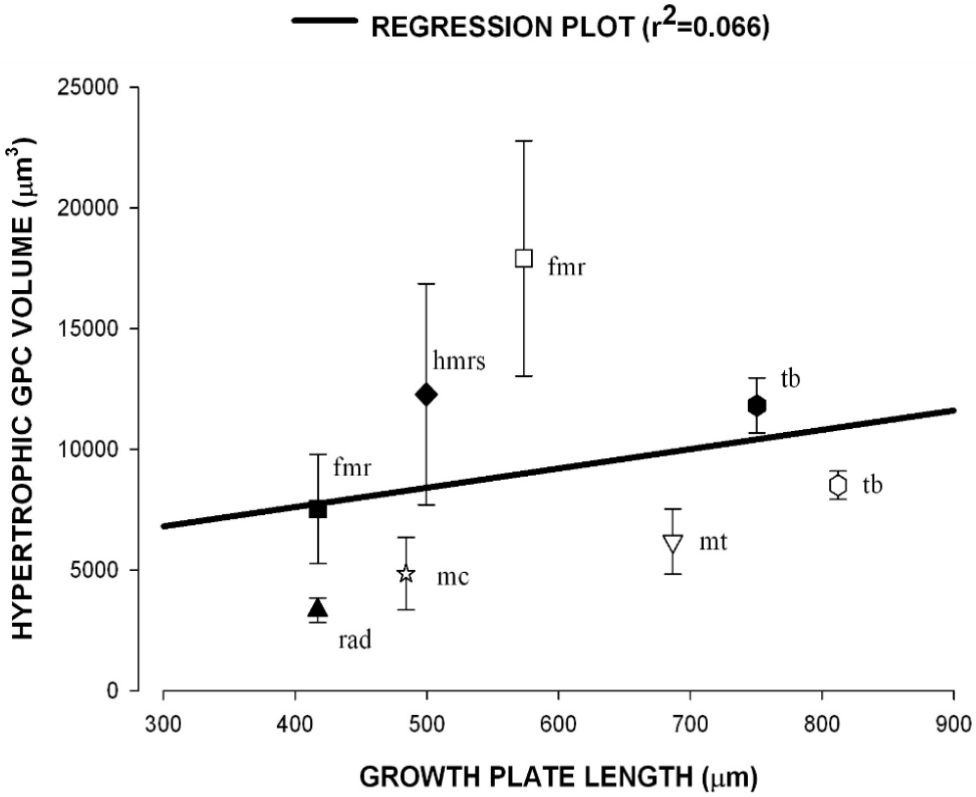

Figure 3.9 Relationship between chondrocytic parameters changes, GP length and the total bone length. (**A**) The regression plot exhibits the linear relationship between GPC swellings and HZ cell volumes from PZ to HZ with the total bone length. (**B**) Proximal and distal GP length linear relationship with the total bone length was shown. Filled pattern = proximal GP length; non-filled pattern = distal GP length. (**C**) Regression plot of HZC volumes with the corresponding GP length was shown. Filled pattern = proximal GP HZ cell volume; non-filled pattern = distal GP HZ cell volume. Data are given as means ± S.E.M; from 3 separate animals (see Table 3.1) for all chondrocytic parameters and each GP and bone length. mc = metacarpal, mt = metatarsal, r = radius, fmr = femur, hmrs = humerus, tb = tibia.

comprised the data from proximal and/ or distal GP. This showed a poor relationship between GPC HZ cell volume with the bone length (r^2=0.394). Furthermore no relationship could be seen between GPC swelling from PZ to HZ, with bone length (r^2=0.151). Figure 3.9B demonstrates the relationship between the GP lengths with the corresponding bone length. There was a good relationship (r^2= 0.829) between the proximal GP length and the bone length. However, the distal GP length showed a weak relationship with the length of the corresponding bone (r^2=0.357). Figure 3.9C displays the hypertrophic GPC volume as plotted with the corresponding GP length. Linear regression test showed no association between the increase in the GP length with the volume of the hypertrophic GPC (r^2=0.066).

Further regression test analysis on the same data suggested the GPC swelling and HZ cell volume showed no significant contribution to the length of the corresponding bone. Likewise, the HZ volume exhibited no influence to the length of corresponding GP (r^2 = 0.019). On the other hand, the length of proximal GP contributed significantly to the bone length (r^2= 0.829); however, the distal GP length gave only very small influence to the bone length (r^2=0.357). In general, this finding suggests that although there was a relationship between the GP length and the bone length, no clear relationship was observed between the HZ cell volume and the corresponding GP and bone length.

3.4 Discussion

This study highlights the differential growth among various growth plates of postnatal rats, which signify the complex regulatory mechanism involved in the longitudinal bone growth. Using the CLSM method, it was found that all *in situ* living GPs exhibited the cell differentiation cascade along the GP. The proliferative cell volume in all GPs was not significantly different; however the final hypertrophic GPC volume at the end of the differentiation cascade in different GPs was markedly varied depending on the bone under investigation. The hypertrophic GPC volume to some extent was influenced by the rate of hypertrophic cell formation along the GP. However there was no obvious relationship between the hypertrophic GPC volumes with the resulted bone length.

Conventional histological methods on fixed tissue to study GP cells has commonly been used by many workers (Buckwalter *et al.,* 1985; Buckwalter *et al.,* 1986; Hunziker *et al.,* 1987b; Breur *et al.,* 1991; Breur *et al.,* 1994; Kuhn *et al.,* 1996; Noonan *et al.,* 1998; Wilsman *et al.,* 1996b; Wilsman *et al.,* 2008). The use of the CLSM technique to study *in situ* living GP cells as in the present study has a number of advantages over the histological methods. The *in situ* living cells could be visualized following labeling with calcein circumventing tissue processing steps which could potentially cause the alteration of the original morphology of the cells. Among these steps was the fixation of the GP tissue using conventional fixatives which was shown to cause significant shrinkage artifact to the GP cells due to their high osmolarity (see Chapter 4). Three dimensional morphology of the individual cell or the orientation of a group of cells could be viewed and examined using the CLSM imaging software. Using a calibrated quantification method (Bush and Hall, 2001b), accurate volume measurement and other dimensional parameters could be performed on the 3-dimensional images of the proliferative cells through to the hypertrophic cells permitting the measurement of the volume changes along the GP.

However as a note of caution, as the preparation of the tissue warranted the bisection of the bone to allow the fluorescence dye to be loaded into the cells, some cell death induced by the cut could not be avoided as what has been observed at the edge of articular cartilage cut where the nuclei of dead cells seen stained red by propidium iodide (Huntley *et al.,* 2005). In this respect, it was noticed that the bigger the size of the cells the more the cells susceptible to the traumatic cell death (unpublished observation). The release of internal pressures upon bisecting the bone could also potentially lead to the changes the *in vivo* properties of the chondrocytes (Guilak and Mow, 2000). To minimize all these artefactual consequences, relatively deeper (>20 μm) optical planes were selected during the cell imaging to exclude any cut-induced dead cells or intact cells that exposed to the cut surface. Possible GPC change (*e.g.* volume) over the period of measurement could be minimized by keeping the GP section under medium at all

times at 37^{o} C until use; and keeping the imaging time as short as possible (~25 min per sample).

It was also noticed during the present experiments, some terminal large hypertrophic GPC that survived the cut injury and were close to the mineralized area tended to be stained poorly by calcein, and inevitably had to be excluded given that the poor quality image produced. The reason for this poor staining was not clear but could be for two different reasons. First, the terminal hypertrophic GPCs were mainly of the GPC cells undergoing degeneration and apoptosis (Farnum and Wilsman, 1989), in which might have relatively reduced levels of the esterases which metabolise the non-fluorescent dye molecules into fluorescent by-product upon entering the cell cytoplasm. Smaller GPC could take some time to die as shown by the slow deterioration of fluorescent staining intensity. Second, the terminal hypertrophic GPCs are metabolically active (Cowell *et al.,* 1987; Farnum *et al.,* 1990; Hunziker *et al.,* 1987b) so can rapidly break down intracellular fluorescent molecules reducing the fluorescent intensity staining of hypertrophic cells if the imaging could only take place after several hours following the staining. If it was because of the first reason, it would not affect the validity of the data obtained but instead facilitated the exclusion of the dying cells from the present data acquisition and analysis. On the other hand, if it was due the second reason, the imaging of relatively larger hypertrophic GPCs had to be performed soon after calcein being loaded (after 1/2 to 1 hrs) to ensure decent quality of the fluorescent GPCs images could be obtained for later analysis before the fluorescence faded. Having taken this into account, scatter ranges were noted in the mean GP hypertrophic cell volume (S7-S8) in some GPs (Figure 3.4A, 4B, 4C and 5A). The possible explanation of this was the GPC within the HZ of the bone GPs showed wider range of cell volume than the other GP zones and could imply an important physiological property of the GP at the HZ. The physiological variation was especially observed in the HZ of proximal femur, distal femur, proximal humerus and pelvic ilium GPs.

The GPC along the GP displayed the profile of volume increase, which corresponded to the cascade of cell differentiation in the GP. The GPC volume

measurement demonstrated various profile of volume increase from PZ through to HZ, which appeared to be independent of the type of bones, GP locations (proximally or distally located) and load function (load-bearing bone or non-bearing). This was in line with the different GPC hypertrophy displayed by different GP. The GPC hypertrophy in the present work were determined by measuring two relevant parameters namely the GPC swelling and the HZ cell volume. The GPC swelling allowed us to determine the total volume increase in the PZ cell that gave rise to the final HZ cell volume, regardless of the rate of the cell transformation from proliferative to hypertrophic cell along the GP. The total cell volume increase ranged from around 2-18 fold increase. Since there was no significant difference in PZ cell volume among different GPs, the difference in the GPC swelling and HZ cell volume among different GPs implied a difference in the chondrocytic performance along the GPC differentiation cascade. When the rate of GPC hypertrophy over the GP section (S4-S8) was examined, which was represented by the slope of the semi-logarithmic volume increase plot, it appeared to have a good influence in determination of the HZ cell volume (r^2=0.569; data not shown). This suggests that relatively higher HZ cell volume produced if the GPC is transformed swiftly towards the hypertrophic cell during the proliferative – hypertrophic cell differentiation process. General comparison among different GPs using the above-mentioned chondrocytic parameters showed the proximal tibia GP exhibited relatively high GPC swelling, large hypertrophic cell mean volume and high rate of the cell hypertrophy conversion from proliferative cell across the GP zones. Therefore it appeared that this GP was the most suitable GP to be used as a model for studying GP chondrocytic performance in P7 rat in future.

In the present study the relationship between the GP lengths with the post natal bone length was examined. As shown in the results, the proximal and distal GP length showed distinct contribution to the bone length (r^2=0.829 and r^2=0.357 respectively). However, the length of the GP was independent of the HZ cell volumes. The data showed that there was no clear relationship between the HZ cell volumes or rates of hypertrophy to the bone length which could be associated with the end result of longitudinal bone growth performance. This experiment was

repeated in older animals (10-month-old rats), and showed the same result of a lack relationship between the HZ cell volume with the adult bone length (data not shown). One possible explanation for this is that different growth plates even from the opposite cartilaginous ends of the same bone elongates at different rates at a given time point. This phenomenon of differential growth has been linked to the different hypertrophic GPC volume manifested by different GP at a given point of time (Wilsman *et al.,* 1996b). Nevertheless, the net effect of the cell hypertrophy against the final bone length might not be seen at a single time point as in the present study. The involvement of other chondrocytic factors therefore, such as growth plate cell division and bone matrix deposition (Hunziker *et al.,* 1987b; Wilsman *et al.,* 2008) could not be ruled out to play some important roles in influencing the bone longitudinal growth at some stages. However the relative contributions of each could differ in GPs growing at different rates. Generally, cellular enlargement during hypertrophy is relatively more important in faster growing bone, whereas matrix synthesis makes a more important contribution in those growth plates that have slower growth rates (Wilsman *et al.,* 1996b). At the same time, the regulation for GPC hypertrophy must be tightly coupled with the controls for proliferation, as the regulation of kinetics of either proliferation or hypertrophy or both determine the final growth velocity of each different bone (Wilsman *et al.,* 2008).

Those results allude to the importance of locally mediated regulatory controls of GP elongation (Wilsman *et al.,* 1996a), that could tailor the need of individual bone accordingly which has a specific final bone length as the end product (see Figure 3.10 for comparison of different bone length increases in various bones of rats from day 7 to week 40 of age). This is the complement to systemic control systems such as hormones, growth factors and nutrient status (Hunziker *et al.,* 1994; Loveridge, 1993; Nilsson *et al.,* 2005), which simultaneously controls the overall regulation of chondrocytic performance in all GPs. However, there was no clear evidence that the load bearing factor inherited by certain GP played any role in the differential growth phenomenon as shown in the present results. The relative contributions of the three factors (cell proliferation,

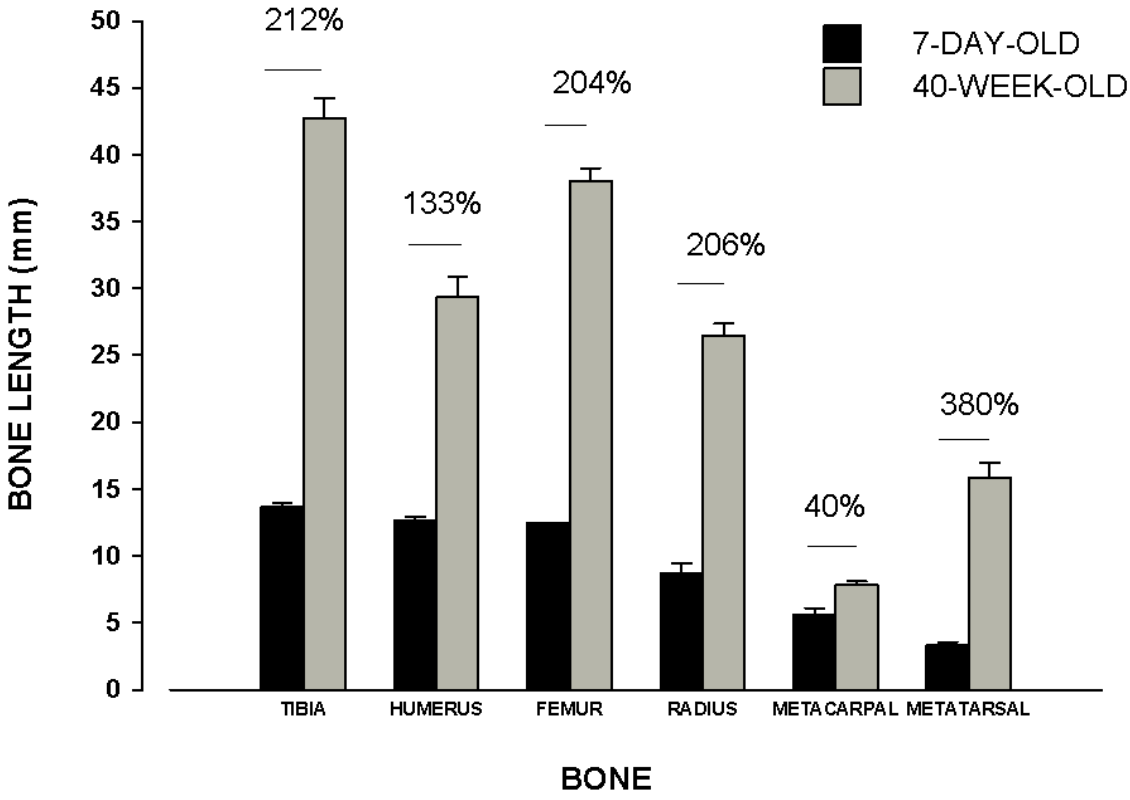

Figure 3.10 Comparison of bone lengths between P7 and 40-week-old rats. The lengths of various bones were measured from Sprague Dawley rats at two different ages. The differences in length (%) between the two age groups, which represent the bone length increase between the two periods, are shown on top of each corresponding grouped bar. Error bars represent SD (n=3).

cell hypertrophy and matrix deposition) to bone elongation in the postnatal animal have been quantitatively evaluated previously using stereological estimation method (Hunziker, 1987b; Wilsman *et al.,* 2008; Wilsman *et al.,* 1996b). The previous results suggested the importance of other factors than HZ cell volume to the bone lengthening growth in some bones. Future experiment could be designed to study the topic using the living *in vivo* GPC model (as used in the present study) since multiple chondrocytic variables could be directly quantified using this method and no longer based on mathematical models as in the previous reports.

An interesting question that arises when observing the variety in GPC volume increase and the HZ cell volume between opposite GPs of the same bone (*i.e.* proximal and distal ends) is whether the cumulative performance produced between the two GPs is tightly controlled in order to finally produce a specific final shape and length of the respective bone. Does any perturbation in one GP trigger compensatory consequence in the other GP of the same bone? To answer this question, the analytical approach in the present study, which measured the GPC volume increase and HZ cell volume among different GPs individually should be optimized by also looking at the cumulative effect of the studied chondrocytic variables from the two opposite GPs of the same bone to the final bone length. The contributions of the chondrocytic variables studied in the present work (*i.e.* GPC volume increase, HZ cell volume, GP length) to the final bone length could be different if the cumulative effect of the variables could be taken into account in the quantitative analysis.

The results also point out the different shape and orientation among different GPs as the cells differentiated from PZ to HZ. It was noted that as the GPC volume increases towards the hypertrophic zone, the length, width and depth of the cell were also increased. It was also found that based on the comparison between two long bones with clearly different length (tibia and radius), GPC in the longer bone demonstrated preferential GPC length increase over the width and depth than the shorter bone. As shown in the present study, the GPC volume increase of proximal tibia GP was followed by 2.9-fold increase in the GPC length as compared to 1.8-fold increase for proximal radius GP. The previous study has

shown this GPC preferential growth character in digital bone GP of two other mammalian namely laboratory rat and big brown bat (Farnum *et al.,* 2008) and it seemed the GPC length increase in the direction of the bone growth is the important feature of GPC hypertrophy that could confer the key contribution to the longitudinal bone growth. The preferential linear dimensional increases of GPC at a single direction instead of equally in all directions as the volume increases could imply the involvement of complex control of the cell morphology, possibly intracellular cyto-skeletal elements (Iscru *et al.,* 2008) and intracellular microtubules to the final GPC shape modulation (Farquharson *et al.,* 1999).

The GPC hypertrophy has been postulated to some extent to involve the transporters of the GPC plasma membrane (Bush *et al.,* 2010) in mediating the cell swelling or hypertrophy during GPC differentiation. In view of the present findings, it would be interesting to know how GPC volume was regulated differently at different time points throughout the phase of longitudinal bone growth. If plasma membrane transporters have important roles in the GPC hypertrophy, it is then intriguing to know whether membrane transporter(s) is expressed at different time at a particular zone of GPC differentiation cascade during the active phase of the bone growth.

In conclusion, the results of the present study underline the significant phenomenon of differential growth among different growth plates. All postnatal GPs showed cell differentiation cascade manifested by GPC volume increase and change in the cell shape particularly the cell length. However, different GPs had distinct postnatal GPC volume increase and HZ cell volume. In addition, there was no apparent relationship between the post natal GPC hypertrophy with bone length, which suggests the overall bone length could not possibly be determined by a change in HZ cell volume at a single time point (*e.g.* day-7 post natal) but instead throughout the active period of the bone growth.

Chapter 4

A Cell Shrinkage Artifact in Growth Plate Chondrocytes with Common Fixative Solutions: Importance of Fixative Osmolarity for Maintaining Morphology

4.1 Introduction

The accurate study of the morphology of living cells as they appear within tissues is difficult but fundamental for an understanding of normal cell biology, and the changes that occur in disease states. Accordingly a vast amount of research has been performed on chemically-fixed cells and tissues, with the intention of retaining the fine morphology and constituents of living *in situ* cells so that they can be studied without the complications of deleterious changes to cell metabolism and loss of viability during the investigation (see Hopwood, 1985). In addition, tissue fixation should protect against cell autolysis, attack by bacteria, and changes to cell volume and shape especially during subsequent preparative treatment (Baker, 1960) when tissue dehydration is frequently performed. Thus, fixative solutions should serve to stabilize the specimen and protect it from rigorous physical tissue processing and staining as required for study (Hopwood, 1969). The particular research emphasis of this chapter has been on the cellular mechanisms underlying the structure and function of the mammalian growth plate. There has been extensive study on chemically-fixed growth plates, and particular interest in the remarkable increase in chondrocyte volume which is a major determinant of bone growth (Buckwalter *et al*., 1986). The large volumes of growth plate chondrocytes (typically ranging from 1,000 to 10,000 μm^3; Bush *et al*., 2008b) potentially makes them extremely sensitive to osmotic artifacts during fixation.

Para-formaldehyde (PFA) and glutaraldehyde (GA) and their combinations have long been used as fixative solutions (Fox *et al*., 1985; Hopwood, 1969) to retain tissue and cell properties (Kiernan, 1999; Renshaw, 2007). Examples of these aldehyde preparations used conventionally are (a) 4% (w/v) PFA (Fox *et al*., 1985; Hosoya *et al*., 2005; solution A, Table 4.1 which has the same formaldehyde concentration (4%) as 10% Formalin (Kiernan, 1999)), (b) 2% (w/v) GA & RHT (ruthenium hexamine trichloride) combined with 2% (w/v) PFA (Farnum *et al*., 2002; solution B, Table 4.1) and (c) 2% GA (w/v) with 0.7% (w/v) RHT (Hunziker *et al*., 1983; solution C see Table 4.1). Although the fixative properties have been widely known, less appreciated is the fact that the *osmolarity* of these solutions is markedly greater than that of typical physiological extracellular solutions (Table

4.1). The osmolarity of the fixative solutions and their effects on cell and tissue morphology have received relatively little attention recently – indeed often appear ignored – despite the fact that there are studies in the literature highlighting this issue. For example, Schultz and Karlsson (1965) observed that hypertonic fixative solutions perfused into the central nervous system caused cellular shrinkage and increased extracellular spaces, whereas isotonic (300-320 mOsm) and hypotonic fixatives could result in cell swelling. Mathieu *et al*., (1978) have reported the importance of both the concentration of GA and the molarity of the vehicle used for the fixative solution for the preservation of lung tissue. Even with these early studies, there are recent examples of investigators using hyper-osmolar fixative solutions (Farnum *et al*., 2002) but little if any comment on the morphology of the fixed cells which frequently appear shrunken/distorted (Buckwalter *et al*., 1985; Erben, 1997; Hosoya *et al*., 2005; Kouri *et al*., 1996; Lee *et al*., 1996; Ross and Reith, 1985; Sanchez *et al*., 2000; Van Der Eerden *et al*., 2000) and no attempt at quantification of the shrinkage artifact. The present study, therefore (a) re-visited this issue to emphasize the importance of osmotic correction to fixative solutions in order to retain cell morphology and (b) provide quantitative data on the extent of cell shrinkage and specifically report on the influence of fixative osmolarity on connective tissue cells.

During preliminary experiments when we were attempting to optimize the chemical fixation protocols for mammalian growth plates to permit a detailed morphological study of hypertrophic zone chondrocytes, we noticed that their appearance in histological sections obtained from whole bones fixed with conventional fixatives was markedly different compared to sagittally sectioned bones fixed using exactly the same methods. The morphology of the cells in the whole bone fixed samples appeared considerably mis-shapen and shrunken, whereas in the bisected bone morphology was relatively normal. From our previous studies on the shape/volume of chondrocytes exposed to osmotic challenge (Bush & Hall, 2001b) we suspected that an artifact of the relatively high osmotic pressure of the fixative solution could be responsible.

Thus, in the present study, using standard fixative solutions which are widely used in the histological preparation of tissues, experiments were undertaken to quantify the osmotic shrinkage effect on hypertrophic growth plate chondrocytes. The present data show that a shrinkage artifact is particularly marked when whole bones were chemically fixed, and significantly reduced when bones are sagittally bisected prior to fixation. The present findings also demonstrate that adjusting the fixative solution to an osmolarity close to that of typical extracellular solutions (approx. 280 mOsm; (solution D, Table 4.1) abolishes the artifact.

4.2 Materials and Methods

4.2.1 Animals and Growth Plate Preparation

The tibia of each limb with intact proximal GP from twenty-five Sprague-Dawley rats (7-day-old; P7) was prepared as described previously (2.1.3).

For the preparation of samples for histology, fifty tibias from 25 animals were used and placed in fixative solutions of differing composition as follows: (a) conventional fixative solutions (Table 4.1), (b) fixatives with GA concentration maintained constant, but with osmolarity similar to that used for conventional fixative solutions (Table 4.2), and (c) fixatives with various concentrations of GA but with osmolarity maintained at approx. 550 mOsm (Table 4.3). The growth plates were fixed for 24 hrs at room temperature for subsequent paraffin-embedding for histological sectioning. For group (a) three intact tibias and 3 bisected tibias were fixed in each fixative solution, whereas in group (b) and (c), three and five intact tibias were used in each fixative solution respectively.

For the preparation of growth plates for the analysis of *in situ* growth plate chondrocyte (GPC) volume, 15 tibias from 8 rat pups were used. They were grouped into two: (i) five bones maintained intact, and (ii) ten bones that were bisected sagittally (Figure 4.6(A)). Both groups of bones were incubated with either CMFDA-green for 60 mins (if the bones were subsequently fixed) or calcein AM (for non-fixed bones). Then, all bones from group (i) and four bones from group (ii) were fixed in solution A. The other three bones from group (ii) were fixed in osmotically-corrected fixative solution (solution D, Table 4.1). All the bones were fixed for 24 hrs at room temperature. The remaining 3 bones in group

Solution ID	Fixative solution	Cacodylate Buffer (mM)	pH	Osmolarity (mOsm)	References
A	PFA 4%	None	7.11	1148 ± 2	Hosoya, *et al*, 2005
B	PFA 2% + GA 2% + RHT 0.7%	100	7.06	1135 ± 32	Farnum, *et al.*, 2002
C	GA 2% + RHT 0.7%	50	6.72	420 ± 20	Hunziker, *et al.*, 1983
D	GA 1.3% + RHT 0.5%	30	5.67	270 ± 10	(present study)

Table 4.1 Composition of fixative solutions used in the study. Fixative solutions were prepared as described in the references cited which reported the morphology of growth plate chondrocytes following fixation. For solution A, distilled water was used instead of cacodylate buffer. Fixative solution D was prepared by diluting solution C with distilled water. [Concentrations are given as % (v/v) for GA= glutaraldehyde and PFA= paraformaldehyde, and as % (w/v) for RHT= ruthenium hexamine trichloride].

Solution ID	Fixative Solution	Cacodylate buffer (mM) pH 7.4	pH	Osmolarity (mOsm)
280	0.7% RHT + 1% GA	50	6.76	273 ± 13
480	0.7% RHT + 1% GA	50	6.60	467 ± 28
640	0.7% RHT + 1% GA	50	6.55	637 ± 20
1200	0.7% RHT + 1% GA	50	6.49	1141 ± 116

Table 4.2 Modified fixative solutions with constant concentrations of GA and RHT, but with osmolarity varied using NaCl. Fixative solutions were prepared with the constituents at the concentrations indicated (see Materials and Methods), with the osmolarities and pH of the resulting solutions as shown. Concentrations are given as % (w/v) for RHT, and % (v/v) for GA. Data expressed as means ± S.E.M. from at least 3 independent determinations

Solution ID	Fixatives	Glutaraldehyde concentration (%)	Cacodylate buffer (mM), pH 7.4	pH	Osmolarity (mOsm)
0.5GA	0.7% RHT + GA	0.5	50	6.81	543 ± 1
1GA	0.7% RHT + GA	1.0	50	6.73	542 ± 4
2GA	0.7% RHT + GA	2.0	50	6.72	556 ± 18
4GA	0.7% RHT + GA	4.0	50	6.35	577 ± 11

Table 4.3 Modified fixative solutions with varying GA concentration, but with similar final osmolarity. Fixative solutions were prepared with the constituents including different GA concentrations (% v/v) as indicated (see Materials and Methods), with the osmolarities of the resulting solutions as shown. Concentrations of RHT are given as % (v/v). Data expressed as means ± S.E.M from at least 3 independent determinations.

(ii) were maintained unfixed for *in situ* living cell imaging. The osmolarity of all solutions was determined using a freezing point micro-osmometer (Model 3300, Vitech Scientific Ltd., Partridge Green, U.K.) with solid NaCl or distilled water added to adjust the osmolarity to the required range. The pH of all solutions was measured at room temperature using a SevenEasy™ pH meter (Mettler Toledo, UK) with the pH of fixative solutions altered as required by adding either HCl or NaOH.

4.2.2 Histology of the Growth Plate

Bones were embedded in paraffin wax using a standard procedure as described in 2.3.2. The sections were then mounted on poly-l-lysine-coated microscope slides (Polysine™, VWR International, Leicestershire, UK) and dried overnight. After removing paraffin, the sections were stained with 0.1% (w/v) Toluidine blue O (see 2.3.3.1).

4.2.3 Measurement of Growth Plate Chondrocyte Shrinkage

Histological sections of fixed hypertrophic GPC stained with 0.1% Toluidine blue O were observed under an x63 (oil-immersion) objective lens. Several histological views of chondrocytes within sections S5 and S6 of the hypertrophic zone (see details in the section *In situ* volume measurement (below), and Figure 4.1(A)) were randomly selected and the images recorded using a mounted digital camera (Coolpix 4500, Nikon, Japan) with Coolpix MDC2 Relay lens (MXA 2900, Nikon, Japan). The captured images were then transferred to a computer for further image analysis. Java-based scientific image processing software (ImageJ, NIH, Bethesda, Maryland, U.S.A.) was then used to measure the cell shrinkage from the images of the histological sections.

In order to determine the extent of chondrocyte shrinkage it was necessary to identify the area of individual chondrocytes and that of their lacuna – *i.e.* the 'cavity' in which the cell resided. It was in fact relatively straightforward to do this as the outermost edge of the cell area stained distinctly with Toluidine blue O, and the perimeter of the corresponding lacuna was identified as the edge of the extracellular matrix that demarcated the border between the stained area of the

matrix and the 'space' of the lacuna which was relatively unstained. It was noted that the area of the lacuna could only be observed if there was cell shrinkage. For each group of treatments, 4 fields of view from each image were selected and up to 11 cells and their corresponding lacunae randomly taken for area measurement. The area of each cell and that of its associated lacuna were selected by outlining their perimeters using the freehand selection tool (see Figure 4.2A), panel a). The total area of the cell and its lacuna were then determined using the 'analyze' and 'measure' toolbar in the software. Cell shrinkage was calculated as {100 – [(cell area/lacuna area) x 100]} and expressed as a percentage of the initial volume (see Fig. 4.2A(a)). When the cell and its corresponding lacuna shared the same perimeter, the value of cell shrinkage was defined as zero as defined above.

4.2.4 Confocal Laser Scanning microscopy

An upright Zeiss Axioskop LSM 510 CLSM was used to acquire fluorescent images of *in situ* hypertrophic growth plate chondrocytes using the protocol that has been described previously (2.4.2).

4.2.5 *In situ* Volume Measurement

Whole growth plates imaged from the proliferative to hypertrophic zones were divided into eight equal parts and labeled S1 to S8 (Figure 4.1(A)). This was done so that a comparative analysis could be made between corresponding sections from different individuals (see 2.5.1). Since the greatest number of hypertrophic cells that was consistently found to be intact was in the sections S5 and S6, the *in situ* growth plate cell volume analysis was performed only at these sections. Chondrocytes in S7-S8 often appeared to be in poor condition, possibly as a result of cutting trauma during the preparation of the tissue (Huntley *et al*., 2005; Amin *et al.,* 2008). Volume analysis was performed using high performance 3D imaging software (Volocity®) on scanned CLSM images using the calibrated cell volume method as previously described (2.5.2).

4.3 Results

4.3.1 Volume and Morphology of Rat Growth Plate Chondrocytes

Initially, to determine live cell volumes and the morphology of *in situ*, unfixed chondrocytes, *in situ* growth plate chondrocytes were labelled with calcein as shown (Fig. 4.1). Imaging of the fluorescently-labelled *in situ* living growth plate chondrocytes demonstrated a clear increase in the size of GPC from the proliferative through to hypertrophic zones (Fig. 4.1(a)). Chondrocytes within the proliferative zone (between the reserve and hypertrophic zone) appeared ellipsoidal and usually arranged in columns of at least three to eight cells. In the hypertrophic zone (between the proliferative zone and the zone of calcification) the cells were larger and frequently more rounded although there were cells with a height greater than half of the cell's width (Buckwalter *et al*., 1985; Farnum and Wilsman, 1986).

In accordance with the visual appearance of chondrocytes along the growth plate, the quantified volume of *in situ* cells increased although it was clearly not a linear process as there was a relatively poor fit to a linear regression (correlation coefficient $r^2 = 0.793$). The volume increase was initially gradual through to S5, but then became more rapid from S5-S8 similar to an exponential growth relationship (Fig. 4.1(b)). When the volume data were transformed to $\log_{10}$ and plotted semi-logarithmically (see inset to Fig. 4.1(b)) there was a much better fit to the data ($r^2 = 0.955$) supporting the notion of a logarithmic increase in chondrocyte volume associated with hypertrophy. In the present study, a focus was made on chondrocytes within these latter sections of the growth plate. Although the shrinkage artifact was apparent in the smaller cells, it was very difficult to quantify the phenomenon. It was found that using our imaging methods (see Materials and Methods) the distinction between the perimeter of the lacuna and the cell edges of smaller (shrunken) cells was difficult to determine accurately, resulting in large variations. Therefore, the phenomenon was studied only on chondrocytes in the hypertrophic zone to ensure accurate measurements, and the cells within S5-S6 were chosen because an adequate number of intact cells from these segments could consistently be observed.

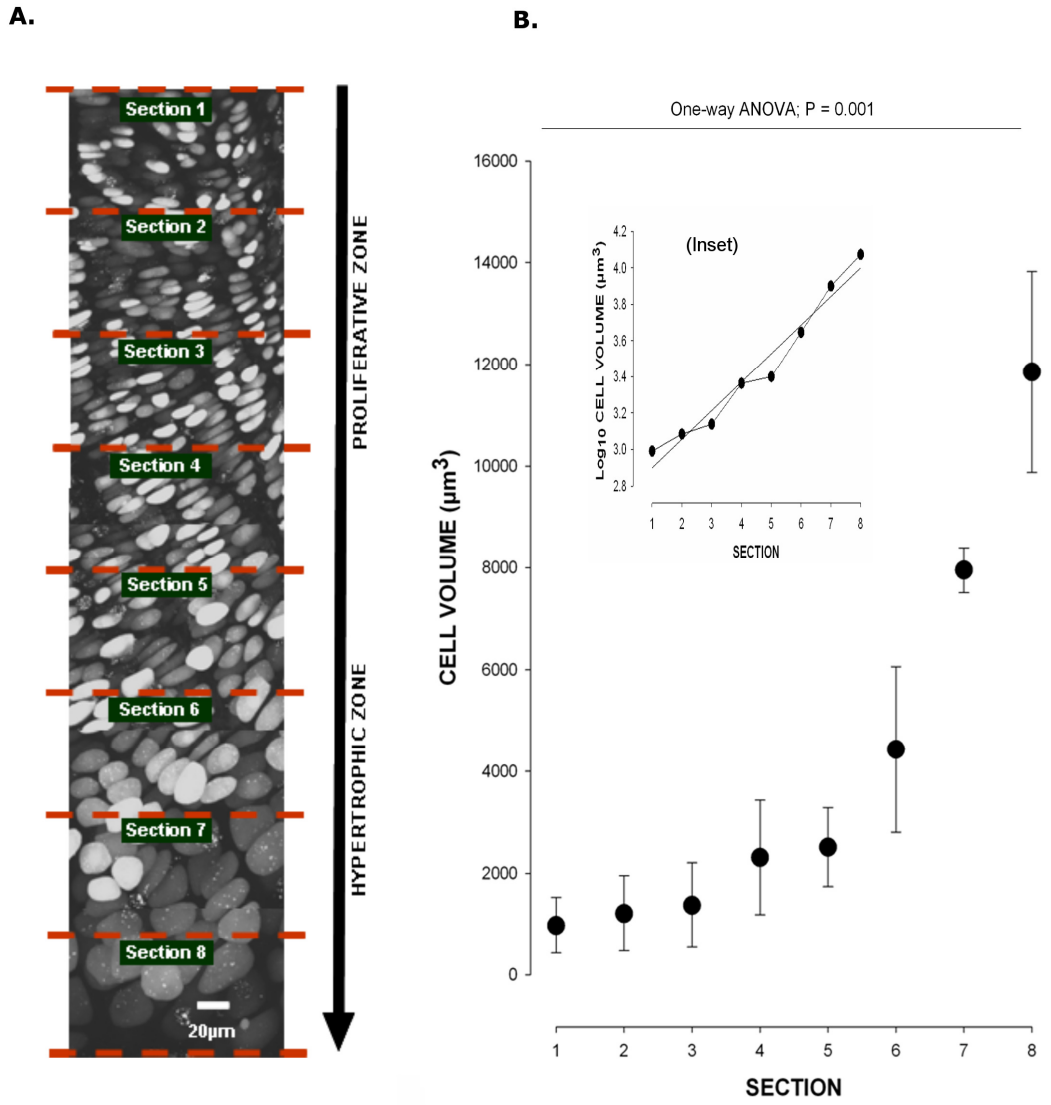

Figure 4.1. Overview of the rat growth plate, and division of *in situ* living rat chondrocytes (GPC) into sections from proliferative to hypertrophic zones. Living chondrocytes in a bisected proximal tibia of a 7-day-old rat pup were labeled with calcein AM, and sequential CLSM images taken with a x63 water-dipping objective (see Materials and Methods). Panel (**A**) demonstrates the projected image of a section of the growth plate showing the increase in chondrocyte volume from proliferative to hypertrophic zone. The zones were divided into eight equal sections (labeled S1-S8) from early proliferative zone to late hypertrophic zone. Panel (**B**) shows the changes in the volume along the growth plate sections as measured using Volocity® software on living *in situ* growth plate chondrocyte images captured with CLSM. Also shown is an inset where the same data points were transformed to $\log_{10}$. (Data shown are means ± S.E.M. or S.D. as appropriate, with n = 2 for S1-S4 and S7-S8, and n = 3 for S5-S6; and at least N=15 cells measured at each section).

4.3.2 Measurement of Cell Shrinkage

The accuracy of the method used for assessing chondrocyte shrinkage in histological sections as described in Materials & Methods (Fig. 4.2A(a)) was initially determined by measuring the area of GPC cells that had distinct and well-defined perimeters. The cell measurement was made independently using the free-hand selection tool on the same cell twice and the difference between the two readings compared. The mean difference between the two measurements was 2.7±1.9 % (mean ± S.D., for 11 cells) indicating the measurement method had an appropriate level of accuracy.

4.3.3 Morphology of Growth Plate Chondrocytes Fixed Using Conventional Solutions

An ideal fixative should successfully preserve tissue for subsequent staining procedures, but it is important to accurately retain the original morphology of the living cells in the tissue, free from artifacts occurring during the fixation process. To demonstrate the morphology of GPC fixed with conventional fixatives (Farnum *et al*., 2002; Hosoya *et al*., 2005; Hunziker *et al*., 1983), we used three standard and widely-used solutions (Table 4.1). These fixative solutions were all hyper-osmotic (Table 4.1), and therefore for comparison an iso-osmotic fixative with osmolarity adjusted to close to that of typical extracellular physiological solutions (280 mOsm; Table 4.1), was also included.

In whole (non-bisected) bone samples, fixed and processed as described for histology (see Materials and Methods), there was a clear cell shrinkage artifact observed in tissue fixed with the three conventional fixatives (solutions A, B & C; Table 4.1; Fig. 4.2A(a-c)). Among the three fixatives, chondrocyte shrinkage assessed visually was most marked for solutions A and B and least for solution C (Fig. 4.2A(c,d)). When osmotically corrected solution D (~280 mOsm) was used, no apparent cell shrinkage was observed (Fig. 4.2A(d)). Quantitatively, solution A caused the highest cell shrinkage (44 ± 3 % (3[44])), followed by tissue fixed in solution B (31 ± 4% (3[44]), then cells in solution C 17 ± 5% (3[44]) and finally for the osmotically-corrected fixative solution D, there was no measurable cell

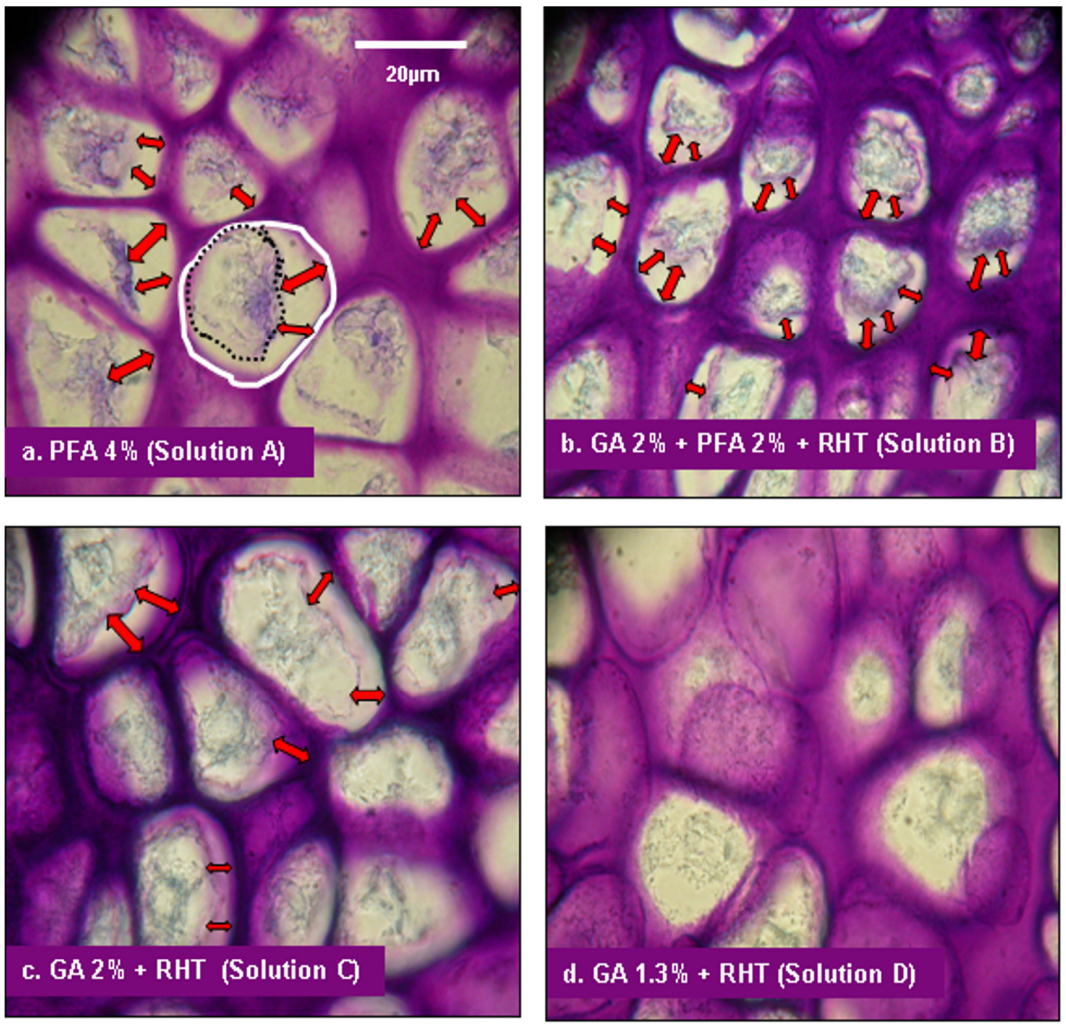

Figure 4.2A. Conventional fixatives cause considerable shrinkage of hypertrophic growth plate chondrocytes when applied to whole (intact) bones. Intact proximal tibias of 7-day-old rat pups were fixed using various standard fixative solutions (Table 4.1) and sections prepared and stained with 0.1% Toluidine blue O (see Materials and Methods). The method used to calculate the extent of chondrocyte shrinkage was illustrated in panel **a**. The thick white line was drawn free-hand around the perimeter of the lacuna and the black broken line drawn around the membrane edge of its resident chondrocyte (see details in Materials and Methods). The gap between the cells and the border of the lacuna is illustrated by double headed arrows. Cell shrinkage was observed in all conventional fixatives (panels **a - c**) but not when the osmolarity of the fixative was adjusted to a 'physiological' osmolarity (panel **d**). For pooled data see Figure 4.3. The scale bar of 20µm in this and the following Figure applied to all panels.

shrinkage (5.5 ± 0.8% (3[44])). When analysing the extent of the shrinkage from solutions A to D (lowering osmolarity, Table 4.1), there was a significantly decreasing trend (one-way ANOVA test; $p = 0.010$) however only the shrinkage for cells in solutions A and B were significantly different (unpaired Student's t-test, $p<0.05$) from the osmotically-corrected fixative solution D. Note that although shrunken cells were routinely observed microscopically in cells fixed in solution C (Fig. 4.2A(c)) the pooled data did not show a significant difference and this was mainly because of the range in the magnitude of the shrinkage effect.

In bisected bones (Fig. 4.2B), microscopic inspection showed clearly that the extent of the chondrocyte shrinking artifact was considerably reduced with the four fixatives when compared to the cells within fixed whole bones (Fig. 4.2A(a-d)). When the shrinkage was quantified (Fig. 4.3B), the same decreasing trend in cell shrinkage with the four fixatives was also observed and the trend significant over the whole range (one-way ANOVA test; $p = 0.024$). The absolute level of shrinkage and the trend with decreasing osmolarity, was less compared to the data for intact bones (Fig. 4.3A). When the data sets for intact and bisected bones over the range of fixatives were compared using a two-way ANOVA, the difference was significant ($p=0.004$). In solution A cell shrinkage in bisected bones was 22 ± 2.6%, which was significantly less than the shrinkage of chondrocytes fixed in intact tibias ($p = 0.030$). Fixative solution B caused 17 ± 1.4% (3[44]) shrinkage whereas solution C caused 9 ± 0.4% (3[44]) cell shrinkage and these values were less than for intact bones but did not reach the level of significance ($p> 0.05$). Cell shrinkage in the iso-osmotic fixative solution D for GPC in bisected bones was only 4 ± 0.4% (3[44]; Fig. 4.3) and this was not significantly different from the data in intact bones (see above). These results showed that the shrinkage artifact was considerably reduced if the bones were bisected prior to fixation, and with osmotic correction, there was no shrinkage artifact of GPC in either intact or bisected bones.

As noted in Table 4.1, the pH of the fixatives varied over the range 5.67 to 7.11, which was the result of different types and concentration of fixative agents and buffer concentration. A further experiment to examine whether pH contributed

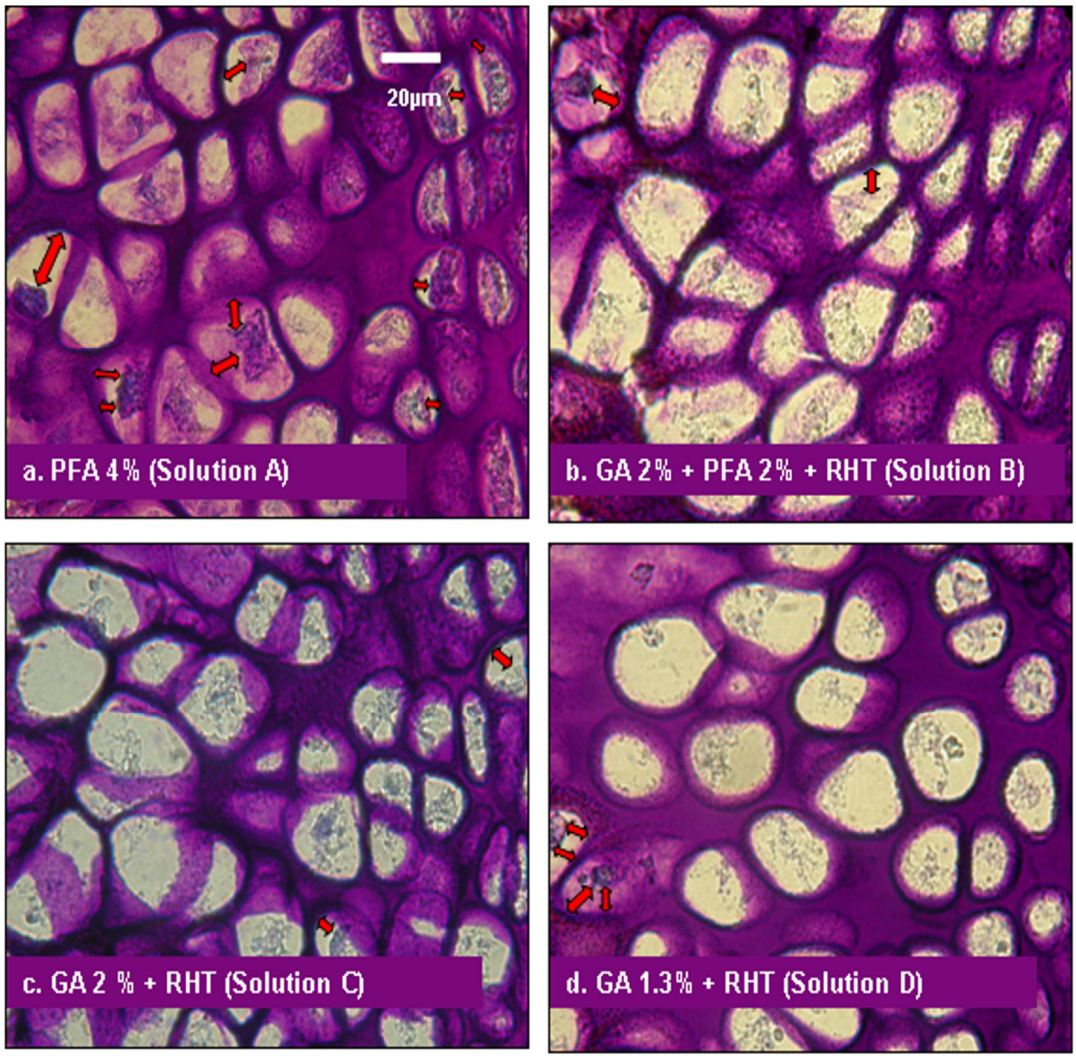

Figure 4.2B. Reduced cell shrinkage in GPC of sagittally-bisected bones following fixation. Bisected sections prepared and stained with 0.1% Toluidine blue O (see Materials and Methods). With these bisected bones the extent of cell shrinkage was markedly less compared to the intact bones (Figure 4.2A) and shrunken chondrocytes were only occasionally observed as illustrated by the double headed arrows (panel **a**). The morphology of chondrocytes within the three other fixative solutions (panels **b – d**) was relatively normal (see pooled data in Figure 4.3).

INTACT BONES

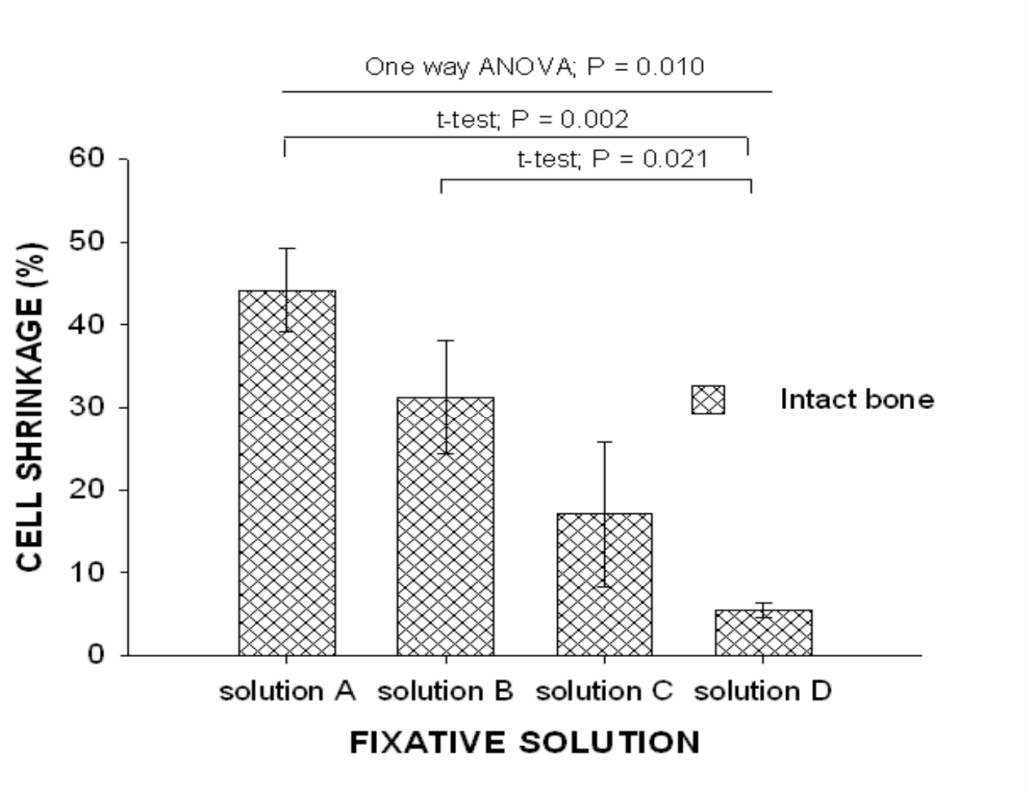

Figure 4.3A. Growth plate chondrocyte shrinkage in histological sections from intact bones fixed in four different solutions. Cell shrinkage of *in situ* chondrocytes fixed in solutions A (1148 ± 2 mOsm), B (1135 ± 32 mOsm), C (420 ± 20 mOsm)or D (270 ± 10 mOsm) (for composition see Table 4.1) in intact tibias from 7 day-old rats were measured as described (see Materials and Methods). Data in this and the subsequent Figure were from at least (3[44]) for each condition. In this and the following Figure, P values for unpaired Student's t-tests are shown. (Data are given as means ± S.E.M.).

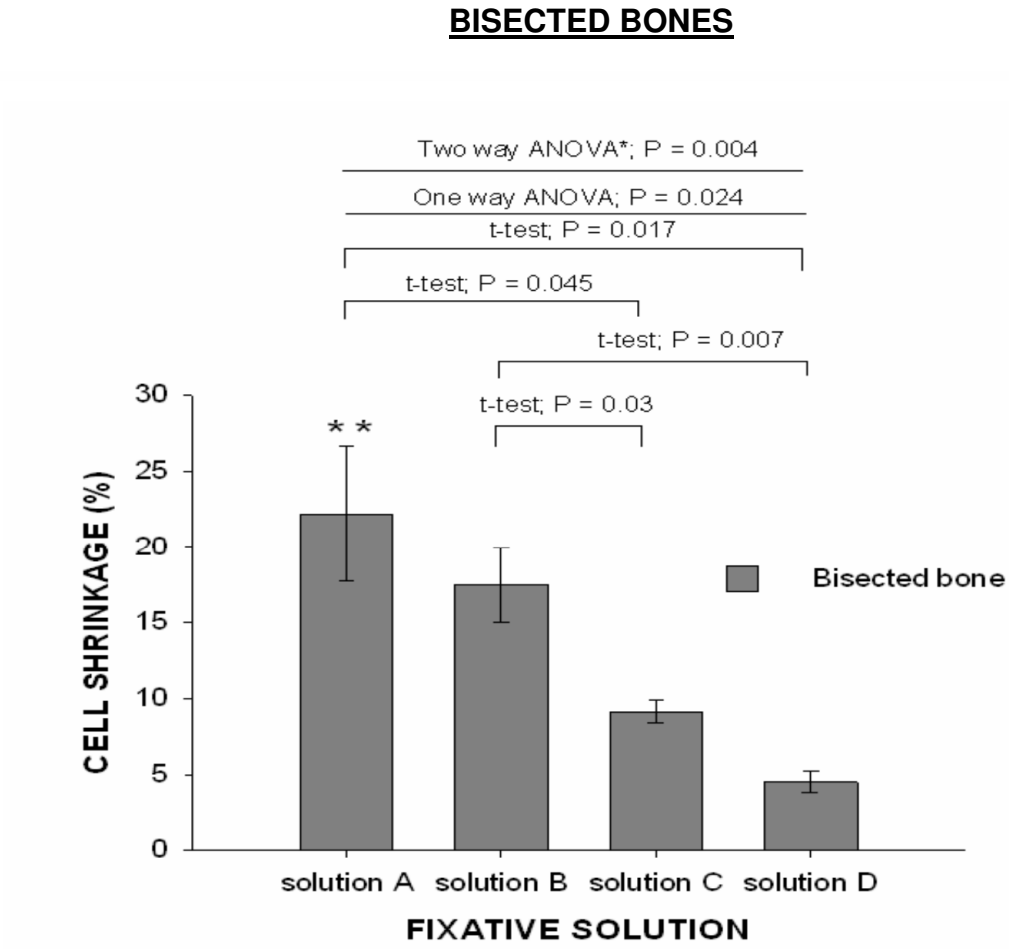

Figure 4.3B. Growth plate chondrocyte shrinkage in histological sections from bisected bones fixed in four different solutions. Cell shrinkage of *in situ* chondrocytes fixed in solutions A (1148 ± 2 mOsm), B (1135 ± 32 mOsm), C (420 ± 20 mOsm)or D (270 ± 10 mOsm) (Table 4.1) in sagitally-bisected tibias from 7 day-old rats were measured as described (see Materials and Methods). A single asterisk (*) denoted a significant difference when the two-way ANOVA tested the trend of cell shrinkage between intact and bisected bones in various fixative solutions. A double asterisk (**) denoted a significant difference compared to the intact bone fixed in solution A (Student's unpaired t-test).

significantly to the quality of tissue preservation was conducted. Two pH values (*i.e*. 5.6 and 7.2) were tested using the same fixative solution (solution D) to fix two groups of growth plate tissue from proximal tibia of P7 rats (n=3). Using the same method to quantify the cell shrinkage as described previously, the result showed that at pH 5.7 there was 8 ± 0.6 % (mean ± S.E.M.) cell shrinkage, whereas at pH 7.2 there was 7 ± 1.5 % of cell shrinkage. These were not significantly different ($p<0.05$) and so we concluded that pH over this range had a negligible effect on cell shrinkage compared to the osmolarity of the fixative solutions.

4.3.4 Fixation of GPC Using Different Concentrations and Osmolarities of Glutaraldehyde (GA) Solution

To test whether the osmolarity or concentration of fixative was responsible for the shrinkage artefact, whole bones were immersed in solutions with varying osmolarity (273-1141 mOsm) and standard fixative concentrations (GA 1%, RHT 0.7%; Table 4.2), or in solutions varying fixative concentration (GA 0.5-4%) whilst maintaining osmolarity relatively constant (555± 8 mOsm; Table 4.3). At the lowest osmolarity (273 ± 13 mOsm), cell shrinkage was minimal (13 ± 0.6% (3[44])), but as it was raised, there was a progressive and significant increase (ANOVA, $p<0.001$) in the extent of cell shrinkage (Fig. 4.4(A)). At the highest osmolarity studied (1141 mOsm) cell shrinkage was 52 ± 1.6% (3[44]) and significantly greater (unpaired Student's t-Test, $p<0.001$ for both) than the shrinkage observed in 273 and 467 mOsm solutions. When the GA concentration was varied over the range 0.5 to 4%, but with the osmolarity of all solutions maintained constant, the shrinkage of GPC fixed in intact bones with 1%, 2% and 4% GA was 15 ± 2.4%, 12 ± 0.5%, and 16 ± 2.1% respectively, and not significantly different ($p>0.05$; data from at least (5[44]); Fig. 4.4(B)). It was notable that GA at 0.5% showed slightly higher cell shrinkage (25 ± 4.1% (5[44])) compared to 1% GA, but this was not significantly different from the lowest cell shrinkage produced by GA at 2% ($p > 0.05$). The morphology of a noticeable number of these cells was abnormal, suggesting that they were not properly fixed, and thus it was possible that the cells were susceptible to the post-fixation

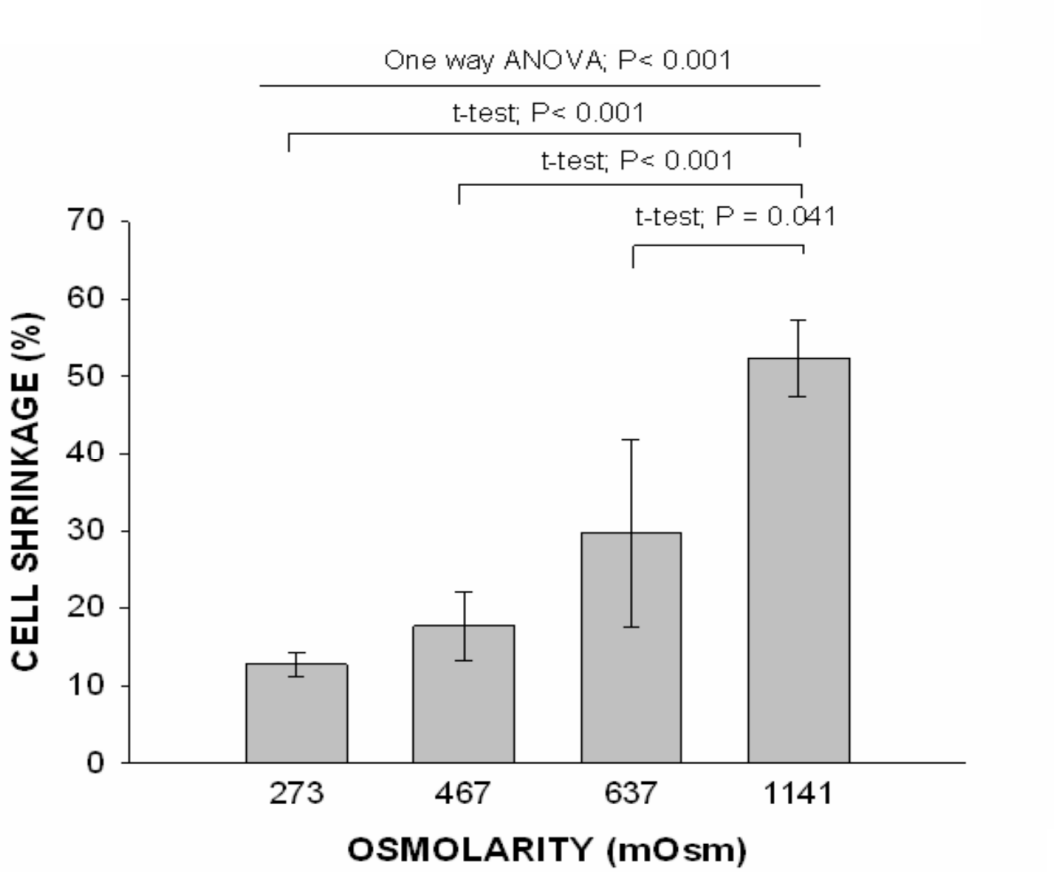

Figure 4.4A. Chondrocyte shrinkage increased with elevated osmolarity of the fixative solution. Whole bones were fixed in solutions composed of 1% GA and 0.7% RHT, with osmolarity varied over the range 273 to 1141 mOsm by the addition of NaCl (see Table 4.2). Shrinkage of GPC was determined as described (see Materials and Methods, and Fig. 4.2(A(a))). Data were from at least 3 animals and in total 44 cells (3[44]) for each condition and presented as means ± S.E.M.

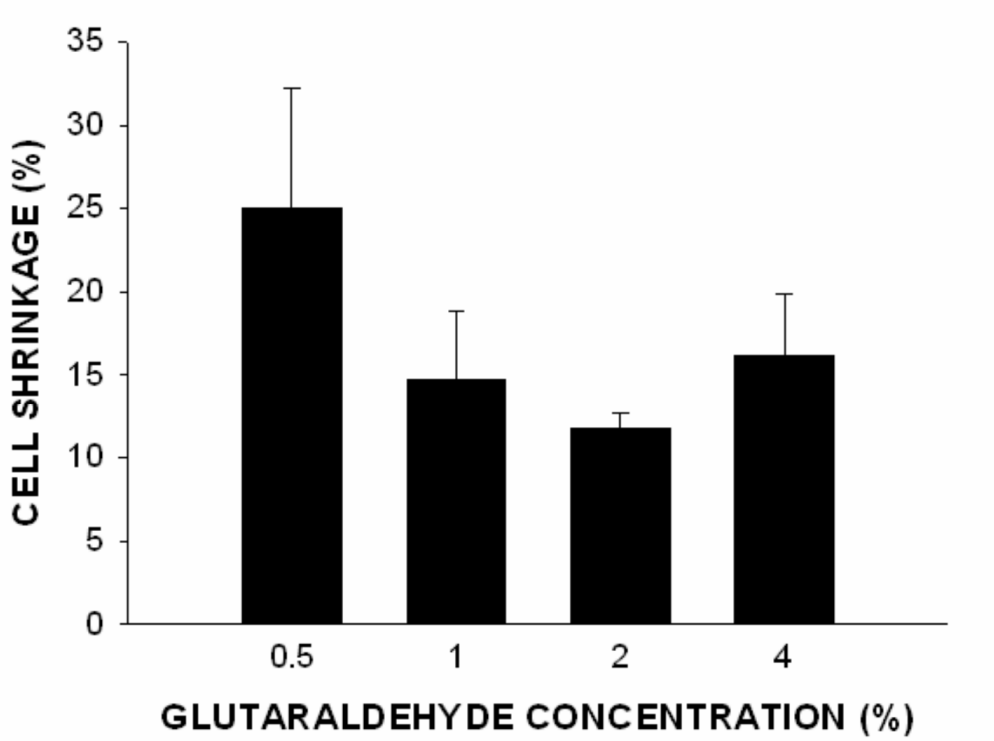

Figure 4.4B. There was no difference in cell shrinkage with an increase of fixative concentration if osmolarity was kept constant. Whole bones were fixed in fixative solutions with the GA concentration varied over the range 0.5 to 4%, but with the osmolarity maintained constant at ~550 mOsm (see Table 4.3 for composition of solutions). Shrinkage of GPC was determined as described (see Materials and Methods, and Fig. 4.2(A(a)). There was no significant difference between any pairs of data (Student's unpaired t-test). Data were from at least (5[44]) for each condition and presented as means ± S.E.M.

dehydration protocols (unpublished observations).Taken together, these data suggest that the shrinkage and morphological changes of GPC fixed using standard solutions could be accounted for by the osmolarity of the fixative solutions and not by the concentration of the fixative.

4.3.5 *In situ* Growth Plate Chondrocyte Volume Following Fixation in Solution A in Intact and Bisected Bones

The volume of *in situ* GPC within intact or sagittally-bisected bones and fixed under various conditions was also assessed using another method. Solution A was chosen as it had the highest osmolarity among the different conventional fixative solutions used in the present study and has been used previously in the study of growth plate chondrocytes (see Table 4.1). Images of fluorescently-labelled *in situ* chondrocytes taken by Clhands howeverSM showed the majority of cells with abnormal shrunken morphology in intact bone fixed with this solution (Fig. 4.5(a)). When the bone was sagitally bisected and then fixed using the same solution, the proportion of shrunken chondrocytes was markedly less (Fig. 4.5(b)), and similarly when these bones were fixed in the osmotically-corrected solution (solution D, Table 4.1) there were almost no shrunken cells observed (Fig. 4.5(c)) with the cells appearing morphologically normal. The volume of GPC fixed in the intact bone was only 40% of those fixed in the bisected bone (Table 4.4; unpaired t-Test: $p = 0.016$, $n=5$). For comparison, GPCs volume of living non-fixed bone and of bisected bone fixed in solution D was not significantly different from the GPC volume of bisected bone fixed in solution A (unpaired t-Tests, $p>0.05$). However, the GPC fixed in solution A showed no significant volume decrease than the GPC fixed in solution D and non-fixed GPC as expected due to cell shrinkage, as shown previously (Figure 4.3B). The reason for this was not immediately obvious, although it should be noted that the errors associated with the measurement of *in situ* GPC volume were relatively large (Table 4.4). In summary, the reduction in cell volume was significantly greater for GPC within intact bones compared to bisected bones when fixed in a conventional fixative solution (Table 4.4).

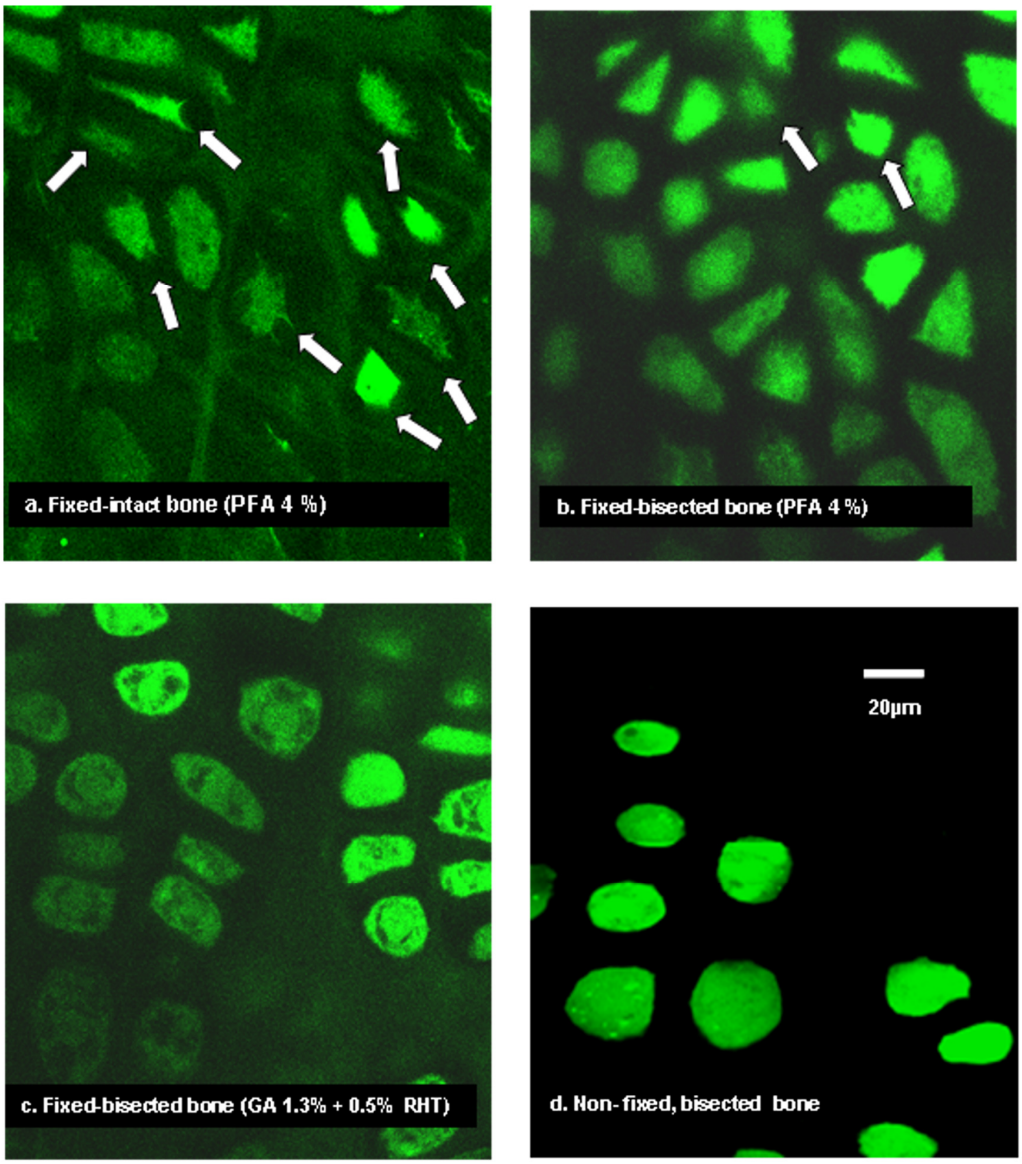

Figure 4.5 Reduced volume and altered morphology of *in situ* GPC fixed within intact bone compared to those within bisected bones. Panels (**a-c**) showed the typical appearance of fluorescently (CMFDA-green)-labeled chondrocytes within intact (panel **a**) or bisected (panels **b, c**) bones, and fixed under the various conditions indicated. The shrinkage of some cells was observed in the fixed *in situ* cells (examples indicated with white arrows, panels **a** and **b**) but not in the osmotically-corrected fixative solution D (panel **c**). Panel (**d**) shows the appearance of unfixed (*i.e.* living) *in situ* hypertrophic GPCs labeled with calcein. All images were taken by CLSM using a x63 water-dipping objective. Cell volume measurements were performed as described (see Materials and Methods) with pooled data given in Table 4.4. Details of the composition of fixative solutions are given in Table 4.1. Scale bar = 20 µm.

Nature of the bone specimen	Fixatives	*In situ* GPC volume (μm^3)
Intact	PFA 4% (solution A)	1698 ± 166*
Bisected	PFA 4% (solution A)	4064 ± 571
Bisected	GA 1.3% + RHT 0.5% (solution D)	3389 ± 659
Bisected	No fixative	3411 ± 1148

Table 4.4 Reduction of *in situ* GPC volume in fixed intact bones compared to bisected bones. CMFDA-labeled *in situ* chondrocytes were fixed under the conditions shown (see Figure 4.5), their volume determined as described (see Materials and Methods) and the pooled data presented. Data (as means ± S.E.M.) are from n = 5 animals with 5-29 chondrocytes measured from each animal. *Denotes a significant difference (Student's unpaired t-test) between the data for the intact bone and the three other solutions.

4.4 Discussion

This study demonstrated that the osmolarity of fixative solutions was of critical importance for maintaining the normal morphology of *in situ* hypertrophic chondrocytes within the mammalian growth plate following chemical fixation. The shrinkage artifact evident when using conventional fixatives, was abolished when the osmolarity of the medium was reduced to close to that of normal physiological solutions or markedly reduced when the bones were sagitally bisected prior to fixation. These results raise important issues in relation to the accurate preservation of cell morphology by these widely-used chemical fixative solutions.

The first point to consider is the identification of a fixative concentration that ensured proper fixation of the cells/tissue without the osmolarity being too high to cause a shrinkage artifact and the present data suggest that solution D was optimal (Table 4.1; Fig. 4.3). This osmolarity would be close to that normally present in physiological extracellular solutions meaning that the osmolarity of the cells within the extracellular matrix of the growth plate would similarly be optimal for normal chondrocyte morphology. (Note however that the exact extracellular osmolarity around the GPC will most likely be higher due to the presence of glycosaminoglycans present in the extracellular matrix (Urban *et al.*, 1993)). A

lower concentration of GA (0.5%) produced what appeared to be a shrinkage artifact (Fig. 4.4B) but although individual shrunken cells were present on visual examination, statistical analysis of pooled data showed this was not significant. However we would caution against using such a low concentration as the fine appearance of the cells suggested that there were cells that were not properly fixed, resulting in morphological changes/distortions during post-fixation protocols (unpublished observations). Previous studies have, however, successfully utilized low fixative concentrations. For example Maunsbach (1966) investigating the kidney and Hopwood (1967) studying the brain noted that GA was an effective fixative down to 0.25% (Hopwood, 1967; Maunsbach, 1966). It is possible that low fixative concentrations could be used successfully in these studies because of the different physical nature of hard tissues compared to soft tissues, as in the latter the diffusion rate and thus penetration of the fixative would be expected to be considerably greater. The present findings were in general agreement with a previous report that identified the importance of fixative osmolarity to produce correct soft tissue preservation. Mathieu *et al.,* (1978) reported both the GA percentage and molarity of the fixative vehicle were of importance for the preservation of lung tissue. In this study, they noted the shrinkage was induced by the osmolarity of buffer and fixative combined, as evidenced by shape changes of erythrocytes in capillaries and small vessels of the trachea, and a reduction in the air-blood tissue barrier of the trachea with different fixative osmolarities. Higher fixative concentrations (*e.g*. 2-4% GA) could of course be used for some applications where cell shrinkage is not a concern (*e.g*. for tissue perfusion fixation (Santoreneos *et al.,* 1998) or biomaterial fixation (Nuss *et al.,* 2006)), but clearly the results from the present study emphasize the importance of researchers being aware of the potential for an osmotic shrinkage artifact to cell shape.

In the present study RHT (ruthenium hexamine trichloride) was included in most of the fixative solutions (Table 4.1). Hunziker *et al.,* (1982) have proposed that this cationic dye stabilized the GPC plasma membrane within the lacuna by establishing electrostatic cross-linkage between anionic components within the plasma membrane and the proteoglycans of the pericellular matrix which surrounds

chondrocytes. They suggested that this could prevent the rupture or detachment of the plasma membrane from the pericellular matrix when conventional aldehyde solution was used simultaneously (Hunziker *et al.,* 1982; 1987a, 1992b) (Fixative solution B and C; Table 4.1). In our hands however, the presence of RHT could not prevent the shrinkage artifact (see Fig. 4.3). Thus, although the % shrinkage was not significantly different from the osmotically-corrected fixative solution (solution D) it was still clearly greater than the solution B & C. In addition, abnormal/shrunken cells were routinely observed (Fig. 4.2A(c)) as also reported in the original Hunziker *et al.,* (1982) study. Therefore, although it is possible that RHT does protect against the shrinkage effect to some extent by stabilizing the cell membrane against the pericellular matrix, it appears that osmotic correction is the preferred procedure to eliminate the artefact (Fig. 4.3) and the presence of any abnormal cells (Fig. 4.2A(d)).

The nature of the chemical fixative is also an issue of importance as there is not one fixative suitable for all applications. For example, GA has been associated with antigen masking due to its excessive and aggressive cross-linking of proteins, and is therefore normally considered unsuitable for tissues intended for immunochemical staining (Renshaw, 2007). GA is usually used as a mixture with PFA (termed Karnovsky's fixative; (Karnovsky, 1965) so as to take advantage of the latter which has rapid tissue penetration although the fixation rate is not as rapid as that of GA (Kiernan, 1999). Therefore, PFA (4%) alone probably gives the best compromise between good cytological preservation and immunolocalisation, while at the same time maintaining antigen masking to a minimum. However, as it is a fixative solution with high osmolarity (Table 4.1), tissues should be bisected beforehand to maximize rapid fixative access to limit undesirable cell shrinkage artifacts although it should be noted that they were still clearly apparent (Fig. 4.2B(a)) and still significant (~20% shrinkage, Fig. 4.3).

The finding that the shrinkage artifact was significantly reduced in bisected compared to whole bones, strongly suggested that the rate of penetration of the fixative compared to the osmotic changes to chondrocytes resulting from the high osmolarity of the fixative solutions are important. In the whole bone, the large

shrinkage artifact suggested that osmotically-induced cell shrinkage occurred before the tissue was fixed. Thus when the bone was placed in the fixative solution, water movement out of the bones to the hyper-osmolar fixative solution occurred rapidly, and before the fixative fully penetrated the bone/cartilage matrix to fix the cells throughout the sample. Dempster (1960) has shown that fixatives obeyed the diffusion laws, that is, the depth penetrated (d) was proportional to the square root of time and the coefficient of diffusibility of the fixative, which was specific for each fixative. As the diffusion is directly proportional to the concentration gradient based on Fick's Law (Mehrer, 2007), the diffusibility of the fixative molecules (PFA, FA, GA) through the extracellular matrix of the tissue will undoubtedly be less than that for water molecules because of their different molecular shape and molecular weight. Thus, the diffusibility of the fixatives will be markedly less than that of water, leading to a greater shrinkage effect in thicker and denser tissues such as bone/cartilage, compared to 'soft' tissues such as brain and kidney (see Figure 4.6(B) that illustrates the comparative diffusion rate of fixative and water into the bone tissue). For thick tissues where preservation of cell morphology deep in the tissue is of importance, osmotic adjustment with lower fixation concentrations and longer fixation times would be advisable. Most workers set the fixation period using conventional fixatives of between 1- 4 hrs, or even longer (Hopwood, 1969). The optimum time will depend on several factors including the physical properties of the tissue (*e.g*. bone/cartilage *vs* brain) concentration of the fixative and thickness of tissue sections. Higher fixative concentrations require shorter fixation times (Monis *et al*., 1965) whereas thicker blocks and harder tissues will necessitate longer fixation times as the penetration of the fixative will be slower.

The present results demonstrated that the shrinkage artifact could also be significantly reduced - although not abolished - when the bone was bisected before being fixed in standard (high osmolarity) fixative solutions (Fig. 4.3). Bone bisection would markedly reduce the physical obstacles and diffusional distances thereby providing a more direct and far more rapid exposure of the GPC that were being visualized to the fixative solutions. The rate of fixation would thus be much more rapid compared to GPC within intact bone (Figure 4.6(B)), although the fact

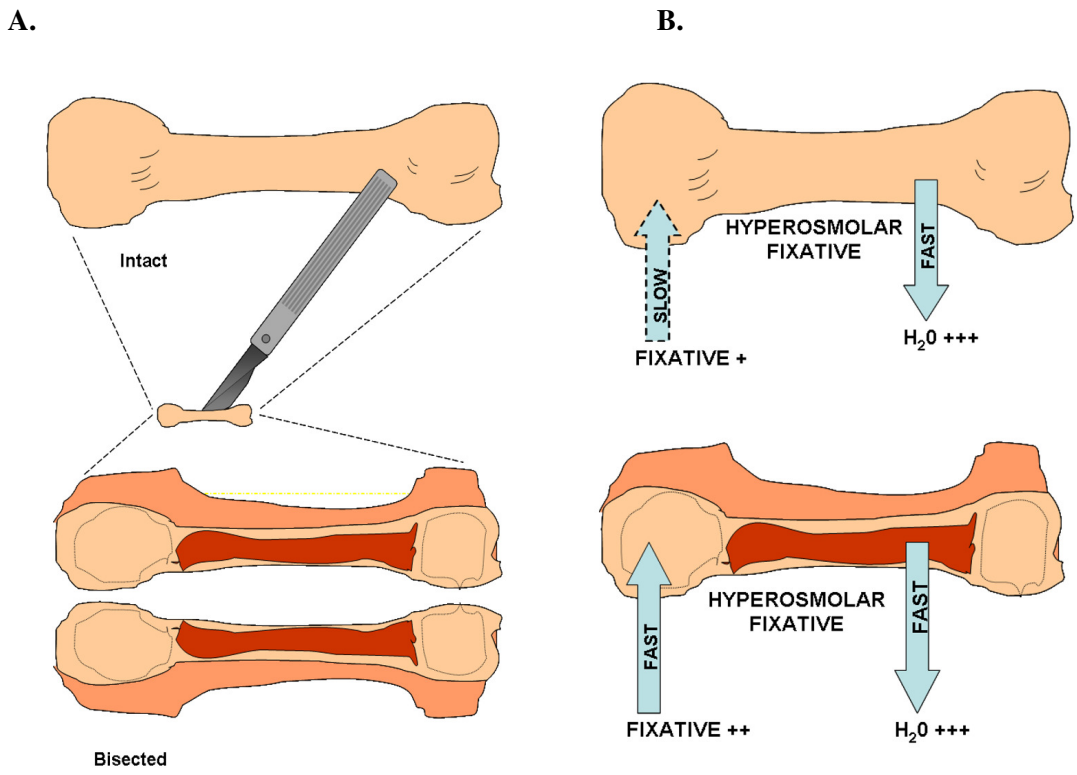

Figure 4.6 A-Schematic illustration of intact and bisected bones; B- The rate of fixative and water diffusion into the intact bone compared to the bisected bone.

that the shrinkage artifact was still present indicated that despite the increased access provided to the fixative, significant cell shrinkage still occurred before the tissue was effectively fixed (Fig. 4.3). However, the drawback with bone bisection as a manoeuvre to reduce the fixation artifact would be that it could cause physical trauma/death to the cells at the cut edge (Huntley *et al*., 2005) and unless care was taken with imaging protocols by optically sectioning deeper into the tissue, the damaged surface cells would be the ones that are visualized. Bone bisection would also release internal (physiological) pressures within the bone and result in the loss/damage to matrix constituents (loss of proteoglycans, damage to the collagenous network, altered ionic/osmotic environment) potentially leading to changes to the *in vivo* properties (volume/morphology) of chondrocytes prior to fixation (Guilak and Mow, 2000).

The present measurements of cell shrinkage by a histological method (Fig. 4.2A, B; Fig. 4.3) were supported to some extent by volume analysis of fluorescently-labeled living *in situ* GPC images taken by CLSM (Figure 4.5 and Table 4.4). Although the latter technique was more time-consuming, it served as a useful additional and direct measure of cell volume to confirm the cell shrinkage due to hyper-osmolar fixatives. The results from this method clearly showed the reduction in the cell volume of chondrocytes fixed with PFA (4%) in intact bone compared to bisected bone (Table 4.4). However we would have expected that in parallel with the histological shrinkage measurements (Fig. 4.3A & B), the volume of cells within the bisected bone samples would not have been reduced in the PFA solution to the same extent as cells fixed with the osmotically-corrected fixative solution. At present no explanation could be given for this finding, but it was noted in the present study that the volume method was not as sensitive for detecting the chondrocyte shrinkage compared to the histological method.

Both of these approaches provided us with more accurate quantitative measurements of the cell shrinkage artifact, compared to previous indirect methods *e.g*. counting the number of cell nuclei per unit area of tissue (Fox *et al.,* 1985). Previous studies had suggested fixation artifacts arose from subsequent steps in tissue processing *e.g*. during ethanol-induced dehydration and embedding

(Hopwood, 1969). However the present data suggest that before it is possible to determine these secondary artifacts resulting from further preparation of tissue for histological analysis, it is essential that as far as possible the fixed tissue was as close as possible to its native state by abolishing the osmotic shrinkage artifact reported here.

In summary, the present study demonstrated that the high osmolarity of conventional fixatives caused a shrinkage artifact to chondrocytes within the hypertrophic zone of the mammalian growth plate. This was particularly noticeable when whole bones were fixed, but was still present when the bones were bisected prior to fixation. This problem could be avoided by adjusting the osmolarity of the fixatives to the osmotic pressure of normal extracellular fluids (~280 mOsm). In conclusion, in order to preserve the normal volume/morphology of cells within tissue samples, careful consideration should be given to the osmotic pressure of the fixative solution.

Chapter 5

The Role of Sodium–Hydrogen and Anion Exchangers in Longitudinal Bone Growth

5.1 Introduction

Longitudinal bone growth occurs by endochondral ossification in which cartilage is first formed, calcified and then replaced by bone tissue. Central to this process is the growth plate (GP), in which chondrocytes undergo proliferation, hypertrophy and extra-cellular matrix secretion (Gerber *et al.,* 1999; Olsen *et al.,* 2000; Mackie *et al.,* 2008). The hypertrophic differentiation has a significant contribution to longitudinal growth as the chondrocyte height can increase by 6 to 10-fold during the terminal stage of hypertrophy (Hunziker *et al.,* 1994). This contributes up to 60% of the overall longitudinal growth of rats (Wilsman *et al.,* 1996b). Until now the mechanism(s) that regulates the GP hypertrophy has received relatively little attention. However one possible mechanism has been proposed to involve the plasma membrane transporters (Bush *et al.,* 2008b; Bush *et al.,* 2010).

The existence of both anion exchanger (AE) and sodium-hydrogen exchanger (NHE) has been described in virtually all tissues and cells (Wakabayashi *et al.,* 1997; Romero *et al.,* 2004). These transporters are always coupled functionally to sustain the normal physiological cellular milieu (Hofmann and Simonsen, 1989; Jiang *et al.,* 1997, Lang *et al.,* 1998; Alrefai *et al.,* 2000). AEs, which exchange chloride for bicarbonate (Boron, 2001), are vital for several physiological processes including the carbon dioxide (CO_2) carriage from the systemic capillaries to the pulmonary capillaries, the secretion or resorption of acid-base equivalents by a range of epithelia (*e.g.,* $NaHCO_3$ reabsorption by the kidney, HCl secretion by the stomach), NaCl reabsorption by certain epithelia (*e.g.* ileum, proximal colon), and the regulation of intracellular pH in nearly every cell of the body (Romero *et al.,* 2004). It was also shown to have a possible role in cell volume regulation albeit not in all type of cells (Alper, 1991; Guizouarn *et al.,* 2001). For NHE, it mediates transmembrane exchange of sodium for hydrogen (Malo & Fliegel, 2006), and specifically plays a critical role in cellular homeostatic processes by maintaining intracellular pH, Na^+ concentration, and cell volume (Mahnensmith & Aronson, 1985; Seifter & Aronson, 1986). NHE is also involved in cell growth, proliferation and differentiation (Shrode *et al.,* 1997; Wang *et al.,* 1997), which implicates the transporter as being an important player in normal

developmental processes. NHE is also thought to be involved in cell apoptosis (Khaled *et al.,* 2001; Reshkin *et al.,* 2003; Wu *et al.,* 2004).

Given the broad range of vital roles played by the transporters in other cell types and tissues, it is perhaps surprising that relatively little is known about their exact role in growth plate chondrocyte. It is interesting to speculate their function in mediating transport of osmolytes and water into the cell through the osmotic gradient as normally occurs during regulatory volume increase (RVI) (Lang *et al.,* 1998; Waldeggar *et al,* 1998), which contribute to the net chondrocyte cell enlargement by swelling and hypertrophy (Bush *et al.,* 2008b).

Microarray analysis of the adult rat GP showed higher expression of a number of plasma membrane transporters in the hypertrophic zone (HZ) compared to the proliferative zone (PZ), which included the NKCC, GLAST and AE (Wang *et al.,* 2004; Bush *et al.,* 2006b; Bush *et al.,* 2010). This raises the question of whether the increased expression reflects their specific roles in chondrocyte hypertrophy. A previous study has suggested a possible role for NKCC and AE in growth plate chondrocyte (GPC) hypertrophy and longitudinal bone growth (Bush *et al.,* 2010). In this study, using a specific NKCC inhibitor (bumetanide), P7 rat metatarsal bone growth was significantly inhibited by 30% after 24 hrs culture. In the presence of the AE inhibitor, DIDS (4,4-diidothiocyano-2,2-stilbenedisulfonate) bone lengthening was further reduced by up to 80%. This finding suggests the possibility that more than one membrane transporters is involved in regulating the rate of longitudinal bone growth.

To expand the previous work that has suggested a role for NKCC1 in GPC volume increase (Bush *et al.,* 2010), the present study examined the role of AE and NHE in regulating the rate of longitudinal bone growth by studying the effects of their inhibitors namely DIDS and EIPA (5-(N-Ethyl-N-isopropyl) amiloride) respectively (Figure 5.1; Vigne *et al.,* 1984; Cabantchik & Greger, 1992; Shen *et al.,* 2002). The study was undertaken to test the hypothesis that AE or NHE have functional roles in GPC hypertrophy and consequently longitudinal bone growth, and this function would be impaired to some extent should the normal activity of

the transporters be inhibited. In the present study, histological examination on the GP was also performed using established methods to determine any changes to the

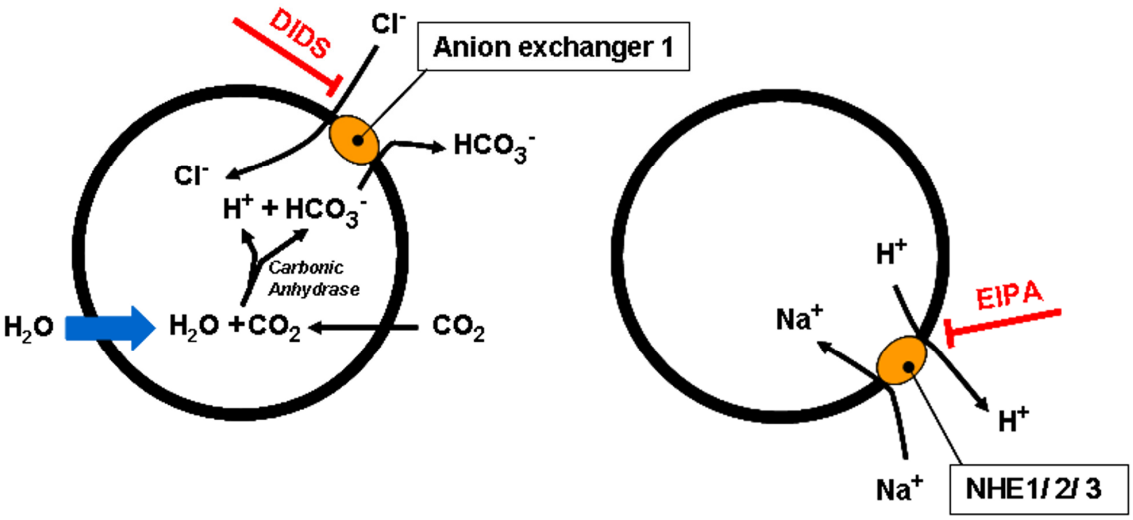

Figure 5.1 Schematic of AE and NHE transport activity. Adapted from Kunzelmann and Mall (2001); Seidler *et al.* (2001). An AE subfamily (Anion exchanger 1) and two NHE isoforms, NHE 2 or 3 (NHE 2/3) are indicated. The inhibitors of these systems are also shown. DIDS, 4,4'-diisothiocyano-2,2'-stilbenedisulfonate; EIPA, isopropylamiloride.

height of the HZ as a result of the AE and NHE inhibition (Bush *et al.,* 2010). The HZ cell volume of *in situ* GPC treated with the inhibitors was also examined to determine the effect of the drugs on cell enlargement. Cell viability tests on living *in situ* GPC of post natal rat metatarsals were also conducted after the drug treatment to rule out bone growth cessation caused by possible cytotoxic effect of the inhibitors. To further confirm this, the cell density in the HZ was also studied to ensure no significant decrease in the HZ cell numbers following treatment with the inhibitors. Micro-computed tomography (micro-CT) was also undertaken to examine if the effect of the drugs on the bone growth lengthening might be influenced by changes in the physical bone morphometry. The *ex vivo* experiment was repeated in foetal mouse metatarsals to allow observation of the DIDS and EIPA effects on longitudinal bone growth beyond 24 hrs period and to study the

difference in bone growth response to the drugs in foetal compared to postnatal GP, and between 2 species namely mice and rats.

5.2 Materials and Methods

5.2.1 Animals and Growth Plate Tissue Preparation

5.2.1.1 Seven-day-old Post Natal Rat Metatarsals

Metatarsals from forty-nine P7 Sprague-Dawley rats were prepared using the method that has been described in 2.2.1. For inhibitor dose-response curve experiments, whole metatarsal rudiments from n=40 animals with intact growth plate cartilage were dissected and temporarily placed in bone dissection media. The overall length of the metatarsal rudiments was measured as described below (5.2.2) before being cultured individually in 1 ml standard culture media supplemented with different concentrations of DIDS or EIPA (Figure 5.2). For DIDS inhibition experiments, 24 metatarsal bone rudiments were pooled from four animals, and 4 bones from different animals were each cultured in five different final concentrations of DIDS (50, 100, 250, 500 and 1000 μM). For EIPA inhibition study, a minimum of 8 bone rudiments pooled from 36 separate animals were cultured in each 7 different final concentrations of EIPA (28, 56, 111, 222, 444, 888, and 1333 μM). The vehicle-alone control was prepared by adding the standard culture media with the vehicle without the inhibitor (potassium bicarbonate for DIDS; and DMSO for EIPA). All the bone rudiments were maintained at 37^{o} C (CO_2 5%: air 95%; pH 7.4) for 24 hrs, before the second bone length measurement was taken.

For histological analysis, 6 metatarsal rudiments from 6 different animals were cultured in each of four treatment groups namely 250 μM DIDS, 444 μM EIPA and their controls. Bone rudiments were maintained at 37^{o} C for 24 hrs as mentioned above, and then fixed (see below) for paraffin wax embedding (see below). These concentrations of inhibitors were chosen because these were the minimal concentration of the inhibitors that were found to give maximum growth inhibition to the whole metatarsal rudiment culture (see Results; Figure 5.3).

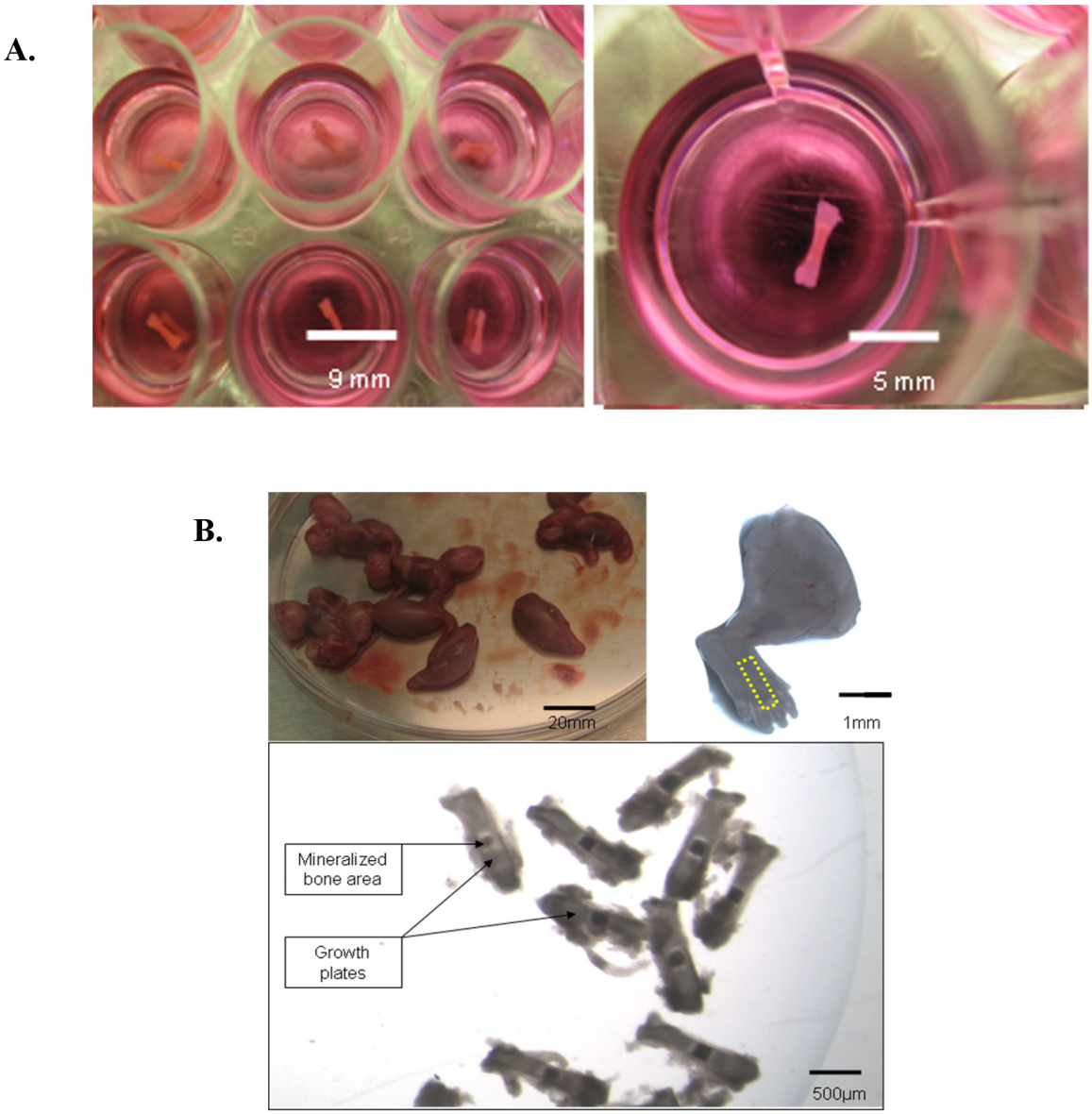

Figure 5.2 *Ex vivo* rat and mouse metatarsal bone culture. (**A**) The P7 rudiment bones were individually cultured in 24-well plate with bone culture medium with or without the DIDS and EIPA inhibitors and incubated for 24 hrs (left). The right figure is the close-up image of an individual bone culture from the 24-well plate. The bone measurement was performed initially at 0 hrs and repeated 24 hrs later (see the Materials & Methods). (**B**) The mice foetal rudiment bones were collected E18 mice (left upper panel) and the middle three metatarsals from the hind limbs were isolated (a single mid-metatarsal is shown within the rectangle, upper left panel) and pooled together (lower panel) before individually cultured in 24-well plate with bone culture medium with or without the presence of the DIDS and EIPA and incubated for 7 days (see the Materials & Methods).

For *in situ* GPC volume analysis, 18 metatarsal rudiments from 6 rat pups were used. At least three bones from different animals were each cultured in medium supplemented with inhibitors with final concentrations of (i) 0 μM DIDS (vehicle alone), (ii) 250 μM DIDS, (iii) 0 μM EIPA (vehicle alone), and (iv) 444 μM EIPA. All the bone rudiments were maintained at 37^{o} C for 24 hrs as described above. Bones were then washed in fresh culture media before being bisected sagitally, and incubated with the CMFDA, 5μM for 60 mins. Then, they were fixed in 4% (v/v) paraformaldehyde (PFA) overnight, and stored at 4^{o}C in PBS until analysed using a CLSM.

For *in situ* GPC viability test, at least three bones from each different treatment group as described for the GPC volume analysis above were prepared. After 24 hrs incubation at 37^{o} C, bones were washed, sagitally bisected and then exposed to CMFDA or calcein AM (5 μM) concomitantly with PI (5 μM) for 60 mins. CMFDA or calcein was used to label the viable cells, whereas PI the dead cells (see 2.3.4). The region of interest (ROI; Figure 5.4) incorporating the proliferative and the hypertrophic zones of the GP was viewed under low power CLSM lens (x10 dry objectives). Cell viability was evaluated qualitatively by comparing the distribution of dead over the live cells within the ROI between treatment groups.

For the micro-CT analysis, 16 metatarsal rudiments from 4 rat pups were used. Four bones from 4 separate animals were cultured in each of 4 different medium treatments as described for the GPC volume analysis experiment above. After 24 hrs, the bones were fixed in 70 % ethanol until analysed.

5.2.1.2 Eighteen-Day-Old Embryonic Mouse Metatarsals.

The experimental protocol was described in 2.2.2. The middle three metatarsals were aseptically dissected under a dissecting microscope from up to ten 18-day-old embryonic Swiss mice (E18; Figure 5.2(B)). All the bones were pooled together before being cultured individually in each well of a 24-multi-well plate. Six bone rudiments were assigned to each treatment groups: (i) 0 μM DIDS (vehicle alone), (i) 100 μM DIDS, (ii) 250 μM DIDS, (iii) 0 μM EIPA (vehicle alone), and (iv) 200 μM EIPA. Membrane transporter inhibitors (EIPA or DIDS, where appropriate)

were added to the cultured bones. Each culture well contained 300 µl of a standard culture medium with the different treatments, and placed at 37^{o} C in a humidified atmosphere of 95% air / 5% CO_2 for up to 11days. In all experiments, the medium was changed every second/third day. For histology, a total of 2 bones from DIDS control, 3 bones from 250 µM DIDS and 4 bones from the rest of treatment groups above, were fixed at d 11 and prepared for histological examination as described later.

5.2.2 Measurement of Whole Metatarsal Rudiment Length

For P7 rat metatarsals, images (640x480 pixels) of rudiments were acquired immediately after dissection and after 24 hrs in the presence or absence of DIDS/EIPA, using an eyepiece camera (DCM 35 350K Pixel Digital Eyepiece Camera, Brunel Microscopes, U.K.) fitted to a dissecting stereomicroscope (Wild M3, Switzerland). An image of a rule was acquired to provide calibration, and bone lengths were measured using ImageJ software (National Institutes of Health, Bethesda, Maryland, U.S.A.).

For E18 mouse metatarsals, the bone rudiment length was taken using a digital camera (COHU, San Diego, CA) attached to an Eclipse T300 inverted microscope (Nikon, Surrey, UK) on day 0, 3, 5, 7 and 11. The total lengths of the bones were determined using Image Tool (Image Tool version 3.00, University of Texas Health Life Science Centre, San Antonio, Texas). All results are expressed as a percentage change from the length at day 0, which was regarded as baseline to demonstrate the rate of growth over time.

5.2.3 Histology of the Growth Plate

The metatarsals were fixed overnight with GA (1.3% v/v with 0.5% w/v RHT) or PFA (4% w/v in 0.01M phosphate buffer; pH 7.4). The histological sections were prepared as described in 2.3.2. For P7 rats, the sections were stained with 0.1% toluidine blue O, whereas for E18 mice with Hematoxylin and Eosin (see 2.3.3).

E18 mouse metatarsal bone histological sections were examined under a Leica DMR microscope (Peterbrough, U.K.) which connected to a Leica DFC 490 digital camera (Peterbrough, U.K.). Image acquisition and analysis was performed

with the Leica application suite (LAS, Peterbrough, U.K.) software in conjunction with the use of the microscope and digital camera. Histological evaluation of the sections under high magnification views was made based on identification of various zones of chondrocyte differentiation in foetal mouse metatarsals as previously reported (Van Bezooijen *et al.,* 2002). P7 rat metatarsal histological sections were examined using CLSM (see 5.2.4 below).

5.2.4 Measurement of Growth Plate Length and Cell Density

Images of distal growth plates were taken using the transmitted light detector of an upright confocal laser scanning microscope (Zeiss LSM510, U.K.) fitted with a x10 dry objective lens. To determine the beginning and terminal points of the GP, several subjective criteria based on the cell size and organization were used as described in 2.5.1. The GP length and the late HZ height were then identified and measured using an established procedure that has been described previously (Bush *et al*., 2010). Briefly, three zones were identified by eye and marked by drawing a horizontal freehand line along the top of the proliferating cells border, the clear demarcation of cell enlargement between proliferative and hypertrophic regions, and the zone of mineralization at the base of the hypertrophic zone. Another straight line was drawn vertically at right angles along the mid GP section (Zeiss LSM Image Browser Software, Carl Zeiss Microlmaging GmbH, Germany) (see Fig. 5.6). The GP length was determined from the distance between the two points where the vertical and horizontal lines met most proximally and distally using ImageJ software (National Institutes of Health, Bethesda, Maryland, U.S.A.). The late HZ height was determined from the distance between the two points the lines met at the PZ-HZ cell enlargement regions proximally and the zone of mineralization distally. The total number of cells within the late hypertrophic zone was counted by eye and the surface area of the zone was selected using freehand selection and measured using ImageJ. The cell density was determined based on the total cell numbers counted over the measured area of the late HZ (cells/mm^2).

5.2.5 Confocal Laser Scanning Microscopy

An upright Zeiss Axioskop LSM 510 CLSM was used to acquire fluorescent images of *in situ* proliferative and hypertrophic growth plate chondrocytes. The same protocol as described in 2.4.2 was used.

5.2.6 *In Situ* Cell Volume Measurement

Whole growth plates imaged from the proliferative to hypertrophic zones were divided into eight equal parts and labeled S1 to S8 (see 2.5.1) and volume analysis was performed on scanned CLSM images using the previously described method (2.5.2).

5.2.7 Micro-CT Analysis

The micro-tomography was performed using established method as has been previously reported (Idris *et al*., 2009). Briefly, the metatarsal bone rudiments were scanned (300 slices directly distal of the growth plate) using SkyScan 1172 instrument (Kontich, Belgium) set at 60 kV and 167 μA, at a resolution of 4.9 μm. The images were reconstructed using the SkyScan NRecon program and analyzed using SkyScan CTAn software (Aartselaar, Belgium).

5.3 Results

5.3.1 DIDS and EIPA Treatment in P7 Rat Metatarsal Bone Culture (24 hrs)

5.3.1.1 DIDS and EIPA Dose–Response Curve

In order to study the roles of AE and NHE on bone lengthening, the effects of the inhibition of the membrane transport systems by DIDS or EIPA was studied.

The mean increase in bone length from the overall baseline length in the control medium was 6.2 ± 1.3% (n=4) over 24 hrs. Exposure to DIDS (0-1 mM) for 24 hrs resulted in dose dependent reduction of bone lengthening (Figure 5.3(A)). The rate of reduction was most dramatic in 50 μM DIDS solution, bone lengthening reduced to 1.9 ± 0.9% (n=4), and all [DIDS] tested resulted in a significant reduction in longitudinal growth (unpaired Student's *t*-Test; $P<0.05$; n=4). A DIDS concentration of 250 μM appeared to provide maximal inhibition

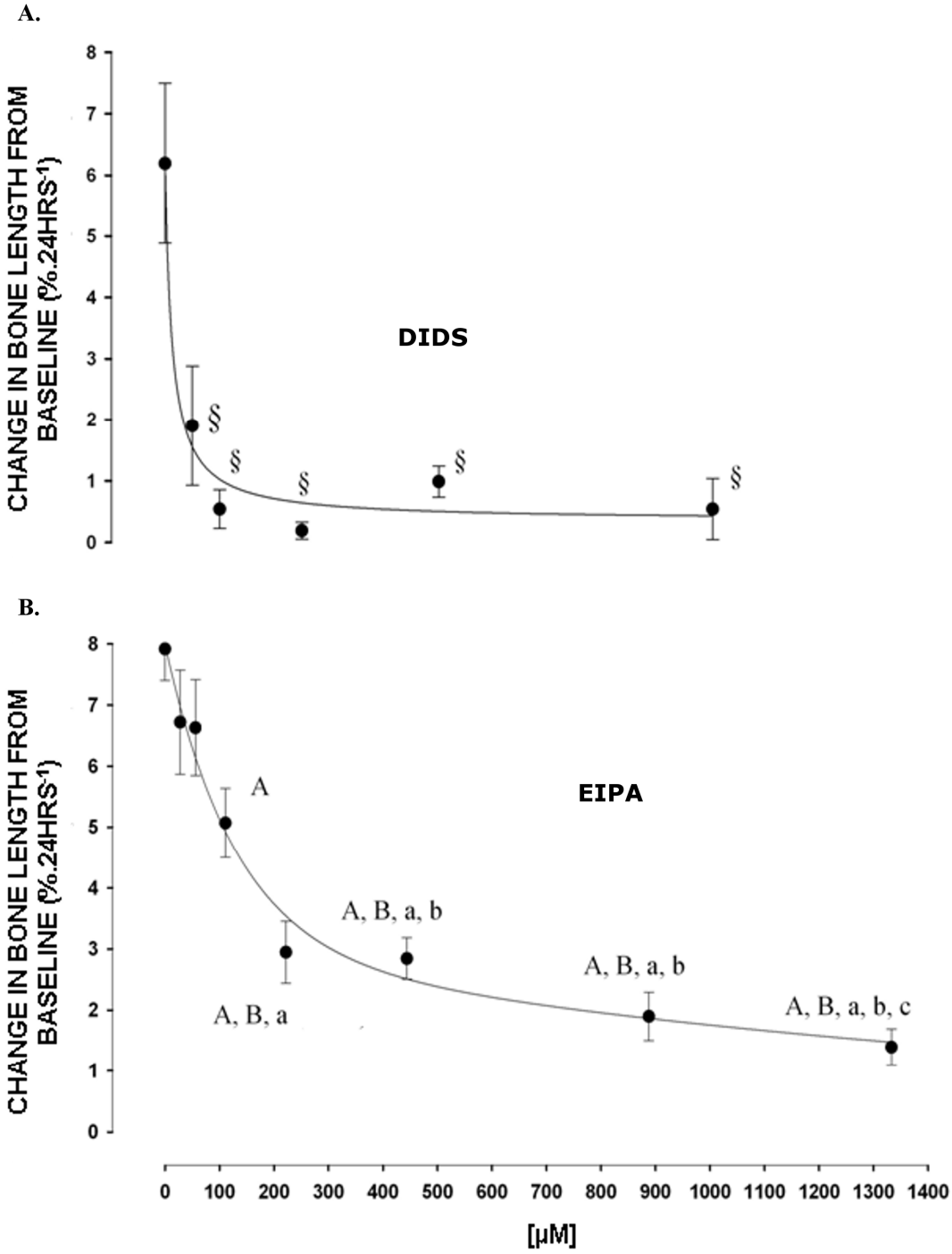

Figure 5.3 The inhibitory effect of the DIDS and NHE EIPA on rat metatarsal bone rudiment growth. **A**. Five different final concentrations of DIDS were used in the dose-response curve experiment (see the Materials and Methods). Each data point contains results from four metatarsals (n=4) from four different animals which were cultured for 24 hrs in the presence/ absence of the drugs at the concentration as shown. The mean bone increase was measured as described in Materials and Methods. There was a dose dependent relationship for DIDS

inhibition, individual points were significantly different from control (contains no DIDS) with all the other DIDS concentrations ($^{\S}P<0.05$; unpaired Student's t-test). **B**. The effect of metatarsal mean bone increase in response to the increasing EIPA concentrations is shown. Each data point contains a number of metatarsals (n) each pooled from different individual animals which were cultured in the presence/ absence of EIPA in the shown concentration for 24 hrs and measured (see Materials and Methods). There was a dose dependent relationship for EIPA inhibition, and some individual points were shown as significantly different (unpaired Student's t-test; $P<0.05$) from control (no EIPA) and from lower concentration treatment groups when the indicated data point was compared to ^{A} control, ^{B} 28 μM, ^{a} 56 μM, ^{b} 111 μM and ^{c} 222 μM. Data expressed as means ± S.E.M.

and was therefore used for the remaining studies. Figure 5.3(B) illustrates the effect of EIPA (0-1.3 mM) on metatarsal bone longitudinal growth. The mean control bone length increase after 24 hrs was 7.9 ± 0.5% (n=36). A one way ANOVA study demonstrated a significant trend of overall bone longitudinal growth decrease as the DIDS concentrations increased ($P<0.001$). *Post-hoc* pairwise (*vs* control) comparison analysis (Holm-Sidak method) showed a significant overall bone lengthening difference from the control ($P<0.05$).

EIPA resulted in a dose dependent decrease in bone lengthening, but only becoming significantly reduced at an [EIPA] of 111μM and above (unpaired Student's *t*-Test; $P<0.05$; at least n=8). Whilst an EIPA concentration of 1.3 mM showed the maximum reduction of bone lengthening (1.4 ± 0.3%), 444 μM was the lowest concentration that produced the optimal reduction of bone lengthening and was therefore used in the later experiments. The effective concentration of EIPA which resulted in a 50% inhibition (EC_{50}) was approximately 250 μM. A one way ANOVA study showed a significant trend reflecting overall bone growth decrease as the EIPA concentrations increased ($P<0.001$). *Post-hoc* multiple comparison analysis against the control (0 mM)(Holm-Sidak method) showed a significant bone lengthening difference in 111, 222, 444, 888, and 1333 μM EIPA-treated groups ($P<0.05$).

This result showed dose-response relationship between the DIDS or EIPA to the bone lengthening growth and the DIDS effective at lower concentrations compared with EIPA.

5.3.1.2 Viability of the GPC after Treatment with DIDS and EIPA

DIDS and EIPA could potentially induce cell cytotoxicity or cell death in some cells (Lieu *et al.,* 2008; Park *et al.,* 2009). This could consequently impair the bone lengthening growth and give a false indication that the decrease in bone growth is a result of the inhibition of their respective transport system by the drugs. To rule out this, a cell viability test was undertaken on the GPC after the 24 hrs treatment with 250 μM DIDS or 444 μM EIPA. Bisected metatarsal bones were incubated in CMFDA or calcein AM concomitantly with the PI to examine and compare the ratio of dead: living *in situ* cells (see Materials and Methods). Figure 5.4 shows viable intact CMFDA-labelled cells could be observed in all bones after 24 hrs incubation in the drugs. Although DIDS control bone appeared to reveal more PI-stained cells than the other groups in the Figure 5.4, the overall examination on the rest of the GP sections showed no clear difference in dead cell ratio over live cells observed between the treatment group (250 μM DIDS or 444 μM EIPA) and the controls. This suggested that the reduction in the bone growth was likely not to be associated with cytotoxic or apoptotic induced effects of the inhibitors.

5.3.1.3 Gross Morphology of the Bones Post Treatment

There was no obvious difference in the gross appearance and morphology of rat metatarsal bone after 24 hrs treatment in DIDS compared to the control (Figure 5.5(A & B) far left respectively). However, EIPA-treated bones showed that the diaphyseal zone looked paler in colour (Figure 5.5(D) far left) when compared to the control (Figure 5.5(C) far left) after 24 hrs. This raised question of whether EIPA caused any changes to the morphometric properties of the treated bones and this was studied in the following section.

5.3.1.4 Three-Dimensional Morphometric Parameters Analysis of the Treated Bones

To examine whether the morphological changes observed in EIPA-treated metatarsal involved changes in bone mineralization particularly at the diaphyseal region, micro-CT scanning was undertaken to evaluate the three-dimensional

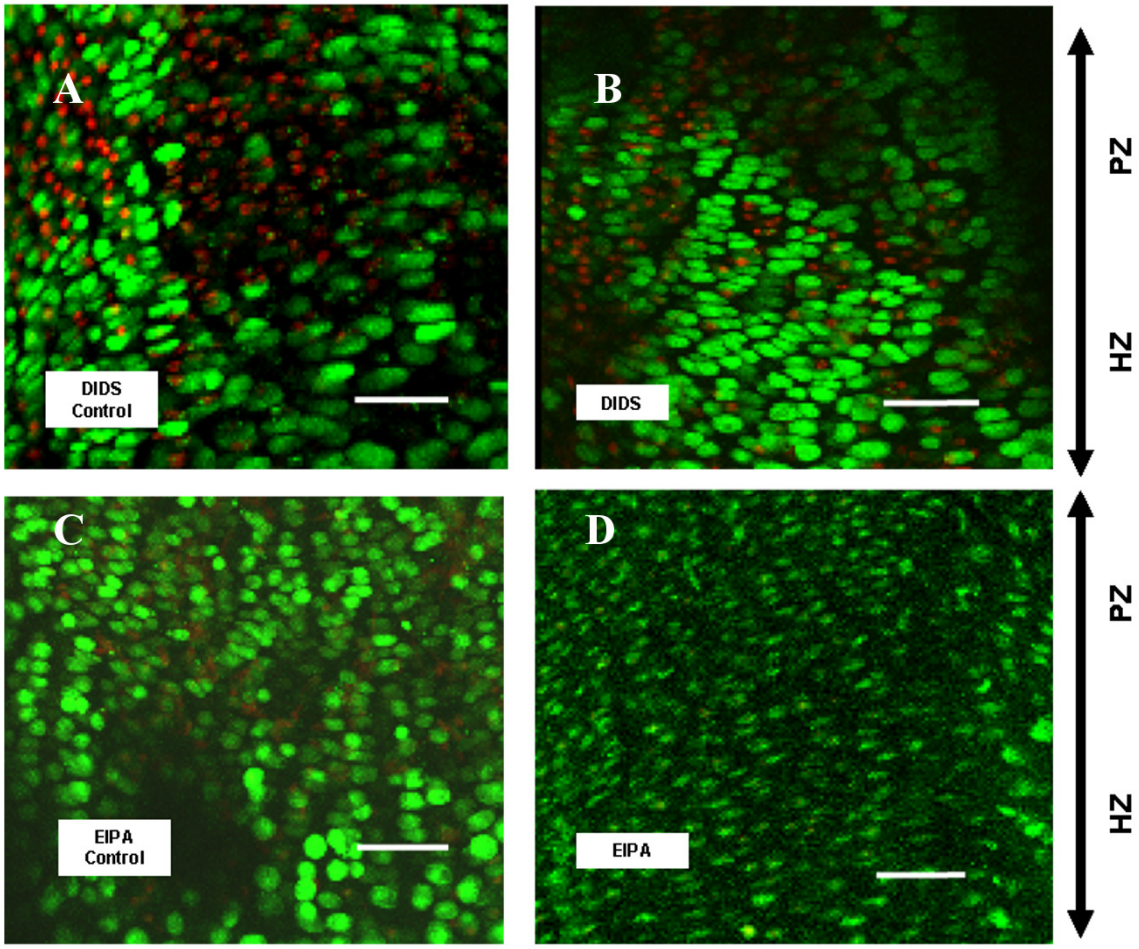

Figure 5.4 DIDS or EIPA caused no apparent effects on the GPC viability. P7 rat metatarsal bones were bisected and incubated in CMFDA fluorescent dyes and PI, fixed and then viewed using low power objective lens of confocal microscope following 24 hrs treatment with the DIDS (250 μM) and EIPA (444 μM). The similar ROI (proximal GP) was identified in all bones, and the cells viability were determined by whether the cells were positively stained by the CMFDA or calcein AM (live cells) or PI (dead cells): **A**. DIDS control, **B**. DIDS-treated, **C**. EIPA control, **D**. EIPA-treated. HZ, hypertrophic zone; PZ, proliferative zone Scale bar = 50 μm in all panels.

morphometry of the bone specimens after the EIPA treatment. For a comparison, the micro-CT scanning on DIDS-treated bones and the controls were also undertaken. Figure 5.5(A-D) (middle and far right), showed the 3-D reconstructed micro-CT images of the metatarsal bones as viewed at upright-lateral (middle) and ventral-dorsal (right). No clear differences (unpaired Student's t-test; $P>0.05$) in three dimensional structural changes were observed between the different treatment groups. All metatarsals showed the absence of mineralization in the trabecular bones of the diaphyseal area as shown by hollow bone shaft. The diaphyseal cortical bone thickness between treatment groups and controls showed no clear difference. In addition to the visual assessment of the bone microarchitecture, analysis was made on the following morphotomographic determinations: (i) bone density (grayscale index), (ii) tissue volume (μm^3), (iii) bone volume (μm^3), (iv) percent of bone volume (%),v. bone surface/ volume ratio ($x10^{-3}$ μm^{-1}), (vi) trabecular thickness (μm), (vii) trabecular separation (μm), (viii) trabecular number (μm^{-1}), (ix) degree of anisotropy (DA), and (x) total porosity (%). The results of the analysis were tabulated in Table 1 and revealed no significant difference in the effect of DIDS or EIPA to the bone morphometric parameters.

5.3.1.5 Histological Measurement of the GP Length and Late HZ Height Following Treatment

Having recorded the dose-response relationship between the DIDS or EIPA with *ex vivo* bone longitudinal growth (Figure 5.3), the histological changes were then examined. Emphasis was placed on the GP HZ cells, as the size of these cells are the key determinant to the rate of longitudinal bone growth (Wilsman *et al,* 1996b). The total length of the GP, the height of the late HZ and the cell density in the late HZ were measured (see Materials and Methods; Figure 5.6). Table 5.2 shows the histological analysis results of the metatarsals cultured in the presence or absence of DIDS (250 μM) or EIPA (444 μM). There was no significant difference in the total growth plate length between the control and DIDS treated group (657 ± 99μm and 670 ± 76μm respectively; unpaired Student's *t*-Test; $P>0.05$; n=4 to 6). Similarly there was no significant difference in the total growth plate length

between the non-treated and EIPA-treated group (683 ± 99µm and 668 ± 68µm respectively; $P>0.05$). The height of the HZ in the control was also not significantly different from the DIDS-treated GP (144 ± 18µm and 116 ± 11µm respectively; $P>0.05$). Likewise, there was no significant difference between the height of the HZ in the control as compared to the DIDS-treated GP (147 ± 19µm and 117 ± 19µm respectively; $P>0.05$). However, when HZ height was expressed as a percentage of the total GP length, the relative HZ height in the DIDS and EIPA-treated groups (17.5 ± 0.7% and 17.3 ± 1.5% respectively) were found to be significantly different compared to the controls (22.6 ± 1.8% and 21.9 ± 1.1%; unpaired Student's *t*-Test; $P<0.05$; n=4 to 6). This result reveals the effect of DIDS and EIPA on the HZ heights over the GP length, which possibly implies the perturbation of normal GPC hypertrophy in the presence of the drugs.

5.3.1.6 Histological Measurement of the Cell Density

The reduction in the size of the late HZ height over the total GP length was possibly as a result of changes in GPC size (*e.g.* caused by perturbation of normal cell enlargement) or the cell numbers (*e.g.* caused by cell death possibly associated with cytotoxic effect of the drugs). To further investigate this, the cell density in the HZ was measured. The result presented here (Table 5.2) showed no difference in number of GPC in the HZ of the DIDS and EIPA-treated metatarsals (4404 ± 884 cells/mm^2 and 4019 ± 1300 cells/mm^2 respectively) as compared to the controls (4383 ± 25 cells/mm^2 and 4007 ± 1316 cells/mm^2; unpaired Student's *t*-Test; $P>0.05$; n=3). This suggests that the transport protein inhibitors used did not cause significant hypertrophic GPC death, and confirms the finding from the viability assessments, which showed no evidence of direct effect of the inhibitors on the viability of living *in situ* GPC after 24 hrs culture period.

5.3.1.7 Effect of the GP and EIPA to the GPC Volume

Having established that the effect of the DIDS and EIPA was non-cytotoxic to the GPC, further examination of the effect of DIDS and EIPA inhibition on *in situ* GPC volume was made using CLSM technique. The reduction in cell enlargement should be detectable by volume measurement if the drugs inhibited normal cell

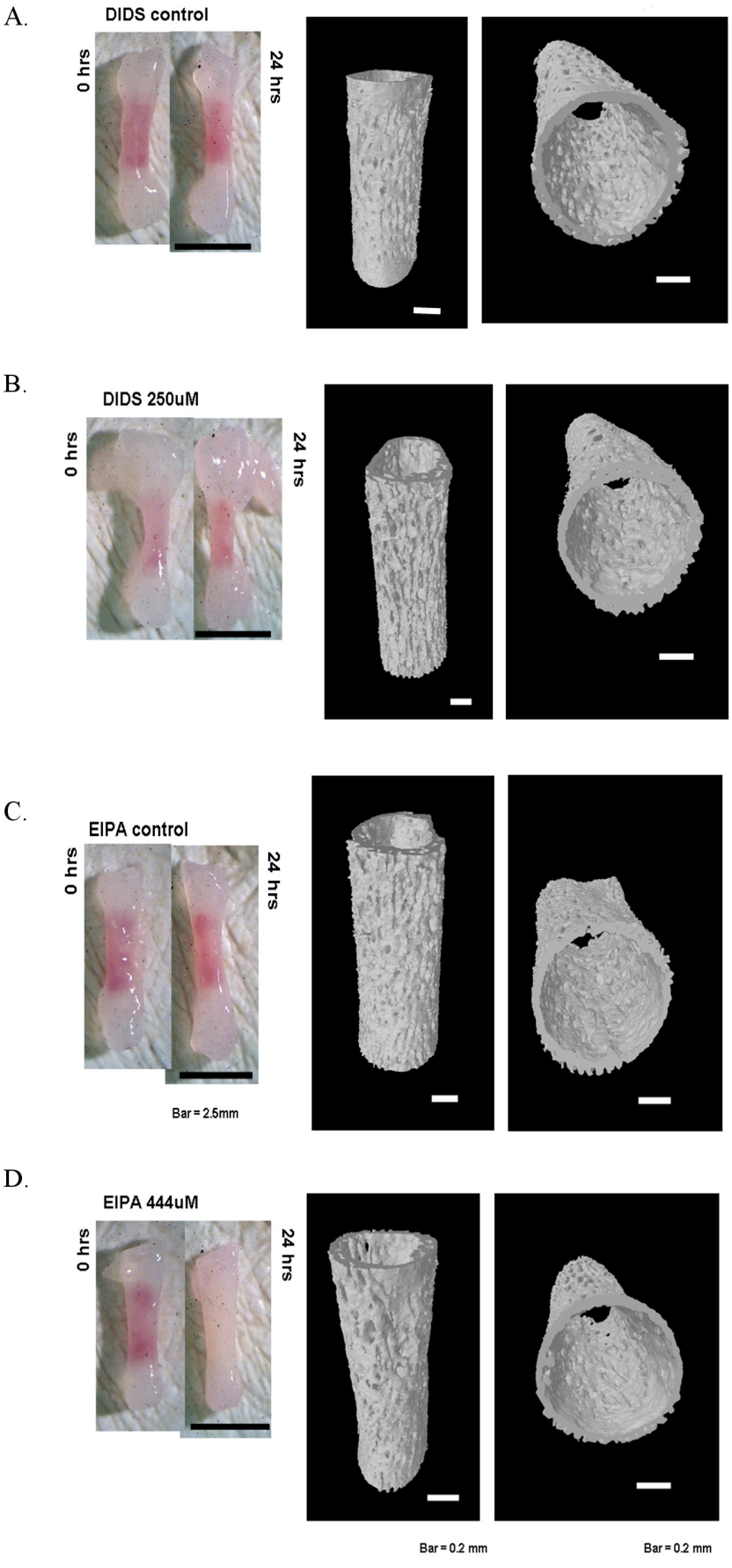
A.
DIDS control
0 hrs
24 hrs
B.
DIDS 250uM
0 hrs
24 hrs
C.
EIPA control
0 hrs
24 hrs
Bar = 2.5mm
D.
EIPA 444uM
0 hrs
24 hrs
Bar = 0.2 mm
Bar = 0.2 mm

Figure 5.5 Gross morphology and three-dimensional micro-CT images of metatarsal bones after DIDS or EIPA treatment. The far left images show the gross morphology of the bones before and after 24 hrs culture in each indicated treatment group: **A**. DIDS control, **B**. DIDS treated (250 μM), **C**. EIPA control, **D**. EIPA treated (444 μM). The middle and far right images showed the corresponding reconstructed three-dimensional micro-CT images after 24 hrs as viewed at two different angles: upright-lateral (middle) and ventral-dorsal (right). Scale bar = 2.5 mm in all gross morphology images and 0.2 mm in all the reconstructed 3-D micro-CT images.

enlargement. In these experiments, volume analysis was performed at the PZ (S1-P2) and the HZ (S7-S8; see Materials and Methods). Using a high power objective lens, no clear difference was observed in the appearance of the GPC treated with DIDS and the control (Figure 5.7 (A & B)). However there was a clear difference between the EIPA-treated GP and the control cell size (Figure 5.7 (C & D)). Volume analysis was also performed on the GPC in the PZ and HZ from the metatarsal bones of each treatment group (Table 5.3). The result showed the mean volume of the control cells in PZ (609 ± 46μm^3; 6[29]) was not significantly different from DIDS-treated (572 ± 71μm^3; 3[25]); unpaired Student's *t*-Test; $P>0.05$). Likewise, the mean volume of the control cells in HZ (1880 ± 230μm^3 6[44]) was not significantly different from the mean GPC volume in DIDS-treated GP (2660 ± 419 μm^3; 3[27]; $P>0.05$). On the other hand, there was significant difference between the mean volume of the control cells in PZ and HZ (761 ± 50 μm^3 (6[33]); and 2044 ± 219 μm^3 (6[38]) respectively) and the volume of the respective EIPA-treated cells in PZ (211 ± 26 μm^3; 3[15]) and HZ (586 ± 54 μm^3; 3[19]); unpaired Student's *t*-Test; $P<0.05$; n=3 to 6). Taken together, these data suggest that the DIDS treatment resulted in no significant changes to the size of the PZ cells and HZ cells whereas EIPA treatment resulted in a significant reduction in size of the cells of both the PZ and HZ.

Treatment [μM]	Bone density, BD (Grayscale index)	Tissue volume, TV ($x10^8$ μm^3)	Bone volume, BV ($x10^8$ μm^3)	Percent of bone volume, BV/TV (%)	Bone surface/ volume ratio, BS/BV ($x10^{-3}$ μm^{-1})	Trabecular thickness, Tb.Th (μm)	Trabecular separation, Tb.Sp (μm)	Trabecular number, Tb.N ($x10^{-3}$ μm^{-1})	Degree of anisotropy, DA	Total porosity, Po(tot) (%)
Control	101 ± 1	7.54 ± 0.35	1.69 ± 0.62	22 ± 1	65 ± 3	49 ± 1	232 ± 12	4.6 ± 0.1	1.60 ± 0.24	77.6 ± 4
DIDS [250]	100 ± 1	7.58 ± 0.32	1.77 ± 0.18	23 ± 1	67 ± 4	47 ± 1	221 ± 12	4.9 ± 0.3	1.91 ± 0.18	76.6 ± 1
Control	101 ± 3	13.23 ± 5.29	1.79 ± 0.89	18 ± 4	64 ± 1	49 ± 1	285 ± 60	3.7 ± 0.8	2.11 ± 0.30	78.4 ± 0.4
EIPA [444]	103 ± 2	8.04 ± 0.43	1.74 ± 0.88	22 ± 0	64 ± 1	49 ± 2	222 ± 11	4.4 ± 0.1	2.12 ± 0.28	81.8 ± 4.0

Table 5.1 Micro-CT bone mineral and morphometric analysis of metatarsal bones after DIDS or EIPA treatment. The metatarsals were from four P7 rats (n=4) that were cultured for 24 hrs in the absence/ presence of DIDS or EIPA at the indicated concentrations. Ten morphometric parameters were measured using SkyScan CTAn software from the reconstructed three-dimensional bone images acquired using micro-CT instrument (see Materials and Methods). Data were shown as means ± S.E.M.

DIDS CONTROL **DIDS**

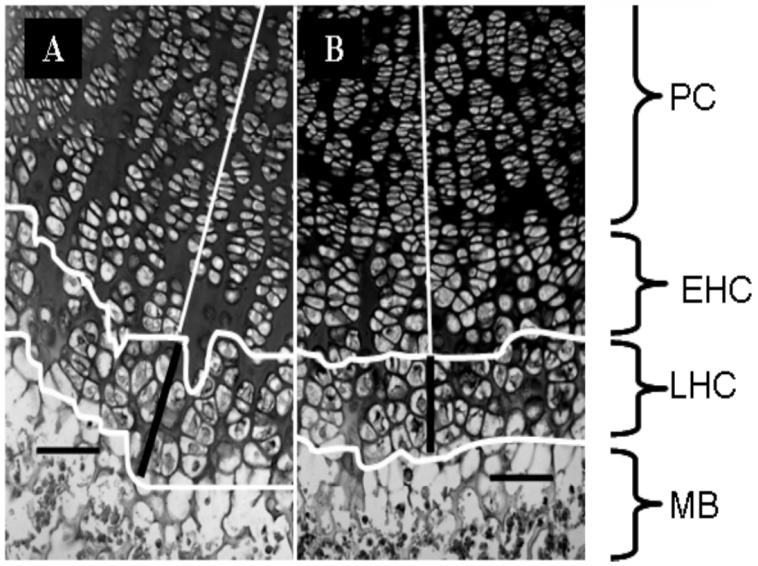

EIPA CONTROL **EIPA**

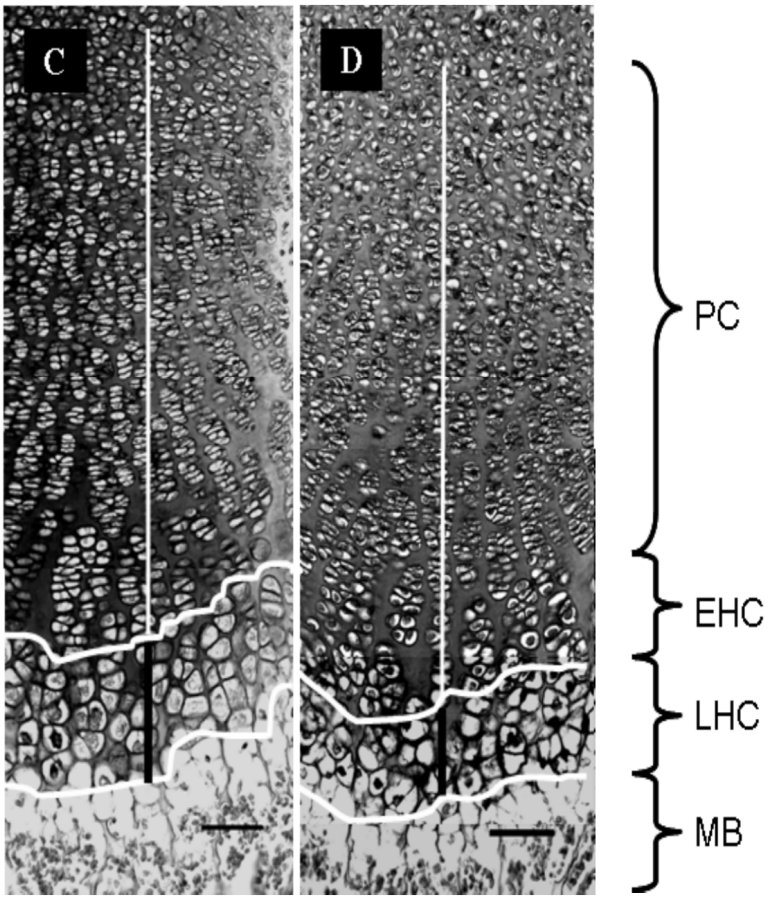

Figure 5.6 The total percentage height of the late hypertrophic GP zone decreased significantly in the presence of DIDS or EIPA. P7 rat metatarsal bones were fixed; sections prepared and stained with 0.1% Toluidine blue O following 24 hrs treatment with 250 μM DIDS or 444 μM EIPA. Using light microscopy the proximal GP was located and the late GP hypertrophic zone cells (LHC) were identified by eye in between the beginning of the late hypertrophic zone cells and the mineralized bone (MB) at the bottom (between the 2 horizontal lines). The vertical black line at the mid GP section and between the two horizontal lines indicates the average height of late hypertrophic GP zone in DIDS and EIPA-treated bones (**B & D**), and the controls (**A & C**). The straight black and white vertical line at the mid GP section were used to determine the total length of the GP as defined in the Materials and Methods. PC, proliferating zone cells; EHC, early hypertrophic zone cells. Scale bar =100 μm in all panels.

5.3.2 DIDS and EIPA Treatment in E18 Mouse Metatarsal Bone Culture

Having found the inhibitory effect of DIDS and EIPA on the post natal bone growth, the investigation was extended to foetal bones. Foetal mouse metatarsal bone cultures were treated with either DIDS or EIPA for seven days as described in Materials and Methods.

5.3.2.1 Foetal Metatarsal Gross Morphological Changes

Preliminary results (data not shown) showed clear abnormal gross morphology changes following treatment with 250 μM of DIDS. Therefore, a lower DIDS concentration (100 μM) was also used in the present study in order to compare the effect between the two different concentrations on bone morphology and particularly on bone lengthening growth. For EIPA, a preliminary experiment using 250 μM (as had been used in postnatal rat metatarsals) resulted in total bone growth arrest and poor bone morphology following 72 hrs of treatment. This raised concerns about possible cytotoxic effects incurred by the inhibitor at the given dose (250 μM; data not shown). Therefore slightly lower EIPA concentration (200 μM) was used in the present experiment on foetal mouse metatarsal bone culture.

Treatment [µM]	Total growth plate (µm)	Late HZ (µm)	HZ (% of total)	Treatment [µM]	Late HZ cell density (cell/mm^2)
Control (n=4)	657 ± 99	144 ± 18	22.6 ± 1.8	Control (n=3)	4383 ± 25
DIDS [250] (n=6)	670 ± 76	116 ± 11	17.5 ± 0.7*	DIDS [250] (n=3)	4404 ± 884
Control (n=5)	683 ± 99	147 ± 19	21.9 ± 1.1	Control (n=3)	4007 ± 1316
EIPA [444] (n=5)	668 ± 68	117 ± 19	17.3 ± 1.5*	EIPA [444] (n=3)	4019 ± 1300

Table 5.2 The effect of DIDS and EIPA on growth plate zone height and cell density. Distal metatarsals from three to six P7 rats were cultured for 24 hrs in the absence/ presence of DIDS or EIPA at the concentrations indicated. Bones were fixed, prepared, and visualized as described in Materials and Methods. There was significant reduction in height (%) of hypertrophic zone from the total height of the growth plate in DIDS or EIPA-treated bones. However the average height of growth plates and hypertrophic zone between control and treated bones were not significantly different. Hypertrophic zone cell density of treated bones also showed no significant difference from the control. * denotes significantly different from the corresponding control ($P<0.05$; unpaired Student's t-test). Data are shown as means ± S.E.M.

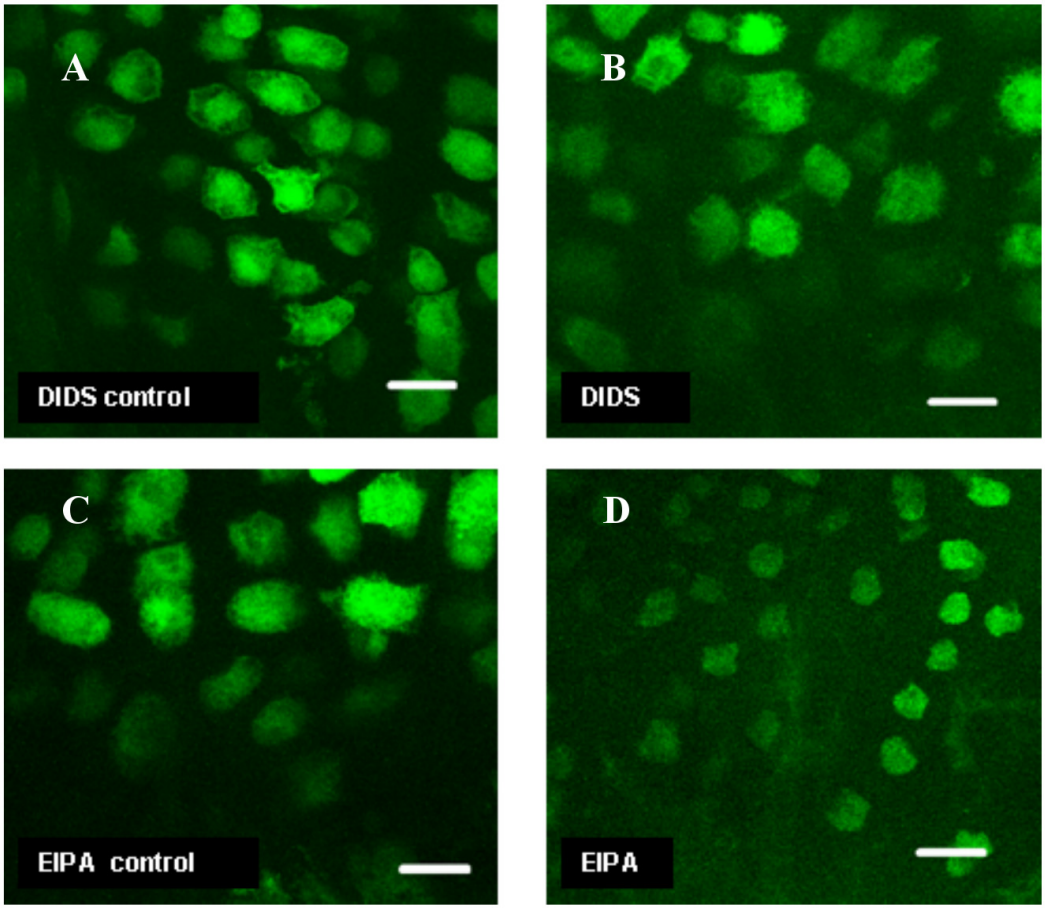

Figure 5.7 *In situ* GPC volume evaluation post 24 hrs of DIDS (250 µM) or EIPA (444 µM) treatment. Bisected bones as described in Figure 5.5 were then examined under high power magnification on the confocal microscope. The ROI was selected at PZ and HZ of the GP and the images were recorded for further cell volume analysis (see Materials and Methods). All the panels shown here demonstrate the HZ cells of the GP from different treatment groups: **A**. DIDS control **B**. DIDS-treated, **C**. EIPA control, and **D**. EIPA-treated. Scale bar = 20 µm in all panels.

Treatment [µM]	GPC volume (µm^3) from (n[N])	
	PZC (S1-S2)	**HZC (S7-S8)**
Control	609 ± 46 (6[29])	1880 ± 230 (6[44])
DIDS [250]	572 ± 71 (3[25])	2660 ± 419 (3[27])
Control	761 ± 50 (6[33])	2044 ± 219 (6[38])
EIPA [444]	211 ± 26* (3[15])	586 ± 54* (3[19])

Table 5.3 The effect of EIPA and DIDS on growth plate chondrocyte volume. Distal metatarsals from three to six P7 rats were cultured for 24 hrs in the absence/ presence of DIDS or EIPA at the concentrations indicated. Bones were bisected, loaded with fluorescent dye (CMFDA), fixed and visualized using CLSM technique as described in Materials and Methods. Data are given as means ± S.E.M. *Significant difference from the control (P<0.05; unpaired Student's t-test).

Figure 5.8 (panels A, D, G, J, M and P) shows the image of gross morphology of the intact foetal metatarsals at d 3 post treatment, as visualized and recorded using a digital camera (see Materials and Methods). No clear gross change to morphology was observed between the 100 μM DIDS treatment group (panel D) and the control (panel A) where the mineralized and non-mineralized zones looked similar. However, besides the straight bone shape formation (panel G) some bones in the 250 μM DIDS treatment groups also showed some degree of peculiar (crooked) bone deformity (panel J). For EIPA treated bones (panel P), there were no obvious changes in shape of the mineralized and non-mineralized zones compared to the control culture (panel M).

5.3.2.2 Longitudinal Bone Growth Measurement

As shown in Figure 5.9, at d 3 of E18 bone culture, 250 μM DIDS showed a significantly higher growth rate (59.54 ± 3.67 %; unpaired Student's t-test; n=4) than the control (40.32 ± 1.64%; P=0.002; n=4) and the 100 μM DIDS treated bones (47.50 ± 2.37%; P=0.023; n=4). DIDS at a concentration of 100 μM also had a significantly higher growth rate compared to control bones (P=0.034). The difference in growth rate noted in the 100 μM DIDS treated bones at d 3 was not seen at any other time points examined. At d 5 culture, the 250 μM DIDS caused a further significant increase in growth rate (76.61 ± 5.41%) compared to the control (56.51 ± 3.39%; P=0.013) and 100 μM DIDS treated bone (54.86 ± 2.32%; P=0.008). At d 7, 250 μM DIDS caused a further increase in growth rate (80.08 ± 3.97 %) and this was significantly different from the control (63.32 ± 3.88%; P=0.013) and 100 μM DIDS treated bone (61.79 ± 2.56%; P=0.004). At d 11, the mean bone increase of the 250 μM DIDS-treated bones (81.82 ± 4.08%) remained significantly higher than the control (65.46 ± 2.72%; P=0.009) and 100 μM DIDS-treated bones (66.98 ± 3.06%; P=0.017). It should be noted that the control and 100 μM DIDS-treated bones grew almost identically between 3 and 11 days of culture. The overall effect of 250 μM DIDS treatment on the bone growth rate compared to the control and 100 μM DIDS was significantly different (two way ANOVA, P <0.001).

The results also demonstrated that at d 3, 5, 7 and 11, the bones treated with 200 μM EIPA (n=4) showed generally less than a 3 % increase in growth rate suggesting that growth rate was, at best, negligible. On the other hand, the EIPA control demonstrated progressive increase in bone growth during the same durations (27.25 ± 2.97% to 55.65 ± 3.93%, from d 3 to 11). The growth rate of the 200 μM EIPA treated bones was significantly much lower than the growth of the EIPA control during these periods ($P<0.0001$, n=4). At d 11 however, the EIPA control bone had a growth rate very similar to that of the DIDS control (no significant difference between the two; $P>0.05$).

When comparing the changes in the growth rate of the same treatment groups at different time points, the mean growth rate of the DIDS control bones was significantly higher at d 5, 7, and 11 compared to d 3 ($P=0.003$, 0.001 and 0.0001 respectively). For 100 μM DIDS-treated bones, the growth rate at d 11 and 7 was significantly greater than at d 3 ($P=0.001$ and 0.002 respectively). The 100 μM DIDS-treated bones at d 11 was also had a significant higher growth rate than at d 5 ($P=0.01$). For the 250 μM DIDS-treated bones, the growth rate reached at d 11 was significantly higher than at d 3 ($P=0.002$). Likewise, the growth rate at d 7 and d 5 was significantly higher than at d 3 ($P=0.004$ and 0.03 respectively). For EIPA, the control showed significant growth rate at d 11 compared to d 3 and 5 ($P=0.0002$ and 0.002 respectively). At d 7, the EIPA control demonstrated significantly higher growth rate than at d 3 ($P=0.005$). For 200 μM EIPA-treated bones, the growth rate at d 11 was significantly higher than at d 3, 5 and 7 ($P=0.0002$, 0.002 and 0.02 respectively). The bone growth rate was also significantly higher in d 7 compared to d 3 ($P=0.005$).

It should be noted that the increase in growth rate of EIPA control bones was significantly less than the growth rate of the DIDS control bones ($P\leq0.005$) on d 3, 5 and 7 of culture which could suggest a possible adverse effect of the 1% DMSO

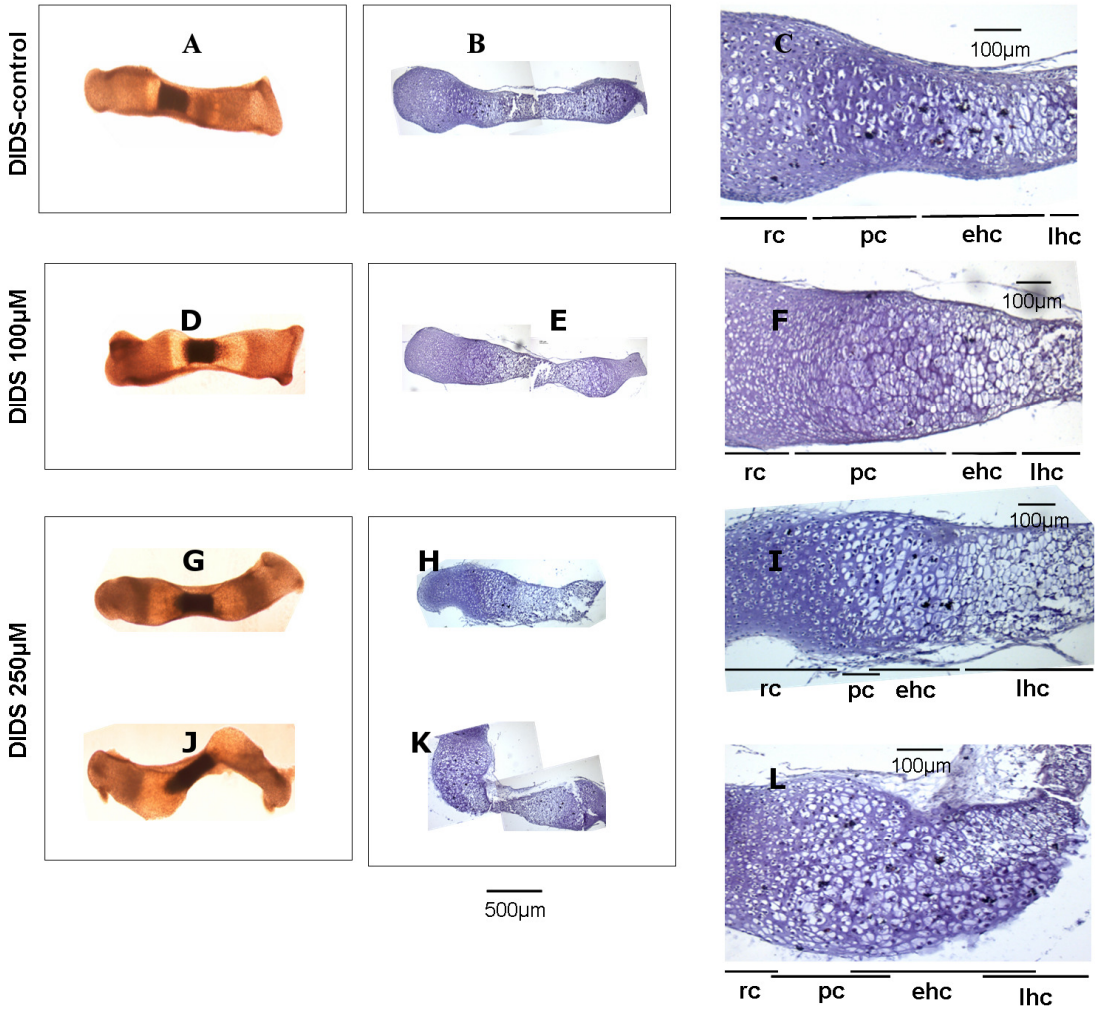
DIDS-control
DIDS 100µM
DIDS 250µM
A
B
C
D
E
F
G
H
I
J
K
L
100µm
rc
pc
ehc
lhc
500µm

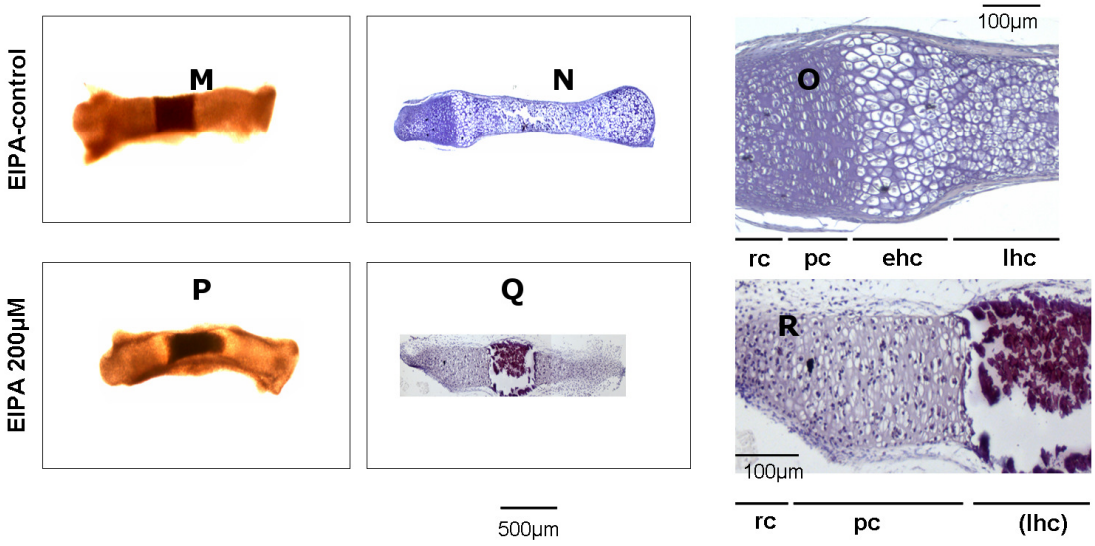
EIPA-control
EIPA 200µM
M
N
O
P
Q
R
100µm
rc
pc
ehc
lhc
(lhc)
500µm

Figure 5.8 Gross morphology and histological staining of foetal mouse metatarsals cultured in the absence or presence of DIDS and EIPA. Eighteen-day-old foetal mouse metatarsals were cultured for seven days in the absence (**A-C**) or presence of DIDS (100 and 250 μM; **D-F** and **G-L** respectively); or in the absence (**M-O**) or presence of EIPA (200 μM; P-R). Panels **A, D, G, J, M** and P show the gross morphology of the intact foetal metatarsals at day 3 culture. Panels **B, E, H, K, N** and **Q** demonstrate the histological sections of the foetal metatarsals after day 5 culture (fixed in 4% PFA and stained for Haematoxylin and Eosin). Higher magnification views of the respective histological sections are shown in panels **C, F, I, L, O** and **R**; with four different zones of chondrocyte differentiation are shown: rc, resting chondrocytes; pc, proliferating chondrocytes; ehc, unmineralized early hypertrophic chondrocytes; lhc, mineralized late hypertrophic chondrocytes.

that was used as the solvent for the EIPA. However it was clear that EIPA completely inhibited longitudinal growth when compared to the EIPA control. These results suggest clear differences between the inhibitory effects of DIDS and EIPA on foetal mouse bone growth. DIDS at both given concentrations significantly stimulated bone growth, whereas EIPA significantly inhibit it over 11-day bone culture period.

5.3.2.3. Foetal Metatarsal GP Histological Changes

To examine further the cause of the contrasting effects of DIDS and EIPA on the bone lengthening, histology was performed on the GP from the d 5 post treatment bone sections. Lower magnification views showed the overall bone shapes at d 5 in all treatment groups (Figure 5.8 panels B, E, H, K, N) and demonstrated no clear changes from those at d 3 as described earlier. An exception was in the EIPA-treated bone (Figure 5.8 (Q)) that showed relatively smaller bone size.

The sections were analysed at higher magnification where the various zones of chondrocyte differentiation were identified (see Materials and Methods). At lower DIDS concentration (100 μM), there was an increase in the proliferative chondrocytes (PC) and reduction in the early un-mineralized hypertrophic chondrocytes (EHC) (Figure 5.8 (F)) as compared to the control (Figure 5.8 (C)). At higher concentration (250 μM), the cell differentiation (*i.e.* proliferation and hypertrophy) appeared to be non-uniform along the GP. The PC zone was generally reduced whereas the resting chondrocytes (RZ) and EHC zone length were

variable, with both a slight increase and a slight decrease observed (see Figure 5.8 (I & L)). The late mineralized hypertrophic chondrocytes (LHC) zone appeared became relatively longer than in the control and the 100 μM DIDS groups. For EIPA, there was a complete elimination of the EHC zone (Figure 5.8 (R)). The PC zone increased as compared to the control (Figure 5.8 (O)). These histological findings demonstrate irregular changes in the foetal metatarsal GPC differentiation pattern as a consequence of DIDS or EIPA treatment.

5.4 Discussion

This study identifies a possible role of AE and NHE in postnatal bone longitudinal growth as shown by dose-response relationship of the inhibitors to the two transporters namely DIDS and EIPA respectively with the bone lengthening. The results show that both NHE and AE are implicated in the GPC enlargement mechanism. However, prenatal bone growth in the presence of the AE inhibitor DIDS exhibited the opposite effect, with bone lengthening stimulated.

5.4.1 The Specificity of DIDS and EIPA Effects

DIDS was used as it has recognized inhibitory effects on the AEs (Cabantchik & Greger 1992), whereas EIPA (an amiloride analogue) was found to potentially produce full inhibition on NHE activities up to 140 times more than amiloride itself (Vigne *et al.,* 1984). The inhibition of bone growth in P7 rat metatarsals by DIDS and EIPA was shown to be dose-dependent, where the optimal concentration that produced the maximum inhibition effect was approximately 250 μM for DIDS and 444 μM for EIPA as estimated from the dose-response curve (Figure 5.3).

The effects of DIDS and EIPA have been studied previously in various cell types. For DIDS, it has been found to provide protection against apoptosis in cardiomyocytes (100-250 μM; Wang *et al.,* 2005 Okada *et al.,* 2006, Liu *et al.,* 2008), N1E 115 cells (clonal mouse neuroblastoma)(250 μM; O'Reilly *et al.,* 2002), MDCK cells (renal epithelial cell line) (10-500 μM; Araki *et al.,* 2002), human adenocarcinoma KB cells (100 μM; Ise *et al.,* 2005); and HeLa cells and U937 (human monocytic cell) (500μM; Wang *et al.,* 2005). It also has been shown to inhibit cell proliferation and induce cell apoptosis in hepatocellular carcinoma

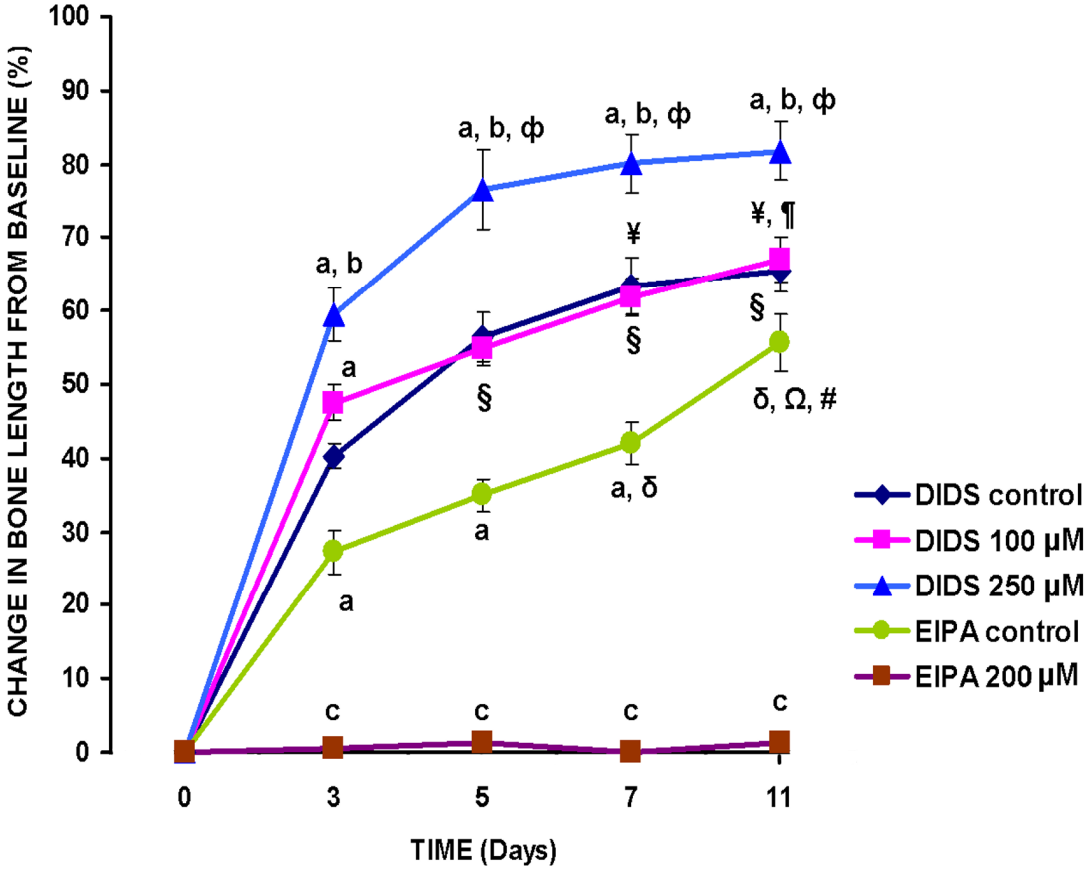

Figure 5.9 Effect of DIDS (100 and 250 µM) and EIPA (200 µM) on foetal metatarsal bone growth. Each data point contains results from four metatarsals (n=4) from at least 10 foetuses of 18-day old that were pooled together in a same dish. Each bone was cultured individually in 24-well plate for 7 days in the presence/ absence of the drugs in the concentration shown and measured as described in Materials and Methods. The mean bone increase (% change in bone length from the baseline) was significantly different (unpaired Student's t-test) when the indicated data point was compared to [a] DIDS control at the same time point ($P \leq 0.034$), [b] 100 µM DIDS at the same time point ($P \leq 0.023$), [c] EIPA control at the same time point ($P < 0.0001$), [ф] 250 µM DIDS at d 3 ($P \leq 0.029$), [¥] 100 µM DIDS at d 3 ($P \leq 0.002$), [¶] 100 µM DIDS at d 5 ($P < 0.011$), [§] DIDS control at d 3 ($P \leq 0.004$), [δ] EIPA control at d 3 ($P \leq 0.005$), [Ω] EIPA control at d 5 ($P \leq 0.002$), and [#] EIPA control at d 7 ($P \leq 0.021$). Data expressed as means ± S.E.M.

cells (400-1000 μM; Liu *et al.,* 2008). Besides AE, DIDS also inhibit some bicarbonate-transporter family members of HCO_3^- transporters namely the Na^+-coupled HCO_3^- transporters such as NBC1 (Romero *et al.,* 2004). NBC1 could be found ubiquitously in many tissue such as in the basolateral membranes of renal proximal tubule, pancreatic ducts, and epididymis, as well as in astrocytes and neurons in several regions of the brain, several tissues within the eye, and blood vessels and intercalated disks within the heart (Romero *et al.,* 2004). Even though, it has been suggested has a role in cell pH regulation (Bernardo *et al.,* 2006), contrary to AE this system has no coupling function with NHE (Alrefai *et al.,* 2000), which was also associated with other roles in cellular mechanisms such as volume regulation (Alper, 1991).

For EIPA, at 10 μM it induced total NHE inhibition in MCF-7 (human breast cancer cells) and CNE-1 (nasoparyngeal carcinoma) cells. However when this was coupled with heating factor (43^{o}C, 2 hrs) it induced cell cytotoxicity (Li and Liu, 1997). It was also reported that at 1μM it substantially reduced myocardial infarct size in isolated rabbit hearts when it was administered either prior to or after the onset of ischemia (Sato *et al.,* 1997). Besides that, EIPA at 5-1000 μM could induce cell apoptosis through the inhibition of intracellular alkalinization (Khaled *et al.,* 2001; Wu *et al.,* 2004). However since some of these were cancer cells, the signaling pathway may not represent a typical mechanism in healthy cells (Malo and Fliegel, 2006). Na^+ channel (found in electrically high resistance epithelia) is another transport system besides NHE that sensitive to EIPA. However compared to Na^+ channel, NHE is found in many different cellular preparations and seems to function in cell proliferation and differentiation (Shrode *et al.,* 1997), volume regulation and intracellular pH regulation (Seifter & Aronson, 1986), which related to cellular events involving GPC. In addition, this exchange pathway becomes operational usually after some external stimuli and to inhibit the system much higher concentrations of amiloride are required than those required for the Na^+ entry pathway (Beno, 1982).

These observations serve to provide general overview of the effects of DIDS and EIPA in various cells, which seems varies depending to dose and the

type of cells studied. Therefore, the present study on *ex vivo* GPC undertook several methods including histology and *in situ* cell viability test and volume analysis in order to identify the relevant effect of the agents on the GP that could specifically explain the growth retardation.

The concentration of DIDS used in the present *ex vivo* study was within the range of concentrations used previously in the culture of other cells (O'Reilly *et al.,* 2002; Araki *et al.,* 2002; Ise *et al.,* 2005; Wang *et al.,* 2005; Okada *et al.,* 2006; Liu *et al.,* 2008). However for EIPA, a relatively much higher concentration was needed to give optimal effects in the present study than what was reported previously in other cell types (Li and Liu, 1997; Sato *et al.,* 1997; Khaled *et al.,* 2001; Wu *et al.,* 2004; Malo and Fliegel, 2006). Considering the P7 rat metatarsal bones were relatively small and have less amount of calcification (Table 5.2) serving as barriers between the culture media containing the drug and the chondrocytes, it was reasonable to expect that the concentration range needed was not much different from the one used in *in vitro.* This was the case with DIDS in the present *ex vivo* study. However, the higher concentration required for EIPA could be due to the presence of competitive inhibitors for EIPA which reduced the EIPA binding to the target protein receptors. A possible factor that could act as competitive inhibitor was the increase in the extracellular Na^+ ion (Vigne, 1984; Kleyman and Cragoe, 1988). DMSO, the solvent for EIPA, has been shown to induce leakage of Na^+ ion from other cells (Santos *et al.,* 2002). Other sensible explanation is the negatively charged dense GP cartilage, due to the presence of proteoglycans (Ng *et al.,* 2002; Ng *et al.,* 2003) caused electrostatic repulsion of negatively polar EIPA compound (Kleyman and Cragoe, 1988). This resulted in a decrease of the drug concentration upon reaching the target tissue and subsequently reduced the EIPA binding.

The relatively much higher concentration of EIPA than the dose used previously in other cell types (Li and Liu 1997; Sato *et al.,* 1997) could potentially expose the cells to toxicity that in turn could adversely affect bone growth. To rule this out, an *in situ* viability test and histology was performed on the GPC after incubation with the EIPA. No clear difference in the appearance of dead cells over

live cells was observed in treated bones compared to the control bones after 24 hrs incubation of the *in situ* GPC (Figure 5.4). The intact CMFDA-labelled cells could be observed across the GP in all bones exposed to the drugs. However, as a note of caution the *in situ* viability cell test in the present study could only serve as a general qualitative cell viability evaluation of the bone tissues. No attempt to further quantify cell viability was made since it would not have offered extra evidence; the process of bisecting these delicate bones causes significant cell death over and above that due to cytotoxicity of any drug. This is especially true for the largest cells, those in the early and late HZ, being most affected by this cutting artifact. Therefore further assessment was undertaken using histological examination described earlier. The histology results support the *in situ* qualitative viability observations, showing no significant changes in the density of HZ cells in the presence of the inhibitors (Table 5.3). This implies that any drug toxic effect was limited and that any affect was through the inhibition of HZ cell volume increase.

The *in situ GPC* culture model used in this study better mimics the physiological milieu of the GPC than the use of cells in monolayer culture. However exposing the entire bones to the drugs could also trigger responses from cells other than those in zones of the growth plate. For example, it has been reported that DIDS can block completely the sulphate transport activity of DTDST (diastrophic dysplasia sulphate transporter) that speculated to play a role in endochondral bone formation, at a concentration of 1 mM (Satoh *et al.,* 1998). Even though the present study did not rule out an effect of DIDS on epiphyseal matrix sulphated proteoglycans synthesis activity (critically affected in the absence of DTDST), the histology results narrowed down the possible effect of DIDS to a decrease in GPC hypertrophy. In addition, the microCT results do not suggest any significant effects of DIDS on the bone morphometric parameters.

It was also interesting to know if 250 μM DIDS used in the current post natal bone growth study could induce protection against cell apoptosis in GPC as reported in various other cell types cells (Araki *et al.,* 2002; O'Reilly *et al.,* 2002; Ise *et al.,* 2005; Wang *et al.,* 2005; Okada *et al.,* 2006 and Liu *et al.,* 2008). In bone

growth, cell apoptosis is considered to be an important mechanism to remove the terminally mature hypertrophic chondrocytes in order to match the rate of chondrocyte proliferation, and transform the composite chondroid bone into mineralized bone which has relatively superior mechanical, physical and structural properties (Adams and Shapiro 2002; Shapiro, 2005). It is also one of the key factors in the bone formation process by initiating the recruitment of the bone cell precursors and blood vessel formation at the terminal HZ (Gibson, 1998). How significant the effect of DIDS on the apoptosis of the HZ cells at the terminal HZ was not specifically studied in the present work but if apoptosis was inhibited a relatively longer HZ would be expected as the number hypertrophic chondrocytes progressively increased. The present results showed the HZ height over the GP length of DIDS-treated GP of postnatal rats was found significantly lower than in the control (Table 5.2). It can be reasoned from this observation that DIDS at the given dose used in the postnatal rat metatarsal study inhibited bone growth most likely through the inhibition of HZ cell volume increase and not through the blocking of the apoptosis of terminal HZ cells. This was further supported by the evidence of no changes in the cell numbers, which suggest that the rate of apoptosis is not affected by DIDS.

As could be noted in the result (Figure 5.3) there was no significant difference in bone growth between the DIDS and EIPA controls of post natal rat metatarsals after 24 hrs treatment. On the other hand, the DIDS and EIPA controls showed marked difference in the bone growth of foetal mouse metatarsals during d 3 to 7 incubation periods (Figure 5.9). The EIPA control that contained only the vehicle solution of the drug showed significantly lower growth rate compared to the DIDS control during the duration of culture. This suggested at exposure of 1% (v/v) of DMSO used as the solvent (vehicle) for EIPA in the current study could adversely effect the normal bone growth of foetal metatarsals. A toxic effect of DMSO has been reported previously in post natal rat cochlear organotypic cultures and how this could be minimized if the concentration of DMSO used was between 0.1-0.25% (Qi, 2008). However for the present study, since all the EIPA experiments were run in parallel with the control groups that contained DMSO

alone, the result clearly demonstrated the significant net effect on the bone lengthening was EIPA-dependent (Figure 5.9).

The Micro-CT results reveal no difference in the three-dimensional bone morphometry between treated bones and the controls (Table 1), which suggests that the paler colour appearance seen grossly in EIPA-treated bones (Figure 5.5(D) far left) compared to the control (Figure 5.5(C) far left) was not as the result of changes in the bone mineralization and architecture. However the actual cause for these gross morphological changes was not clearly identified but could be due to the effect of the drug on bone marrow. The three-dimensional micro-CT morphometry on Sprague Dawley rat metatarsal bones have not been reported previously to the best of my knowledge. However almost all the present morphometric parameter results showed approximately the same range values as have been reported in male Wistar rat tibia (4-week-old; Bielohuby *et al.,* 2010), Wistar rat femoral diaphysis (53 to 56-day-old; Freeman *et al.,* 2008) and C57BL/6 mouse distal femur metaphysis (10-week-old; Gudberg *et al.,* 2004).

5.4.2 Possible AE and NHE Roles in Bone Longitudinal Growth

The current hypothesis suggests that the AE and NHE have roles in GPC hypertrophy and consequently in longitudinal bone growth. This hypothesis fits well with the present finding and demonstrates the dose-response relationship between DIDS or EIPA to the inhibition of postnatal bone growth. The results indicate that 250 μM DIDS or 444 μM EIPA inhibited ~97% and 64% of longitudinal bone growth in P7 rat metatarsals, respectively. Both drugs caused a significant decrease in the height of the hypertrophic zone over the total GP length.

The decrease in the height of the GP HZ over the GP length suggests that the inhibition of the transporters have direct effects on GPC hypertrophy, probably through the inhibition of normal cell regulatory volume mechanism. In this experiment, all bones in this experiment were fixed in fixative solution of 1.3% GA with 0.5% RHT, with the osmolarity was adjusted to the osmotic pressure of normal extracellular fluids (Chapter 4) to avoid fixative-induced cell artefact shrinkages having bias towards the decrease of the HZ height over the GP length. To examine this further, the post treatment *in situ* GPC volume of the DIDS and

EIPA treated bones was measured at PZ and HZ of the GP. The results showed a marked decrease in GPC volume in the PZ and HZ of EIPA-treated bones but no significant volume changes were observed in DIDS-treated bones.

The HZ cell height has been shown to be significantly higher than in the PZ cell due to preferential increase in cell height over the cell width and depth in normal HZ chondrocytes (Farnum *et al.,* 2008). This fact could explain why the effect of EIPA on the HZ cell volume subsequently caused a significant decrease in the GP HZ height over the GP length (Table 5.2), although GPC volume decrease was observed in both the PZ and HZ (Table 5.3).

It was interesting to find that the effect of EIPA on GPC volume was across the PZ and HZ (Figure 5.4 & 5.7; Table 5.3). Related to this, there is accumulating evidence suggesting that the inhibition of NHE leads to cell death possibly by an apoptotic process (Khaled *et al.,* 2001, Reshkin *et al.,* 2003; Wu *et al.,* 2004). The NHE inhibition could have caused cell death in at least two possible ways. First, it induces apoptotic volume decrease (AVD), a hallmark of apoptotic mechanism that could be simply referred as abnormal RVI as the decrease of cell volume takes place under hypotonic condition (Okada and Maeno, 2001; Okada *et al.,* 2001). Second, it causes the loss maintenance of the normal intracellular pH (pHi), which has been suggested to lead to the apoptotic cell death (Matsuyama *et al.,* 2000**;** Khaled *et al.,* 2001; Lagadic-Gossmann *et al.,* 2004). Even though no clear indication that the GPCs were dying or in a process of apoptosis (Figure 5.4 & 5.7), the effect of EIPA at a concentration of 444 μM on GPCs volume was evident (Table 5.3). Therefore, it cannot be ruled out that the NHE function in GPC could be critically important in regulation of GPC survival as has been observed in other cells (Schelling and Jawdeh, 2008). The NHE role in regulating cells viability could be achieved by enhancing the Na^+ entry as a part of RVI-mediated defense against AVD (Okada and Maeno, 2001; Okada *et al.,* 2001**;** Okada *et al*., 2006). When cells are induced to shrink, RVI is coordinated by activation of NHE and, in some cells, the AE and NKCC (Lang *et al.,* 1998). The net effect is Na^+, K^+ and Cl^- and H_2O influx, which leads to cell volume re-expansion (Schelling and Jawdeh, 2008) and consequently prevents the progression of AVD.

While it was clear from the current findings that the reduction of the HZ height in EIPA treated bone was partly due to a decrease in hypertrophic GPC volume, the reduction in the HZ height of the DIDS-treated bones could be explained differently. The AE could have a critical role in the initial stage of PZ cell transformation into HZ cells during PZ-HZ cell differentiation. Inhibition of the AE by DIDS could plausibly delay the transformation rate of PZ cells into HZ cells. As the transformation rate from the proliferative to hypertrophic GPC could contribute to the final HZ volume (unpublished data/ Chapter 4 of this thesis), the delay in the transformation would affect the final HZ cell volume and consequently the HZ height. Nevertheless, this could not rule out a more extensive effect of DIDS on the majority of the GP cells *e.g.* by disruption of AE intracellular pH regulation function (Romero *et al.,* 2004). How ever this would not prevent terminally differentiated HZ from progressing to apoptotic process. This plausible broader effect of DIDS would explain the almost total inhibition of bone lengthening, the maintenance of HZC volume, and the decrease in % HZ height. This finding also highlights the possibility that the AE was not the main plasma membrane transporter system involved in mediating the GPC volume increase at the later stage of the hypertrophy. The main role could be taken up by other membrane transport system, which was not affected by the inhibition of the AE function and could also be able to compensate perturbed functions of other membrane transporters at the earlier HZ. A good candidate for this is $Na^+/K^+/2Cl^-$ co-transporter (NKCC), which has previously been shown to demonstrate cellular localisation in GP HZ and increase in mRNA expression of the cells (Bush *et al.,* 2010). In addition, a reduction in bone growth by 35% was observed when the NKCC activity was blocked by its specific inhibitor, bumetanide (Bush *et al.,* 2010).

5.4.3 Response of Foetal Mouse and Postnatal Rat Bone Growth to DIDS and EIPA

The present results indicate the markedly different effects of the drugs at different development stages (prenatal and postnatal) as well as in two different species. Even though different species (mouse and rat) were used at the different

time points, it is interesting to find that EIPA caused ~100% inhibition of bone lengthening in prenatal (E18) mouse GPs, whereas DIDS generated a significant ~50% increase in bone length compared to the control (Figure 5.9). The growth promoting effects of DIDS on the prenatal bones was contradictory with it inhibition effects on postnatal bones (Figure 5.3), which caused a ~97% reduction in longitudinal bone growth. The growth-promoting effect of DIDS was noted at d 3 at a concentration of 100 μM; and at d 3, 5, 7 and 11 bone cultures at a concentration of 250 μM (Figure 5.9). Microscopic examination and histology revealed that at a concentration of 250 μM, the DIDS induced bone deformity (crooked bones) (Figure 5.8(J)). This was in contrast to that observed in P7 rat metatarsals 24 hrs bone culture. At lower concentrations (100 μM) DIDS caused the increase in the proliferative cells and reduction in the early non-mineralized hypertrophic cells. In higher concentration (250 μM), there was irregular cell differentiation particularly at the proliferative and hypertrophic zones along the GP which could contribute to the deformed bone formation in some of DIDS-treated bones. The late mineralized hypertrophic cells zone appeared to increase probably due to the effect of apoptosis inhibition in the HZ cells as discussed earlier. However the histological observation was based on general qualitative evaluation of the histological sections, since the very tiny sections made it impossible to produce sufficient and decent quality histological sections for quantitative and statistical analysis of different zone of GPC differentiations. Nevertheless, this result highlights the different effect of DIDS at different stage of GP development (*i.e.* foetal vs postnatal animals); or at different days of bone culture (24, 72 or 120 hrs); or at different DIDS concentration used. For EIPA, the inhibitor demonstrated the consistent longitudinal bone growth inhibition in both E18 mouse and P7 rat metatarsals. Gross examination on the EIPA treated mouse foetal metatarsals showed the relatively smaller bone size than the control, whereas the histology examination demonstrated the complete elimination of the EHC zone (Figure 5.8 (R)). However, since no cell viability test was performed on the foetal bone rudiments, further examination would be required to rule out any cytotoxic effect of the inhibitor at the given concentration on the foetal bone tissues. To do this,

other feasible viability test technique should be employed on the foetal bone since the present method requires the cutting of these bones that would causes a greater cell death artifact than earlier discussed for the P7 bones.

The variation between the skeletal development in foetal and postnatal mouse and rat have also been reported in the changes of bone longitudinal growth rates (Patton and Kaufman 1995; Wilsman *et al.,* 2008), the first appearance of the ossification centre and ossification pattern (Patton and Kaufman 1995); changes in hypertrophic volume increase and GPC production/ turnover (Wilsman *et al.,* 2008), and catch-up growth response following withdrawal of dexamethasone treatment (Chagin *et al.,* 2010).

The different GPC performances at different periods of skeletal development could influence the behaviour or the response of the GPC to both DIDS and EIPA. The process of skeletal development in foetus and neonatal animals by endochondral bone development through chondrogenesis and osteogenesis are tightly coordinated in time and space. The histology of the growth plate changes: as shown during the second half of human foetal development is more cellular, is less organised in columns, and shows less development of the matrix than at the end of the period studied. On the other hand, at birth, the growth plate, although thinner and less cellular than in foetuses, has well-organised hypertrophic cell columns separated from one another by the longitudinal septa of the matrix (Rodriguez-Zavala *et al.,* 2005).

The difference between both bone development stages could be demonstrated further by the important contribution of the GPC proliferation in the prenatal period to the bone growth in comparison with the postnatal period, in where the GPC hypertrophy is relatively more important in the bone length growth (Wilsman, *et al.* 2008). The species difference adds to this variation as for example the process of ossification of majority of the mouse skeleton and the growth takes places relatively more rapidly when compared with that of the rat (Patton & Kaufman, 1995).

The fact that the inhibitors could bring about various effects in different type of cells as shown in the earlier discussion, does raise the possibility that the

mode of action of the drugs on the GPC could also be different between different species and age of the animal. Beside that, we also could not rule out a possible manifold effects of the drugs on the foetal bones such as the inhibition by DIDS of DTDST activity that was suggested as an important requirement for chondrocytes to grow and crucially important for endochondral bone development (Satoh *et al.,* 1998). The irregular and abnormal changes in the foetal metatarsal GPC differentiation pattern following treatment with the DIDS could imply the important effect of the DTDST inhibition on the early age of skeletal bone formation.

In accord with the present results, it can be reasoned that the inconsistent findings between the possible existence role of the transporter in the bone lengthening (as implied by the present result) and the non increase of NHE mRNA expression between PZ cells and HZ cells (Bush *et al.,* 2010), could be due to the difference in the expression level of the transporters (*e.g.* NHE) between different stages of the skeletal development *i.e*. between animals at postnatal age (used in the current study) and at the later age (used in the previous microarray analysis study).

5.5 Conclusion

In summary, the present findings underscore a possible role for AE and NHE in post natal bone longitudinal growth. The inhibition of the AE or NHE by DIDS or EIPA respectively, resulted in bone lengthening inhibition in a dose-dependent manner. The inhibition of both membrane transporters caused a significant decrease in the hypertrophic zone over the total growth plate length. Whilst the inhibition of the AE resulted in no clear effect on the growth plate chondrocyte volume, the NHE inhibition caused a significant decrease in the cell volume of the proliferative and hypertrophic chondrocyte cells. It also highlights the different response to the DIDS and EIPA between the prenatal and postnatal bones that warrants further examination. These findings might imply a possible important involvement of the AE and NHE in the growth plate chondrogenesis and bone longitudinal growth.

Chapter 6

Changes to Sodium/ Hydrogen (NHE1) and Anion Exchanger (AE2) Expression Levels with Growth Plate Chondrocyte Hypertrophy: A Fluorescence Immunohistochemical Study

6.1 Introduction

6.1.1 A Possible Role for NHE and AE

The previous results in Chapter 5 have demonstrated a possible function of NHE and AE in post natal mammalian bone growth. The reported data showed dose-dependent inhibition of bone growth by EIPA or DIDS known to respectively block the NHE or AE activity. Histology on the DIDS and EIPA-treated bones showed a significant decrease in the percentage height of the growth plate (GP) hypertrophic zone (HZ), which could explain how both drugs affect the bone longitudinal growth. Analysis of the GP chondrocytes revealed that the HZ cell volume decreased significantly following treatment with a NHE inhibitor, whereas AE inhibitor did not result in any cell volume changes at the same zone. The present study was designed to further investigate the presence of the transporters by examining cellular and tissue localisation of specific NHE and AE isoforms (NHE1 and AE2) in post natal rat GP using fluorescence immunohistochemistry (FIHC).

6.1.2 FIHC Technique

Immunohistochemical staining is the detection of antigens in histological tissue sections (frozen or paraffin embedded) through the use of specific antibodies that are labeled (*e.g.* with the use of enzyme or fluorescence) so that the sites of antibody become microscopically visible (Haines and Chelack, 1991). The term FIHC or immunofluorescence being used in the present study refers to the immunostaining technique using a fluorescent label (Renshaw, 2007). It has proved an invaluable investigative tool for the visualization of tissue antigens in healthy and pathologic tissues. When coupled with high resolution imaging methods (*e.g.* confocal laser scanning microscopy) immunohistochemistry (IHC) has the potential to reveal further information about the complex three-dimensional composition and organization of cellular and extracellular matrix compartments in GP cartilage. These technologies can also be used to quantify signal intensities and thereby facilitate numerical computation of image data (Hayes *et al.*, 2008).

It cannot be overemphasised the importance of every IHC result to be consistently accurate and reproducible. A good result could be hampered by the type of tissue sections used. For instance, although paraffin embedded sections are

preferred to frozen tissue sections as the former offers better morphological appearance, the antigen (Ag) preservation in paraffin embedded sections might be affected by excessive fixation and processing regime such as Ag masking and background autofluorescent problems (Renshaw, 2007). Autofluorescence is the ability of a tissue or cellular component to fluoresce naturally, such as the fluorescent pigment lipofuscin in mammalian tissue. This occurs independent of the binding of immunochemical staining reagents conjugated to fluorochromes. Autofluorescence can potentially mask specific fluorescent signals or be mistaken for fluorescent labels (Baschong *et al.*, 2001; Renshaw, 2007). In order to overcome this, appropriate tissue section pretreatment inevitably should be first undertaken prior to FIHC procedure to constantly produce high quality FIHC results.

6.1.3 A Review on NHE and AE Isoforms and the Distribution in Other Tissues

Previous research work has studied protein expression and localisation, regulatory features and physiological roles for NHE and AE protein in other tissues (Alrefai *et al*., 2001; Malo & Fliegel, 2006). The family of NHE proteins includes 9 isoforms (NHE1-9), each with unique tissue and cellular distribution, inhibitor sensitivities, regulatory elements, and subsequent physiological roles. NHE1, the first isoform identified, is distinct in that it is ubiquitously expressed in all mammalian cells and plays a housekeeping role (Malo & Fliegel, 2006). This isoform was the most sensitive to amiloride and its derivatives (Masereel *et al.,* 2003).

NHE2 shared 42% identity in an amino acid sequence with NHE1 (Wang *et al.,* 1993) and is expressed in the epithelial tissue of the intestinal tract and kidney, skeletal muscle, and the testis (Malakooti *et al.,* 1999). Within the digestive tract, NHE2 is quite prominent with strong expression in the jejunum, ileum, and colon (Bookstein *et al.,* 1997) and specific expression in renal tissue (Chambrey *et al.,* 1998; Peti-Peterdi *et al.,* 2000). This isoform has similar inhibition constants for both amiloride and nonamiloride compounds as that observed for NHE1 (Yu *et al.,* 1993). Overall, NHE2 appears to be involved in several secretory processes.

NHE isoforms 3 and 4 were both identified to have 39% and 42% amino acid identity to NHE1, respectively (Orlowski *et al.,* 1992). Furthermore, both NHE3 and NHE4 were identified as having significant levels of expression in the kidney and gastrointestinal tract (GIT). In the gastrointestinal tract, NHE3 has higher expression in the intestine, whereas NHE4 appears to be localized predominantly in the stomach. In renal tissue, NHE3 has been identified as an apical membrane protein in the proximal tubule and thick ascending limb (Amemiya *et al.,* 1995), whereas the NHE4 isoform has basolateral epithelial distribution and is found specifically in the inner medulla of the kidney (Bookstein *et al.,* 1997; Pizzonia *et al.,* 1998). More recently, both isoforms have also been identified in the submandibular gland in rats, with NHE3 having apical expression in duct cells and NHE4 having basolateral expression in acinar and ducts cells (Oehlke *et al.,* 2006). Both NHE3 and NHE4 are relatively resistant to amiloride and nonamiloride inhibitors (Brant *et al.,* 1995; Yu *et al.,* 1993) and NHE4 requires hyperosmolarity for activation (Bookstein *et al.*, 1994; Bookstein *et al.,* 1996).

Studies on NHE5 have revealed that its expression is restricted to the brain in both rats and humans. Sequence analysis demonstrated that NHE5 has 39% amino acid identity to NHE1, but also 53% identity to NHE3. In addition to having similar primary structure to NHE3, NHE5 also has similar inhibitor sensitivities to NHE3 (Attaphitaya *et al.*, 1999; Baird *et al.,* 1999). Overall, NHE5's restricted expression in the brain suggests a specialized role for the isoform, but as of yet no physiological role has been elucidated. NHE isoforms 6–9 are unique in that they are localized to the membranes of the Golgi and post-Golgi endocytic compartments. It is likely that these NHE isoforms contribute to pH maintenance of these intracellular organelles (Nakamura *et al.,* 2005).

For AE, there are at least three structurally and functionally related genes for AE, termed as AE1, AE2 and AE3 (Alper, 1991). AE1 or band-3 AE of erythrocytes was the first described AE and is expressed in greatest abundance in the erythrocyte plasma membrane. Outside the erythrocytes the predominant site of AE1 expression is the kidney in the basolateral plasma membrane of Type A

intercalated cells of the renal cortical and medullary collecting ducts. It is also expressed at lower levels in heart, distal colon, and other tissues (Alper, 1991).

AE2 is the most widely expressed form of AE, and in nearly all epithelial cells resides in the basolateral plasma membrane. Membrane localisation studies revealed that AE2 polypeptide was present at highest levels in the epithelial cell basolateral membrane of choroid plexus, gastric parietal cells, throughout the GI tract, and in some cell types of the respiratory and genital tracts. AE2 in exocrine glands is expressed in acinar cell basolateral membranes, but minimally in duct epithelial cells. It is also expressed throughout the nephron, but most abundantly in the medullary thick ascending limb and the inner medullary collecting duct (Alper, 2006). Whereas AE1 shows little sensitivity to pH over the physiological range, intracellular and extracellular acidification both inhibit AE2 (Alper *et al.,* 1991).

AE3 is expressed at highest level in excitable tissues, throughout the GI tract, and at lower levels in other tissues (Kudrycki *et al*., 1990). The AE3 gene has been shown to code at least two transcripts and two protein isoforms, bAE3 (brain subtype) and cAE3 (cardiac subtype). Adult hearts of rat, rabbit, chicken and human express both bAE3 and cAE3 at almost equal levels (Yannoukakos *et al.,* 1994). To date, very little is known about the expression of the AE3 isoforms in epithelial tissue (Alrefai *et al.,* 2001). The latest reported AE4 isoform (Tsuganezawa *et al.,* 2001) was cloned from kidney and is more closely related in sequence to the NBC Na-bicarbonate cotransporters than to AE anion exchangers, although it is reported to mediate Na^+-independent Cl^- /HCO_3 - exchange (Alper *et al.,* 2001).

6.1.4 Aim of the Study and Hypothesis

Having found evidence of functional roles of NHE and AE in longitudinal bone growth (Chapter 5), the present study explored further the presence of the NHE1 and AE2 isoforms in P7 rat GP cartilage using FIHC. These two were the most ubiquitously found isoforms in other tissues and cells (Alper 2006; Malo & Fliegel, 2006). Other isoforms (AE1 and AE3) were also tested but the antibodies used to detect these isoforms were found ineffective (see Table 6.1). The study was undertaken to test the hypothesis that changes in chondrocyte size during the

transition from the proliferative to hypertrophic zones is associated with changes in the distribution of NHE and AE expression. Collagen type X distribution in the growth plate tissue was also examined in the preliminary FITC staining optimization studies as it known to be only produced by GP hypertrophic chondrocytes and uniquely present in the extracellular matrix of the hypertrophic zone (Kielty *et al.,* 1985; Sasano *et al.,* 1998).

In this study, proximal tibia growth plates of P7 rats were fixed and processed for immunofluorescence microscopy. The pretreatment procedure for the FIHC comprising heat-induced antigen (epitope) retrieval (HIAR) and autofluorescence quenching was initially optimized. Ag retrieval is defined as an enzymatic or high-temperature heating method to recover the antigenicity of tissue sections that had been masked by formalin fixation or paraffin-embedding tissue processing (Shi *et al.,* 2001). The established FIHC pretreatment technique was then used to test for collagen type X distribution in GP sections. Having established the methods, the immunostaining study of NHE1 and AE2 within the GP was performed. CLSM was used to record high resolution images of the immunofluorescent GP sections. A semi-quantitative method was used to measure the immunofluorescence intensity in order to determine the tissue and cellular localisation of the transporters from the proliferative through to the hypertrophic GP zones.

6.2 Materials and Methods

6.2.1 Animals and Growth Plate Preparation

Tibiae from each hind limb of P7 Sprague-Dawley rats were prepared and fixed as described previously (Chapter 2). The tibias with intact proximal GP from five different animals were used (n=5). Kidney and gastrointestinal tract tissues were collected to be used as positive control tissues for the antibodies used in this FIHC study.

For histological sections preparation, tibiae were bisected sagitally and placed in fixative solution (4% (w/v) PFA or 2% (v/v) GA with 0.7% (w/v) RHT) for 24 hrs at room temperature (RT). Sagital bisection of the GP prior to fixation has been shown to significantly reduce the shrinkage artefacts associated with high

osmolarity of the conventional fixatives used (Chapter 4). Kidneys and GITs were also fixed in the same fixatives. All the fixed tissues were dehydrated though a series of graded ethanol solutions prior to paraffin embedding using a standard procedure for histological sectioning. Tissue sections (10 μm) were prepared using the method described in 2.3.2.

For *in situ* GPC imaging, a tibia from a 7-day-old rat pup were bisected sagitally and stained with Calcein AM (5 μM) for image scanning using CLSM as described previously (2.3.4.1).

6.2.2 Optimization of Pretreatment Method for the FIHC on Growth Plate Histological Sections

For FIHC optimization, techniques comprising heat-induced antigen retrieval (HIAR) and autofluorescence quenching (*i.e.* $NaBH_4$) were assessed. GP histological sections were de-waxed in xylene, rehydrated in 100, 95, and then 75% ethanol followed by PBS. Four groups of treatment were tested: (i) no treatment given (control), (ii) 1% (w/v) sodium borohydride ($NaBH_4$), (iii) HIAR, and (iv) a combination of HIAR and 1% $NaBH_4$. For HIAR, histological slides were immersed in boiling Tris-EDTA-T80 HIAR buffer for 20 mins and then cooled in water for 10 mins (a domestic microwave was used in the HIAR procedure, and a plastic rack vessel was used to hold the slides during the Ag retrieval process). For pretreatment with 1% $NaBH_4$, GP sections were incubated with $NaBH_4$ in 0.1M PBS, refreshing 3 times at 20 mins intervals. For combination methods, GP sections were first treated with HIAR and followed by treatment with 1% $NaBH_4$. For this experiment, the pretreatment steps were then followed by FIHC protocol using anti-collagen type X primary antibody (Ab).

6.2.3 Fluorescence Immunohistochemistry

FIHC was performed (see details in 2.3.4.2) after pretreatment procedures being applied to the GP histological sections. Rabbit polyclonal 1^o Ab for the NHE1 and AE2 were used at 1:500 and 1:100 dilution respectively. Other antibodies used are shown in Table 6.1. For the negative control section, the primary Ab was omitted

and replaced with goat serum. FITC-tagged goat anti-rabbit was used as the 2^{o} Ab. The experiments were repeated in at least 5 different GP sections of 5 separate animals.

6.2.4 Confocal Laser Scanning Microscopy

An upright Zeiss Axioskop LSM 510 CLSM was used to acquire fluorescent images of GP sections using the protocol that has been described previously (2.4.2) A series of high power images were obtained along the GP under examination, starting from the osteochondral junction distally to the early proliferative zone cells proximally. For immunofluorescence studies, the negative control sections were imaged first followed by other respective sections under examination. The same confocal settings used were maintained throughout the procedures.

6.2.5 Semi Quantitative-Measurement of NHE1 and AE2 Cellular Localisation

In order to measure cellular immunofluorescence staining intensity and the localisation of the transporters across the GP, the GPCs in high power images were recorded using a CLSM. GP images of sequential zones were 'stitched' together to produce a montage of the whole length of a GP from the proliferative zone (PZ) to the hypertrophic zone (PZ). Each imaged growth plate was divided into 8 equal sections (S1-S8) as described previously (2.5.1). An average fluorescence labeling intensity associated with AE2 or NHE1 in individual GPC was analyzed along GP zones in an unbiased semi-quantitative manner using ImageJ Java-based scientific image processing software as described before (Bush *et al.,* 2010). The average intensity of intracellular and plasma membrane fluorescence were further determined for chondrocytes at the PZ (S1) and HZ (S7-8) (Bush *et al.,* 2010; Figure 6.6). To achieve this, a line was drawn centrally across a middle optical section for each chondrocyte and the peaks of fluorescence intensity at the two opposite plasma membrane surfaces (2 selected plasma membrane segments) from each individual chondrocyte to give the average of fluorescence intensity on the membrane of the cell. For a single line this can be observed as 2 peak values from

	Antibody	Target	Isotype	Notes on the cross reactivity and other remarks provided by the supplying company	Company	Fluorescent IHC test in the present study	
						Ab Titre	Comments
1.	Band 3 (C-17) goat polyclonal antibody against a peptide mapping within an internal region of band 3 of human origin (sc-20559).	AE1 (band 3)	IgG	Is recommended for detection of band 3 of mouse, rat and human origin. Detection by Western Blotting, immunofluorescence (starting dilution 1:50, dilution range 1:50-1:500) and solid phase ELISA.	Santa Cruz Biotechnology Inco., U.K.	1: 50; 1:100	Ineffective Ab. No +ve immunostaining detected when tested on the positive control tissue (rat red blood cells, kidney).
2.	Rabbit polyclonal to AE2 (ab42687)	AE2	IgG	Mouse and human. Predicted: rat, rabbit, horse, guinea pig, cow, orangutan	Abcam, UK	1:500	(see Results in 6.3.2)

Table 6.1 The antibodies against AE and NHE isoforms used in the present IHC study.

	Antibody	Target	Isotype	Cross reactivity and other remarks from the supplying company	Company	Fluorescent IHC test	
						Ab Titre	Comments
3.	SLC4A3 rabbit anti-rat polyclonal antibody (LS-C20639)	Solute Carrier Family 4, Anion Exchanger, Member 3 (SLC4A3, AE3)	IgG	Recognizes rat anion exchanger 3 (bAE3). No significant sequence homology is detected with other AE or other proteins. Does not recognize cardiac AE3. Species sequence homology: mouse 100%: human 95%: rabbit 90%. Does not recognize cardiac isoform of AE3. Actual crossreactivity of antibodies in various species has not been studied. Suitable for use in ELISA. Other applications not tested.	LifeSpan Biosciences Ltd., U.K.	1:100	Ineffective Ab. No +ve immunostaining detected when tested on the positive control tissue (rat kidney).
4.	Rabbit polyclonal to Sodium/ Hydrogen Exchanger 1 (ab67313)	NHE1	IgG	Mouse, rat, human	Abcam, UK	1:100	(see Results in 6.3.2)

Table 6.1 The antibodies against AE and NHE isoforms used in the present IHC study (cont.)

the graph (Figure 6.6B). Similarly, fluorescence intensity from the cytoplasm of a cell could be determined from any peak values between the first 2.5 µm and before the last 2.5 µm from the graph depicted (2.5 µm is the consistent approximate distant allocated to observe fluorescence intensity at plasma membrane surfaces along a line drawn across the chondrocyte optical section). Although the plasma membrane thickness is relatively very much less than this, it was chosen for reasons of convenience for the present method. The total average fluorescence signal of the 2 plasma membrane segments and the central intracellular portion gave the average of whole cellular fluorescence intensity for each GPC. The fluorescence intensity (in gray value) was expressed as a percentage with the highest intensity measured was assigned 100% thus normalizing the staining intensity of images from different GPs. Fluorescence signals at the plasma membrane were further corrected for cell surface area: volume ratio in light of previous studies that showed a relatively large reduction in the cell surface area and volume ratio in the late GP hypertrophic zone (see Chapter 4).

6.3 Results

6.3 1 Pretreatment Optimization for GPC FIHC Staining

In order to improve the quality of FIHC staining, a pretreatment technique was initially optimized. Two main procedures were tried namely the autofluorescence quenching method (using $NaBH_4$) and HIAR technique (see Materials and Methods). In this study, FIHC staining with an Ab to collagen type X was tested in P7 GPs. Collagen type X was used as it is known to be synthesized in GP only by hypertrophic chondrocytes (Kielty *et al.,* 1985; Poole & Pidoux, 1989; Sasano *et al.,* 1998). It is also a major component of the matrix and by reducing its autofluorescence the background levels could be reduced and the fluorescently-labeled Ab would be visualised more easily. Figure 6.1A shows none of the FIHC pretreatment techniques employed could remove auto-fluorescence background in GP tissue sections fixed in 2% GA + 0.7% RHT. No obvious difference in the fluorescence staining could be seen between GP sections pretreated with $NaBH_4$, HIAR or the combination of both pretreatments with the non-pretreated sections, which stained virtually the whole GP sections. There was also no apparent

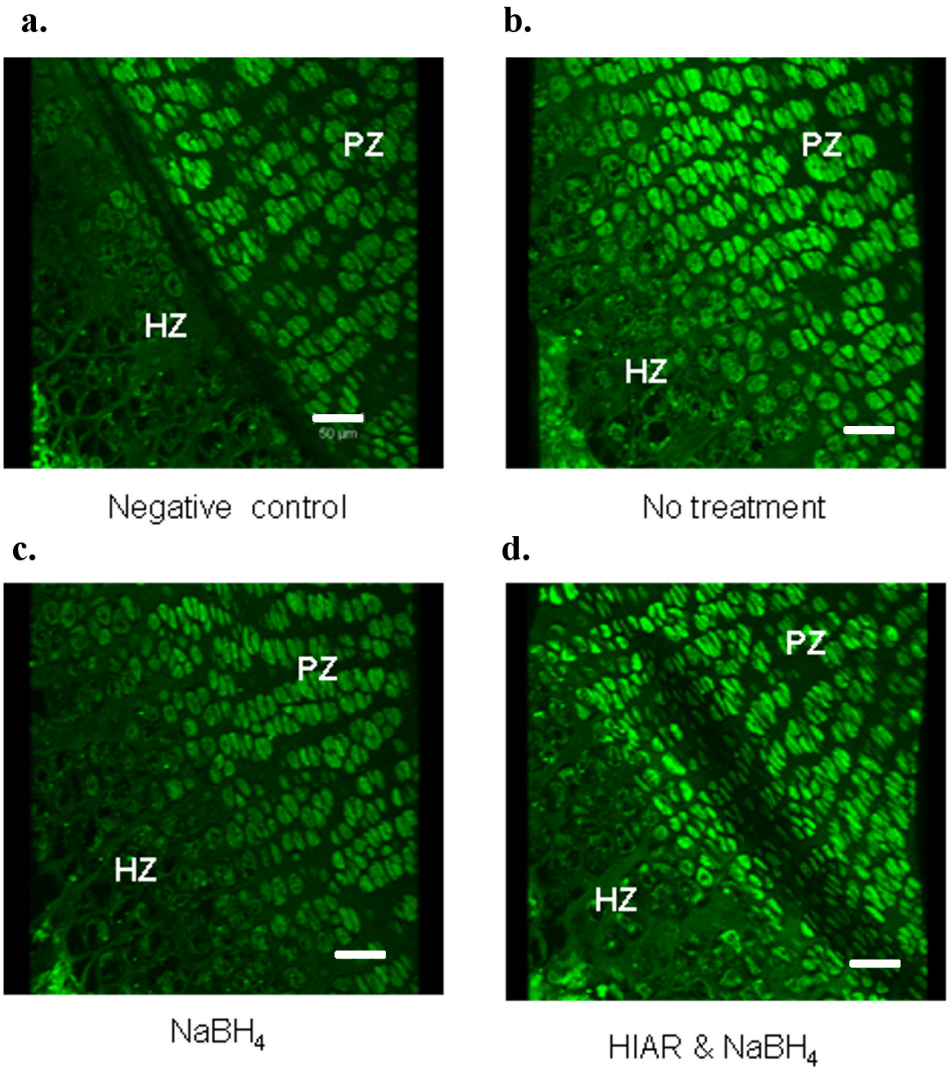

Figure 6.1A FIHC pretreatment did not remove fixative-induced autofluorescence in GA-fixed GP tissue sections. FIHC staining of collagen type X in P7 rat histological GP sections fixed with 2% GA + 0.7% RHT as observed under x20 objective of CLSM using the same settings throughout (see Materials and Methods). Sections were subjected to the following pretreatment procedures: (**a**) negative control (goat serum), (**b**) no pretreatment, (**c**) autofluorescence quenching with $NaBH_4$ and, (**d**) HIAR and $NaBH_4$. Bar scale in all panels = 50 µm. HZ, hypertrophic cells zone; PZ, proliferative cells zone.

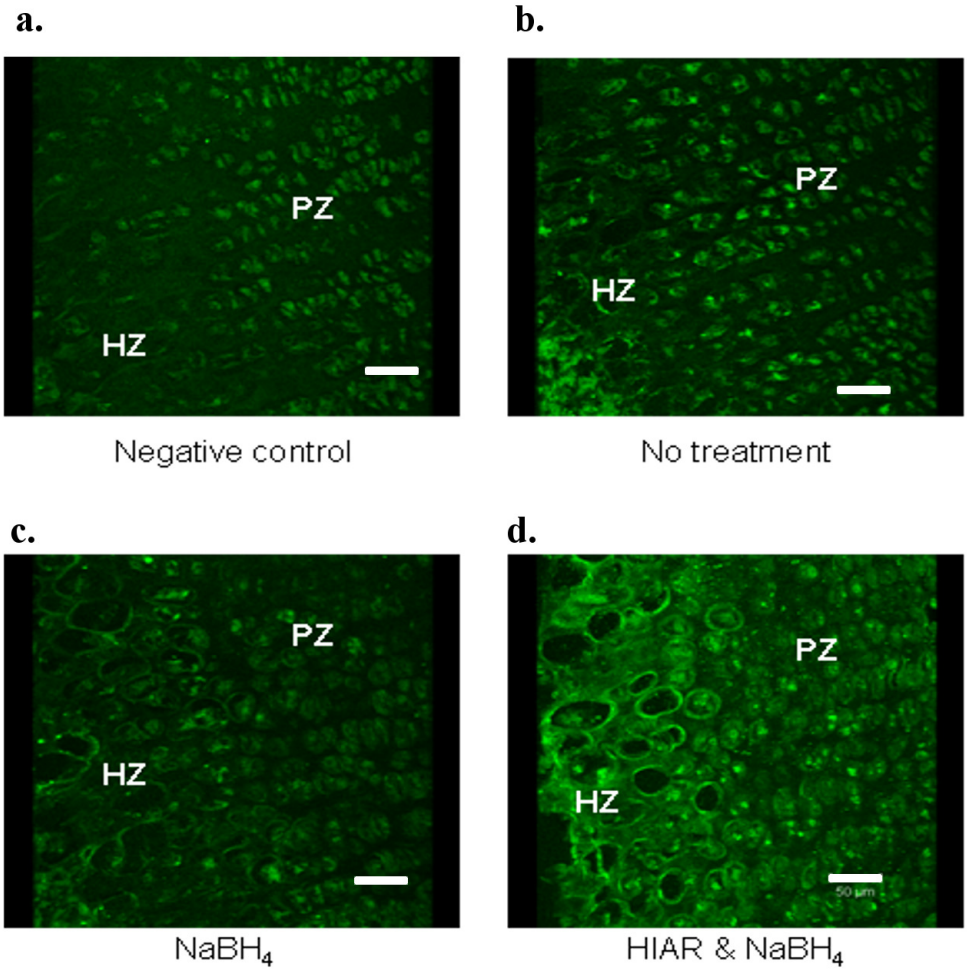

Figure 6.1B Effects of antigen retrieval and autofluorescence quenching in PFA-fixed GP tissue immunostaining. FIHC staining of collagen type X in P7 rat histological GP sections, sagitally bisected before being fixed with 4% PFA as observed under x20 objective of CLSM using the same settings throughout (see Materials and Methods). The sections were subjected to different pretreatment procedures as follows before being stained with collagen type X antibodies: (**a**) negative control (goat serum), (**b**) no pretreatment, (**c**) autofluorescence quenching with $NaBH_4$, (**d**) HIAR and $NaBH_4$. Bar scale in all panels = 50 µm. HZ, hypertrophic cells zone; PZ, proliferative cells zone.

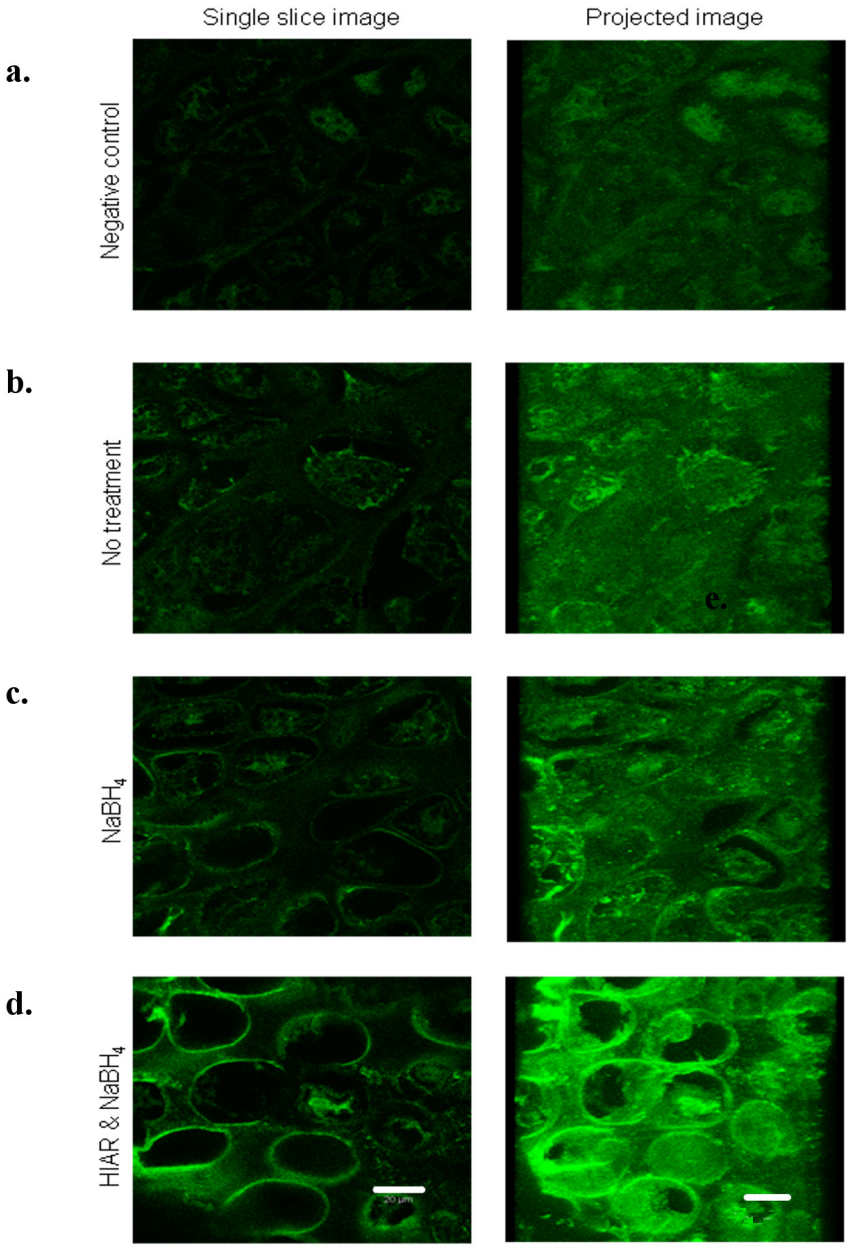

Figure 6.1C Ag retrieval and fixative-induced autofluorescence quenching in PFA-fixed GP hypertrophic cells. FIHC staining of collagen type X in P7 rat histological GP sections, sagitally bisected before being fixed with 4% PFA as observed under x63 objective of CLSM where the field of view (FOV) was selected at hypertrophic cells zone. Each section was subjected to different pretreatment procedures: (**a**) negative control (goat serum), (**b**) no pretreatment, (**c**) autofluorescence quenching with $NaBH_4$ and, (**d**) HIAR and $NaBH_4$. Images are presented as single slice optical images (2-D images, left panels) and their corresponding stack (3-D, projected) images (right panels). Bar scale in all panels = 20 µm.

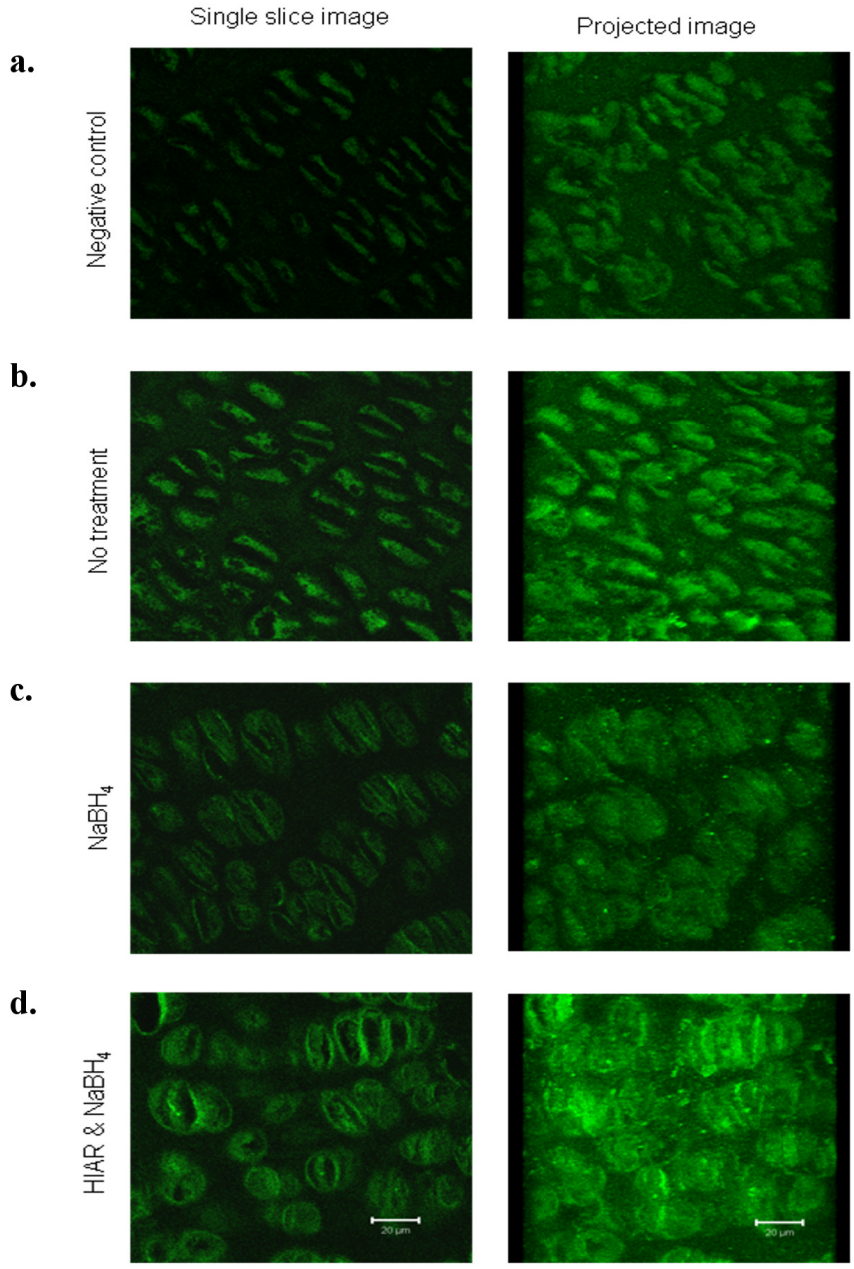

Figure 6.1D Ag retrieval and fixative-induced autofluorescence quenching in PFA-fixed GP proliferative cells. FIHC staining of collagen type X in P7 rat histological GP sections, sagitally bisected before being fixed with 4% PFA as observed under x63 objective of CLSM where the FOV was selected at proliferative cells zone. Each section was subjected to different pretreatment procedures: (**a**) negative control (goat-serum), (**b**) no pretreatment, (**c**) autofluorescence quenching with $NaBH_4$, (**d**) HIAR and $NaBH_4$. Images are presented as single slice optical images (2-D images, left panels) and their corresponding stack (3-D, projected) images (right panels). Bar scale in all panels = 20 µm.

difference with the negative control sections (Figure 6.1A (a)), which suggests that the auto-fluorescence background was mainly due to the GA (Renshaw, 2007) that was used to fix the GP tissues. When the FIHC staining was performed in GP tissue sections fixed in 4% PFA, pretreatment with the combination of $NaBH_4$ and HIAR demonstrated an obvious improvement in the fluorescence labeling of collagen type X compared to the un-pretreated or singly pre-treated sections (Figure 6.1B, 1C and 1D). The sections treated with HIAR alone gave inconsistent results (data not shown). The autofluorescence background produced by the PFA fixed tissue was relatively lower as shown in the negative control sections (Figure 6.1B(a), 1C and 1D). The staining of collagen type X was detected mainly around the hypertrophic chondrocytes and the surrounding matrix of GP cartilage (Figure 6.1B (d) and 1C). In GP proliferative zone, the collagen type X staining was observed occasionally around the chondrocytes (Figure 6.1D). This study has optimized the right pretreatment steps for FIHC staining on GP sections fixed in 4% PFA. The stepwise procedure was summarized in Figure 6.2. In light of the present result, the following FIHC study would avoid using GA-fixed GP tissues since the relatively strong autofluorescence background induced by the fixative could not be satisfactorily removed by the current established pretreatment method.

6.3 2. NHE1 and AE2 Positive FIHC Staining in Kidney and GIT

Having established the optimum FIHC pretreatment steps for the GP, the FIHC study was performed for NHE1 and AE2. As a part of quality assurance of the FIHC results obtained, the anti-NHE1 and AE2 Ab staining were first tested on tissues known for positively expressing the proteins in relatively high levels. For NHE1 and AE2, P7 rat kidney and GIT were used as the control tissues respectively (Mahnensmith and Aronson, 1985; Alrefai *et al.,* 2001). Figure 6.3A shows no fluorescence staining of NHE1 in the negative control kidney section (a-b) compared to the positively stained section (c-f). Guided by the corresponding transmitted light image (d and f), the localisation of the NHE1 based on the fluorescence labeling (c and e) was mainly observed in renal corpuscles and renal convoluted tubules of the renal cortex region. For the AE2, the localisation of the transporters was confined at the mucosa membrane of the GIT (Figure 6.3B (c-f)).

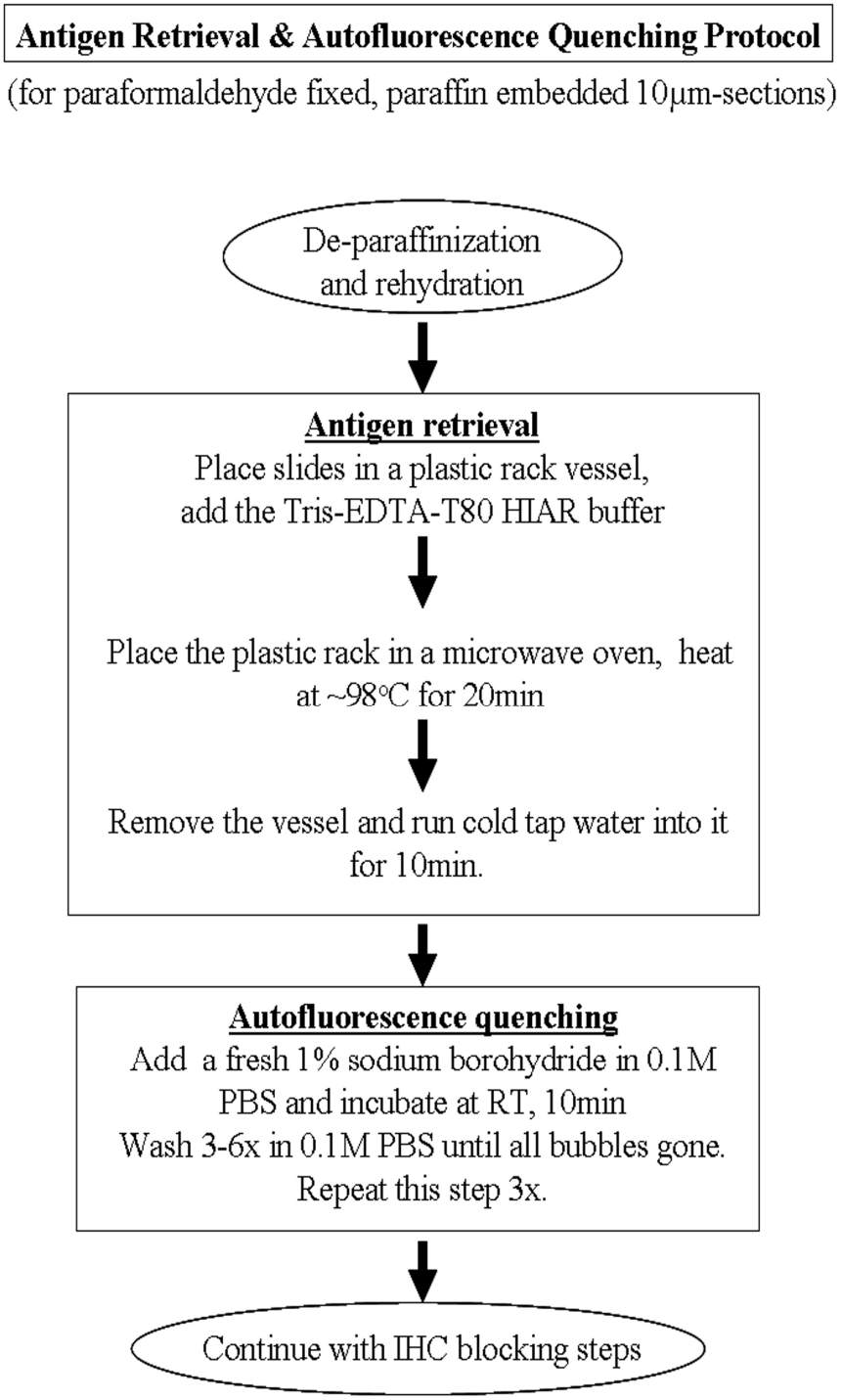

Figure 6.2 Summary of Ag retrieval and autofluorescence quenching protocol. Optimized techniques for Ag retrieval and fixative-induced autofluorescence quenching of GP histological sections (10 µm in thickness) fixed in 4% PFA, as pretreatment steps prior to FIHC procedure. pretreatment steps prior to FIHC procedure.

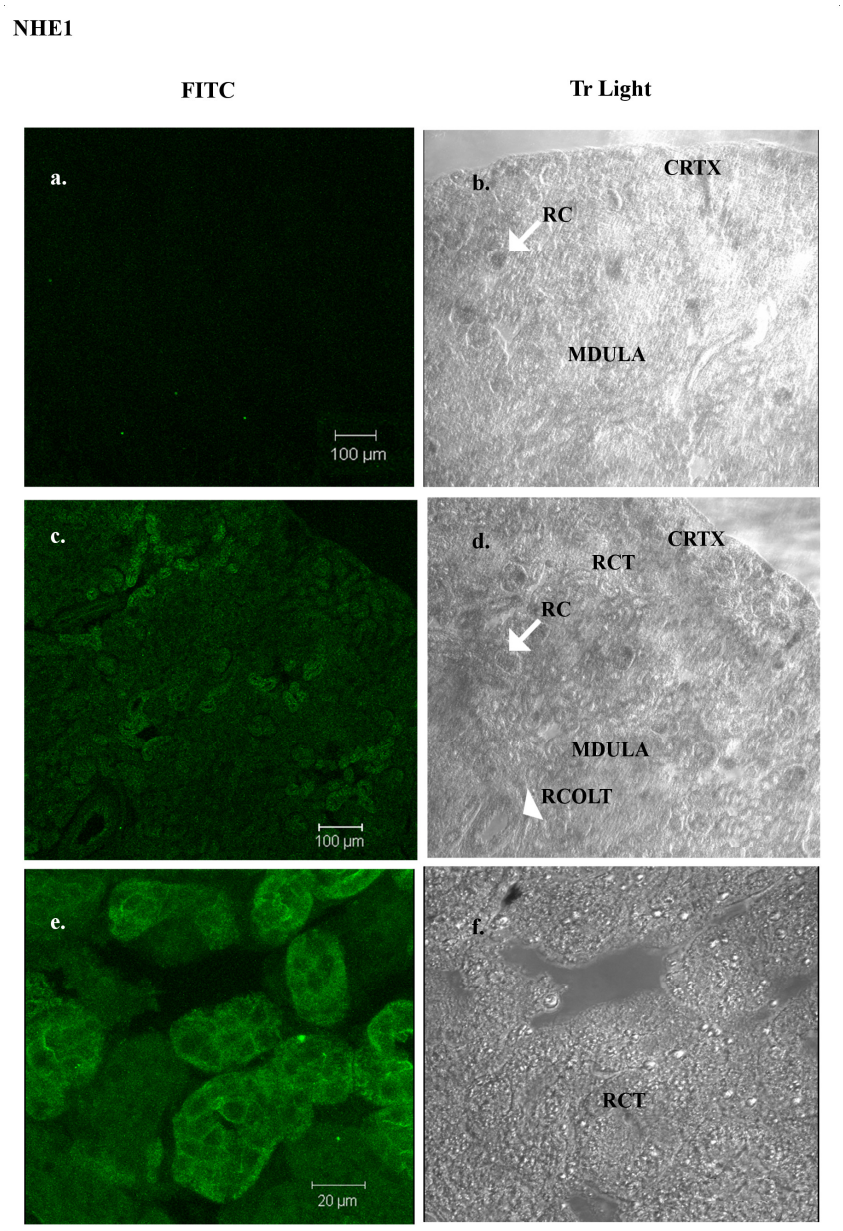

Figure 6.3A Positive NHE1 FIHC staining in the rat kidney. NHE1 was positively labeled by FIHC staining in P7 rat histological kidney sections fixed with 4% PFA. Primary Ab at 1:300 dilution was used and the secondary Ab was conjugated with FITC for FIHC staining. The fluorescence images (FITC) were shown in the left panels and their corresponding transmitted light images (Tr Light) were shown in the right. The negative control sections (a and b) are shown in comparison to the positively labeled NHE1sections (c and d) as observed under x10 objective of CLSM. The (e) and (f) showed the higher magnification images of positively NHE1 labeled sections as observed under x63 objective of CLSM. Bar scale = 100 µm and 20 µm in (a-d) and (e-f) respectively. CRTX, cortex; MDULA, medulla; RC, renal corpuscle; RCT, renal convoluted tubule; RCOLT, renal collecting tubule.

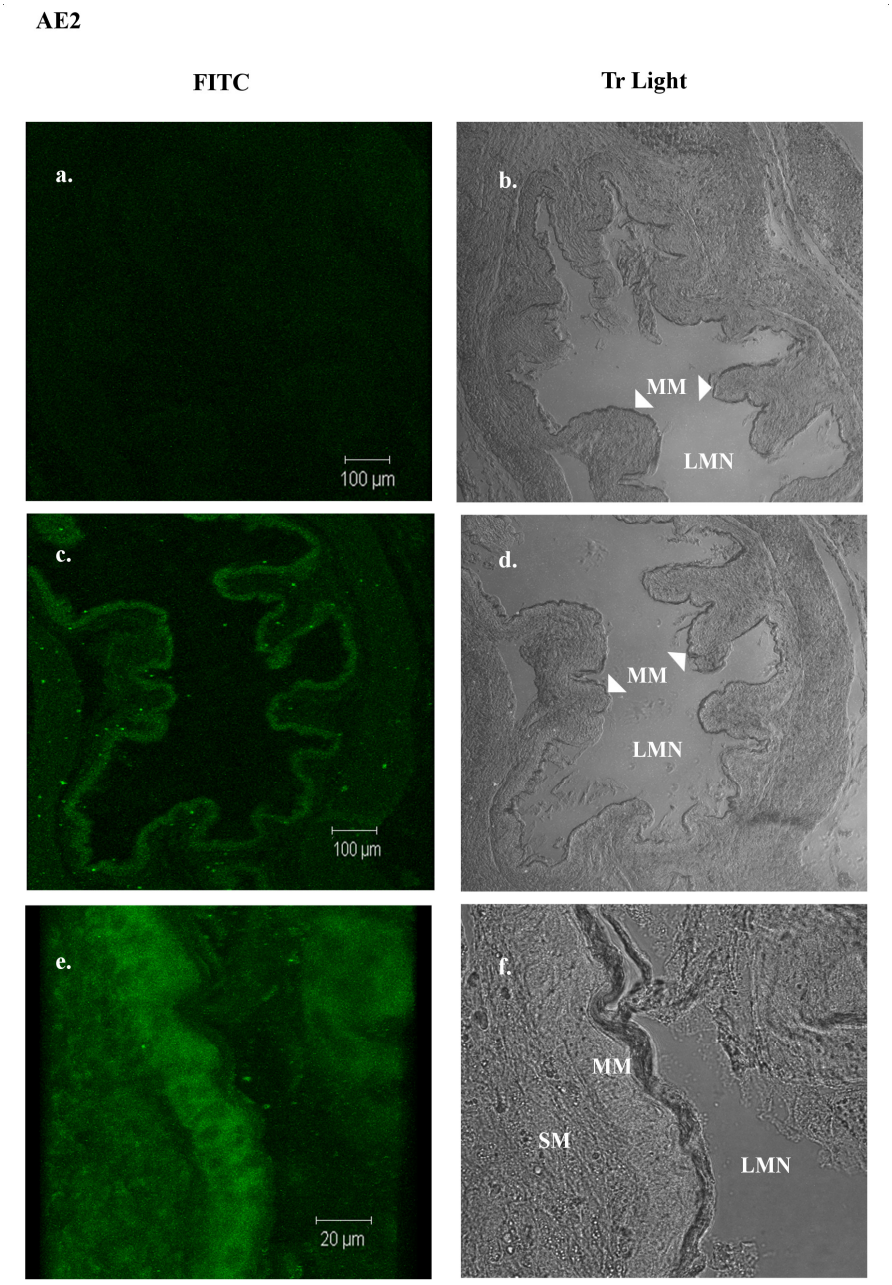

Figure 6.3B Positive AE2 FIHC staining in the rat gastrointestinal tract (GIT). AE2 was positively labeled by FIHC staining in P7 rat histological GIT sections fixed with 4% PFA. Primary Ab of 1:500 dilution was used and the secondary Ab was conjugated with FITC for the FIHC staining. The fluorescence images (FITC) were shown in the left and their same scale corresponding transmitted light images (Tr Light) were shown in the right panels. The negative control (a and b) are shown in comparison to the positively labeled AE2 sections (c and d) as observed under x 10 objective of CLSM. The (e) and (f) showed the higher magnification images of positively AE2 labeled sections observed under x63 objective of CLSM. Bar scale = 100 µm and 20 µm in (a, c) and (e) respectively. MM, mucosal membrane; LMN, lumen; SM, submucosa.

This was confirmed with no fluorescence labeling observed in the negative control section (a-b). This result gave assurance that the antibodies of NHE1 and AE2 used in the current FIHC study was reliable and validated the next immunochemical staining study that identified the presence and distribution of NHE1 and AE2 in GP tissues.

6.3 3 NHE1 and AE2 Positive FIHC Staining in P7 Rat GPC

This section presents the result of NHE1 and AE2 localisation in P7 rat GP tissues using anti NHE1 and AE2 FIHC staining. Low power (x10 objective lens) CLSM images showed no NHE1 fluorescence staining in the negative control sections (Figure 6.4A (a-b)) in comparison with the tested GP sections, which revealed distribution of fluorescence staining along the GP (Figure 6.4A (c-f)). The fluorescent signal was less intense at the early PZ but increasing at the late PZ and early HZ, before decreasing in the middle to late HZ. Almost the same distribution of fluorescence staining could be observed for AE2, with the most intense fluorescence staining observed at the late PZ and early hypertrophic GP zone (Figure 6.4B (c-f)). As for comparison, no fluorescence signal was observed in the negative control sections (Figure 6.4B (a-b)). Further examination in high power (x63 objective lens) CLSM images (FITC and transmitted light images) revealed the cellular distribution of both NHE1 and AE2 fluorescence labeling in GPCs was mainly at S1-S6 of the GP proliferative and hypertrophic zones (Figure 6.5). This finding was consistent across proximal tibial GP of all five animals. This finding indicates the localisation of both the NHE1 and AE2 in GPC were site-specific within the zones of GPC differentiation.

6.3 4 Localisation of NHE1 and AE2 in GPC Plasma Membrane and Intracellular Cytoplasm

In order to specify the localisation of NHE1 and AE2 in GPC, the cellular distribution of immunofluorescence staining was further determined semi-quantitatively by measuring fluorescence intensity of the plasma membrane and intracellular immuno-staining of PZ (S1) and HZ (S7-S8) cells in P7 proximal tibial GP (Figure 6.6; see Materials and Methods). For NHE1, the

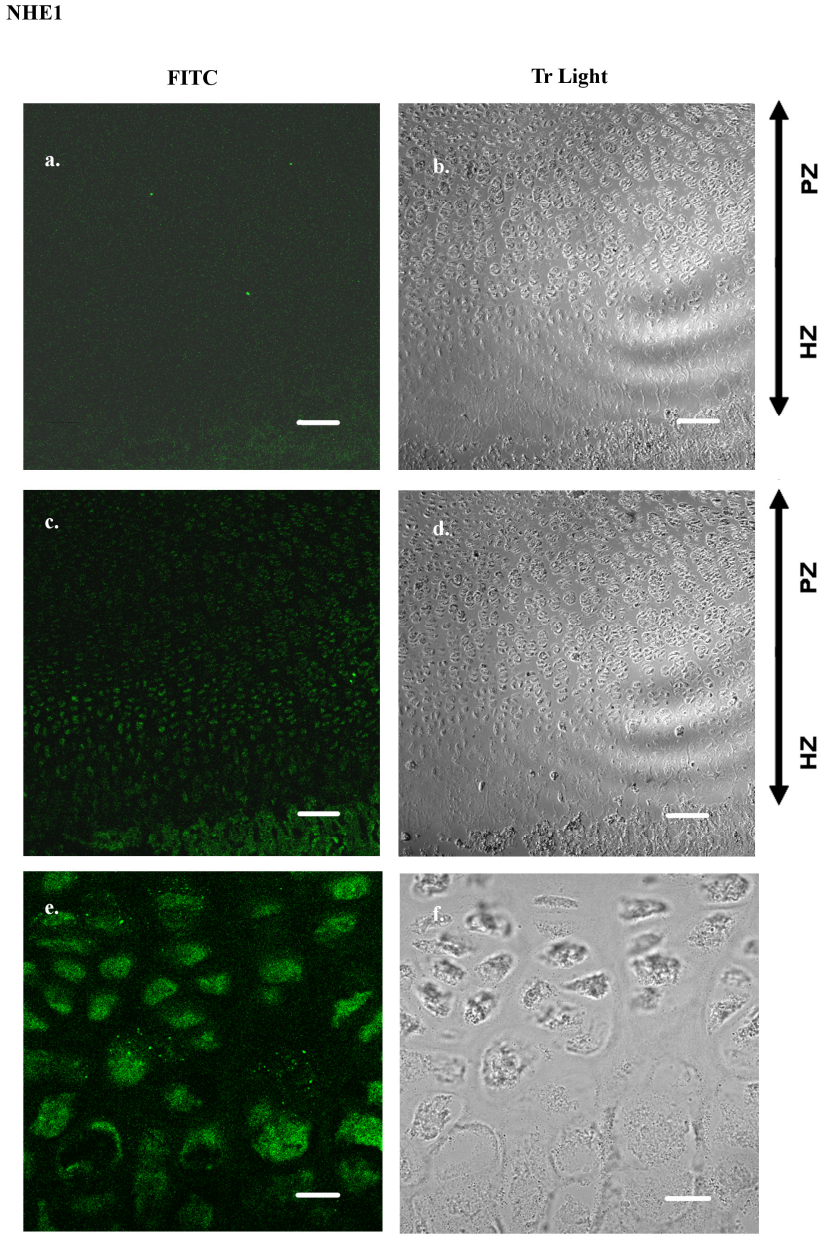

Figure 6.4A Positive NHE1 FIHC staining in rat P7 GPs. NHE1 was positively labeled by FIHC staining in P7 rat histological proximal tibia GP sections, sagitally bisected before being fixed with 4% PFA. Primary Ab of 1:100 dilution was used and the secondary Ab was conjugated with FITC for the FIHC staining. The fluorescence images (FITC) were shown in the left and their corresponding transmitted light images (Tr Light) were shown in the right panels. The negative control (a and b) were shown in comparison to the positively labeled NHE1 sections (c and d) as observed under x10 objective of CLSM. The (e) and (f) show the higher magnification images of positively NHE1 labeled sections at the hypertrophic GPC zones observed under x 63 objective of CLSM. Bar scale = 100 μm and 20 μm in (a-d) and (e-f) respectively. HZ, hypertrophic cells zone; PZ, proliferative cells zone.

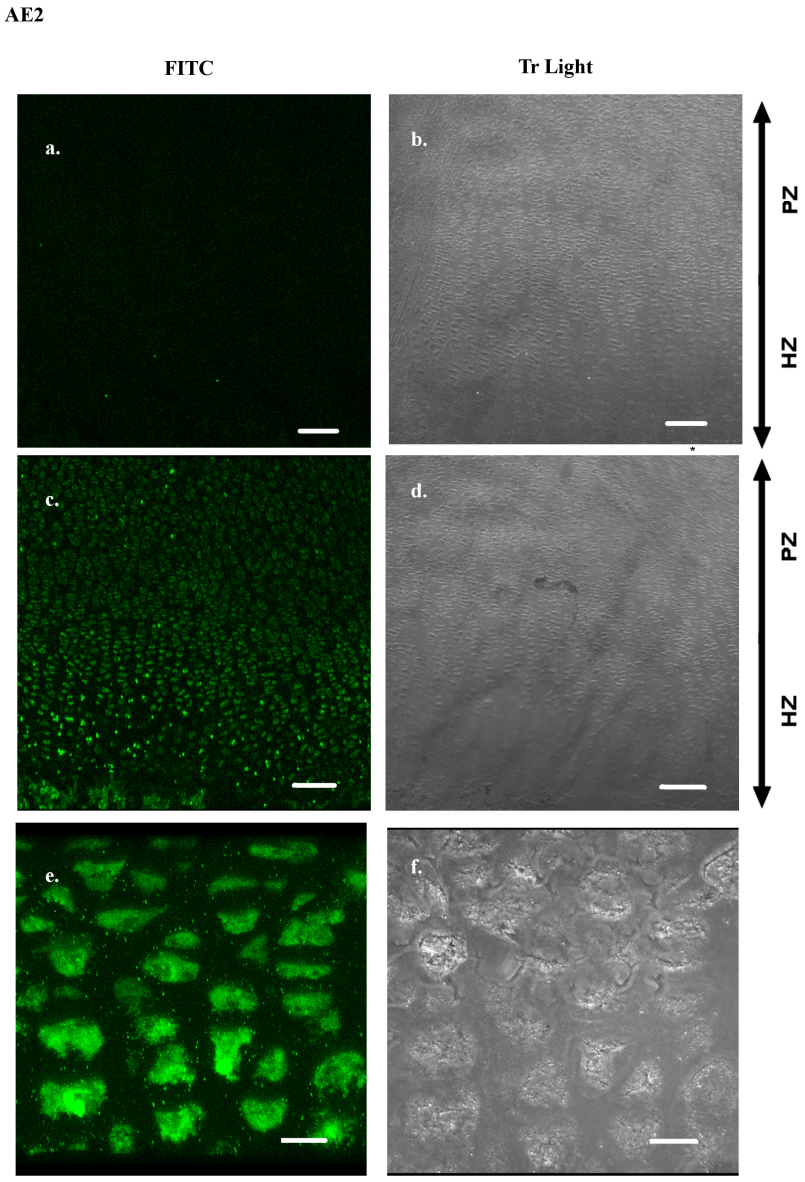

Figure 6.4B Positive AE2 FIHC staining in rat P7 GPs. AE2 was positively labeled by FIHC staining in P7 rat histological proximal tibia GP sections, sagitally bisected before being fixed with 4% PFA. Primary Ab of 1:500 dilution was used and the secondary Ab was conjugated with FITC for the FIHC staining. The FITC were shown in the left and their corresponding transmitted light images (Tr Light) were shown in the right panels. The negative control (a and b) were shown in comparison to the positively labeled AE2 sections (c and d) as observed under x10 objective of CLSM. The (e) and (f) showed the higher magnification images of positively AE2 labeled sections at the hypertrophic GPC zones observed under x63 objective of CLSM. Bar scale = 100 μm and 20 μm in (a-d) and (e-f) respectively. HZ, hypertrophic cells zone; PZ, proliferative cells zone.

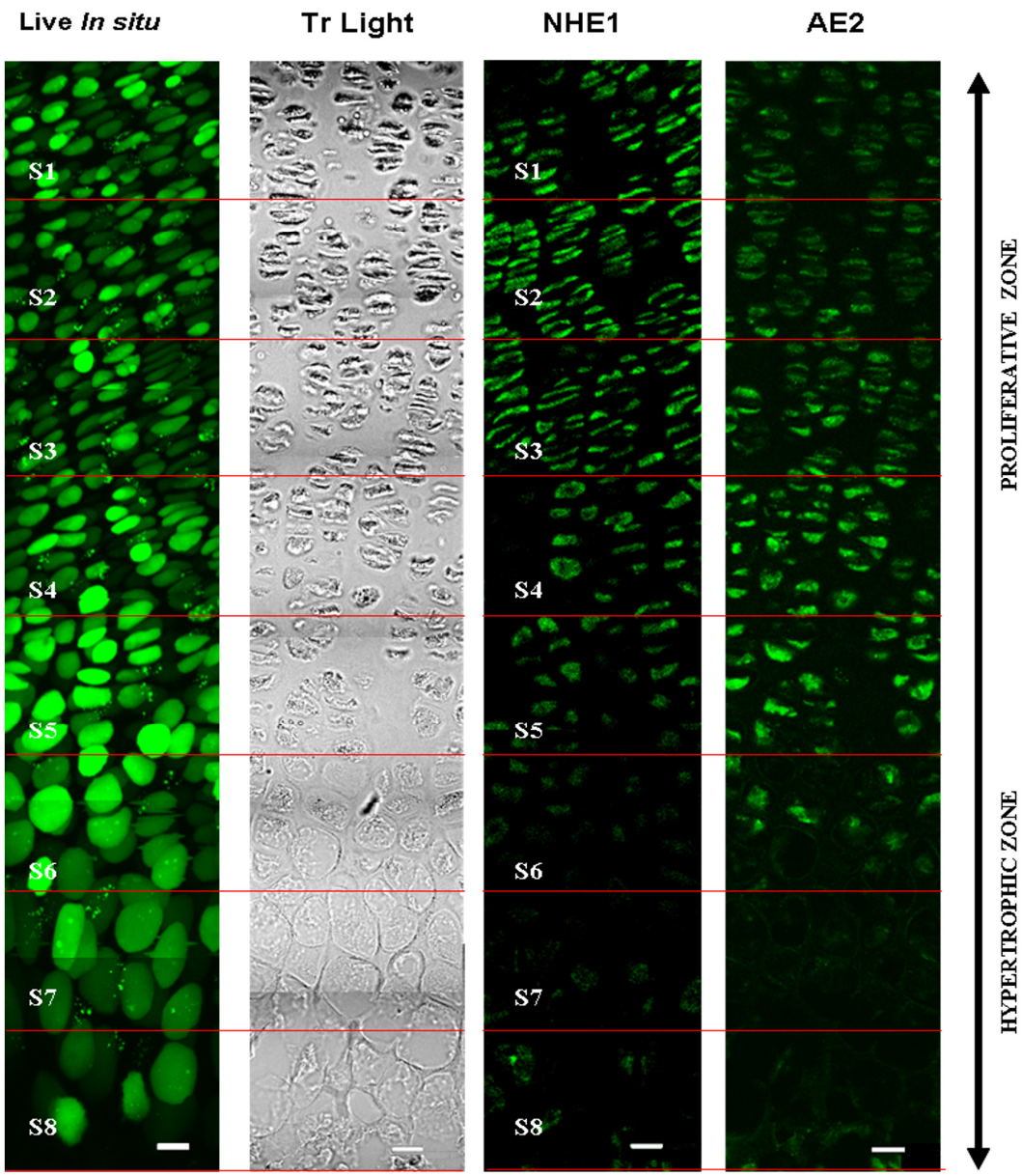

Figure 6.5 Positive fluorescence signal associated with NHE1 and AE2 in the GP IHC. Paraffin embedded sections (10 µm-thick) of proximal tibia GP of 7-day old rat showed positive fluorescence (FITC) in GPC at different zone sections of proliferative zone and hypertrophic zone cells (S1-S8). Tr Light = transmitted light image corresponding to the fluorescence images. *In situ* GPC (figure far left) as viewed in unfixed live (calcein-loaded) GP tissue was shown for comparison. Images were taken using CLSM (x63 objective lens). Bar = 20 µm.

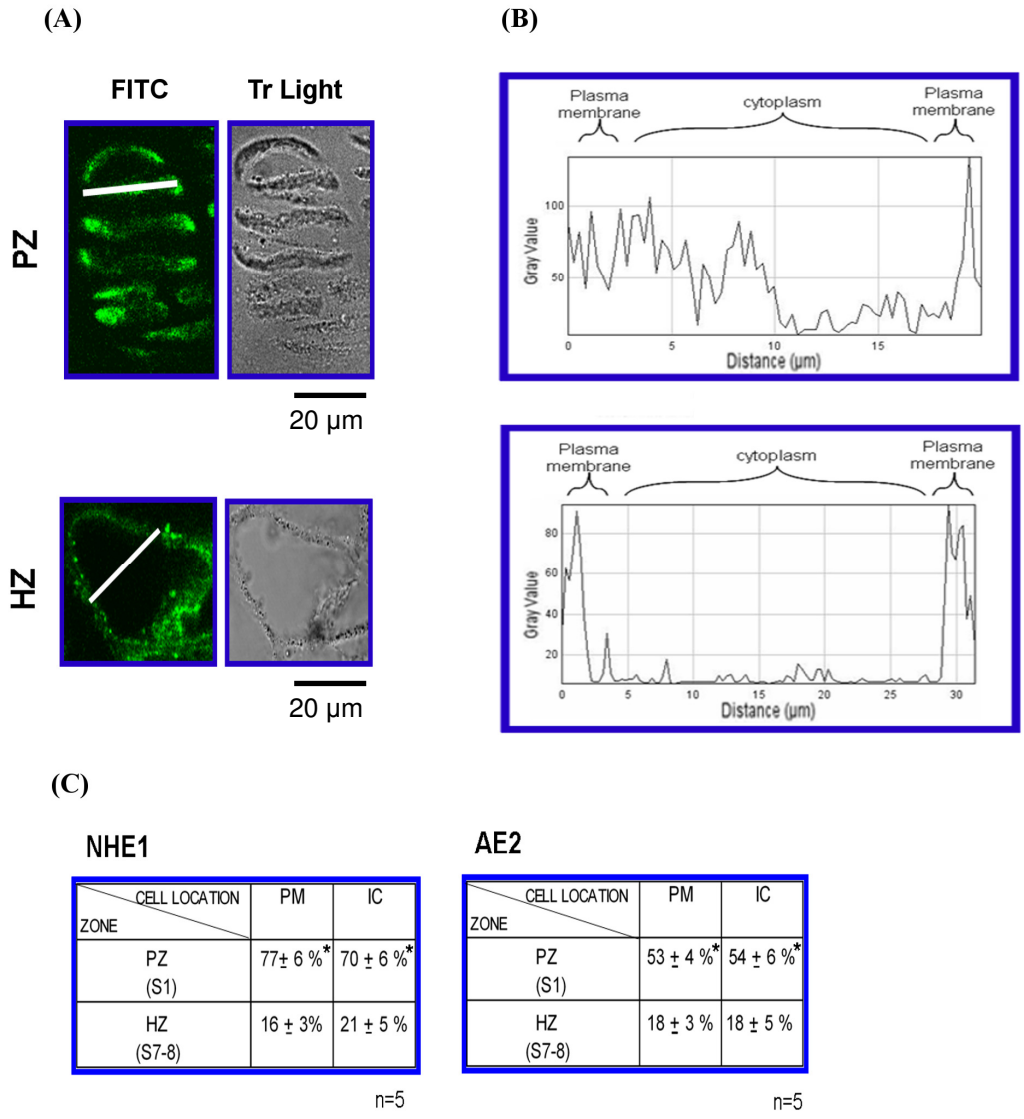

Figure 6.6 Localisation of NHE1 and AE2 in GPC plasma membrane and cytoplasm. Localisation of NHE1 and AE2 in GPC plasma membrane (PM) and intracellular cytoplasm (IM) by FIHC was measured semi-quantitatively (see Materials and Methods). Bar = 20 µm. (**A**) GPC NHE1 or AE2 localisation is shown in typical proliferative (PZ, top) and hypertrophic (HZ, bottom) chondrocyte(s) determined from the corresponding transmitted light (Tr Light) image. (**B**) Examples of the intensity profiles of fluorescence associated with NHE1 and AE2 as determined along a line drawn across an optical section of a proliferative (top) and hypertrophic (bottom) chondrocyte using ImageJ. Fluorescence intensity is in gray scale value. (**C**) Table of values (% highest intensity) representing cellular localisation of NHE1 (left) and AE2 (right) in GPC PM and IC; and in the corresponding PZ (S1) and HZ (S7-8). *Significantly different from corresponding HZ (Student's unpaired *t*-test; $P<0.05$, n=5).

immunofluorescence intensity in GPC plasma membranes was significantly 5-fold higher in PZ cells compared to HZ cells (Student's unpaired *t*-test; $P<0.05$; n=5). The intracellular cytoplasm of PZ cells also had significantly higher fluorescence intensity (~3-fold) than the HZ cells ($P<0.05$). However there was no significant difference in the fluorescence intensity between the plasma membrane and intracellular membrane of the cells from the same zones. For AE2, the fluorescence intensity in both plasma membrane and intracellular cytoplasm of the PZ cells was significantly higher than the HZ cells (~3-fold; $P<0.05$). The fluorescence intensity between plasma membrane and intracellular cytoplasm within the same zones was not significantly different. These results demonstrate that PZ cells had significantly higher fluorescent intensity of NHE1 and AE2 immunostaining than in HZ cells. However, there was no apparent difference in localisation of NHE1 and AE2 between plasma membrane and intracellular cytoplasm within a same cell in either PZ or HZ. Fluorescence intensity of the plasma membrane and intracellular immuno-staining of other zone sections between S1 and S7-S8 were not determined due to inconsistent quality of the GPC sections to allow the discrimination between the plasma membrane and intracellular cytoplasm fluorescent labeling.

6.3 5 Semi-quantitative Distribution Pattern of NHE1 and AE2 in GPC along the GP

To examine the overall semi-quantitative distribution pattern of NHE1 and AE2 in GPCs along P7 proximal tibia GP (S1-S8), the average fluorescence labeling intensity associated with membrane transporter localisation was determined as described in Materials and Methods. Figure 6.7A shows a relatively high level of NHE1 immunofluorescence intensity throughout S1-S5 before decreasing dramatically from S6-S8 (One-way ANOVA; $P<0.001$). The fluorescence intensity was significantly lower in S8 compared to the maximum intensity that was reached in S5 (Student's unpaired *t*-test; $P<0.001$; 5[15]). Figure 6.7B demonstrates a significant increase in immunofluorescence intensity of AE2 throughout S1-S5 (One-way ANOVA; $P<0.001$). The peak intensity was observed in S5, which was significantly higher than the original intensity recorded in S1 (Student's unpaired *t*-

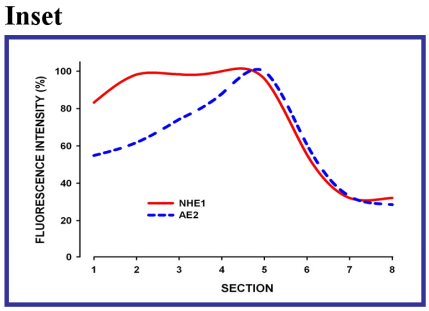
Inset
FLUORESCENCE INTENSITY (%)
SECTION
NHE1
AE2

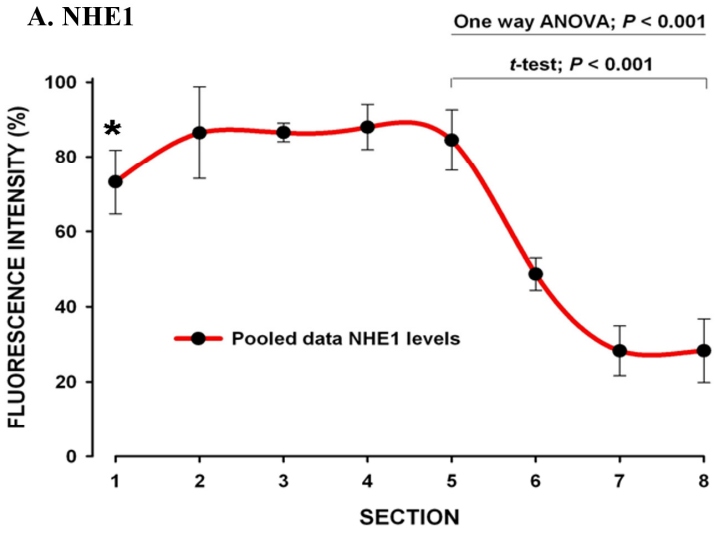
A. NHE1
One way ANOVA; P < 0.001
t-test; P < 0.001
*
Pooled data NHE1 levels
FLUORESCENCE INTENSITY (%)
SECTION

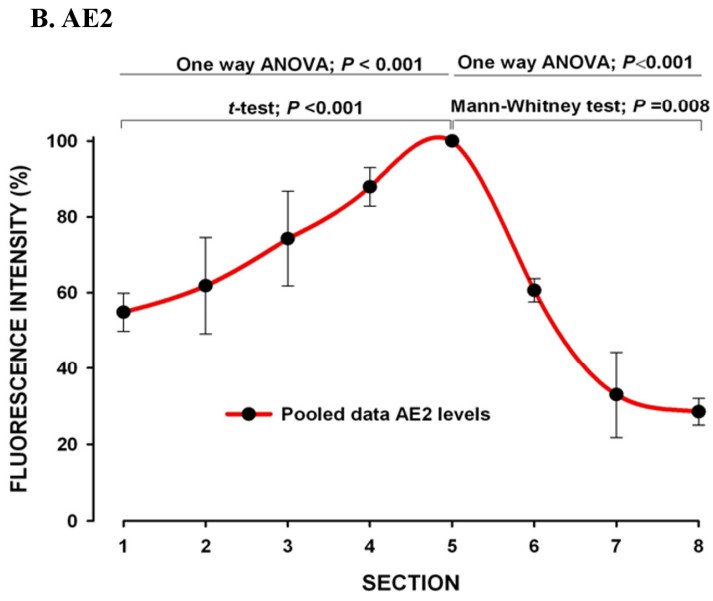
B. AE2
One way ANOVA; P < 0.001
One way ANOVA; P<0.001
t-test; P <0.001
Mann-Whitney test; P =0.008
Pooled data AE2 levels
FLUORESCENCE INTENSITY (%)
SECTION

Figure 6.7 Localisation of NHE1 and AE2 in GPC along the GP. Overall NHE1 (A) and AE2 (B) fluorescence labelling intensity (%) pattern are shown as seen at the plasma membrane and intracellular compartments of chondrocytes along P7 rat proximal tibia GPs. Data pooled from five separate animals and at least 15 cells/ section. Section 1 (S1) is nearest to the epiphyseal end and marks the early proliferative zone and section 8 (S8) is nearest to the metaphyseal end and denotes the late hypertrophic zone of the GP. The inset shows the graphs in (A) and (B) were re-plotted together for easier comparison by normalising the data to 100% at S5. *Significant difference compared to S1 of AE2 (Student's unpaired *t*-test; $P< 0.005$, n=5).

test; $P<0.001$; data from at least 5[15]). After reaching the highest fluorescence intensity in S5, there was a significant decrease in the intensity from S6-S8 (One-way ANOVA; $P<0.001$). The fluorescence intensity of AE2 in S8 was significantly lower than in S1 (Mann-Whitney test; $P=0.008$; 5[15]). Although immunofluorescence labeling of both NHE1 and AE2 shared the highest intensity in S5 and the lowest in S8, the intensity of NHE1 in S1 was significantly higher than in AE2 (Student's unpaired *t*-test; $P<0.005$; 5[15]). Figure 6.7 (inset) demonstrates direct comparison between NHE1 and AE2 immunofluorescent intensity along GP after the data from Figure 6.7(A & B) being normalized to 100% at S5 (peak intensity in both graphs). It shows that while NHE1 was maintaining a constantly higher level of immunofluorescent labeling throughout S1-S5, the AE2 labeling has initially lower immunofluorescence labeling and was gradually increasing toward S5. Both NHE1 and AE2 immunofluorescence decreased dramatically after S5 toward S8.

6.4 Discussion

6.4 1 The Key Findings

This study has optimized FIHC staining technique for NHE and AE detection on PFA-fixed and paraffin-embedded GP cartilage histological sections. The FIHC result identified a consistent distribution pattern of AE2 and NHE1 in postnatal GP cartilage. The NHE1 was found at a relatively higher level throughout proliferative and early hypertrophic zones, whereas AE2 level was initially lower at early proliferative zone but gradually increased toward the late proliferative and early hypertrophic zones. Both NHE1 and AE2 levels decreased dramatically from early

to late hypertrophic zones. At the cellular level, the NHE1 and AE2 showed almost equal distribution within the intracellular and plasma membrane compartments of the proliferative and hypertrophic zone, with the overall immunofluorescent staining being significantly higher in PZ compared to HZ.

6.4 2 FIHC Technique

The basis of IHC comprises three scientific disciplines: immunology, histology, and chemistry. The fundamental concept behind IHC is the demonstration of antigens within tissue sections by means of specific antibodies. Once antigen–antibody binding occurs, it can be demonstrated with a coloured histochemical reaction visible by light microscopy (enzymatic immunolabeling) or fluorochromes with excitation light (fluorescent immunolabeling) (Ramos-Vara, 2005). An advantage of using fluorescent-label immunostaining is it is relatively quick and easy to perform compared to enzyme-immunolabeled histochemistry, which is more complex and time-consuming (Renshaw, 2007). In addition, the present study used indirect fluorescent immunostaining method to localize the NHE1 and AE2, which is simple and economical to do because the reaction is only a two-step process with a secondary Ab conjugated directly with fluorescent label (Renshaw, 2007).

6.4 3 Background Staining and Ag Masking Problems in FIHC Study

However, one setback of the fluorescent immunohistochemistry method is the presence of unwanted back-ground fluorescence, which is either due to autofluorescence of the tissue of interest, or presents as a fluorescent background caused by nonspecific binding of the fluorescent antibody giving a false positive staining (Ramos-Vara, 2005). Besides, the indirect immunostaining method used provides little amplification of the visible signal, so their use is limited to detection of plentiful Ag but lacks sufficient sensitivity for the detection of relatively low concentrations of Ag in question.

Therefore understanding the source of the background staining is the key strategy to improve the discrimination of the Ag labeling when using the indirect fluorescent immunostaining technique. There are three common types of

autofluorescence, which can be categorized as intrinsic or induced by fixation media and tissue processing: i) elastin and collagen autofluorescence, ii) lipofuscin autofluorescence and iii) aldehyde (fixative)-induced autofluorescence (Renshaw, 2007). Native fluorescence of elastin and collagen is typically found in blood vessel walls and skin; whereas lipofuscin is prominent in neurons, glial cells cardiac muscle cells but is also found in a wide range of cell types (Billinton and Knight, 2001). For GP sections, the presence of native autofluorescences was less problematic compared to the autofluorescence caused by aldehyde fixative during FIHC staining. Aldehyde fixative served as a good choice for the preservation of GP tissue morphological details for electron microscopy (Paljarvi *et al.,* 1979), or for general histology when the fixative was coupled with a cationic dye (Hunziker *et al.,* 1983). However the fixative has a major drawback as it may further augment background fluorescence when the aldehyde-fixed tissue is destined for immunochemical staining. Formaldehyde forms covalent bonds between adjacent amine-containing groups through Schiff acid-base reactions. As a consequence, fluorescent products are formed, resulting in an intense fluorescent background. Moreover, these products may also non-specifically react with antibodies (Vieges *et al.,* 2007). Molecules that contribute to the intrinsic and induced autofluorescence are responsible for an emission of fluorescence between 450 and 650 nm that overlaps the emission wavelength of fluorophores widely used in immunofluorescence studies such as fluorescein isothiocianate (FITC) (Vieges *et al.,* 2007)

Besides that, background staining could also be contributed by hydrophobic protein interactions, and non-specific attachment of conjugated antibodies to free aldehyde groups in aldehyde-fixed specimens (Ramos-Vara, 2005). Tissue proteins are rendered more hydrophobic by fixation with aldehyde containing fixatives as the result of cross-linking of reactive epsilon- and alpha-amino acids, both within and between adjacent tissue proteins. The increase hydrophobicity of proteins during fixation increases the background staining in immunohistochemical procedures (Ramos-Vara, 2005; Renshaw, 2007). The non-specific attachment of conjugated antibodies to free aldehyde groups introduced by aldehyde-containing

fixatives present in the tissue is more common when glutaraldehyde is being used, but prolonged fixation in formaldehyde can also produce free aldehydes (Ramos-Vara, 2005).

Moreover, Ag masking due to cross linking of proteins in aldehyde-fixed tissue section has been recognized as one of the major causes for immunohistochemical failures in the past (D'Amico *et al.,* 2009). Although adequate fixation is an important factor in successful IHC localisation of Ag through preservation of tissue morphology and immobilization of the Ag, it could adversely affect the preservation of Ag immunoreactivity and hinder adequate penetrability of tissue to the immunochemical reagents (Berod *et al.,* 1981). As discussed earlier, this Ag masking by cross linking proteins also causes other related background staining problems in FITC.

6.4 4 Pretreatment of FIHC Study

Having understood the issues related to FIHC method, coping with the Ag masking and background staining is therefore particularly important when adopting FIHC technique. This study has found that a combination of HIAR technique and the use of 1% $NaBH_4$ (Figure 6.2) were effective to improve FIHC staining of PFA-fixed GP tissues in pre detection phase. The theory behind HIAR remains unclear (Renshaw, 2007), but a possible mechanism of the technique was the loosening or breaking of the cross-links (methylene bridges) between proteins induced by aldehyde fixation (Shi *et al.,* 1991 & 1992). The breakage of the cross-links allows the proteins to take on a more tertiary-like structure, allowing antibodies access to the epitope. This technique demonstrates that cross-linking of protein may be a reversible chemical reaction under certain conditions, serving to unmask antigenicity after aldehyde fixation (Shi *et al.,* 2001).

Besides that, calcium precipitation (and also that of other divalent metal cations) is currently thought to play a significant role in effective Ag retrieval. Methylene bridge formation allows bonding of proteins to calcium ions and their removal or precipitation is thought to be a critical step in salt-mediated Ag retrieval (Renshaw, 2007). Morgan *et al.* (1997) demonstrated that the chelating effects of EDTA to be improved at high pH compared with low pH. The present study

showed that to detect NHE1 and AE2 antigens, HIAR solution comprising of with 0.01 M Tris Base buffer, 0.001 M EDTA (pH 9.0) gave satisfactory FIHC results.

However, care has to be taken when using the HIAR technique. Tissues undergoing this procedure should be on tissue-adhesive-coated slides to improve tissue adherence to the glass. Harsh conditions of heat-induced Ag retrieval often cause tissue to lift off the slides, and friable tissues are prone to lifting, even on coated slides (Renshaw, 2007)

The use of sodium borohydrate in the present study reduces aldehyde-induced autofluorescence by reducing Schiff bases ($R_1HC=NR_2$) that are formed between the aldehyde and NH_2 groups (Renshaw, 2007). This also removes non-specific attachment of conjugated antibodies to free aldehyde groups introduced by the aldehyde-containing fixatives present in the tissue. Other compounds that can abolish this binding include ammonium chloride, ammonium carbonate buffer, lysine, and glycine (Baschong, 2001).

For GA-fixed sections, the Ag masking by the proteins cross-linking is a major drawback for immunochemical staining due to the excessive and aggressive cross-linking compared to PFA or formaldehyde (Renshaw, 2007). In addition, there is a relatively higher degree of autofluorescence compounds formed between the aldehyde fixatives and proteins or amines. All these could be the reasons why antigens in GA-fixed tissue could not be restored by the current FIHC optimization method (Figure 6.1A).

There are a number of other different FIHC pretreatment approaches that could be attempted for GA-fixed tissue sections. Baschong *et al.* (2001) summarized different types of strategies to control autofluorescence that were (a) extraction of the autofluorescent constituent by dissolution such as treatment with ammonia/ethanol; (b) chemical modification of the fluorochrome such as the use of photochemical methods, *e.g.* photobleaching, through which the molecular structure of a fluorophore is changed so that it loses its ability to fluoresce; and (c) masking of the autofluorescent structure by appropriate staining. Autofluorescence masking can be achieved using Trypan Blue and Sudan Black B by its veiling activity on autofluorescence without interfering with the surface fluorescent label

resembles the effect of counterstains (Baschong *et al.* 2001). Other strategies involve using instruments, such as optimized filter sets, CLSM and post-measurement image correction also allow discrimination of autofluorescence through the use of mathematical models (Steinkamp and Stewart, 1986; Van de Lest *et al.* 1995).

A number of workers have reported several methods that combined or modified the above mentioned strategies that could be worthwhile on GA-fixed GP sections. An example is the use of water-bath heating for 30 mins at 80°C in 10–50 mM sodium citrate at pH of 8.5–9.0, which considerably enhances the immunolabeling that can be obtained in fixed sections without any evident deleterious effect of the treatment on tissue integrity at the light microscopy or electron microscopy (EM) level (Jiao *et al.,* 1999). Vieges *et al.* (2007) proposed the combined use of high-intensity (30W), short-duration (2 hrs) photobleaching and Sudan Black B as the sections pretreatment for FIHC staining, which can be used regardless of tissue type as similar results were obtained for highly vascularised, lipofuscin-rich tissues, such as kidney and liver, and tissues with reduced vascularisation and low lipofuscin content. This approach is even more effective when poorly vascularised and low lipofuscin content tissues, such as the pancreas. Having discussed the various pretreatment methods, a possible simple way to reduce aldehyde-related fluorescence is to use the fixative in low concentrations or to avoid it altogether if the tissue is destined for FIHC (Tokumasu and Dvorak, 2003).

6.4 5 Other Pretreatment Techniques Studied

Other pretreatment methods have been tried in the present study (data not shown) in order to improve the signal-to-background noise ratios in FIHC staining. However the results were unsatisfactory compared with the combination of HIAR and $NaBH_4$. These include the use of thiol-based blocking strategies (Rogers *et al.,* 2006, and CAS-Block™ (Invitrogen). Thiol-based blocking approach has been proposed to inhibit the mechanism of intermolecular disulfide bridge formation and/or other thiol linkages between antibodies and substrate chemical side groups, whereas CAS-Block™ is used as a universal blocking agent for reducing

nonspecific background staining using non species-specific serum. Using enzymatic Ag retrieval methods such as trypsin or proteinase K were also attempted but gave poor and inconsistent results.

Allthough there are other wide range of strategies to tackle autofluorescence problems as discussed earlier, the results of the present study highlight the fact that there is no general methodology available for all antigen demasking and the control of autofluorescence. Success in exploiting them was found in a tactical approach to choose appropriate reagent(s) by trial and error, either individually or in combination, tailored for a specific tissue type and fixation medium and other relevant factors such as processing technique, and wavelength of excitation light (Baschong *et al.,* 2001). Optimizing FIHC techniques is laborious and time consuming, however it is worth endeavouring as it is an indispensable step to obtain reliable FITC results where quality assurance is of utmost importance.

6.4 6 FIHC Quality Assurance

One of quality assurance measures in fluorescence IHC procedure that applied in the present works was simultaneous staining of sections of known positive (positive control tissue) such as the kidney (Figure 6.3A) and GIT (Figure 6.3B) for NHE1 and AE2 antigens, respectively (Mahnensmith and Aronson, 1985; Alrefai *et al.,* 2001). The appearance of tissue staining in the positive control tissue in an expected distribution corresponding to the Ag under investigation provides evidence of the specificity of the antiserum used. Conversely, staining in an unexpected location or pattern suggests that the staining may not be specific. Thus the reproducibility of the technique is assured because the staining intensity and distribution in this tissue should remain consistent. In addition, the control and unknown case tissues were sampled, fixed, embedded and stored identically to ensure the antigens in the test and control tissues have been equally preserved thus avoiding false negative results from occurring. Otherwise, the interpretation of negative findings in FIHC result must be made with caution (Haines and Chelack, 1991).

6.4.7 FIHC Result Quantification and Analysis

Quantification of FIHC staining is not non-straightforward and can only be performed subjectively according to a semi-quantitative grading, which can have poor reproducibility depending on the skills. Therefore standardisation of the quantification method used and consistency in the results from a repeated number of studies is important.

Even though there is a number of automatic image analysis facilities available to study FITC results (Renshaw, 2007), some basic technical issues like morphological quality of the tissue need to be addressed beforehand. The quality of the sections is particularly important to study a specific cellular localisation at sub-cellular level *e.g.* antigens distribution to the plasma membrane and cytoplasm because this requires good detail of cellular morphology. Based on this study, using PFA 4% gave a good trade off between adequate morphological preservation and providing acceptable quality of FIHC staining with manageable background staining and Ag masking induced by the fixative. Future work could be attempted to optimize FIHC staining technique for GP tissue fixed in 2% GA with 0.7% RHT solutions (osmolarity adjusted to ~280 mOsm) as it has shown to provide superior preservation of the original GPC morphology with minimal artifacts compared to other conventional fixatives (Chapter 4).

CLSM allowed a careful morphological observation and analysis at a cellular resolution (Paddock, 2000) that make the localisation of the Ag at cellular level possible based on the acquired 2D and 3D images. However, because of the limitation of the image analysis technique used in the present study, the distribution of NHE1 and AE2 fluorescent staining either in the plasma membrane and cytoplasm was based on a rather subjective approximation of plasma membrane thickness and cytoplasm diameter range.

In future, improved measurement of cellular localisation of membrane transporters could be attained by exploiting the advantage CLSM method that permits the determination of the location of multiple fluorescently tagged molecules in the same tissue preparation without fear of the signal from one molecule contributing to the others (Renshaw, 2007). For instance, the *in situ* GPC

colocalisation of specific membrane transporters and plasma membrane could be performed by using a specific antibody for the membrane transporters and fluorescent probes for plasma membrane (*e.g.* 1-43FX fixable analog of FM®, Invitrogen) and *in situ* live cell (*e.g.* fixable CellTracker™ Blue CMAC (7-amino-4-chloromethylcoumarin), Invitrogen). Preliminary works on this approach showed lack of specificity in the labeling of the plasma membrane (data not shown), but warranted further optimization. However, overall observation of NHE1 and AE2 immunofluorescence staining in GPCs along P7 proximal tibia GP (S1-S8) in this study clearly showed the transporters fluorescent-labeled signals were detected specifically from within the chondrocyte compartments (Figures 3, 4 and 5).

To allow comparison between the result values acquired from different animals using semi-quantitative method, normalization of the values based on the highest percentage value in each individual GP tissue was performed. Alternatively, normalization using a standard reference value based on a universal parameter could be utilized similar to the use of loading control in Western blots technique (Aldridge *et al.,* 2008). The parameter of reference should be consistently present and measurable in cells from different individual animals. For example, normalization of immunofluorescent staining of the Ag of interest measured in parallel to the immunofluorescence of a high-abundance housekeeping protein such as actin and tubulin (Spector *et al.,* 2001; Ferguson *et al.,* 2005; Romero-Calvo *et al.,* 2010). This could ensure the reliability of the data that were pooled and compared from different samples or animals. However this normalization method has its own limitation due to the influence of various physiological and pathological factors on the control of gene expression (Ferguson *et al.,* 2005), besides extra technical and optimization steps required in the FIHC technique compared to the present method used.

6.4 8 Collagen Type X

Collagen type X was found mainly in the hypertrophic cartilage zone peri- and extracellularly. This finding was in agreement with previous reported studies that showed the secretion of collagen type X in hypertrophic chondrocytes of chick GP (Poole & Pidoux, 1989), condylar cartilage of fetal mouse mandible (Shibata *et al.,*

1997), developing rat trachea (non GP cartilage) (Sasano *et al.,* 1998); and newborn rat tibia GP (Sasano *et al.,* 1998); chick embryo epiphysial cartilages (Kielty *et al.,* 1985), and human fetal and juvenile articular cartilage-bone metamorphosis (Nerlich *et al.,* 1992). Thus this result further supports the notion that collagen types X can be utilised as markers of chondrocyte hypertrophy (Farquharson & Whitehead, 1995; Shibata *et al.,* 1997) in numerous cartilage cells that have been studied.

6.4 9 NHE1 and AE2 Distribution in Postnatal GP

Previous work on NHE in rat GP has demonstrated the presence of activity NHE activity in the HZ cells but not in the PZ cells, based on pH recovery measurement in a HCO_3-free medium following intracellular acidification using the ammonium rebound technique (Bush *et al.,* 2006b). The subsequent work also showed absolute expressions of the AE gene families in PZ and HZ of 6 week rats with the fold change between PZ and HZ (Bush *et al.,* 2010). The microarray analysis highlighted AE3 alone as changing expression between proliferative and hypertrophic zones, with an approximately 14-fold increase compared with no change for AE1 or AE2.

The results appeared to be not fully in agreement with the present immunofluorescence staining results that showed the NHE distribution was found to be almost consistent along the PZ before decreasing through to the late HZ (Figure 6.5 and 6.7A). The current result also specifically demonstrated the distribution of AE2 was relatively higher at the late PZ and early HZ compared to the rest of GPC differentiation zones (Figure 6.5 and 6.7B). A possible explanation for this lies with the fact that there was a difference in a categorical selection of the GP PZ and HZ zone for tissue sampling between these studies. For an example the microarray analysis to analyze mRNA levels of the membrane transporters was based on a group of GP cells that was procured using laser capture microdissection (LCM) (Wang *et al.,* 2004) and not the distribution of the protein from stained PZ or HZ segments, whereas in FIHC study the fluorescent labelling was examined in individual GPC across the different GP zones. In this respect, even though neither method is a specific measure of protein activity, FIHC offers a more specific

definition of the transporter distribution and localisation along the GP tissue. Another possible explanation for the contradictory results was the difference in the age of animals studied *i.e.* day-7 and day-42. The expression of transporters or their subfamily could be affected by the animal age and this was demonstrated by alkaline phosphatase, a known HZ marker that showed 4 times greater in the enzyme expression from GP PZ to HZ in 6-week-old compared to 7-week-old rats (Wang *et al.,* 2004). Further FIHC study of other subfamily AE or NHE localisation in GP could give a complete picture of the role of the transporters in the bone growth. To achieve this, reliable specific antibodies for FIHC studies are essential.

6.4 10 NHE1 and AE2 Possible Roles in Bone Growth

The relatively high levels of NHE1 throughout the proliferative (PZ) and early hypertrophic zones (Figure 7A) support a 'housekeeping' role of this transporter in the maintenance of optimal pH_i (Schelling & Abu Jawdeh, 2008). However the increased levels of AE2 appeared to correspond with early chondrocyte enlargement (Fig. 7B). The FIHC results suggested that both transporters were localized at the plasma membrane and cytoplasm of both PZ and HZ cells (Fig. 6). The increased AE2 labelling along the GP (along with NHE1 activity) might give rise to the accumulation of intracellular Cl^- and Na^+ (leading to the stimulation of the $3Na^+/2K^+$ pump), creating an osmotic gradient into the cell resulting in water accumulation and subsequent cell enlargement. It is also possible that raised levels of AE2 might correspond to the increased requirement for the maintenance of steady-state pH_i in the face of elevated metabolism of HZ chondrocytes (Brighton *et al.,* 1973; Hunziker *et al.,* 1987b). The decreased levels of both transporters in S5 to S6 appeared to occur when hypertrophic chondrocytes are maximally enlarged (Chapter 3) and this could accelerate cell death thus allowing calcification and new bone formation. These results suggest complex changes to levels of these transporters along the GP which might be associated with GPC hypertrophy and thus bone lengthening. Hypertrophy and survival in other cell types has also been associated with changes to levels of these transporters (Schelling & Abu Jawdeh,

2008; Hwang *et al.,* 2009) raising the possibility that they play similar roles in the GP.

6.4 11 Comparison of Growth Plate Chondrocyte Hypertrophy Mechanisms with Other Cell Types

Hypertrophy in cell types other than chondrocytes was usually observed in pathological conditions. For examples, cardiac hypertrophy (Geisterfer *et al.,* 1988; Shubeita *et al*., 1990; Wang *et al.,* 1998; Colella *et al.,* 2008), systemic and pulmonary hypertension (Tseng and Berk, 1992; Tajsic and Morrell, 2011) and compensatory renal hypertrophy (Johnson and Vera Roman, 1966; Bonvalet *et al.,* 1972; Liu and Preisig, 2002; Chen *et al.,* 2005). The pathological cell hypertrophy is controlled by paracrine factors, as also occurs in normal cell growth and differentiation (Shubeita *et al.,* 1990; Wolf and Nelson, 1990; Wolf *et al.,* 1993; Franch *et al.,* 1997; Flyvbjerg *et al.,* 1999; Huet *et al.,* 2001; Colella *et al.,* 2008).

Hypertrophy of non-chondrocytes is predominantly associated with influx of water and ions into the intracellular spaces via alteration of plasmalemmal ion channel and transporter proteins expression to maintain the increase in cells volume (Tseng and Berk, 1992; Tajsic and Morrell, 2011). Other mechanisms have also been suggested, which include cell-cycle-dependent or independent mechanisms that mediate the increase in RNA and cellular protein synthesis (Bonvalet *et al.,* 1972; Ouellette *et al.,* 1987; Liu and Preisig, 2002; Chen *et al.,* 2005), and endoreduplication process that increases the DNA content (Soonpaa and Field, 1994; Lippin and Roth*.,* 1997; Larkins *et al.,* 2001**).**

The hypertrophic cells could increase their volume without DNA synthesis, but instead through the synthesis of RNA and cellular protein. This could be achieved with or without cell cycle activation. The cell cycle-dependent mechanism of cell hypertrophy involves entry of cells into the G_1 phase of the cell cycle, initiating G_1 -related events, followed by arrest of cell cycle progression prior to the G_1 /S checkpoint (Liu and Preisig, 2002**)** as a result of coordinated effects of a mitogen and antiproliferative agent (Wolf and Nelson, 1990; Liu and Preisig, 2002). These agents block progression of the cell cycle before entry into S

phase so cells do not divide but continue to synthesize protein, yielding hypertrophy (Franch *et al.,* 1997). This mechanism was shown to mediate renal tubular cell hypertrophy following unilateral nephrectomy (Liu and Preisig, 2002).

On the other hand, cell-independent mechanism involves an imbalance between rates of cellular protein synthesis and degradation by lysosomal enzymes (Liu and Preisig, 2002). This form of hypertrophy is induced by alkalinization of acidic intracellular vesicles (*e.g.* lysosomes) by certain compounds that inhibit the activity of lysosomal enzymes in protein degradation (Liu and Preisig, 2002), or by suppression of lysosomal proteolysis under influence of growth factors such as epidermal growth factor (EGF) and transforming growth factor- β (TGF-β) (Franch *et al.,* 1997).

Hypertrophy of cells is irreversible if it is coupled with increase in the DNA content via endoreduplication, as observed in vascular smooth muscle cells (Tajsic and Morrell, 2011). Endoreduplication is a form of nuclear polyploidization that results in multiple, uniform copies of chromosomes. This process is common in plants and animals, especially in tissues with high metabolic activity, and generally in cells that are terminally differentiated. During this process, cells amplify their genome without chromatin condensation, segregation or cytokinesis, resulting in what appears to be multiple, uniform copies of the nuclear DNA. Clearly, some of the mechanisms that direct sequential progression of the G_1-, S-, G_2- and M-phases of the cell cycle are modified in this an 'alternative' cell cycle to allow the chromosomes to replicate without consequent nuclei and cells division. Typically, cells that have undergone endoreduplication are larger than comparable cells that have not. Being bigger and having a larger number of organelles (mitochondria or plastids in plants) would potentially confer the cells with greater transcriptional and translational capacities, manifested functionally by high cellular metabolic activities (Larkins *et al.,* 2001). It was suggested the large cells have the capacity to increase their volume faster than smaller cells, and this could be advantageous in the case of rapidly growing tissues, as observed in some species of fruits and seeds (Grime and Mowforth, 1982).

However, the characterization of the mechanisms involved in the development of hypertrophy in the other cell types than chondrocytes was only demonstrated in in vitro (Iwaki et al., 1990; Shubeita *et al.,* 1990; Wolf and Nelson, 1990; Tseng and Berk, 1992; Wolf *et al.,* 1993; Franch *et al.,* 1997; Chu *et al.,* 2008). Nonetheless from those studies and the present results, there are a number of common features shared between chondrocytes and other cell types with regards to cell hypertrophy. These include regulatory functions of paracrine factors in the cell enlargement process and potential roles of membrane transporters in mediating cell volume increase associated with the hypertrophy.

6.4 12 Future Study

Previous studies have shown roles of growth factors and hormone in controlling membrane transporters activity in AE regulation in rat ventricular myocytes (Malo & Fliegel, 2006). This and the fact that growth hormone has been known for many years to be an important regulator of longitudinal bone growth (Nilsson *et al.,* 2005) raises an intriguing question whether growth hormone has any contributory effects on the GPC membrane transporters activity and sets an interesting direction of future study on the current topic.

6.4 13 Summary

This study suggests that the NHE1 presence in the GP could be associated with its maintenance role in chondrocytes survival from the onset of chondrocyte proliferation through to the early stage of chondrocyte hypertrophy, whereas AE2 appeared to be specifically involved in the transition of cells from proliferative to hypertrophic zones.

Chapter 7

General Discussion, Conclusions and Future Studies

7.1 General Discussion and Conclusions

The study highlighted the importance of the well-coordinated chondrogenesis as a 'making space' mechanism model that allow the normal growth plate development in a mammalian. The study has also emphasised the importance of GPC hypertrophy in longitudinal bone growth and a possible involvement of plasma membrane transporters in the GPC enlargement. Based on the hypothesis that plasma membrane transporters have a role in driving the cell swelling associated with chondrocyte hypertrophy, the focus of the investigations were centered on the NHE and AE - two membrane transporters ubiquitously found in mammalian cells. The functions and distributions of these membrane transporters in the growth plate of a mammalian species were studied by using tissue culture and immunohistochemistry coupled with the powerful micro-imaging tools of CLSM.

The experimental findings of this project are presented under four broad headings: (i) characterization of *in situ* living GPC in the rat GP, (ii) GPC fixation and shrinkage artifact incurred by conventional fixatives, (iii) possible roles for NHE and AE in longitudinal bone growth, and (iv) expression of NHE1 and AE2 within hypertrophic GPC hypertrophy in the rat GP.

(i) Characterization of *in situ* living GPC in the rat GP

Studying GPC volume changes within GP cartilage without artefacts caused by GP tissue fixation was essential. Therefore this work initially studied unfixed fluorescently labeled living GPCs *in situ* by using high resolution confocal scanning microscopy.

This study identified a number of important observations of live *in situ* GPC in the different maturational zones. All GPs exhibited the cell differentiation cascade characteristic of GPs. The final hypertrophic GPC volume varied markedly depending on the bone under investigation although the cell volume at the proliferative zone was not significantly different between different GPs. In other words, all of these bones start with the same sort of growth plate chondrocytes. The hypertrophic GPC volume to some extent was influenced by the rate of cell volume changes between the proliferative zone and hypertrophic zone.

Interestingly, there was no obvious relationship between the final hypertrophic GPC volumes and bone length based on a single time point (*i.e.* post natal) cell volume measurement. It could be reasoned that the final hypertrophic GPC volume changes dynamically during the bone growth phase to attain specific final bone lengths for different bones. This result highlighted differential growth (Wilsman *et al.,* 1996b, 2008) among different growth plates of postnatal rats that signify the complex regulatory mechanism involved in longitudinal bone growth.

(ii) GPC shrinkage artifact incurred by conventional fixative solutions. Having characterized living *in situ* GPCs, the second scope of study examined was the effect of conventional fixatives on GPC morphology. Optimal fixation methods that maintain the original morphology of the GPCs are vital when fixed GP tissues are used to study the tissue and cellular distribution of plasma membrane transporters in GP using the immunohistochemistry technique.

This study demonstrated that the osmolarity of fixative solutions was important for maintaining the normal morphology of hypertrophic chondrocytes within the mammalian growth plate following chemical fixation. The shrinkage artifact incurred by conventional fixatives, was abolished when the osmolarity of the medium was reduced close to that of normal physiological solutions or markedly reduced when the bones were sagitally bisected prior to fixation. These results raised important issues in relation to the accurate preservation of cell morphology by widely-used conventional fixative solutions. The subsequent works in the thesis took a careful note of this finding *e.g.* when fixed GP sections were prepared for FIHC studies.

(iii) A possible role for NHE and AE in longitudinal bone growth. The third part of the present study determined if plasma membrane transporters have a role in growth plate chondrocyte enlargement and subsequent longitudinal bone growth

This study identified an essential role of AE and NHE in postnatal longitudinal bone growth as shown by dose-response relationship of the inhibitors to the two transporters with bone growth in an *ex vivo* bone growth model (Figure 5.3). The results indicated that both NHE and AE are implicated in the postnatal GPC enlargement mechanism. However, the role of the transporters in prenatal

bone growth appeared more complicated and warranted further examination with additional number of samples, and adjustment of the inhibitor drugs concentration to avoid drug-induced cytotoxicity of the relatively smaller and delicate embryonic bones.

(iv) Changes to sodium hydrogen 1 (NHE1) and anion exchanger (AE2) expression levels with GPC hypertrophy in the postnatal rat GP. In light of the *ex vivo* results indicating a possible functions of NHE and AE in GPC enlargement and longitudinal bone growth, the subsequent study was undertaken to investigate the GP tissue distribution and cellular localisation of NHE1 and AE2 along the GPC differentiation cascade using optimized FIHC staining technique.

FIHC examination described the expression and distribution pattern of NHE1 and AE2 in postnatal GP cartilage. These findings highlighted a distinct relationship between NHE1 and AE2 expression levels and GPC hypertrophy in rat postnatal GPs. The transporter GP and cellular localisation suggested that the role of NHE1 in the GP was associated with maintenance of chondrocyte survival from the onset of chondrocyte proliferation through to the early stage of chondrocyte hypertrophy. In contrast, AE2 appeared to be specifically involved in the transition of cells from the proliferative to hypertrophic zones.

While GPC hypertrophy of bone growth could be considered physiological, hypertrophy in other cell types is usually pathological. For examples hypertrophy of smooth muscle cells (Geisterfer *et al.*1988; Tseng and Berk, 1992; Tajsic and Morrell, 2011), cardiomyocytes (Iwaki *et al.,* 1990; Shubeita *et al*., 1990; Wang *et al.,* 1998; Colella *et al.,* 2008), neurons (De Souza *et al*., 2000) and nephrons (Johnson and Vera Roman, 1966; Liu and Preisig, 2002; Chen *et al.,* 2005). These cells hypertrophy is controlled by paracrine factors as in normal cell growth and differentiation (Shubeita *et al.,* 1990; Huet *et al.,* 2001; Colella *et al.,* 2008) dominantly associated with activities of channel and transporter systems to maintain the cell volume increase (Tseng and Berk, 1992; De Souza *et al*., 2000**;** Tajsic and Morrell, 2011). However other mechanisms have been implicated in the pathological cell hypertrophy including cell hypertrophy attributable to the increase in RNA, cellular protein and DNA content (Soonpaa and Field, 1994; Lippin and

Roth., 1997). Even though the hypertrophy mechanisms of these cells have been only characterized using *in vitro* systems (Iwaki *et al.,* 1990; Shubeita *et al*., 1990; Wolf and Nelson, 1990; Tseng and Berk, 1992; Wolf *et al.,* 1993; Franch *et al.,* 1997), those previous studies and the present results, chondrocytes and other cell types shared a number of common characteristics with regards to cell hypertrophy mechanisms. These include regulatory functions of paracrine factors in the cell enlargement process and potential roles of membrane transporters in mediating cell volume increase associated with the hypertrophy.

Taken together, the *ex vivo* experiment and IHC results provided important evidence to support the hypothesis proposed in the thesis that plasma membrane transporters are important for GPC enlargement and longitudinal bone growth.

7.2 Future Studies

Future areas of research, based on the data from this studentship have been outlined in the discussion sections of Chapter 3, 4, 5 and 6. However for clarity, they are summarized below:

(i) In view of the present findings that show differential growth (Wilsman *et al.,* 1996b, 2008) among various growth plates and a role of plasma membrane transporters in the GPC hypertrophy (Bush *et al.,* 2010), future studies could examine whether membrane transporter(s) are temporally expressed within a particular GPC zone during the active phase of bone growth.

(ii) The roles of growth factors and hormones in controlling membrane transporter activity have been shown in AE regulation of rat ventricular myocytes (Malo & Fliegel, 2006). This and the fact that GH has been known to be an important regulator of longitudinal bone growth (Nilsson *et al.,* 2005) raises an intriguing question whether GH modifies GPC membrane transporters activity and expression, and sets an interesting direction of future study on the current topic. The fetal murine growth bone culture model (Mushtaq *et al.,* 2004) could be used to examine the effect of specific bone regulatory factors (*e.g.* IGF or glucocorticoid) on the expression of the transporters at different time points.

(iii) In addition, future studies could examine the cellular mechanism of chondrocyte hypertrophy in an established chondrocyte cell line. This study would

offer some basic understanding of membrane transporters involvement in chondrocyte hypertrophy without the presence of other confounding factors *e.g.* circulating growth hormones or local factors found in *in vivo* GP.

The current work has undertaken preliminary studies using ATDC5 cells (Atsumi *et al.,* 1990) as a model system to study the cellular process of chondrocyte hypertrophy (data not shown). The finding showed that the ATDC5 cells became hypertrophic only at the centre of cartilage nodules, which formed after 24 days of culture (Shukunami *et al.* 1997). Suspension of cells derived from the monolayer cells comprised mixed cell population of various sizes (see Appendix 2), which made it technically difficult to study hypertrophic cells without parallel biochemical evaluation using specific hypertrophic cell markers (*e.g.* collagen type X expression and ALPase activity; Shukunami *et al.* 1997). Further work is required to optimize the technique so that quantitative evaluation can be made to study the function of membrane transporters in the cellular enlargement process.

(iv) As discussed earlier (6.4.11), pathological hypertrophy in other cell types has been shown to involve cell cycle mechanisms and endoreduplication. Although the current study suggest the role of plasma membrane transporters in GPC hypertrophy, the involvement of cell cycle mechanisms and endoreduplication are still largely unknown. Therefore it is interesting to know whether the cell cycle and endoreduplication mechanisms have any alternative or complementary role to plasma membrane transport regulation in GPC hypertrophy complex mechanisms - an interesting area to be explored in future study. Furthermore, better insight into physiological mechanism(s) of cell hypertrophy in GPCs could increase the understanding of the principles in pathophysiology of cell hypertrophy at cellular levels of other organs under diseased conditions.

References

Abad V, Meyers JL, Weise M, Gafni RI, Barnes KM, Nilsson O, Bacher JD, Baron J (2002): The role of the resting zone in growth plate chondrogenesis. Endocrinology **143**:1851-7.

Abu EO, Horner A, Kusec V, Triffitt JT, Compston JE (1997): The localization of androgen receptors in human bone. J Clin Endocrinol Metab **82**:3493-7.

Abu EO, Horner A, Kusec V, Triffitt JT, Compston JE (2000): The localization of the functional glucocorticoid receptor α in human bone. J Clin Endocrinol Metab **85**:883-9.

Adams CS, Shapiro IM (2002): The fate of the terminally differentiated chondrocyte: Evidence for microenvironmental regulation of chondrocyte apoptosis. Crit Rev Oral Biol Med **13**:465-473.

Ahmed SF, Farquharson C (2010): The effect of GH and IGF1 on linear growth and skeletal development and their modulation by SOCS proteins. J Endocrinol **206**:249-59.

Ahmed YA, Tatarczuch L, Pagel CN, Davies HM, Mirams M, Mackie EJ (2007a): Hypertrophy and physiological death of equine chondrocytes in vitro. Equine Vet J **39**:546-52.

Ahmed YA, Tatarczuch L, Pagel CN, Davies HM, Mirams M, Mackie EJ (2007b): Physiological death of hypertrophic chondrocytes. Osteoarthritis Cartilage **15**:575-86.

Aigner T (2002): Apoptosis, necrosis, or whatever: how to find out what really happens? J Pathol **198**:1-4.

Akagi M, Ueda A, Teramura T, Kanata S, Sawamura T, Hamanishi C (2009): Oxidized LDL binding to LOX-1 enhances MCP-1 expression in cultured human articular chondrocytes. Osteoarthritis Cartilage **17**:271-5.

Aldridge GM, Podrebaraca DM, Greenougha WT, Weiler IV (2008). The use of total protein stains as loading controls: An alternative to high-abundance single-protein controls in semi-quantitative immunoblotting. J Neurosci Methods **172**:250-54.

Alper SL (1991): The band 3-related anion exchanger (AE) gene family. Annu Rev Physiol **53**: 549-64.

Alper SL (2006): Molecular physiology of SLC4 anion exchangers. Exp Physiol **91**:153-61.

Alper SL, Chernova MN, Stewart AK (2001): Regulation of Na^+-independent Cl^- /HCO_3^- exchangers by pH. JOP. **2**:171-75.

Alrefai WA, Tyagi S, Nazir TM, Barakat J, Anwar SS, Hadjiagapiou C, Bavishi D, Sahi J, Malik P, Goldstein J, Layden TJ, Ramaswamy K, Dudeja PK (2001). Human intestinal anion exchanger isoforms: expression, distribution, and membrane localization. Biochim Biophys Acta **1511**:17-27.

Amemiya M, Loffing J, Lotscher M, Kaissling B, Alpern R, Moe OW (1995): Expression of NHE-3 in the apical membrane of rat renal proximal tubule and thick ascending limb. Kidney Int **48**:1206 -15.

Amin AK, Huntley JS, Bush PG, Simpson AHRW, Hall AC (2008). Osmolarity influences chondrocyte death in wounded articular cartilage. J Bone Joint Surg Am **90**:1531-42

Amin AK, Huntley JS, Simpson AHRW, Hall AC (2009): Chondrocyte survival in articular cartilage, the influence of subchondral bone in a bovine model. J Bone Joint Surg Br **91**:691-9.

Amini S, Veilleux D, Villemure I (2010): Tissue and cellular morphological changes in growth plate explants under compression. J Biomech **43**:2582-8

Anderson HC (1969): Vesicles associated with calcification in the matrix of epiphyseal cartilage. J Cell Biol **41**:59-72.

Araki T, Hayashi M, Watanabe N, Kanuka H, Yoshino J, Miura M, Saruta T (2002). Down-regulation of Mcl-1 by Inhibition of the pI3-K/Akt pathway is required for cell shrinkage-dependent cell death. Biochem Biophys Res Commun **290**:1275-81.

Aszodi A, Bateman JF, Gustafsson E, Boot-Handford R, Fassler R (2000): Mammalian skeletogenesis and extracellular matrix: What can we learn from knockout mice? Cell Struct Funct **25**:73-84.

Atsumi T, Miwa, Y., Kimata, K., and Ikawa, Y. (1990): A chondrogenic cell line derived from a differentiating culture of AT805 teratocarcinoma cells. Cell Differentiation and Development **30**:109-116.

Attaphitaya S, Park K, Melvin JE (1999). Molecular cloning and functional expression of a rat Na^+/H^+ exchanger (NHE5) highly expressed in brain. J Biol Chem **274**:4383-88

Bailey DA, Baxter-Jones ADG, Mirwald RL, Faulkner RA (2003): Bone growth and exercise studies:The complications of maturation. J Musculoskel Neuron Interact **3**:335-7.

Baird NR, Orlowski J, Szabo ED, Zaun HC, Schultheis PJ, Menon AG, Shull GE (1999): Molecular cloning, genomic organization, and functional expression of Na^+/H^+ exchanger Isoform 5 (NHE5) from human brain. J Biol Chem **274**:4377-82.

Baker JK (1960): "Cytological technique: The principles underlying routine methods." London: Methuen

Baker J, Liu JP, Robertson EJ, Efstratiadis A (1993): Role of insulin-like growth factors in embryonic and postnatal growth. Cell **75**:73-82.

Ballock RT, O'Keefe RJ (2003): The biology of the growth plate. J Bone Joint Surg Am **85**:715-26.

Bancroft JD & Cook HC (1994): Manual of histological techniques and their diagnostic application. Edinburgh, Churchill Livingstone.

Bannister LH, Berry MM, Collins P, Dyson M, Dussek JE, Ferguson WWJ (1995): Gray's anatomy London: Churchill Livingstone, pp 432-33.

Barbera A, Jones OW, Zerbe GO, Hobbins JC, Battaglia FC, Meschia G (1995): Early ultrasonographic detection of fetal growth retardation in an ovine model of placental insufficiency. Am J Obstet Gynecol 173.

Baschong W, Suetterlin, R., and Laeng, R.H. (2001): Control of autofluorescence of archival formaldehyde-fixed, paraffin-embedded tissue in Confocal Laser Scanning Microscopy (CLSM). J Histochem Cytochem **49**:1565-1571

Beck BR (2009): Muscle forces or gravity—What predominates mechanical loading on bone?: Introduction. Med Sci Sports Exerc **41**:2033-6.

Bennett BD, Jetton TL, Ying GT, Magnuson MA, Piston DW (1996): Quantitative subcellular imaging of glucose metabolism within intact pancreatic islets. J Biol Chem **271**:3647-3651.

Benya PD, Shaffer JD (1982): Dedifferentiated chondrocytes reexpress the differentiated collagen phenotype when cultured in agarose gels. Cell **30**:215-24.

Benos DJ (1982). Amiloride: A molecular probe of sodium transport in tissues and cells. J Physiol **242** (Cell Physiol. 11):C131-45.

Bernardo AA, Bernardo CM, Espiritu DJ, Arruda JAL (2006): The sodium bicarbonate cotransporter: Structure, function, and regulation. Semin Nephrol **26**:352-60.

Berod A, Hartman BK, Pujol JF (1981). Importance of fixation in immunohistochemistry: Use of formaldehyde solutions at variable pH for the localization of Tyrosine Hydroxylase. J Histochem Cytochem **29**:844-50.

Bielohuby M, Matsuura M, Herbach N, Kienzle E, Slawik M, Hoeflich A, Martin Bidlingmaier M (2010). Short-term exposure to low-carbohydrate, high-fat diets induces low bone mineral density and reduces bone formation in rats. J Bone Miner Res **25**:275-84.

Billinton N, Knight AW (2001): Seeing the wood through the trees: A review of techniques for distinguishing green fluorescent protein from endogenous autofluorescence. Anal Biochem **291**:175-97.

Blair HC, Zaidi M, Schlesingers PH (2002): Mechanisms balancing skeletal matrix synthesis and degradation. Biochem J **364**:329-41.

Bonvalet JP, Champion M, Wanstok F, Berjal G (1972): Compensatory renal hypertrophy in young rats: Increase in the number of nephrons. Kidney Int **1**:391-6.

Bookstein C, Musch MW, DePaoli A, Xie Y, Rabenau K, Villereal M, Rao MC, Chang EB (1996): Characterization of the rat Na^+/H^+ exchanger isoform NHE4 and localization in rat hippocampus. Am J Physiol **271**:Cl629-38.

Bookstein C, Musch MW, DePaoli A, Xie Y, Vlereall M, Rao MC, Chang EB (1994). A unique sodium-hydrogen exchange Isoform (NHE-4) of the inner medulla of the rat kidney is induced by hyperosmolarity. J Biol Chem **269**:29704-9.

Bookstein C, Xie Y, Rabenau K, Musch MW, Mcswine RL, Rao MC, Chang EB (1997): Tissue distribution of Na^+/H^+ exchanger isoforms NHE2 and NHE4 in rat intestine and kidney. Am J Physiol **273**:C1496-505.

Boron WF (2001): Sodium-coupled bicarbonate transporters. JOP **2**:176-81.

Boyan BD, Sylvia VL, Dean DD, Toro FD, Schwartz Z (2002): Differential regulation of growth plate chondrocytes by 1 alpha 25 and 24R,25-

(OH)3D2 involves cell-maturation-specific membrane-receptor-activated phospholipid metabolism CROBM 13.

Brant SR, Yun CHC, Donowitz M, Tse CM (1995): Cloning, tissue distribution, and functional analysis of the human Na^+/H^+ exchanger isoform, NHE3. Am J Physiol **269**:C198-C206.

Breur GJ, Farnum CE, Padgett GA, Wilsman NJ (1992): Cellular basis of decreased rate of longitudinal growth of bone in pseudoachondroplastic dogs. J Bone Joint Surg Am **74**:516-28.

Breur GJ, Turgai J, Vanenkevort BA, Farnum CE, Wilsman NJ (1994): Stereological and serial section analysis of chondrocytic enlargement in the proximal tibial growth plate of the rat. Anat Rec **239**:255-68.

Breur GJ, VanEnkevort BA, Farnum CE, Wilsman NJ (1991): Linear relationship between the volume of hypertrophic chondrocytes and the rate of longitudinal bone growth in growth plates. J Orthop Res **9**:348-59.

Brighton C (1978): Structure and function of the growth plate. Clin Orthop Relat Res **136**:22-32.

Brighton CT, Ray RD, Soble LW, Kuettner KE (1969): Epiphyseal-plate growth in various oxygen tensions in vitro J Bone Joint Surg Am **51**:1383-96.

Brighton CT, Sugioka Y, Hunt RM (1973): Cytoplasmic structures of epiphyseal plate chondrocytes. Quantitative evaluation using electron micrographs of rat costochondral junctions with special reference to the fate of hypertrophic cells. J Bone Joint Surg Am **55**:771-84.

Browning JA, Wilkins RJ (2004): Mechanisms contributing to intracellular pH homeostasis in an immortalised human chondrocyte cell line. Comp Biochem Physiol A Mol Integr Physiol **137**:409-18.

Buckwalter JA, Mower D, Schafer J, Ungar R, Ginsberg B, Moore K (1985): Growth-plate-chondrocyte profiles and their orientation. J Bone Joint Surg Am **67**: 942-55.

Buckwalter JA, Mower D, Ungar R, Schaeffer J, Ginsberg B (1986): Morphometric analysis of chondrocyte hypertrophy. J Bone Joint Surg Am **68**: 243-55.

Burch WM, Wyk JJV (1987): Triiodothyronine stimulates cartilage growth and maturation by different mechanisms. Am J Physiol (Endocrinol Metab15) 252 El76-82.

Burr DB (2002): Targeted and nontargeted remodeling. Bone **30**:2-4.

Bush PG, Hall AC (2001a): Regulatory volume decrease (RVD) by isolated and *in situ* bovine articular chondrocytes. J Cell Physiol **187**:304-314.

Bush PG, Hall AC (2001b): The osmotic sensitivity of isolated and *in situ* bovine articular chondrocytes. J Orthop Res **19**:768-78.

Bush PG, Hall AC (2005a): Passive osmotic properties of *in situ* human articular chondrocytes within non-degenerate and degenerate cartilage. J Cell Physiol **204**:309-319.

Bush PG, Hodkinson PD, Hamilton GL, Hall AC (2005b): Viability and volume of *in situ* bovine articular chondrocytes- changes following a single impact and effects of medium osmolarity. Osteoarthritis Cartilage **13**:54-65.

Bush PG, Hall AC, Macnicol MF (2008a): New insights into function of the growth plate: Clinical observations, chondrocyte enlargement and a possible role for membrane transporters. J Bone Joint Surg Br **90**:1541-7.

Bush PG, Parisinos CA, Hall AC (2008b): The osmotic sensitivity of rat growth plate chondrocytes *in situ*; clarifying the mechanisms of hypertrophy. J Cell Physiol **214**:621-29.

Bush PG, Pritchard M, Loqman MY, Damron TA, Hall AC (2010): A key role for membrane transporter NKCC1 in mediating chondrocyte volume increase in the mammalian growth plate. J Bone Miner Res **25**:1594-603.

Bush PG, Huntley JS, Macnicol MF, Hall AC (2006a): Volume regulation by *in situ* growth plate chondrocytes. J Bone Joint Surg Br **88**:369-b.

Bush PG, Wang Y, Lisle J, Damron TA, Hall AC (2006b): Evidence for increased sodium/ hydrogen and anion exchange activity with growth plate chondrocyte hypertrophy Transactions of the 52nd Annual Meeting, March 31:paper #1401.

Bush PG, Wokosin DL, Hall AC (2007): Two-versus one photon excitation laser scanning microscopy: Critical importance of excitation wavelength. Front Biosci **12**:2646-57.

Cabantchik ZI, Greger R (1992). Chemical probes for anion transporters of mammalian cell membranes. Am J Physiol **262** (Cell Physiol 31):C803-C827.

Campo RD (1988): Effects of cations on cartilage structure: Swelling of growth plate and degradation of proteoglycans induced by chelators of divalent cations. Calcif Tissue Int **43**:108-21.

Cancel M, Grimard G, Thuillard-Crisinel D, Moldovan F, Villemure I (2009): Effects of in vivo static compressive loading on aggrecan and type II and X collagens in the rat growth plate extracellular matrix. Bone **44**:306-15.

Carani C, Qin K, Simoni M, Faustini-Fustini M, Serpente S, Boyd J, Korach KS, Simpson E (1997): Effect of testosterone and estradiol in a man with aromatase deficiency. N Engl J Med **337**:91-5.

Carey D, Liu X (1995): Expression of bone morphogenetic protein-6 messenger RNA in bovine growth plate chondrocytes of different size. J Bone Miner Res **10**:401-5.

Chagin AS, Chrysis D, Takigawa M, Ritzen EM, Sävendahl L (2006): Locally produced estrogen promotes fetal rat metatarsal bone growth; an effect mediated through increased chondrocyte proliferation and decreased apoptosis. J Endocrinol **188**:193-203.

Chagin AS, Karimian E, Sundström K, Eriksson E, Sävendahl L (2010): Catch-up growth after dexamethasone withdrawal occurs in cultured postnatal rat metatarsal bones. J Endocrinol **204**:21-29.

Chambrey R, Warnock DG, Podevin RA, Bruneval P, Mandet C, Be´ lair MF, Barie´ty J, Paillard M (1998). Immunolocalization of the Na1/H1 exchanger isoform NHE2 in rat kidney. Am J Physiol **275**:F379-86.

Cheah SS, Behringer RR (2001): Contemporary gene targeting strategies for the novice. Mol Biotechnol **19**:297-304.

Chen J, Chen J, Neilson EG, Harris RC (2005): Role of mammalian target of rapamycin signaling in compensatory renal hypertrophy. J Am Soc Nephrol **16**:1384-91.

Chen TL, Klein L (1978): Fetal rat bone in organ culture: effect of bone growth and bone atrophy on the comparative losses of ^{45}Ca and ^{3}H-tetracycline. Calcif Tissue Res **25**:255-63.

Chu CH, Tzang BS, Chen LM, Kuo CH, Cheng YC, Chen LY, Tsai FJ, Tsai CH, Kuo WW, Huang CY (2008): IGF-II/mannose-6-phosphate receptor signaling induced cell hypertrophy and atrial natriuretic peptide/BNP expression via Galphaq interaction and protein kinase C-alpha/CaMKII activation in H9c2 cardiomyoblast cells. J Endocrinol **197**:381-90.

Chrysis D, Ritzen EM, Savendahl L (2003): Growth retardation induced by dexamethasone is associated with increased apoptosis of the growth plate chondrocytes. J Endocrinol **176**:331-7.

Clarke B (2008): Normal bone anatomy and physiology. Clin J Am Soc Nephrol **3**:S131-9.

Colella M, Grisan F, Robert V, Turner J, Thomas A, Pozzan T (2008): Ca^{2+} oscillation frequency decoding in cardiac cell hypertrophy: role of calcineurin/NFAT as Ca^{2+} signal integrators. Proc Natl Acad Sci USA **105**:2859-64.

Colnot C, Sidhu SS, Balmain N, Poirier F (2001): Uncoupling of chondrocyte death and vascular invasion in mouse galectin 3 null mutant bones. Dev Biol **229**:203-14.

Cook ME (2000): Skeletal deformities and their causes: Introduction. Poult Sci **79**:982-4.

Cowell HR, Hunziker EB, Rosenberg L (1987): The role of hypertrophic chondrocytes in endochondral ossification and in the development of secondary centers of ossification. J Bone Joint Surg Am **69**:159-61.

Crockett JC, Rogers MJ, Coxon FP, Hocking LJ, Helfrich MH (2011): Bone remodelling at a glance. J Cell Sci **124**:991-8.

D'Amico F, Skarmoutsou E, Stivala F (2009). State of the art in antigen retrieval for immunohistochemistry. J Immunol Methods **341**:1-18.

Davies CM, Jones DB, Stoddart MJ, Koller K, Smith E, Archer CW, Richards RG (2006): Mechanically loaded ex vivo bone culture system 'Zetos': systems and culture preparation. Eur Cell Mater **11**:57-75.

de Cingolani GC, Morgan P, Mundina-Weilenmann C, Casey J, Fujinaga J, de Hurtado MC, Cingolani H (2001): Hyperactivity and altered mRNA isoform expression of the Cl^-/HCO_3^- anion-exchanger in the hypertrophied myocardium. Cardiovasc Res **51**:71-9.

de Luca F (2006): Impaired growth plate chondrogenesis in children with chronic illnesses. Pediatr Res **59**:625-9.

Dean DD, Schwartz ZV, Muniz OE, Gomez R, Swain LD, Howell DS, Boyan BD (1992): Matrix vesicles contain metalloproteinases that degrade proteoglycans. Bone Miner **17**:172-6.

Delezoide A-L, Benoist-Lasselin C, Legeai-Mallet L, Merrer ML, Munnich A, Vekemans M, Bonaventure J (1998): Spatio-temporal expression of FGFR 1, 2 and 3 genes during human embryo-fetal ossification. Mech Dev **77**:19-30.

Dempster WT (1960): Rates of penetration of fixing fluids. J Amer Anat **107**:59-72

De Souza RR, Gama EF, Silva RD, Heimann JC, Maifrino LB, Liberti EA (2000): Dietary sodium intake induced myenteric neuron hypertrophy in Wistar rats. Braz J Med Biol Res **33**:847-50.

Di Nino DL, M.L. C, Linsenmayer TF (2002): Multiple mechanisms of perichondrial regulation of cartilage growth. Dev Dyn **225**:250-9.

Dittmer KE, Thompson KG (2011): Vitamin D metabolism and Rickets in domestic animals: A review. Vet Pathol **48**:389-407

Drury RAB, Wallington EA (1980). Carleton's Histological Technique Oxford, UK: Oxford University Press.

Drury RAB, Wallington EA (1980). Carleton's Histological Technique Oxford, UK: Oxford University Press.

Effting C, de Paula DJ, Nunes Junior GP (2004): A model for the study of skeletal anomalies in rat fetuses. Braz Arch Biol Technol **47**:33-9.

Egerbacher M, Helmreich M, Rossmanith W, Haeusler G (2002): Estrogen receptor-alpha and estrogen receptor-beta are present in the human growth plate in childhood and adolescence, in identical distribution. Horm Res **58**:99-103.

Ehrlich PJ, Lanyon LE (2002): Mechanical strain and bone cell function: A review. Osteoporos Int **13**:688-700.

Erben RG (1997): Embedding of bone samples in methylmethacrylate: An improved method suitable for bone histomorphometry, histochemistry, and immunohistochemistry. J Histochem Cytochem **45**:307-313

Errington RJ, Hall AC (1995): Volume regulatory properties of porcine articular chondrocytes measured *in situ* using confocal microscopy (Abstract). J. Physiol **482**:12-13P.

Errington RJ, Fricker MD, Wood JL, Hall AC, White NS (1997): Four dimensional imaging of living chondrocytes in cartilage using confocal microscopy: a pragmatic approach Am J Physiol **272** (Cell Physiol. 41):C1040-51.

Ertem K, Karakoc Y, Duzova H, Kekilli E, Emre MH, Kilinc E, Yagmur C (2008): Effects of different durations of treadmill training exercise on bone mineral density in growing rats Biol Sport **25**:187-93.

Farnum CE, Wilsman NJ (1986): *ln situ* localization of lectin-binding glycoconjugates in the matrix of growth-plate cartilage. Am J Anat **176**:65-82.

Farnum CE, Wilsman NJ (1989): Cellular turnover at the chondro-osseus junction of growth plate cartilage: Analysis by serial sections at the light microscopial level. J Orhtop Res **7**:654-66.

Farnum CE, Turgai J, Wilsman NJ (1990): Visualization of living terminal hypertrophic chondrocytes of growth plate cartilage *in situ* by differential interference contrast microscopy and time-lapse cinematography. J Orthop Res **8**:750-63.

Farnum CE, Lee R, O'Hara K, Urban JPG (2002): Volume increase in growth plate chondrocytes during hypertrophy: The contribution of organic osmolytes. Bone **30**:574-581

Farnum CE, Tinsley M, Hermanson JW (2008): Postnatal bone elongation of the manus versus pes: Analysis of the chondrocytic differentiation cascade in Mus musculus and Eptesicus fuscus. Cells Tissues Organs **187**:48-58.

Farquharson C, Whitehead CC (1995): Differentiation and mineralization in chick chondrocytes maintained in a high cell density culture: A model for endochondral ossification. In Vitro Cell Dev Biol **31**:288-294.

Farquharson C, Lester D, Seawright E, Jefferies D, Houston B (1999): Microtubules are potential regulators of growth-plate chondrocyte differentiation and hypertrophy. Bone **25**:405-12.

Farquharson C, Jefferies D (2000): Chondrocytes and longitudinal bone growth: the development of tibial dyschondroplasia. Poult Sci **79**:994-1004.

Farquharson C, Jefferies D, Seawright E, Houston B (2001): Regulation of chondrocyte terminal differentiation in the postembryonic growth plate: the role of the PTHrP-Indian hedgehog axis. Endocrinology **142**:4131-40.

Farquharson C (2003): Bone Growth. In Scanes CG (ed): "Biology of growth of domestic animals." Iowa: Iowa State Press, pp 170-85.

Ferguson RE, Carroll HP, Harris A, Maher ER, Selby PJ, Banks RE (2005). Housekeeping proteins: A preliminary study illustrating some limitations as useful references in protein expression studies. Proteomics **5**:566-71.

Ferrara N, Davis-Smyth T (1997): The biology of vascular endothelial growth factor. Endocr Rev 18 4-25.

Fleming RH, McCormack HA, McTeir L, Whitehead CC (2006): Relationships between genetic, environmental and nutritional factors influencing osteoporosis in laying hens. Br Poult Sci **47**:742-55.

Flyvbjerg A, Bennett WF, Rasch R, van Neck JW, Groffen CA, Kopchick JJ, Scarlett JA (1999): Compensatory renal growth in uninephrectomized adult mice is growth hormone dependent. Kidney Int **56**:2048-54.

Fox CH, Johnson FB, Whiting J, Roller PP (1985): Formaldehyde fixation. J Histochem Cytochem **33**:845-853

Franch HA, Curtis PV, Mitch WE (1997): Mechanisms of renal tubular cell hypertrophy: mitogen-induced suppression of proteolysis. Am J Physiol **273**:C843-51.

Freeman TA, Patel P, Parvizi J, Antoci V Jr, Shapiro IM (2009). Micro-CT analysis with multiple thresholds allows detection of bone formation and resorption during ultrasound-treated fracture healing. J Orthop Res **27**:673-679.

Frost HM, Schonau E (2000): The "muscle-bone unit" in children and adolescents: a 2000 overview. J Pediatr Endocrinol Metab **13**:571-90.

Fukai A, Kawamura N, Saito T, Oshima Y, Ikeda T, Kugimiya F, Higashikawa A, Yano F, Ogata N, Nakamura K, Chung UI, Kawaguchi H (2010): Akt1 in murine chondrocytes controls cartilage calcification during endochondral ossification under physiologic and pathologic conditions. Arthritis Rheum **62**:826-36.

Gatti R, Belletti S, Orlandini G, Bussolati O, Dall'Asta V, Gazzola GC (1998): Comparison of annexin V and calcein-AM as early vital markers of apoptosis in adherent cells by confocal laser microscopy. J Histochem Cytochem **46**:895-900.

Geisterfer AA, Peach MJ, Owens GK (1988): Angiotensin II induces hypertrophy, not hyperplasia, of cultured rat aortic smooth muscle cells. Circ Res 62:749-56.

Gerber H-P, Vu TH, Ryan AM, Kowalski J, Werb Z, Ferrara N (1999): VEGF couples hypertrophic cartilage remodeling, ossification and angiogenesis during endochondral bone formation. Nat Med **5**:623-28.

Gibson G (1998): Active role of chondrocyte apoptosis in endochondral ossification. Microsc Res Tech **43**:191-204.

Glade MJ, Kanwar YS, Hefley TJ (1991): Enzymatic isolation of chondrocytes from immature rabbit articular cartilage and maintenance of phenotypic expression in culture. J Bone Miner Res **6**:217-26.

Glant T, Mikecz K (1986): Antigenic profiles of human, bovine and canine articular chondrocytes. Cell Tissue Res **244**:359-69.

Glimcher MJ, Shapiro F, Ellis RD, Eyre DR (1980): Changes in tissue morphology and collagen composition during the repair of cortical bone in the adult chicken. J Bone Joint Surg Am **62**:964-73.

Goss RJ (1978): "The physiology of growth." London: Academic Press.

Grant WT, Sussman MD, Balian G (1985): A disulfide-bonded short chain collagen synthesized by degenerative and calcifying zones of bovine growth plate cartilage. J Biol Chem **260**:3798-803

Grime JP, Mowforth MA (1992): Variation in genome size - an ecological interpretation. Nature **299**:151-3.

Grimsrud CD, Romano PR, D'Souza M, Puzas JE, Reynolds PR, Rosier RN, O'Keefe RJ (1999): BMP-6 is an autocrine stimulator of chondrocyte differentiation. J Bone Miner Res **14**:475-82.

Gross TS, Srinivasan S, Liu CC, Clemens TL, Bain SD (2002): Noninvasive loading of the murine tibia: An in vivo model for the study of mechanotransduction. J Bone Miner Res **17**:493-501.

Guadalupe-Grau A, Fuentes T, Guerra B, Calbet JAL (2009): Exercise and bone mass in adults. Sports Med **39**:439-68.

Guilak F, Mow VC (2000): The mechanical environment of the chondrocyte: A biphasic finite element model of cell-matrix interactions in articular cartilage. J Biomech **33**:1663-1673. doi:10.1016/S0021-9290(00)00105-6

Guizouarn H, Gabillat N, Motais R, Borgese F (2001). Multiple transport functions of a red blood cell anion exchanger, tAE1: its role in cell volume regulation. J Physiol **535**:497-506.

Guldberg RE, Lin ASP, Coleman R, Robertson G, Duvall C (2004): Microcomputed tomography imaging of skeletal development and growth. Birth Defects Res (Part C) **72**:250-59.

Haaijman A, Karperien M, Lanskel B, Hendriks J, Lowik CWGM, Bronkers ALJJ, Burger EH (1999): Inhibition of terminal chondrocyte differentiation by bone morphogenetic protein 7 (OP-1) in vitro depends on the periarticular region but is independent of parathyroid hormone-related peptide. Bone **25**:397-404.

Haines DM, Chelack BJ (1991): Technical considerations for developing enzyme immunohistochemical staining procedures on formalin-fixed paraffin-embedded tissues for diagnostic pathology. J Vet Diagn Invest **3**:101-12.

Hall AC (1995): Volume-sensitive taurine transport in bovine articular chondrocytes. J Physiol **484** (Pt 3):755-66.

Hall AC (1999): Differential effects of hydrostatic pressure on cation transport pathways of isolated articular chondrocytes. Journal of Cellular Physiology **178**:197-204.

Hall AC, Bush PG (2001): The role of a swelling-activated taurine transport pathway in the regulation of articular chondrocyte volume. Pflugers Arch **442**:771-81.

Hall AC, Horwitz ER, Wilkins RJ (1996a): The cellular physiology of articular cartilage. Exp Physiol **81**:535-545.

Hall AC, Starks I, Shoults CL, Rashidbigi S (1996b): Pathways for K+ transport across the bovine articular chondrocyte membrane and their sensitivity to cell volume. Am J Physiol **270**:C1300-10.

Ham AW (1952): Some histophysiological problems peculiar to calcified tissues J Bone Joint Surg Am **34**:701-28.

Hamada T, Suda N, Kuroda T (1999): Immunohistochemical localization of fibroblast growth factor receptors in the rat mandibular condylar cartilage and tibial cartilage. J Bone Miner Metab **17**:274-82.

Hosoya A, Hoshi K, Sahara N, Ninomiya T, Akahane S, Kawamoto T, Ozawa H (2005): Effects of fixation and decalcification on the immunohistochemical localization of bone matrix proteins in fresh-frozen bone sections. Histochem Cell Biol **123**:639-646

Hayes AJ, Hughes CE, Caterson B (2008): Antibodies and immunohistochemistry in extracellular matrix research. Methods **45**:10-21.

Heckman JD, Boyan BD, Aufdemorte TB, Abbott JT (1991): The use of bone morphogenetic protein in the treatment of non-union in a canine model. J Bone Joint Surg Am **73**:750-64.

Hochberg Z (2002): Clinical physiology and pathology of the growth plate. Best Pract Res Clin Endocrinol Metab **16**:399-419.

Hoffmann EK, Simonsen LO (1989): Membrane mechanisms in volume and pH regulation in vertebrate cells. Physiol Rev 69:315-82.

Hopwood D (1967): The behaviour of various glutaraldehydes on Sephadex G-10 and some implications for fixation. Histochemie **11**:289-95

Hopwood D (1969): Fixatives and fixation: a review. Histochemical Journal **1**:323-360

Hopwood D (1985): Cells and tissue fixation 1972-1982.Histochem J **17**:389-442.

Horton WA (2003): Skeletal development: insights from targeting the mouse genome. The Lancet **362**:560-569.

Hsieh Y-F, Turner CH (2001): Effects of loading frequency on mechanically induced bone formation. J Bone Miner Res **16**:918-24.

Huet C, Li Z, Liu H, Black R, Galliano M, Engvall E (2001): Skeletal muscle cell hypertrophy induced by inhibitors of metalloproteases; myostatin as a potential mediator. Am J Physiol Cell Physiol **281**:C1624-34.

Hughes PC, Tanner JM (1970): A longitudinal study of the growth of the black-hooded rat: methods of measurement and rates of growth for skull, limbs, pelvis, nose-rump and tail lengths. J Anat **106**:349-70.

Huntley JS, Bush PG, McBirnie JM, Simpson AH, Hall AC (2005): Chondrocyte death associated with human femoral osteochondral harvest as performed for mosaicplasty. J Bone Joint Surg Am **87**:351-60.

Hunziker EB (1994): Mechanism of longitudinal bone growth and its regulation by growth plate chondrocytes. Microsc Res Tech **28**:505-19.

Hunziker EB, Herrmann W, Schenck RK (1982): Improved cartilage fixation by ruthenium trichloride (RHT). A prerequisite for morphometry in growth cartilage. J Ultrstruct Res **81**:1-12

Hunziker EB, Herrmann W, Schenk RK (1983). Ruthenium hexamine trichloride (RHT)-mediated interaction between plasmalemmal components and pericellular matrix proteoglycans is responsible for the preservation of chondrocytic plasma membranes in situ during cartilage fixation. J Histochem Cytochem **31**:717-27.

Hunziker EB, Herrmann W (1987a): In situ localization of cartilage extracellular matrix components by immunoelectron microscopy after cryotechnical tissue processing. J Histochem Cytochem **35**:647-55.

Hunziker EB, Schenk RK, Cruz-Orive LM (1987b): Quantitation of chondrocyte performance in growth-plate cartilage during longitudinal bone growth. J Bone Joint Surg Am **69**:162-73.

Hunziker EB (1992a): The different types of chondrocytes and their function in vivo. In Adolphe M (ed): "Biological regulation of the chondrocytes." London: CRC Press.

Hunziker EB, Ludi A, Hermann W (1992b): Preservation of cartilage matrix proteoglycans using cationic dyes chemically related to ruthenium hexaammine trichloride. J Histochem Cytochem **40**:909-917

Hunziker EB, Wagner J, Zapf J (1994): Differential effects of insulin-like growth factor I and growth hormone on developmental stages of rat growth plate chondrocytes in vivo. J Clin Invest **93**:1078-86.

Hutchison MR, Bassett MH, White PC (2007): Insulin-Like growth factor-I and fibroblast growth factor, but not growth hormone, affect growth plate chondrocyte proliferation. Endocrinology **148**:3122-30.

Hwang J-M, Kao S-H, Hsieh Y-H, Li K-L, Wang P-H, Hsu L-S, Liu J-Y (2009). Reduction of anion exchanger 2 expression induces apoptosis of human hepatocellular carcinoma cells. Mol Cell Biochem **327**:135-44.

Ichinose S, Tagami M, Muneta T, Sekiya I (2005): Morphological examination during in vitro cartilage formation by human mesenchymal stem cells. Cell Tissue Res **322**:217-26.

Idris AI, Sophocleous A, Landao-Bassonga E, Canals M, Milligan G, Baker D, van't Hof RJ, Ralston SH (2009). Cannabinoid receptor type 1 protects against age-related osteoporosis by regulating osteoblast and adipocyte differentiation in marrow stromal cells. Cell Metab **10**:139-147.

Iscru DF, Anghelina M, Agarwal S, Agarwal G (2008): Changes in surface topologies of chondrocytes subjected to mechanical forces: An AFM analysis. J Struct Biol **162** 397-403.

Ise T, Shimizu T, Lee EL, Inoue H, Kohno K, Okada Y (2005). Roles of volume-sensitive Cl- channel in cisplatin-induced apoptosis in human epidermoid cancer cells. J Membrane Biol **205**:139-45.

Isgaard J, Nilsson A, Lindahl A, Jansson JO, Isaksson OG (1986): Effects of local administration of GH and IGF-1 on longitudinal bone growth in rats. Am J Physiol **250**:E367-72.

Ishizaki Y, Burne JF, Raff MC (1994): Autocrine signals enable chondrocytes to survive in culture. J Cell Biol **126**:1069-77.

Iwaki K, Sukhatme VP, Shubeita HE, Chien KR (1990): Alpha- and beta-adrenergic stimulation induces distinct patterns of immediate early gene expression in neonatal rat myocardial cells. fos/jun expression is associated with sarcomere assembly; Egr-1 induction is primarily an alpha 1-mediated response. J Biol Chem **265**:13809-17.

Izbicka E, Dunstan CR, Horn D, Adams R, Mundy GR (1997): Mitogenic lectin concanavalin A induces calvarial bone formation in vivo via indomethacin-sensitive pathway. Calcif Tissue Int **60**:204-9.

Jiang L, Chernova MN, Alper SL (1997). Secondary regulatory volume increase conferred on Xenopus oocytes by expression of AE2 anion exchanger. Am J Physiol **272** (Cell Physiol 41):C191-202.

Jiao Y, Sun Z, Lee T, Fusco FR, Kimble TD, Meade CA, Cuthbertson S, Reine A (1999): A simple and sensitive antigen retrieval method for free-floating and slide-mounted tissue sections. J Neurosci Methods **93**:149-62.

Jingushi S, Scully SP, Joyce ME, Sugioka Y, Bolander ME (1995): Transforming growth factor-beta 1 and fibroblast growth factors in rat growth plate. J Orthop Res:13761-68.

Johnson HA, Vera Roman JM (1966): Compensatory renal enlargement. Hypertrophy versus hyperplasia. Am J Pathol **49**:1-13.

Johnson KA, Howlett CR, Bellenger CR, Armati-Gulson P (1988): Osteogenesis by canine and rabbit bone marrow in diffusion chambers. Calcif Tissue Int **42**:113-8.

Jones CM, Lyons KM, Hogan BLM (1991): Involvement of bone morphogenetic protein-4 (BMP-4) and Vgr-1 in morphogenesis and neurogenesis in the mouse. Development **111**:531-42.

Juul A (2001): The effects of oestrogens on linear bone growth. Hum Reprod Update **7**:303-13.

Kan KW, Cruess RL (1987): Temporal relationship between fetal bovine skeletal growth and circulating hormonal levels. Calcif Tissue Int **40**:137-48.

Karnovsky MJ (1965): A formaldehyde-glutaraldehyde fixative of high osmolality for use in electron microscopy. J Cell Biol **27**:137A-138A

Karp SJ, Schipani E, St-Jacques B, Hunzelman J, Kronenberg HM, McMahon AP (2000): Indian Hedgehog coordinates endochondral bone growth and morphogenesis via parathyroid hormone related-protein-dependent and -independent pathways. Development **127**:543-8.

Karperien M, Lanser P, De Laat SW, Boonstra J, Defize LHK (1996): Parathyroid hormone related peptide mRNA expression during murine postimplantation development: evidence for involvement in multiple differentiation processes. Int J Dev BioI **40**:599-608.

Karperien M, van Dijk TB, Hoeijmakers T, Cremers F, Abou-Samra A-B, Boonstra J, de Laat SW, Defize LHK (1994): Expression pattern of parathyroid hormone/parathyroid hormone related peptide receptor mRNA in mouse postimplantation embryos indicates involvement in multiple developmental processes. Mech Dev 47 29-42.

Kato Y, Gospodarowicz D (1985): Sulfated proteoglycan synthesis by confluent cultures of rabbit costal chondrocytes grown in the presence of fibroblast growth factor. J Cell Biol **100**:477-85.

Kennedy J, Baris C, Hoyland JA, Selby PL, Freemont AJ, Braidman IP (1999): Immunofluorescent localization of estrogen receptor-alpha in growth plates of rabbits, but not in rats, at sexual maturity. Bone **24**:9-16.

Kember NF (1960): Cell division in endochondral ossification: A study of cell proliferation in rat bones by the method of tritiated thymidine autoradiography. J Bone Joint Surg Br **42**: 824-39.

Kerr JFR, Wyllie AH, Currie AR (1972): Apoptosis - basic biological phenomenon with wide-ranging implications in tissue kinetics. Br J Cancer **26**:239-257.

Kerrigan MJ, Hook CS, Qusous A, Hall AC (2006): Regulatory volume increase (RVI) by in situ and isolated bovine articular chondrocytes. J Cell Physiol **209**:481-92.

Kerrigan MJ, Hall AC (2008): Control of chondrocyte regulatory volume decrease (RVD) by $[Ca^{2+}]_i$ and cell shape. Osteoarthritis Cartilage **16**: 312-22.

Khaled AR, Kim K, Hofmeister R, Muegge K, Durum SK (1999): Withdrawal of IL-7 induces Bax translocation from cytosol to mitochondria through a rise in intracellular pH. Proc Natl Acad Sci U.S.A. **96**:14476-81.

Khaled AR, Moor AN, Li A, Kim K, Ferris DK, Muegge K, Fisher RJ, Fliegel L, Durum SK (2001). Trophic factor withdrawal: p38 mitogen-activated protein kinase activates NHE1, which induces intracellular alkalinization. Mol Cell Biol **21**: 7545-57.

Khosla Su, Westendorf JJ, Oursler MJ (2008): Building bone to reverse osteoporosis and repair fractures. J Clin Invest **118**:421-8.

Kielty CM, Kwan APL, Holmes DF, Schort SL, Grant ME (1985): Type X collagen, a product of hypertrophic chondrocytes. Biochem J **27**:545-54.

Kierdorf U, Li C, Price JS (2009): Improbable appendages: Deer antler renewal as a unique case of mammalian regeneration. Semin Cell Dev Biol **20**:535-42.

Kiernan JA (1999): "Histological and histochemical methods: Theory and practice." Oxford: Butterworth-Heinemann.

Kitaoka E, Satomura K, Hayashi E, Yamanouchi K, Tobiume S, Kume K, Obinata M, Nagayama M (2001): Establishment and characterization of chondrocyte cell lines from the costal cartilage of SV40 large T antigen transgenic mice. J Cell Biochem **81**:571-82.

Kjar I (1974): Skeletal maturation of the human fetus assessed radiographically on the basis of ossification sequences in the hand and foot. Am J Phys Anthrop **40**:257-76.

Kleyman TR, Cragoe Jr EJ (1988). Amiloride and its analogs as tools in the study of ion transport. J Membrane Biol **105**:1-21.

Knothe Tate ML, Adamson JR, Tami AE, Bauer TW (2004): The osteocyte. Int J Biochem Cell Biol **36**:1-8.

Kobayashi S, Takahashi HE, Ito A, Saito N, Nawata M, Horiuchi H, Ohta H, to AI, Iorio R, Yamamoto N, Takaokaa K (2003): Trabecular minimodeling in human iliac bone. Bone **32**:163-9.

Kocamis H, Yeni YN, Kirkpatrick-Keller DC, Killefer J (1999): Postnatal growth of broilers in response to in ovo administration of chicken growth hormone. Poult Sci **78**:1219-26.

Kouri JB, Jimenez SA, Quintero M, Chico A (1996): Ultrastructural study of chondrocytes from fibrillated and non- fibrillated human osteoarthritic cartilage. Osteoarthr Cartil **4**:111-125

Krebsbach PH, Kuznetsov SA, Bianco P, Robey PG (1999): Bone marrow stromal cells: characterization and clinical application. Crit Rev Oral Biol Med **10**:165-81.

Kronenberg HM (2003): Developmental regulation of the growth plate. Nature **423**:332-6.

Kudryckil KE, Newman PR, Shull GE (1990). cDNA cloning and tissue distribution of mRNAs for two proteins that are related to the band 3 Cl^- /HCO_3^- exchanger. J Biol Chem **265**:462-71.

Kuhlman RE (1960): A microchemical study of the developing epiphyseal plate. J Bone Joint Surg Am **42**:457-66.

Kuhn JL, DeLacey JH, Leenellett EE (1996): Relationship between bone growth rate and hypertrophic chondrocyte volume in New Zealand white rabbits of varying ages. J Orthop Res **14**:706-11.

Kunzelmann K, Mall M (2001). Electrolyte transport in the mammalian colon: mechanisms and implications for disease. Physiol Rev **82**:245-89.

Lagadic-Gossmann D, Huc L, Lecureur V (2004). Alterations of intracellular pH homeostasis in apoptosis: origins and roles. Cell Death Differ **11**:953-61.

Lang F, Busch GL, Ritter M, Völkl H, Waldegger S, Gulbins E, Häussinger D (1998): Functional significance of cell volume regulatory mechanisms. Physiol Rev **78**:247-306.

Langenskiold A (1998): Role of the ossification groove of Ranvier in normal and pathologic bone growth: a review. J Pediatr Orthop **18**:173-7.

Lappin PB, Roth RA (1997): Hypertrophy and prolonged DNA synthesis in smooth muscle cells characterize pulmonary arterial wall thickening after monocrotaline pyrrole administration to rats. Toxicol Pathol **25**:372-80.

Larkins BA, Dilkes BP, Dante RA, Coelho CM, Woo YM, Liu Y (2001): Investigating the hows and whys of DNA endoreduplication. J Exp Bot **52**:183-92.

Leach RM Jr, Gay CV (1987): Role of epiphyseal cartilage in endochondral bone formation. J Nutr **117**:784-90.

Leach RM Jr, Sokol C, McMurtry JP (1997): Immunolocalization of basic fibroblast growth factor in porcine epiphyseal growth plate. Domest Anim Endocrinol **14**:129-32.

Lee K, Lanske B, Karaplis AC, Deeds JD, Kohno H, Nissenson RA, Kronenberg HM, Segre GV (1996): Parathyroid hormone-related peptide delays terminal differentiation of chondrocytes during endochondral bone development. Endocrinology **137**:5109-5118

Lee KCL, Maxwell A, Lanyon LE (2002): Validation of a technique for studying functional adaptation of the mouse ulna in response to mechanical loading. Bone **31**:407-12.

Lever JP, Heinemann W (1980): "Introducing Anatomy." London: Medical Books Ltd.

Li J-H, Liu F-F (1997): Intracellular pH and heat sensitivity in two human cancer cell lines. Radiother Oncol **42**: 69-76.

Lidor C, Atkin I, Ornoy A, Deke S, Edelstein S (1987): Healing of rachitic lesions in chicks by 24R, 25 -dihydroxycholecalciferol administered locally into bone. J Bone Miner Res **2**:91-8.

Liu C-J, Hwang J-M, Wu T-T, Hsieh Y-H, Wu C-C, Hsieh Y-S, Tsai C-H, Wu H-C, Huang C-Y, Liu J-Y (2008). Anion exchanger inhibitor DIDS induces human poorly differentiated malignant hepatocellular carcinoma HA22T cell apoptosis. Mol Cell Biochem **308**:117-25.

Liu B, Preisig PA (2002): Compensatory renal hypertrophy is mediated by a cell cycle-dependent mechanism. Kidney Int **62**:1650-8.

Lodish H, Baltimore D, Berk A, Zipursky SL, Matsudaira P, Darnell J (1995): "Molecular cell biology." New York: Scientific American Books.

Loveridge N (1999): Bone: More than a stick. J. Anim Sci **77**:190-6.

Loveridge N (1993): Micronutrients and longitudinal growth: "Proceedings of the Nutrition Society." Trinity College, Dublin pp 49-55.

Lyons KM, Pelton RW, Hogan BLM (1989): Patterns of expression of murine Vgr-1 and BMP-2a RNA suggest that transforming growth factor-beta-like genes coordinately regulate aspects of embryonic development. Genes Dev **3**:1657-68.

Lyons KM, Pelton RW, Hogan BLM (1990): Organogenesis and pattern formation in the mouse: RNA distribution patterns suggest a role for Bone Morphogenetic Protein-2A (BMP-2A). Development **109**:833-44.

Macias D, Gañan Y, Sampath TK, Piedra ME, Ros MA, Hurle JM (1997): Role of BMP-2 and OP-1 (BMP-7) in programmed cell death and skeletogenesis during chick limb development. Development **124**:1109-17.

Mackie EJ, Ahmed YA, Tatarczuch L, Chen K-S, Mirams M (2008): Endochondral ossification: How cartilage is converted into bone in the developing skeleton. Int J Biochem Cell Biol **40**:46-62.

MacRae VE, Farquharson C, Ahmed SF (2006a): The pathophysiology of the growth plate in juvenile idiopathic arthritis. Rheumatology (Oxford) **45**:11-9.

MacRae VE, Farquharson C, Ahmed SF (2006b): The restricted potential for recovery of growth plate chondrogenesis and longitudinal bone growth following exposure to pro-inflammatory cytokines. J Endocrinol **189**:319-28.

Mahnensmith RL, Aronson PS (1985): The plasma membrane sodium-hydrogen exchanger and its role in physiological and pathophysiological processes. Circ Res **57**:773-88.

Mai R, Hagedorn MG, Gelinsky M, Werner C, Turhani D, Spath H, Gedrange T, Lauer G (2006): Ectopic bone formation in nude rats using human osteoblasts seeded poly(3)hydroxybutyrate embroidery and hydroxyapatite-collagen tapes constructs. J Craniomaxillofac Surg **34**:101-9.

Malakooti J, Dahdal RY, Schmidt L, Layden TJ, Dudeja PK, Ramaswamy K (1999). Molecular cloning, tissue distribution, and functional expression of the human Na^+/H^+ exchanger NHE2. Am J Physiol **277**:G383-90.

Malo ME, Fliegel L (2006): Physiological role and regulation of the Na^+/H^+ exchanger. J Physiol Pharmacol **84**:1081-95.

Maor G, Rochwerger M, Segev Y, Phillip M (2002): Leptin acts as a growth factor on the chondrocytes of skeletal growth centers. J Bone Miner Res **17**:1034-43.

Marks J, S.C. , Popoff SN (1988): Bone cell biology: The regulation of development, structure, and function in the skeleton. Am J Anat **183**:1-44.

Martin EA, Ritman EL, Turnerc RT (2003): Time course of epiphyseal growth plate fusion in rat tibiae. Bone **32**:261-7.

Masereel B, Pochet L, Laeckmann D (2003): An overview of inhibitors of Na^+/H^+ exchanger. Eur J Med Chem **38**:547-54.

Mataga N, Tamura M, Yanai N, Shinomura T, Kimata K, Obinata M, Noda M (1996): Establishment of a novel chondrocyte-like cell line derived from transgenic mice harboring the temperature-sensitive simian virus 40 large T-antigen gene. J Bone Miner Res **11**:1646-54.

Mathieu O, Claassen H, Weibel ER (1978): Differential effect of glutaraldehyde and buffer osmolarity on cell dimensions: A study on lung tissue. J. Ultrastruct Res **63**:20-34

Matsuyama S, Llopis J, Deveraux QL, Tsien RY, Reed JC (2000). Changes in intramitochondrial and cytosolic pH: Early events that modulate caspase activation during apoptosis. Nat Cell Biol **2**:318-25.

Maunsbach AB (1966): The influence of different fixatives and fixation methods on the ultrastructure or rat kidney proximal tubule. II. Effects of varying osmolality ionic strength, buffer system and fixative concentration of glutaraldehyde solutions. J Ultrastruct Res **15**:283-309

Mehrer H (2007): "Diffusion in solids: Fundamnetals, methods, materials, diffusion-controlled process." Berlin; London: Springer

Mendler M, Eich-Bender SG, Vaughan L, Winterhalter KH, Bruckner P (1989): Cartilage contains mixed fibrils of collagen types II, IX, and XI. J Cell Biol **108**:191-7.

Min BH, Kim HJ, Lim H, Park SR (2002): Characterization of subpopulated articular chondrocytes separated by Percoll density gradient. In Vitro Cell Dev Biol Anim **38**:35-40.

Miura M, Tanaka K, Komatsu Y, Suda M, Yasoda A, Sakuma Y, Ozasa A, Nakao K (2002): Thyroid hormones promote chondrocyte differentiation in mouse ATDC5 cells and stimulate endochondral ossification in fetal mouse tibias through iodothyronine deiodinases in the growth plate. J Bone Miner Res **17**:443–54.

Monis B, Wasserkrug H, Seligman AM (1965): Comparison of fixatives and substrates for aminopeptidase. J Histochem Cytochem **13**:503-509

Morales T, Roberts AB (1988): Transforming growth factor beta regulates the metabolism of proteoglycans in bovine cartilage organ cultures. J Biol Chem **263**:12828-31.

Morgan JM, Navabi H, Jasani B (1997). Role of calcium chelation in high-temperature antigen retrieval at different pH values J Pathol **182**:233-7.

Muir H (1978): Proteoglycans of cartilage. J Clin Pathol Suppl (R Coll Pathol) **12**:67-81.

Muir H (1995): The chondrocyte, architect of cartilage. Biomechanics, structure, function and molecular biology of cartilage matrix macromolecules. Bioessays **17**:1039-48.

Mushtaq T, Farquharson C, Seawright E, Ahmed SF (2002): Glucocorticoid effects on chondrogenesis, differentiation and apoptosis in the murine ATDC5 chondrocyte cell line. J Endocrinol **175**:705-13.

Mushtaq T, Bijman P, Ahmed SF, Farquharson C (2004). Insulin-like growth factor-1 augments chondrocyte hypertrophy and reverses glucocorticoid-mediated growth retardation in foetal mice metatarsal cultures. Endocrinology **145**:2478-86.

Nakajima R, Inada H, Koike T, Yamano T (2003): Effects of leptin to cultured growth plate chondrocytes. Horm Res **60**:91-8.

Nakamura N, Tanaka S, Teko Y, Mitsui K, Kanazawa H (2005). Four Na^+/H^+ exchanger isoforms are distributed to Golgi and post-Golgi compartments and are involved in organelle pH regulation. J Biol Chem **280**:1561-72.

Nerlich A, Kirsch T, Wiest I, Betz P, von der Mark K (1992): Localization of collagen type X in human fetal and juvenile articular cartilage and bone. Histochemistry **98**:275-81.

Ng L, Grodzinsky AJ, Patwari P, Sandy J, Plaas A, Ortizd C (2003): Individual cartilage aggrecan macromolecules and their constituent glycosaminoglycans visualized via atomic force microscopy. J Struct Biol **143**:242-57.

Ng LJ, Plaas AHK, Grodzinsky AJ, Ortiz C (2002): Structure, conformation, and self-assembly of cartilage polyelectrolyte macromolecules studied via atomic force microscopy: "National Meeting " Boston, MA: The American Chemical Society (ACS), Division of Polymer Chemistry, pp 351.

Nilsson O, Marino R, De Luca F, Phillip M, Baron J (2005): Endocrine regulation of the growth plate. Horm Res **64**:157-65.

Nilsson, O, Mitchum, RD Jr, Schrier, L, Ferns, SP, Barnes, KM Troendle, JF, Baron, J (2005): Growth plate senescence is associated with loss of DNA methylation. J Endocrinol **186**: 241-9.

Noonan KJ, Hunziker EB, Nessler J, Buckwalter JA (1998): Changes in cell, matrix compartment, and fibrillar collagen volumes between growth-plate zones. J Orthop Res **16**:500-8.

Nuss KMR, Auer JA, Alois Boos A, Rechenberg BV (2006): An animal model in sheep for biocompatibility testing of biomaterials in cancellous bones. BMC Musculoskelet Disord. **7**:67. doi: 10.1186/1471-2474-7-67

O'Neill WC (1999): Physiological significance of volume-regulatory transporters. Am J Physiol **276**:C995-1011.

Oberbauer AM, Peng R (1995): Fractionation of growth plate chondrocytes: Differential expression of IGF-l and growth hormone and IGF-I receptor mRNA in purified populations. Connect Tissue Res **31**:179-87.

Oehlke O, Sprysch P, Rickmann M, Roussa E (2006). Na^+/H^+ exchanger isoforms are differentially regulated in rat submandibular gland during acid/base disturbances in vivo. Cell Tissue Res **323**:253-62.

Ogden JA, Rosenberg LC (1988): Defining the growth plate. In Uthoff HK, Wiley JJ (eds): "Behavior of the growth plate." New York: Raven Press, pp 1-15.

Oi T, Utsumi N (1980): Ultrastructure of hypertrophic chondrocytes of rat mandibular condyles using lanthanum-containing fixatives. Arch Oral Biol **25**:77-81.

Okada Y, Maeno E (2001): Apoptosis, cell volume regulation and volume-regulatory chloride channels. Comp Biochem Physiol Part A **130**:377-83.

Okada Y, Maeno E, Shimizu T, Dezaki K, Wang J, Morishima S (2001): Receptor-mediated control of regulatory volume decrease (RVD) and apoptotic volume decrease (AVD). J Physiol **532** (Pt 1):3-16.

Okada Y, Shimizu T, Maeno E, Tanabe S, Wang X, Takahashi N (2006): Volume-sensitive chloride channels involved in apoptotic volume decrease and cell death. J Membr Biol **209**:21-9.

Okubo Y, Reddi AH (2003): Thyroxine downregulates Sox9 and promotes chondrocyte hypertrophy. Biochem Biophys Res Commun **306**:186-90.

Olsen BR, Reginato AM, Wang W (2000): Bone development. Annu Rev Cell Dev Biol **16**:191-220.

O'Reilly N, Xia Z, Fiander H, Tauskela J, Small DL (2002): Disparity between ionic mediators of volume regulation and apoptosis in N1E 115 mouse neuroblastoma cells. Brain Res **943**:245-56.

Orlowski J, Grinstein S (1997): Na^+/H^+ exchangers of mammalian cells. J Biol Chem **272**:22373-6.

Orlowski J, Kandasamy RA, Shull GE (1992). Molecular cloning of putative members of the Na^+/H^+ exchanger gene family:cDNA cloning, deduced amino acid sequence, and mRNA tissue expression of the rat Na^+/H^+ exchanger NHE-1 and two structurally related proteins J Biol Chem **267**:9331-9.

Orntiz DM (2000): Fibroblast growth factor, chondrogenesis, and related clinical disorders. In Canalis C (ed): "Skeletal growth factors." Philadelphia Lippincott William & Wilkins, pp 197-209.

Ornitz DM, Itoh N (2001): Fibroblast growth factors. Genome Biol **2**:reviews3005.1-12.

Ornitz DM, Marie PJ (2002): FGF signaling pathways in endochondral and intramembranous bone development and human genetic disease. Genes Dev **16**:1446-65.

Ouellette AJ, Moonka R, Zelenetz AD, Malt RA (1987): Regulation of ribosome synthesis during compensatory renal hypertrophy in mice. Am J Physiol **253**:C506-13.

Ouyang D, Dhall D, Yu R (2011): Pathologic pancreatic endocrine cell hyperplasia. World J Gastroenterol **17**:137-43.

Paddock SW (2000): Principles and practices of Laser Scanning Confocal Microscopy. Mol Biotechnol **16**:127-49.

Paljavri L, Garcia JH, Kalimo H (1979). The efficiency of aldehyde fixation for electron microscopy: Stabilization of rat brain tissue to withstand osmotic stress. Histochem J **11**:267-76.

Palmiter RD, Brinstert RL (1985): Transgenic Mice. Cell **41**:343-5.

Park KS, Poburko D, Wollheim CB, Demaurex N (2009). Amiloride derivatives induce apoptosis by depleting ER Ca^{2+} stores in vascular endothelial cells. Br J Pharmacol 156:1296-304.

Patton JT, Kaufman MH (1995): The timing of ossification of the limb bones, and growth rates of various long bones of the fore and hind limbs of the prenatal and early postnatal laboratory mouse. J Anat **186**:175-85.

Pearce AI, Richards RG, Milz S, Schneider E, Pearce SG (2007): Animal models for implant biomaterial research in bone: a review. Eur Cell Mater **13**:1-10.

Pedersen JF (1982): Fetal crown-rump length measurement by ultrasound in normal pregnancy. Br J Obstet Gynaecol **89**:926-30.

Peti-Peterdi J, Chambrey R, Bebok Z, Biemesderfer D, St. John PL, Abrahamson DR, Warnock DG, Bell PD (2000). Macula densa Na^+/H^+ exchange activities mediated by apical NHE2 and basolateral NHE4 isoforms. Am J Physiol Renal Physiol **278**:F452-63.

Pizzonia JH, Biemesderfer D, Abu-Alfa AK, Wu M-S, Exner M, Isenring P, Igarashi P, Aronson PS (1998): Immunochemical characterization of Na^+/H^+ exchanger isoform NHE4. Am J Physiol **275**:F510-17.

Poole AR, Pidoux I (1989): Immunoelectron microscopic studies of type X collagen in endochondral ossification. J Cell Biol **109**:2547-54.

Prendergast PJ, Huiskes R (1995): The biomechanics of Wolff's law: recent advances. Ir J Med Sci **164**:152-4.

Qi W, Ding D, Salvi RJ (2008). Cytotoxic effects of dimethyl sulphoxide (DMSO) on cochlear organotypic cultures. Hear Res **236** (1-2):52-60.

Ramos-Vara JA (2005): Technical Aspects of Immunohistochemistry. Vet Pathol **42**:405-26.

Renshaw S (2007): Immunochemical staining. In Renshaw S (ed): "Immunohistochemistry." Oxfordshire: Scionm Publishing Limited, pp 45-56.

Reshkin SJ, Bellizzi A, Cardone RA, Tommasino M, Casavola V, Paradiso A (2003). Paclitaxel induces apoptosis via protein kinase A- and p38 mitogen-activated protein-dependent Inhibition of the Na^+/H^+ Exchanger (NHE) NHE isoform 1 in human breast cancer cells. Clin Cancer Res **9**:2366-73.

Revell PA (1986): "Pathology of bone." Berlin: Springer-Verlag.

Riddell C (1980): A survey of skeletal disorders in five turkey flocks in Saskatchewan. Can J Comp Med **44**:275-9.

Rivas R, Shapiro F (2002): Structural stages in the development of the long bones and epiphyses: a study in the New Zealand white rabbit. J Bone Joint Surg Am **84**:85-100.

Roach HI, Aigner T, Kouri JB (2004): Chondroptosis: A variant of apoptotic cell death in chondrocytes? Apoptosis **9**:265-77.

Roach HI, Clarke NMP (1999): “Cell paralysis” as an intermediate stage in the programmed cell death of epiphyseal chondrocytes during development. J bone Miner Res **14**:1367-78.

Roach HI, Clarke NMP (2000): Physiological cell death of chondrocytes *in vivo* is not confined to apoptosis - New observations on the mammalian growth plate. J Bone Joint Surg Br **82**:601-613.

Roach HI, Mehta G, Oreffo ROC, Clarke NMP, Cooper C (2003): Temporal analysis of rat growth plates: Cessation of growth with age despite presence of a physis. J Histochem Cytochem **51**:373-383.

Robinson FE, Classen HL, Hanson JA, Onderka DK (1992): Growth performance, feed efficiency and the incidence of skeletal and metabolic disease in full-fed and feed restricted broiler and roaster chickens. J Appl Poult Res **1**:33-41.

Robson H, Siebler T, Stevens DA, Shalet SM, Williams GR (2000): Thyroid hormone acts directly on growth plate chondrocytes to promote hypertrophic differentiation and inhibit clonal expansion and cell proliferation Endocrinology **141**:3887-97.

Rodriguez-Zavala JS, Moreno-Sanchez R (1998): Modulation of oxidative phosphorylation by Mg^{2+} in rat heart mitochondria. Journal of Biological Chemistry **273**:7850-55.

Rogers AB, Cormier, K.S., and Fox, J.G. (2006): Thiol-reactive compounds prevent nonspecific antibody binding in immunohistochemistry. Laboratory Investigation **86**:526-33.

Romero MF, Fulton CM, Boron WF (2004): The SLC4 family of HCO_3^- transporters. Pflugers Arch **447**:495-509.

Romero-Calvo I, Ocon B, Martinez-Moya P, Suarez MD, Zarzuelo A, Martinez-Augustin O, de Medina FS (2010). Reversible Ponceau staining as a loading control alternative to actin in Western blots. Anal Biochem **401**:318-20.

Ross MH, Reith EJ (1985): "Histology: A text and atlas." New York: Harper & Row, Publishers, J.B. Lippincott Company.

Rubin CT, Lanyon LE (1984): Regulation of bone formation by applied dynamic loads. J Bone Joint Surg Am **66**:397-402.

Saas J, Lindauer K, Bau B, Takigawa M, Aigner T (2004): Molecular phenotyping of HCS-2/8 cells as an in vitro model of human chondrocytes. Osteoarthritis Cartilage **12**:924-34.

Sachs JR (1996): Cell volume regulation. In Shultz SG, Andreoli TE, Brown AM, Fambrough DM, Hoffman JF, Welsh MJ (eds): "Molecular Biology of Membrane Transport Disorders." New York: Plenum Press, pp 379-402.

Salle BL, Rauch F, Travers R, Bouvier R, Glorieux FH (2002): Human fetal bone development: Histomorphometric evaluation of the proximal femoral metaphysis. Bone **30**:823- 8.

Sanchez CP, Kuizon BD, Abdella PA, Juppner H, Salusky IB, Goodman WG (2000): Impaired growth, delayed ossification, and reduced osteoclastic activity in the growth plate of calcium-supplemented rats with renal failure. Endocrinology **141**:1536-1544

Santos NC, Figueira-Coelho J, Saldanha C, Martins-Silva J (2002): Biochemical, biophysical and haemorheological effects of dimethylsulphoxide on human erythrocyte calcium loading. Cell Calcium **31** (4):183-88.

Santoreneos S, Stoodley MA, Jones NR, Brown CJ (1998): A technique for in vivo vascular perfusion fixation of the sheep central nervous system. J Neurosci Methods 79 195–199

Sasano Y, Takahashi I, Mizoguchi I, Kagayama M, Takita H, Kuboki Y (1998). Type X collagen is not localized in hypertrophic or calcified cartilage in the developing rat trachea. Anat Embryol **197**:399-403.

Sato H, Miki T, Vallabhapurapu RR, Wang R, Liu G-S, Cohen MV, Downey JM (1997). The mechanism of protection from 5 (N-ethyI-N-isopropyl)amiloride differs from that of ischemic preconditioning in rabbit heart. Basic Res Cardio **192**:339-50.

Satoh H, Susaki M, Shukunami C, Iyama K, Negoro T, Hiraki Y (1998). Functional analysis of diastrophic dysplasia sulfate transporter: its involvement in growth regulation of chondrocyte mediated by sulfated proteoglycans. J Biol Chem **273**:12307-15.

Sawad AA, Hana BA, Al-Silawi AN (2009): Morphological study of the skeleton development in chick embryo (Gallus domesticus). Int J Poultry Sc **8**:710-4.

Schelling JR, Abu Jawdeh BG (2008): Regulation of cell survival by Na^+/H^+ exchanger-1. Am J Physiol Renal Physiol **295**:F625-32.

Schmid TM, Conrad HE (1982): Metabolism of low molecular weight collagen by chondrocytes obtained from histologically distinct zones of the chick embryo tibiotarsus. J Biol Chem **257**:12451-7.

Schultz RL, Karlsson U (1965) Fixation of the central nervous system for electron microscopy by aldehyde perfusion: II Effect of osmolarity, pH of perfusate and fixative concentration. J Ultrastr Res **12**:187-206.

Segre GV, Lee K, Lanske B, Kronenberg HM (1997): Parathyroid hormone-related protein and Indian hedgehog regulate the pace of cartilage differentiation. J Bone Miner Metab **15**:109-14.

Seidler U, Bachmann O, Jacob P, Christiani S, Blumenstein I, Rossmann H (2001): Na^+/HCO_3^- cotransport in normal and cystic fibrosis intestine. JOP **2**:247-56.

Seifter JL, Aronson PS (1986): Properties and physiologic roles of the plasma membrane sodium-hydrogen exchanger. J Clin Invest **78**:859-64.

Serrat MA, Williams RM, Farnum CE (2009): Temperature alters solute transport in growth plate cartilage measured by *in vivo* multiphoton microscopy. J Appl Physiol **106**:2016-25.

Shapiro F, Holtrop ME, Glimcher MJ (1977): Organization and cellular biology of the perichondrial ossification groove of Ranvier: A morphological study in rabbits. J Bone Joint Surg Am **59**:703-23.

Shapiro IM, Adams CS, Freeman T, Srinivas V (2005): Fate of the hypertrophic chondrocyte: microenvironmental perspectives on apoptosis and survival in the epiphyseal growth plate. Birth Defects Res C Embryo Today **75**:330-9.

Shen MR, Wilkins RJ, Chou CY, Ellory JC (2002). Anion exchanger isoform 2 operates in parallel with Na(+)/H(+) exchanger isoform 1 during regulatory volume decrease of human cervical cancer cells. FEBS Lett **512**:52-8.

Shi S-R, Cote C, Kalra KL, Taylor CR, Tandon AK (1992): A technique for retrieving antigens in formalin-fixed, routinely acid-decalcified, celloidin-

embedded human temporal bone sections for immunohistochemistry. J Histochem Cytochem **40**:787-92

Shi S-R, Cote RJ, Taylor CR (2001). Antigen retrieval techniques: Current perspectives. J Histochem Cytochem **49**:931-37.

Shi S-R, Key ME, Kalra KL (1991). Antigen retrieval in formalin-fixed, paraffin-embedded tissues: An enhancement method for immunohistochemical staining based on microwave oven heating of tissue sections. J Histochem Cytochem **39**:741-48.

Shibata S, Fukada K, Suzuki S, Yamashita Y (1997). Immunohistochemistry of collagen types II and X, and enzyme-histochemistry of alkaline phosphatase in the developing condylar cartilage of the fetal mouse mandible. J Anat **191**:561-70.

Shrode LD, Tapper H, Grinstein S (1997): Role of intracellular pH in proliferation, transformation, and apoptosis. J Bioenerg Biomembr **29**:393-99.

Shubeita HE, McDonough PM, Harris AN, Knowlton KU, Glembotski CC, Brown JH, Chien KR (1990): Endothelin induction of inositol phospholipid hydrolysis, sarcomere assembly, and cardiac gene expression in ventricular myocytes. A paracrine mechanism for myocardial cell hypertrophy. J Biol Chem **265**:20555-62.

Shukunami C, Ishizeki, K., Atsumi, T., Ohta, Y., Suzuki, F., and Hiraki, Y. (1997): Cellular Hypertrophy and calcification of embryonal carcinoma-derived chondrogenic cell line ATDC5 i*n vitro*. J Bone Miner Res **12**:1174-1188.

Siebler T, Robson H, Shalet SM, Williams GR (2001): Glucocorticoids, thyroid hormone and growth hormone interactions: Implications for the growth plate. Horm Res **56**:7-12.

Silvestrini G, Ballanti P, Patacchioli FR, Mocetti P, Di Grezia R, Wedard BM, Angelucci L, Bonucci E (2000): Evaluation of apoptosis and the glucocorticoid receptor in the cartilage growth plate and metaphyseal bone cells of rats after high-dose treatment with corticosterone. Bone **26**:33-42.

Simpkin VL, Murray DH, Hall AP, Hall AC (2007): Bicarbonate-dependent pH(i) regulation by chondrocytes within the superficial zone of bovine articular cartilage. J Cell Physiol **212**:600-9.

Sims N, Baron R (2000): Bone cells and their function. In Canalis C (ed): "Skeletal growth factors." Philadelphia: Lippincott William & Wilkins, pp 1-16.

Smink JJ, Gresnigt MG, Hamers N, Koedam JA, Berger R, Buul-Offers SCV (2003): Short-term glucocorticoid treatment of prepubertal mice decreases growth and IGF-I expression in the growth plate. J Endocrinol **177**:381-8.

Smith EP, Boyd J, Frank GR, Takahashi H, Cohen RM, Specker B, Williams TC, Lubahn DB, Korach KS (1994): Estrogen resistance caused by a mutation in the estrogen-receptor gene in a man. N Engl J Med **331**:1056-61.

Smith EL, Locke M, Waddington RJ, Sloan AJ (2010): An *ex vivo* rodent mandible culture model for bone repair. Tissue Eng Part C Methods **16**:1287-96.

Soonpaa MH, Field LJ (1994): Assessment of cardiomyocyte DNA synthesis during hypertrophy in adult mice. Am J Physiol **266**:H1439-45.

Spector M (2001). Musculoskeletal connective tissue cells with muscle: Expression of muscle actin in and contraction of fibroblasts, chondrocytes, and osteoblasts. Wound Rep Reg **9**:11-18.

Speer DP (1982): Collagenous architecture of the growth plate and perichondrial ossification groove. J Bone Joint Surg Am **64**:399-407.

Steinkamp JA, Stewart CC (1986): Dual-Laser, differential fluorescence correction method for reducing cellular background autofluorescence. Cytometry **7**:566-74.

Steppan CM, Crawford DT, Chidsey-Frink KL, Ke HZ, Swick AG (2000): Leptin is a potent stimulator of bone growth in ob/ob mice. Regul Pept **92**:73-8.

Stevens DA, Williams GR (1999): Hormone regulation of chondrocyte differentiation and endochondral bone formation. Mol Cell Endocrinol **151**:195-204.

Stockwell RA (1978): Chondrocytes. J Clin Path Suppl (R Coll Pathol) **12**:7-13.

Stockwell RA (1991): Cartilage failure in osteoarthritis: Relevance of normal structure and function. A review. Clin Anat **4**:161-91.

Stokes IA, Clark KC, Farnum CE, Aronsson DD (2007): Alterations in the growth plate associated with growth modulation by sustained compression or distraction. Bone **41**:197-205.

Stokes IA, Mente PL, Iatridis JC, E. Farnum C, Aronsson DD (2002): Enlargement of growth plate chondrocytes modulated by sustained mechanical loading J Bone Joint Surg Am **84**:1842-8.

Stokes IA, Spence H, Aronsson DD, Kilmer N (1996): Mechanical modulation of vertebral body growth: Implications for scoliosis progression. Spine **21**:1162-7.

Stratikopoulos E, Szabolcs M, Dragatsis I, Klinakis A, ., Efstratiadis A (2008): The hormonal action of IGF1 in postnatal mouse growth. Proc Natl Acad Sci U S A **105**:19378-83.

Stutzin A, Hoffmann EK (2006): Swelling-activated ion channels: functional regulation in cell-swelling, proliferation and apoptosis. Acta Physiol **187**:7-42.

Sussman MD (1998): Collagen of growth plate cartilage. In Uthoff HK, Wiley JJ (eds): "Behaviour of the growth plate." New York: Raven Press, pp 31-3

Sutfin LV, Holtrop ME, Ogilvie RE (1971): (cited in Revell, 1986) Microanalysis of individual mitochondrial granules with diameters less than 1000 Angstroms. Science **174**:947-9

Tajsic T, Morrell NW (2011): Smooth muscle cell hypertrophy, proliferation, migration and apoptosis in pulmonary hypertension. Compr Physiol **1**:295-317.

Takayama Y, Mizumachi K (2010): Inhibitory effect of lactoferrin on hypertrophic differentiation of ATDC5 mouse chondroprogenitor cells. Biometals **23**:477-84.

Takigawa M, Tajima K, Pan H, Enomoto M, Kinoshita A, Suzuki F, Takano Y, Mori Y (1989): Establishment of a clonal human chondrosarcoma cell line with cartilage phenotypes. Cancer Res:3996-4002.

Thorngren KG HL (1973): Cell kinetics and morphology of the growth plate in the normal and hypophysectomized rat. Calcif Tissue Res **13**:113-29.

Thorp BH (1994): Skeletal disorders in the fowl: a review. Avian Pathol **23**:203-36.

Tokumasu F, Dvorak J (2003): Development and application of quantum dots for immunocytochemistry of human erythrocytes. J Microsc **211**:256-61.

Tonna EA (1961): The cellular complement of the skeletal system studied autoradiographically with tritiated thymidine (H3TDR) during growth and aging. J Biophys Biochem Cytol **9**:813-24.

Torrance AG, Mosley JR, Suswillo RFL, Lanyon LE (1994): Noninvasive loading of the rat ulna In vivo Induces a strain-related modeling response uncomplicated by trauma or periostal pressure. Calcif Tissue Int **54**:241-7.

Trippel SB, Ehrlich MG, Lippiello L, Mankin HJ (1980): Characterization of chondrocytes from bovine articular cartilage: I. Metabolic and morphological experimental studies. J Bone Joint Surg Am **62**:816-20.

Tseng H, Berk BC (1992): The Na/K/2Cl cotransporter is increased in hypertrophied vascular smooth muscle cells. J Biol Chem **267**:8161-7.

Tsuganezawa H, Kobayashi K, Iyori M, Araki T, Koizumi A, Watanabe S-I, Kaneko A, Fukao T, Monkawa T, Yoshida T, Kim DK, Kanai Y, Endou H, Hayashi M, Sarutal T (2001). A new member of the HCO_3^- transporter superfamily is an apical anion exchanger of β-intercalated cells in the kidney. J Biol Chem **276**:8180-9.

Turner CH, Forwood MR (1994): Letters to the editor on animal models for studying bone adaptation. Calcif Tissue Int **55**:316-8.

Urban JPG (1994): The chondrocyte: A cell under pressure. Br J Rheumatol **33**:901-908

Urban JPG, Hall AC, Gehl KA (1993): Regulation of matrix synthesis rates by the ionic and osmotic environment of articular chondrocytes. J Cell Physiol **154**:262-270. doi: 10.1002/jcp.1041540208

Van Bezooijen RL, Wee-Pals LVD, Papapoulos SE, Löwik CWGM (2002). Interleukin 17 synergises with tumour necrosis to induce cartilage destruction in vitro α factor. Ann Rheum Dis **61**:870-76.

Van de Lest CH, Versteeg EM, Veerkamp JH, Van Kuppevelt TH (1995): Elimination of autofluorescence in immunofluorescence microscopy with digital image processing. J Histochem Cytochem **43**:727-30.

van der Eerden BCJ, Karperien M, Gevers EF, Lowik CWGM, Wit JA (2000): Expression of Indian Hedgehog, parathyroid hormone-related protein, and their receptors in the postnatal growth plate of the rat: evidence for a locally acting growth restraining feedback loop after birth. J Bone Miner Res **15**:1045-55

van der Eerden BCJ, Karperien M, Wit JM (2003): Systemic and local regulation of the growth plate. Endocr Rev **24**:782-801.

van der Eerden BCJ, Van Til NP, Brinkmann AO, Lowik CWGM, Wit JM, Karperien M (2002): Gender differences in expression of androgen receptor in tibial growth plate and metaphyseal bone of the rat. Bone **30**:891-6.

van der Rest M, Garrone R (1991): Collagen family of proteins. FASEB J **5**:2814-23.

Van Sickle DC (1985): Control of postnatal bone growth. J. Anim Sci **61**:76-91.

Vander AJ, Sherman JH, Luciano DS (1994): "Human Physiology" New York: WCB/ McGraw Hill.

Vaughan J (1981): "The physiology of bone." Oxford: Clarendon Press.

Verkman AS, Mitra AK (2000): Structure and function of aquaporin water channels. Am J Physiol Renal Physiol **278**:F13-28.

Vico L, Vanacker JM (2010): Sex hormones and their receptors in bone homeostasis: insights from genetically modified mouse models. Osteoporos Int **21**:365-72.

Viegas MS, Martins TC, Seco F, do Carmo A (2007). An improved and cost-effective methodology for the reduction of autofluorescence in direct immunofluorescence studies on formalin-fixed paraffin-embedded tissues Eur J Histochem **51**:59-66.

Vigne P, Frelin C, Cragoe Jr. EJ, Lazdunski M (1984). Structure-activity relationships of amiloride and certain of its analogues in relation to the blockade of the Na^+/H^+ exchange system. Mol Pharmacol **25**:131-6.

Vignolo M, Naselli A, Di Battista E, Mostert M, Aicardi G (1988): Growth and development in simple obesity. Eur J Pediatr **147**:242-4.

Villemure I, Stokes AF (2009): Growth plate mechanics and mechanobiology. A survey of present understanding. J Biomech **42**:1793-1803.

Vortkamp A, Pathi S, Peretti GM, Caruso EM, Zaleske DJ, Tabin CJ (1998): Recapitulation of signals regulating embryonic bone formation during postnatal growth and in fracture repair. Mech Dev **71**:65-76.

Wakabayashi S, Shigekawa M, Pouyssegur J (1997): Molecular physiology of vertebrate Na^+/H^+ exchangers. Physiol Rev **77**:51-74.

Wakita R, Izumi T, Itoman M (1998): Thyroid hormone-induced chondrocyte terminal differentiation in rat femur organ culture. Cell Tissue Res **293**:357-64.

Waldegger S, Steuer S, Risler T, Heidland A, Capasso G, Massry S, Lang F (1998): Mechanisms and clinical significance of cell volume regulation. Nephrol Dial Transplant **13**:867-74.

Wallis GA (1996): Bone growth: coordinating chondrocyte differentiation. Curr Biol **6**:1577-80.

Wang Y, Huang S, Sah VP, Ross JJ, Brown JH, Han J, Chien KR (1998): Cardiac muscle cell hypertrophy and apoptosis induced by distinct members of the p38 mitogen-activated protein kinase family. J Biol Chem **273**:2161-8.

Wang Y, Middleton, F, Horton, JA, Reichel, L, Farnum, CE, and Damron, TA (2004): Microarray analysis of proliferative and hypertrophic growth plate zones identifies differentiation markers and signal pathways. Bone **35**:1273-93.

Wang Z, Orlowski J, Shu GE (1993): Primary structure and functional expression of a novel gastrointestinal isoform of the rat Na/H exchanger. J Biol Chem **268**:11925-8.

Wang H, Singh D, Fliegel L (1997). The Na^+/H^+ antiporter potentiates growth and retinoic acid-induced differentiation of p19 embryonal carcinoma cells. J Biol Chem **272**:26545-9.

Wang X, Takahashi N, Uramoto H, Okada Y (2005): Chloride channel inhibition prevents ROS dependent apoptosis induced by ischemia- reperfusion in mouse cardiomyocytes. Cell Physiol Biochem **16**:147-54.

Warner GP, Hubbard HL, Lloyd GC, Wuthier RE (1983): ^{32}Pi- and ^{45}Ca-metabolism by matrix vesicle-enriched microsomes prepared from chicken

epiphyseal cartilage by isosmotic Percoll density-gradient fractionation. Calcif Tissue Int **35**:327-38.

Weise M, De-Levi S, Barnes K, Gafni RI, Abad V, Baron J (2001): Effects of estrogen on growth plate senescence and epiphyseal fusion. Proc Natl Acad Sci U S A **98**:6871-6.

White A, Wallis G (2001): Endochondral ossification: A delicate balance between growth and mineralisation. Curr Biol **11**:R589-91.

Wilkins RJ, Browning JA, Ellory JC (2000): Surviving in a matrix: Membrane transport in articular chondrocytes. Journal of Membrane Biology **177**:95-108.

Wilkins RJ, Fairfax TP, Davies ME, Muzyamba MC, Gibson JS (2003): Homeostasis of intracellular Ca^{2+} in equine chondrocytes: Response to hypotonic shock. Equine Vet J **35**:439-43.

Wilsman NJ, Bernardini ES, Leiferman E, Noonan K, Farnum CE (2008): Age and pattern of the onset of differential growth among growth plates in rats. J Orthop Res **26**:1457-65.

Wilsman NJ, Farnum CE, Green EM, Lieferman EM, Clayton MK (1996a): Cell cycle analysis of proliferative zone chondrocytes in growth plates elongating at different rates. J Orthop Res **14**:562-72.

Wilsman NJ, Farnum CE, Leiferman EM, Fry M, Barreto C (1996b): Differential growth by growth plates as a function of multiple parameters of chondrocytic kinetics. J Orthop Res **14**:927-36.

Wilson-MacDonald J, Houghton GR, Bradley J, Morscher E (1990): The relationship between periosteal division and compression or distraction of the growth plate. An experimental study in the rabbit. J Bone Joint Surg Br **72**:303-8.

Wolf G, Mueller E, Stahl RA, Ziyadeh FN (1993): Angiotensin II-induced hypertrophy of cultured murine proximal tubular cells is mediated by endogenous transforming growth factor-beta. J Clin Invest **92**:1366-72.

Wolf G, Neilson EG (1990): Angiotensin II induces cellular hypertrophy in cultured murine proximal tubular cells. Am J Physiol **259**:F768-77.

Woods KA, Camacho-Hubner C, Savage MO, Clark ADJL (1996): Intrauterine growth retardation and postnatal growth failure associated with deletion of the insulin-like growth factor I gene. N Engl J Med **335**:1363-67.

Wu SF, De Luca F (2004): Role of cholesterol in the regulation of growth plate chondrogenesis and longitudinal bone growth. J Biol Chem **279**:4642-47.

Wu Y, Sun H, Yakar S, LeRoith D (2009): Elevated levels of insulin-like growth factor (IGF)-I in serum rescue the severe growth retardation of IGF-I null mice. Endocrinology **150**:4395-403.

Yamamah GA, Hassan NE, El-masry SA, Salama EE, Shouman MG (2010): South Sinai Growth Charts of Children and Adolescents J Anim Sci **6**:232-40.

Yamakawa K, Kamekura S, Kawamura N, Saegusa M, Kamei D, Murakami M, Kudo I, Uematsu S, Akira S, Chung UI, Nakamura K, Kawaguchi H (2008): Association of microsomal prostaglandin E synthase 1 deficiency with impaired fracture healing, but not with bone loss or osteoarthritis, in mouse models of skeletal disorders. Arthritis Rheum **58**:172-83.

Yannoukakos D, Stuart-Tilley A, Fernandez HA, Fey P, Duyk G, Alper SL (1994): Molecular cloning, expression, and chromosomal localization of two isoforms of the AE3 anion exchanger from human heart. Circ Res **75**:603 - 14.

Yu FH, Shull GE, Orlowski J (1993): Functional properties of the rat Na/H exchanger NHE-2 isoform expressed in Na/H exchanger-deficient Chinese hamster ovary cells. J Biol Chem **268**:25536-41.

Zachos NC, Tse M, Donowitz M (2005): Molecular physiology of intestinal Na^+/H^+ exchange. Annu Rev Physiol **67**:411-43.

Publications and Abstracts

Refereed Publications

Bush PG, Pritchard M, **Loqman MY**, Damron TA, Hall AC (2010): A key role for membrane transporter NKCC1 in mediating chondrocyte volume increase in the mammalian growth plate. J Bone Miner Res **2**5:1594-603.

Loqman MY, Bush PG, Farquharson C, Hall AC (2010): A cell shrinkage artefact in growth plate chondrocytes with common fixative solutions: Importance of fixative osmolarity for maintaining morphology. Eur Cell Mater **19**:214-27.

Meeting Abstracts

Loqman MY, Bush PG, Hall AC (2008): A Role of Glutamate Aspartate Transporter (GLAST) in growth plate chondrocyte hypertrophy: An immunohistochemical study: "European Workshop on Growth Plate Research." Glasgow, U.K.

Loqman MY, Bush PG, Farquharson C, Hall AC (2008): Fixation of growth plate chondrocytes (GPC) with conventional tissue fixatives causes a shrinkage artifact: "36th Scottish Microscopy Society Symposium." Edinburgh, U.K.

Loqman MY, McAuley P, Bush PG, Hall AC (2010): Changes to anion exchange (AE2) and sodium/hydrogen exchanger (NHE1) levels with growth plate chondrocyte hypertrophy: An immunohistochemical study: "The Physiological Society Meeting." Manchester, U.K.

ORIGINAL ARTICLE

JBMR

A Key Role for Membrane Transporter NKCC1 in Mediating Chondrocyte Volume Increase in the Mammalian Growth Plate

Peter G Bush,[1] Meredith Pritchard,[2] Mohamad Y Loqman,[3] Timothy A Damron,[2] and Andrew C Hall[3]

[1]Centre for Biomedical and Health Science Research, School of Pharmacy and Biomolecular Sciences, University of Brighton, Brighton, UK
[2]Musculoskeletal Sciences Research Laboratory, Department of Orthopedic Surgery, State University of New York Upstate Medical University, Syracuse, NY, USA
[3]Centre for Integrative Physiology, School of Biomedical Sciences, University of Edinburgh, Edinburgh, Scotland, United Kingdom

ABSTRACT

The mechanisms that underlie growth plate chondrocyte volume increase and hence bone lengthening are poorly understood. Many cell types activate the Na-K-Cl cotransporter (NKCC) to bring about volume increase. We hypothesised that NKCC may be responsible for the volume expansion of hypertrophic chondrocytes. Metatarsals/metacarpals from 16 rat pups (P_7) were incubated in the presence/absence of the specific NKCC inhibitor bumetanide and measurement of whole-bone lengths and histologic analysis of the growth plate were done after 24 hours. Fluorescent NKCC immunohistochemistry was visualised using a confocal laser scanning microscopy on seven rat tibial growth plates (P_7). Microarray analysis was performed on mRNA isolated from proliferative and hypertrophic zone cells of tibial growth plates from five rats of each of three ages ($P_{49/53/58}$). Exposure to bumetanide resulted in approximately 35% reduction (paired Student's *t* test, $p < .05$) of bone growth in a dose-dependent manner; histologic analysis showed that a reduction in hypertrophic zone height was responsible. Quantification of fluorescence immunohistochemistry revealed a significant (paired Student's *t* test, $p < .05$) change in NKCC from the intracellular space of proliferative cells to the cytosolic membrane of hypertrophic zone cells. Further, microarray analysis illustrated an increase in *NKCC1* mRNA between proliferative and hypertrophic cells. The increase in *NKCC1* mRNA in hypertrophic zone cells, its cellular localization, and reduced bone growth in the presence of the NKCC inhibitor bumetanide implicate NKCC in growth plate hypertrophic chondrocyte volume increase. Further investigation is warranted to determine the regulatory control of NKCC in the mammalian growth plate and the possible detrimental effect on bone growth with chronic exposure to loop diuretics.

KEY WORDS: GROWTH PLATE; HYPERTROPHIC CHONDROCYTES; NKCC; VOLUME; RAT

Introduction

The growth plate is comprised of a thin layer of columnar chondrocytes lying perpendicular to and responsible for new bone formation during longitudinal skeletal growth. Cells within the column are highly organized, with a "reserve" zone preceding proliferative zone chondrocytes (PZCs). After a regulated period of time, a marked differentiation occurs, signified by a dramatic increase in volume, resulting in the formation of hypertrophic zone chondrocytes (HZCs). This volume increase is predominantly in the longitudinal axis, which accounts for approximately 80% of bone lengthening.[1] The volume of a typical cell increases from approximately 1000 μm^3 in the PZC to approximately 15,000 μm^3 in the HZC.[2] It has been postulated that this cell volume increase occurs through a combination of classic "hypertrophy"[2] and "swelling."[3] However, the mechanisms that drive growth plate HZC volume expansion are unknown.

Cell swelling describes the process arising from the net movement of water into the cell, and in biologic systems, this process relies solely on an osmotic gradient. This can result from a reduction in extracellular osmolarity, an increase in intracellular osmolarity, or a combination of the two. Studies measuring the effect of hypoosmotic challenge on in situ growth plate chondrocytes suggest that for cell swelling to be entirely mediated by a reduction in extracellular osmolarity, these cells would need to be exposed to an approximately 280 mOsmol reduction in osmolarity[2] to approximately 120 mOsmol. Plasma osmolarity therefore would need to be reduced from approximately 300 mOsmol to near 20 mOsmol, which is clearly

Received in original form July 18, 2008; revised form July 8, 2009; accepted January 13, 2010. Published online January 29, 2010.
Address correspondence to: Peter G Bush, PhD, School of Pharmacy and Biomolecular Sciences, University of Brighton, Lewes Road, Brighton, BN2 4GJ UK. E-mail: p.g.bush@brighton.ac.uk

Journal of Bone and Mineral Research, Vol. 25, No. 7, July 2010, pp 1594–1603
DOI: 10.1002/jbmr.47

implausible. Therefore, osmotic gradient–driven water accumulation is more likely to be due to an *increase* in intracellular osmolarity in the transition of a PZC to an HZC.

Intracellular osmolarity can be raised by the catabolism of intracellular macromolecules (eg, proteins and/or complex carbohydrates) into osmotically active components (eg, amino acids and/or simple sugars).[4] However, intracellular organic osmolytes do not account for the volume increase between PZC and HZC.[5] Therefore, the "active" movement of osmolytes across the plasma membrane into the cell is the most probable mechanism. Previous studies suggest that the accumulation of organic solutes (eg, simple sugars and amino acids) is responsible for approximately 9% of the osmolytes required.[5] This strongly suggests other osmolytes are involved, and the activity and/or number of inorganic solute transporters also may be increased in order for cells to amass appropriate quantities of osmolytes to drive such a volume increase.

The intracellular sodium concentration ($[Na^+]_i$) plays a key role in determining cell volume, and Na^+ is moved across the cytoplasmic membrane through a range of transport proteins (see ref. [6]). One of these, the Na-K-2Cl cotransporter (NKCC), is an obvious candidate for HZC expansion owing to its ability to increase cell volume in other cell types.[7] NKCC mediates electroneutral ion transport and is characterized by its sensitivity to loop diuretics (eg, bumetanide and furosemide).[8] In many cell types, activation of NKCC (eg, by exposure to hypertonicity) results in an increase in cell volume, termed *regulatory volume increase* (RVI).[6,7] Typically, RVI describes volume recovery after cell shrinkage, returning a cell to its "normal" volume. In contrast, growth plate chondrocytes require a coordinated, continual volume increase as they progress from PZC to terminal HZC phenotypes. Increased activity of NKCC may be able to drive such cell swelling.

Two NKCC isoforms are known, the near-ubiquitous NKCC1 and NKCC2, which appears to be localized exclusively in the kidney.[7–10] Although considered to be present in all tissues, to our knowledge, only mRNA for *NKCC1* has been reported in growth plates, where it demonstrates increased expression from PZCs to HZCs.[11]

In this study, we tested the hypothesis that NKCC1 was involved with HZC volume increase and longitudinal bone growth using a variety of methodologies. First, whole-metatarsal/metacarpal rudiments were incubated with the loop diuretic bumetanide, a specific NKCC inhibitor, which inhibited bone elongation by approximately 35%. Histologic analysis of growth plates from bumetanide-exposed metatarsal rudiments showed a reduction in HZ height, suggesting an inhibition of NKCC-mediated HZC volume increase. For bumetanide to be acting on NKCC in the hypertrophic zone, NKCC has to be associated with the HZC plasma membrane. To elucidate NKCC tissue and cellular distribution, immunohistochemistry was performed on growth plate sections. While NKCC immunofluorescence was present throughout the growth plate, it was most prevalent in HZCs. Further examination of NKCC cellular distribution revealed a dramatic change from a predominantly intracellular location in PZCs to the cytoplasmic membrane in HZCs. NKCC1-specific antibodies are not available, but gene array microanalysis confirmed the upregulation of *NKCC1* mRNA, with negligible signal for *NKCC2* mRNA.

Materials and Methods

Biochemicals and solutions

Unless otherwise stated, all biochemicals and solutions were obtained from Sigma Chemical Company (Poole, UK). Bone rudiment dissection media consisted of phosphate-buffered saline (PBS) containing α-medium (7.5% v/v; Invitrogen, Ltd., Paisey, UK) and bovine serum albumin V (1 mM). Standard culture medium (α-medium) was supplemented with Na_2 glycerol biphosphate (1 mM), bovine serum albumin V (1 mM), and L-ascorbic acid (5 mg/mL). Bumetanide was prepared as a 20 mM stock solution in ethanol. 4,4′-Diisothiocyanatostilbene-2,2′-disulfonic acid (DIDS) was prepared as a 0.1 M stock solution in 0.1 M potassium bicarbonate.

Animal preparation

For immunohistochemistry and bone rudiment culture, 19 Sprague-Dawley rat pups (7 days old, P_7) were humanely killed by decapitation following UK Home Office guidelines for other experiments. The three middle metatarsals of each hind limb, three middle metacarpals from 14 of the animals, and tibias from 6 animals were dissected out while immersed in dissection medium and carefully cleaned of soft tissue.

Fifteen Sprague-Dawley rats were also used, aged 49, 53, and 58 days old (5 animals in each set). These older animals with larger growth plates were used to obtain sufficient material for microarray analysis studies. Animals were killed by carbon dioxide asphyxiation following procedures reviewed and approved by the Institutional Use and Care of Animals Committee. For the purpose of this study, the left proximal tibial bone including the growth plate then was harvested and immediately frozen in liquid nitrogen and stored at −80°C.

Whole-metatarsal rudiment preparation and measurement

In order to prepare duplicate samples for determination of the effects of six bumetanide concentrations (0 to 200 μM) on bone lengthening, metatarsals and metacarpals of four animals were used (12 bones per animal). Each duplicate consisted of one metatarsal and one metacarpal. Bones were cultured individually in 1 mL of standard culture medium and maintained at 37°C [CO_2 (5%):air (95%), pH 7.4]. Rudiment pairs were randomly selected for either bumetanide (12.5 to 200 μM) or vehicle control (ethanol alone) addition to the medium. Owing to the slower growth rate of metacarpals, further experiments were performed (100 μM of bumetanide or vehicle controls) on metatarsals alone from a further 15 animals. A bumetanide concentration of 100 μM was chosen because it resulted in maximal inhibition of bone lengthening (Fig. 1), but it was still below the concentration known to disrupt the activity of other membrane-transport proteins.[12–14] Similarly, metatarsals and metacarpals were dissected from 10 animals and randomly selected for a range of DIDS concentrations (0 to 1 mM) in the presence of 100 μM of bumetanide. A minimum of four animals was used for each DIDS concentration.

Images (640 × 320 pixels) of rudiments were acquired immediately after dissection and after 24 hours in the presence/absence

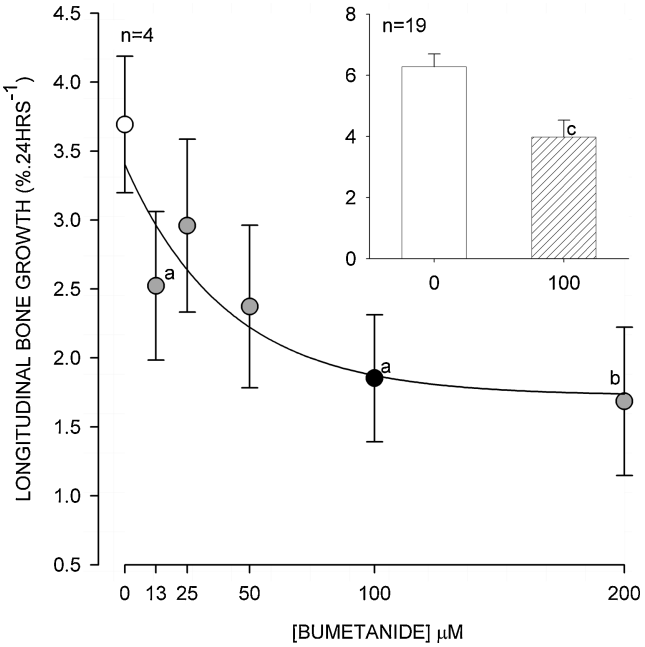

Fig. 1. The effect of NKCC inhibition on rat metatarsal bone rudiment growth by the NKCC inhibitor bumetanide. Each data point contains paired metatarsals, and metacarpals from each animal (*main graph*) or metatarsals alone (*inset*) were cultured for 24 hours and measured as described in "Materials and Methods." There was a dose-dependent relationship for bumetanide inhibition; individual points were significantly different from control (no bumetanide, *open circle*) with bumetanide concentrations of 12.5, 100, and 200 μM ($^{a}p < .05$; $^{b}p < .01$, paired *t* test). The inset chart shows the significant reduction ($^{c}p < .002$, paired *t* test) of bone lengthening by 100 μM of bumetanide (*pattern fill*) on metatarsals alone ($n = 19$). Data expressed as means with errors bars representing SEM.

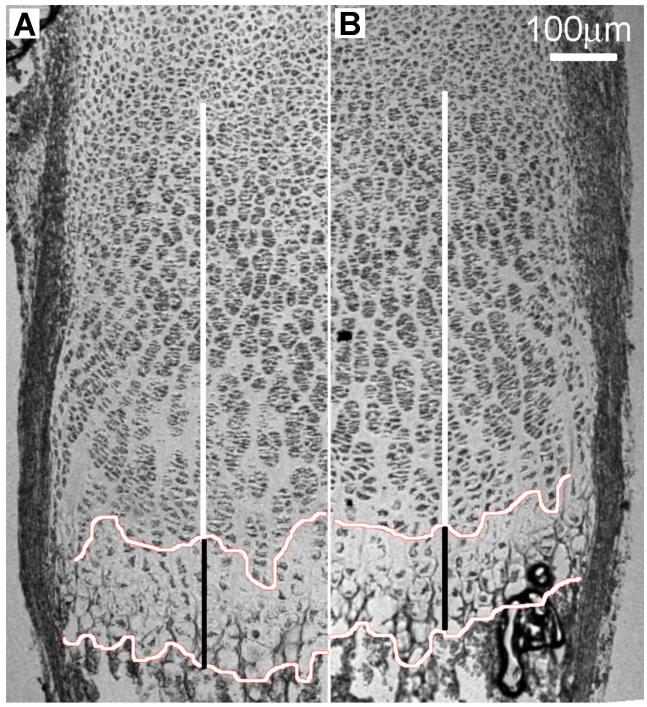

Fig. 2. Light micrograph of rat metatarsal growth plate in the absence (*A*) and presence (*B*) of 100 μM of bumetanide. The irregular horizontal lines were traced by eye along the beginning of late HZCs that exhibited an unambiguous volume enlargement and the bottom at the zone of calcification. The black-and-white vertical bars indicate the average height of the late hypertrophic and remaining growth plate, respectively. Scale bar = 100 μm.

of inhibitor using an eyepiece camera (DCM35, Brunel Microscopes, Chippenham, UK) fitted to a dissecting stereomicroscope (Wild M3, Heerbrugg, Switzerland). An image of a rule was acquired to provide calibration, and bone lengths were measured using ImageJ (National Institute of Health, Bethesda, MD, USA).

After 24 hours of incubation in the presence/absence of bumetanide, metatarsals were fixed with 4% paraformaldehyde in 0.1 M phosphate buffer, pH 7.4, overnight. After dehydration through a graded series of ethanol solutions, tibias were embedded in paraffin wax, cut into longitudinal 10 μm serial sections (Reichert-Jung 1130/Biocut microtome, Leica Biosystems Nussloch GmbH, Nussloch, Germany), and mounted onto polylysine-coated glass slides. Section wax was dissolved in xylene, followed by rehydration through a series of ethanol grades to PBS. Images of both proximal and distal growth plates were taken using the transmitted light detector of an upright confocal laser scanning microscope (Zeiss LSM510, Welwyn Garden City, UK) fitted with a ×10 dry objective lens. Zone heights were determined by eye using a line drawn freehand along the top of proliferating cells, the clear demarcation of cell enlargement between proliferative and hypertrophic regions, and the zone of mineralization at the base of the hypertrophic zone. The distance was measured from a point in the center of the image, and the length between each was recorded using ImageJ (NIH; Fig. 2). The total number of cells between the zone of mineralization and hypertrophy was counted by eye.

Growth plate immunohistochemistry

Dissected tibias were fixed and embedded, and sections were cut as described earlier for metatarsals. Sections were dewaxed and rehydrated to PBS, and nonspecific antigen sites were blocked using donkey serum (1:5 dilution). Sections were incubated with a 1:100 dilution of the mouse monoclonal anti–human NKCC antibody T4[14] (affinity for both NKCC1 and NKCC2). Sections then were exposed to a 1:50 dilution of AlexaFluor 488 donkey anti-mouse (Invitrogen, Ltd.) secondary antibody for 1 hour at 37°C. Omission of the primary antibody served as a control.

Immunohistochemically stained growth plate sections were imaged using a Zeiss LSM510 upright confocal laser scanning microscope (CLSM) at low power [×10 dry objective, numerical aperture (NA) = 0.3] and high power (×63 oil immersion objective, NA = 1.4). Emitted light, following excitation of AlexaFluor 488 (excitation/emission maximum 495/519 nm) with a 488-nm argon laser, was collected through a long-pass 505-nm filter. Transmitted light also was collected to aid cell/zone identification. High-resolution (1024 × 1024) images were acquired representing a field of view 920 and 206 μm^2 and using sequential optical *Z*-steps of either 10 or 1 μm for low- or high-power lenses, respectively. Detector sensitivity was adjusted to

provide maximum contrast without pixel saturation and excessive dye bleaching. Adjacent fields of view were acquired comprising the entire depth of the growth plate.

In order to identify intracellular and cytoplasmic membrane-associated immunofluorescence in an unbiased manner, the cell membrane was visualised using high-power images obtained with transmitted light images. A line was plotted through the central axis of the middle optical section for each cell. The average fluorescent signal between the two cytoplasmic membrane segments and the central intracellular portion were recorded. To correct for variations in sectioning angle between metatarsals, the growth plate was partitioned into eight equidistant sections.[2] The top of section 1 (S_1) was taken as the top of the proliferating zone, with the bottom of section 8 (S_8) at the zone of mineralization. Section average intracellular and cytoplasmic membrane fluorescence was determined from all cells within each section. The fluorescence intensity was expressed as a percentage; the most intense intracellular or cytoplasmic membrane section measurement was assigned 100%, thereby normalizing images from different growth plates.

Microarray analysis

The transcriptional analysis of cDNA by microarray used here has been described previously in detail.[11] Briefly, serial 6-μm sections of snap frozen tibia were cut using a Leica CM3050 cryostat onto Leica polyethylennaphtalae slides (PEN, Leica Microsystems, Bannockburn, IL, USA) and kept on dry ice immediately prior to laser capture microdissection (LCM). A Leica Application Solution Laser Microdissection instrument (Leica Microsystems) with either a ×10 or ×20 objective lens was used to cut freehand-traced areas. The morphology of PZC and HZC was easily identified by eye. Each growth plate fragment fell directly into an RNase-free microfuge tube containing RLT lysis buffer (Qiagen, Valencia, CA, USA). Approximately three regions of PZ and HZ were collected from each slide, with each zone harvested into separate tubes. Total RNA was extracted using the RNeasy RNA isolation kit (Qiagen). Pooled samples contained between 30 and 50 ng of RNA (RNA Pico Labchip, Agilent Technology Bioanalyzer, Santa Clara, CA, USA). After purification and quantification of mRNA,[11] 15 μg of biotinylated cRNA was hydrolyzed to 35 to 200 nucleotides, and known concentrations of positive control genes were added (50 pM Oligo B2 and 1.5, 5, 25, and 100 pM of *Escherichia coli bioB, bioC, bioD*, and *cre*). The hybridization solution was heated (45°C for 5 minutes) and centrifuged (5 minutes) before each sample was injected into an individual RAE230 2.0 GeneChip (Affymetrix, Santa Clara, CA, USA). Chips were hybridized at 45°C for 16 hours with constant rotation (60 rpm) and then were washed and stained on the Fluidics station (Affymetrix) according to the EukGE-WS2v4 protocol. Fluorescent images were acquired using the Agilent G2500A Gene Array Scanner. Affymetrix software (MicroArray Suite 5.0) was used to process the raw images into Cel images files, which were loaded into GeneSpring (Agilent Technologies, Pale Alto, CA, USA) and normalized using the robust multiarray averaging (RMA) method. Differential gene expression ratios were considered significant at the 95% confidence interval (CI).[15]

Real-time RT-PCR

cDNA was produced from the pooled RNA samples used for the arrays by reverse transcription (RT) of 1 μg of total RNA with M-MLV reverse transcriptase and oligo-(dT)15 primers (Promega, Madison, WI, USA). Total RNA from a neonatal (3-day-old) rat kidney was similarly reverse transcribed to generate a positive control for all primer sets, which were run in duplicate. Negative controls included an RT-null control (no RT enzyme), cDNA-null for each primer set, and a template/primer null reaction.

Primers were synthesized by MWG Biosciences (Huntsville, AL, USA): 5′GTCTAAGGACCTGCCACCAA3′ (NKCC1), 5′CGGGTCGTCTA GATCCAAAA3′ (NKCC2), and 5′AGCCATGTACGTAGCCATCC3′ (β-actin, a housekeeping gene sequence, was used for normalization) and antisense primers 5′TGCTGACGATCCAGTCACTC3′, 5′ATGGA CTTGGAAACGACTGG3′, and 5′CTCTCAGCTGTGGTGGTGAA3′, respectively. Prior to performing the real-time assay, the annealing temperature was optimized by gradient PCR using HotStartTaq (Qiagen). Probe specificity was assumed from visualization of a single band at the expected molecular size by agarose gel (2%) electrophoresis.

PCR was performed with Quantitect SYBR Green PCR master mix (Qiagen). The total reaction volume was 25 μL with 12.5 μL of the master mix, primers at 0.3 μM (0.075 μL), and 0.5 μL of the RT product cDNA and brought to balance with nuclease-free water. The reactions were run in duplicate for 40 cycles using an ABI Prism7000 Sequence Detection System (PE Applied Biosystems, Foster City, CA, USA). The reaction parameters were 95°C for 15 minutes (hot start), denatured at 94°C for 15 seconds, annealed at 58°C for 15 seconds, and extension/read at 72°C for 30 seconds. After the fortieth cycle, dissociation data were collected from 66.4 to 91.7°C in 0.9°C increments.

Data analysis

Data were expressed as means ± SEM obtained from a number of individual animals (n). Differences between means were determined by paired Student's t test, with $p < .05$, $p < .01$, and $p < .001$ considered to be significant, highly significant, and extremely significant, respectively. Statistical analysis was performed using SigmaStat (Systat, Chicago, IL, USA).

Results

Bumetanide bone rudiment culture

Duplicate paired metatarsal and metacarpal bones from P_7 rat pups exhibited a dose-dependent inhibition of bone lengthening by bumetanide (Fig. 1). Bone lengthening was significantly reduced with bumetanide concentrations of 12.5, 100, and 200 μM ($p < .05$, t test) compared with controls. A curve fit of the bumetanide dose-response data was best fitted by a three-parameter hyperbolic decay curve ($r^2 = 0.9656$, correlation coefficient), with predicted maximal longitudinal growth of 1.725% as [bumetanide] → ∞ compared with growth in control bones of 3.69% after 24 hours of incubation. Owing to the differing growth rates of metacarpals and metatarsals,[16] further experiments were performed using faster-growing metatarsals alone (Fig. 1, *inset*). Control metatarsals increased in length by

approximately 6% after 24 hours in culture. When incubated with 100 μM bumetanide, bone lengthening was significantly reduced ($p < .01$, Students t test) by approximately 35%.

Measurement of the growth plate of the metatarsals, from uppermost PZC to the zone of mineralization, is shown in Fig. 2. There was no overall difference in total growth plate length between control and bumetanide-treated samples (Table 1), although these measurements were associated with a large SEM. However, there was a significant reduction ($p < .05$, Student's paired t test) in the hypertrophic zone of approximately 50 μm. When the data were normalized with the HZ expressed as a percentage of the total growth plate height, a highly significant reduction of nearly 50% was observed in the bumetanide-exposed specimens (Table 1, $p < .01$, Student's t test).

HZ cell counts of each micrograph were almost identical ($p = .937$, Student's t test), with 193 ± 11.3 cells for the control group and 192 ± 13.6 cells for the bumetanide-treated group. When corrected for the section area, no significant difference ($p = .953$, Student's t test) existed between the cell densities of control and bumetanide-treated groups (1400 ± 125 and 1377 ± 350 cells/mm^2, respectively), showing that the number of HZCs did not change with exposure to bumetanide.

Fluorescence immunohistochemistry

Immunohistochemistry was used to determine both the tissue and cellular localization of NKCC in the mammalian growth plate. The T4 monoclonal anti-NKCC antibody exhibited strong staining for chondrocytes throughout proximal tibial growth plate cartilage from P_7 animals, although the pattern of fluorescence staining was heterogeneous. Low-power (×10 objective lens) CLSM images of NKCC immunohistochemistry (Fig. 3) showed the distribution of staining along the growth plate. It can be seen that the fluorescent signal was strong in the early proliferative zone, decreasing through the late proliferative and early hypertrophic regions, before increasing again in the middle to late hypertrophic zones. This observation was consistent across proximal tibial growth plates of all seven animals.

Table 1. Reduction in Height of the Growth Plate Hypertrophic Zone by Bumetanide

Zone	Control	Bumetanide 100 μM	p Value
Total growth plate (μm)	636 ± 150	689 ± 130	.655
Late HZ (μm)	204 ± 25.6	151 ± 15.0	.015*
HZ (% of total)	33.8 ± 1.57	22.7 ± 0.814	.008**

Note: Growth plate measurements of three P_7 rat metatarsals (proximal and distal) cultured for 24 hours in the absence/presence of 100 μM bumetanide. Bones were fixed, prepared, and visualized (Fig. 2) as described in "Materials and Methods." The average height of growth plates was not significantly different (paired Student's t test) between control and bumetanide-treated bones, whereas there was a significant (*$p < .05$, paired Student's t test) decrease by approximately 50 μm in the late hypertrophic zone (HZ). When normalized and presented as a percentage of total growth plate height, the reduction in growth was highly significant (**$p < .01$, Student's paired t test). Data shown as means ± SEM.

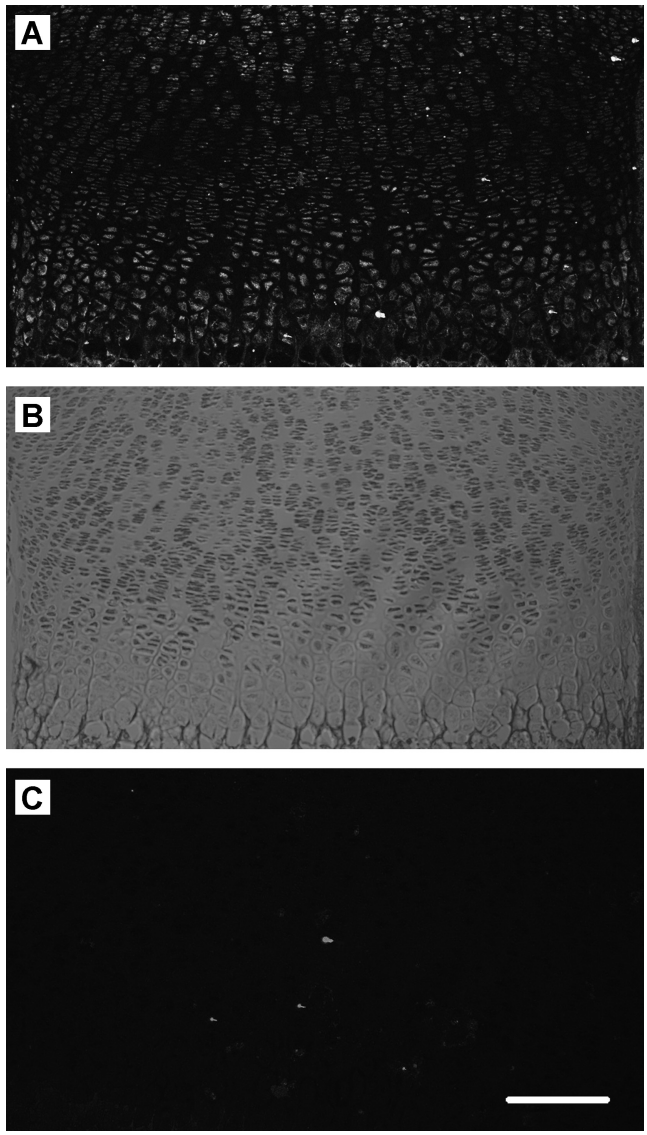

Fig. 3. Growth plate NKCC distribution. Low-power (×10 objective) confocal microscope images (projected) of proximal tibial growth plate stained for NKCC (T4 antibody). Rat proximal tibias were removed and fixed, and transverse sections were prepared for immunohistochemistry as described in "Materials and Methods." (*A*) AlexaFluor 488 secondary antibody fluorescence, (*B*) transmitted light image of the same field of view, and (*C*) as for panel *A* but with primary antibody omitted. The proliferative zone showed some fluorescence that appeared to reduce to the upper edge of the HZ. Cells in the HZ exhibited strong fluorescence, which even at this low magnification appeared to be localized to the plasma membrane. Scale bar = 200 μm.

High-power (×63 objective lens) images allowed the observation of cellular localization, which differed as cells transitioned from early PZCs to late HZCs. Figure 4*A*, *D* shows typical PZCs and an HZC with a predominantly intracellular and cytoplasmic membrane-associated fluorescence, respectively. Quantification of immunofluorescence (Fig. 5) confirmed that qualitative assessment of intracellular fluorescence was highest in the PZC, with S_1 to S_5 being significantly higher than S_6 to S_8 ($p < .05$, paired Student's t test). In contrast, cytoplasmic membrane–associated fluorescence was lowest in S_1 to S_4 PZCs,

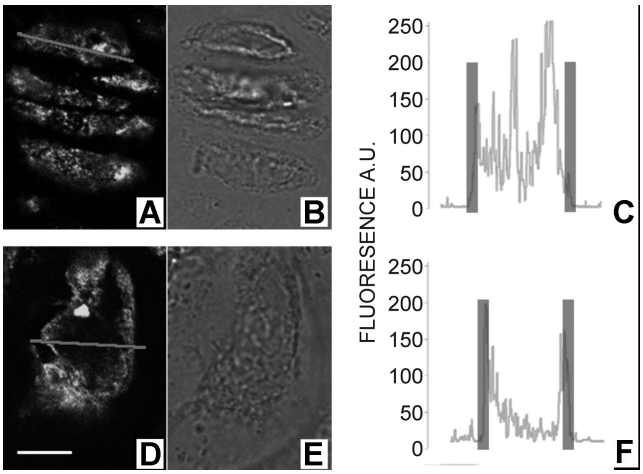

Fig. 4. Growth plate chondrocyte NKCC localization in typical proliferative (*A–C*) and hypertrophic (*D–F*) zone chondrocytes. Rat proximal tibias were prepared for and subjected to immunohistochemical procedures, and then images were acquired as described in "Materials and Methods." NKCC immunofluorescence from a single optical section is shown in panels *A* and *D*, with the corresponding transmitted light images (*B*) and (*E*) for PZCs and HZCs, respectively. The intensity profile along a line drawn through the center of a cell (gray line in *A* and *D*) is shown (*C*, *F*). The overlaid transparent vertical bars in *C* and *F* indicate the approximate position of the cytoplasmic membrane determined from the transmitted light image (*B*, *E*). Fluorescence intensity is in arbitrary units (AUs). For all panels, scale bar = 5 μm.

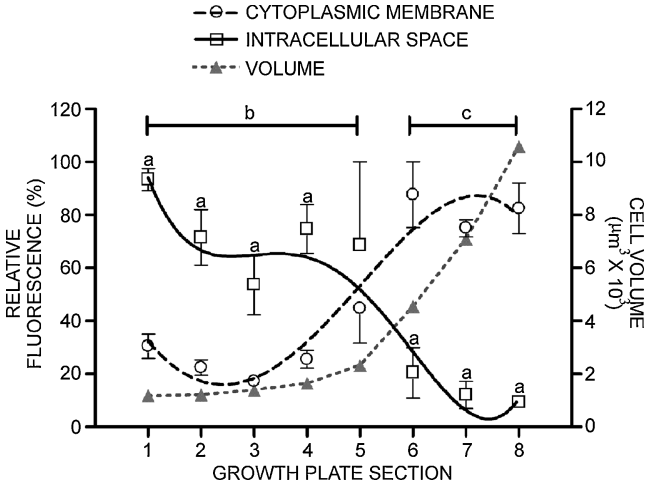

Fig. 5. Quantification of cellular NKCC distribution along the growth plate. The fluorescence associated with the plasma membrane or intracellular space was obtained from images of cells along the entire length of the growth plate (see "Materials and Methods" and Fig. 4). Owing to the variability in section position, angle, and inherent differences in growth plate dimensions, cell positions within the growth plate were expressed in eight equidistant sections; sections 1 to 3 PZC and 5 to 8 HZC. Significant differences ($^a p < .05$, Student's *t* test) between the fluorescent signal of the intracellular space (*solid line*, □) and membrane-associated fluorescence (*broken line*, ○). Similarly, significant differences ($p < .05$, Student's *t* test) between PZC and HZC intracellular fluorescence (*b*) and between PZC and HZC membrane-associated fluorescence (*c*) are shown. An overlay (*gray line*, △) of cell volumes (*right axis*) has been included to highlight the appearance of NKCC in the plasma membrane immediately preceding a volume increase (data replotted from ref. [2]). Data points are for the mean of a minimum of four animals (421 cells) with bars denoting SEM.

increasing significantly in S_6 to S_8 ($p < .05$, paired Student's *t* test). Within each growth plate section S_1 through S_8, there was a significant difference ($p < .05$, paired Student's *t* test) between intracellular and cytoplasmic membrane–associated fluorescence with the exception of cells from S_5.

Gene microarray and RT-PCR analysis

Good-quality antibodies raised against the different isoforms of NKCC (1 and 2) were not available for immunohistochemistry, and hence an alternative approach of gene microarray analysis was required to confirm the presence of NKCC1 over NKCC2. Of the 161 genes examined as part of a wider study into membrane-transport proteins, the majority (approximately 90%) showed low expression levels [<10 arbitrary expression units (AEUs)]. Indeed, the average raw expression levels for the 161 transport-protein genes across both PZCs and HZCs at all time points studied was 8.997 (ranging from 3.15 to 308 AEUs). As expected, the kidney-specific *NKCC2* gene showed background (<10 AEUs) expression levels, whereas the ubiquitous *NKCC1* gene expression levels were above background (Table 2). The positive control proteins for PZC and HZC (procollagen type II and matrix metalloprotease 13 [MMP13], respectively) exhibited high expression levels.

Statistical significance was determined at the 95% confidence interval (CI) with a two-tailed cutoff of 1.96 SD. Log_2 values are shown in Table 3 for the ratios (HZC:PZC) of NKCC1, NKCC2, MMP13, and procollagen type II on rats aged 49, 53, and 58 days. With log_2 values that exceed the 95% CI, it would be expected that there would be a less than 5% risk of false-positive results. For MMP13, since the log_2 ratios exceed the 95% CI by at least 8 SDs in one time point, we should expect no false-positive results. However, of the NKCC transport proteins, only NKCC1 expression on day 49 exceeded the 95% limit. A twofold HZC:PZC ratio was considered relevant[13]; as expected, MMP13 exhibited a large increase between PZCs and HZCs (Table 3), and NKCC1 showed a greater than twofold change on days 49 and 58. There was little change from unity for NKCC2 expression between PZCs and HZCs, near background in both zones across the three animal ages studied.

Owing to the temporal variation in NKCC1 expression by microarray, confirmation was obtained by RT-PCR (Table 4). Log_2 ratios and fold increase in expression between PZ and HZ were identical to those obtained by microarray; indeed, plotting both sets of results by linear regression produced a coefficient of determination (r^2) of 0.986. Similar analysis of NKCC2 revealed a poor correlation ($r^2 = 0.116$), which was more indicative of the levels below threshold associated with NKCC2.

DIDS bone rudiment culture

Metatarsal and metacarpal bones from P_7 rat pups exhibited a dose-dependent inhibition of bone lengthening by DIDS in the presence of 100 μM bumetanide (Fig. 6). Bone lengthening was significantly further reduced by DIDS concentrations of 175 μM

Table 2. Microarray mRNA Expression of *NKCC1*, *NKCC2*, *MMP13*, and *Col II* in Rat Growth Plate Chondrocytes

	Expression (AEUs)					
	Day 49		Day 53		Day 58	
Gene	PZC	HZC	PZC	HZC	PZC	HZC
NKCC1	19.4	56.9	16.1	14.1	79.8	189.4
NKCC2	3.21	4.23	3.31	4.31	4.36	3.15
MMP13	5.72	1019	9.34	676	39.6	5241
Col II	6999	5762	4838	2275	8478	6617

Note: Mean raw levels (AEUs) from five animals each, shown for kidney-specific NKCC2 and ubiquitous NKCC1 transport proteins and the HZC and PZC markers MMP13 and procollagen type II, respectively. The NKCC2 isoform showed no expression above background levels (<10 AEUs), whereas NKCC1 exhibited expression well above average for the 161 transport protein/carrier genes analyzed (~9.0 AEUs). The high expression levels of the standard markers MMP13 and procollagen type II highlight the low levels associated with NKCC1 and NKCC2 isoforms.

Table 3. Microarray Analysis of Growth Plate *NKCC1*, *NKCC2*, *MMP13*, and *Pro-Col II*

	Log 2 ratio (HZ/PZ)			Ratio (HZ/PZ) fold change		
Gene	Day 49	Day 53	Day 58	Day 49	Day 53	Day 58
NKCC1	1.55	−0.20	1.25	2.93	−1.15	2.37
NKCC2	0.40	0.38	−0.47	1.32	1.30	−1.38
MMP13	7.48	6.18	7.05	178.3	72.5	132.3
Col II	−0.28	−1.09	−0.36	0.823	0.470	0.780

Note: Log_2 HZC/PZC ratios and expression ratio fold changes (HPZ/PZC) from microarray analysis (see "Material and Methods") of *NKCC1* and *NKCC2* and the HZC and PZC positive controls *MMP13* and *Procollagen Type II*, respectively. Only the log_2 of *NKCC1* ratio on day 49 (double-scored boundary) was greater than the 95% confidence level (1.20), whereas both day 49 and day 58 exhibited greater than twofold changes in the HZC/PZC ratios. All *MMP13* data showed relevant increases in expression between PZC and HZC and *Procollagen Type II* on day 53.

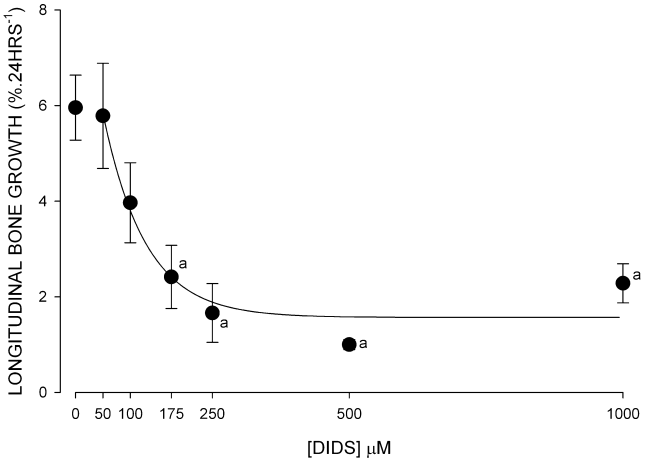

Fig. 6. The effect of the AE inhibitor DIDS (in the presence of 100 μM of bumetanide) on rat metatarsal/metacarpal bone rudiment growth. Each data point represents a metatarsal and metacarpal from of each of at least four animals, cultured for 24 hours, and measured as described in "Materials and Methods." There was a dose-dependent relationship of DIDS inhibition, significantly reduced ($^a p < .05$, *t* test) from control at DIDS concentrations of 175 μM or greater with maximal inhibition at 500 μM. Data points are for the mean of a minimum of four animals with bars denoting SEM.

to 1 mM ($p < .05$, *t* test) compared with 100 μM of bumetanide alone. Rudiment culture for 24 hours in the presence of 500 μM of DIDS resulted in a maximal inhibition of approximately 80% over and above bumetanide alone ($p < .001$, *t* test).

Discussion

This study set out to examine the involvement of NKCC1 in the coordinated volume increase of growth plate HZCs. Using a variety of techniques, we provide evidence that implicates NKCC1 in growth plate chondrocyte hypertrophy and hence longitudinal bone growth. The optimization of different techniques required the use of different bones from differently aged animals. Measurable increases in bone length were possible only with small bones from young animals, but the growth plate chondrocytes of these bones do not withstand crushing injury caused by the bisection required for cell volume determination by CLSM. Hence larger tibias were used from P_7 animals to directly compare the relationship between cell volume and NKCC immunohistochemistry. Although the metatarsals, metacarpals, and tibias used for immunohistochemistry were from age-matched animals (P_7), their relatively small growth plates make extracting sufficient mRNA for microarray analysis technically demanding. Hence older animals with larger growth plates were used, a temporal effect partially checked by examining tibias from P_{49}, P_{53}, and P_{58} animals.

Table 4. Real-Time RT-PCR Analysis of *NKCC1* and *NKCC2*

	Log 2 ratio (HZ/PZ)			Ratio (HZ/PZ) fold change		
Gene	Day 49	Day 53	Day 58	Day 49	Day 53	Day 58
NKCC1	1.7	−0.175	1.12	3.25	−1.13	2.17
NKCC2	0.305	0.8	0.305	1.24	1.74	1.24

Note: Log_2 HZC/PZC ratios and expression ratio fold changes (HPZ/PZC) from real-time RT-PCR (see "Material and Methods") of *NKCC1* and *NKCC2*. The results for *NKCC1* mimic those obtained in the microarray analysis, with both day 49 and day 58 animals exhibiting greater than twofold changes in the HZC/PZC ratios. The coefficient of determination (r^2) for the linear regression between RT-PCR and microarray analysis was 0.986 for *NKCC1* and 0.116 for *NKCC2*.

Microarray analysis of raw data (Table 2) indicated a substantial increase for P_{49} and P_{58} animals but no increase at P_{53}. This may be an indication of temporal changes in NKCC activity, but when compared with MMP13 and Pro-Col II data, it is more likely due to a general suppression of hypertrophy-related genes in this experimental set. Further analysis revealed that while both P_{49} and P_{58} animals showed a greater than twofold increase in NKCC1 expression between PZCs and HZCs, only the data from P_{49} animals exceeded the 95% confidence limit. Some confusion therefore exists with the microarray data; however, subsequent RT-PCR analysis of the samples provided confirmation of these results. It must be remembered that the primary role for this technique was to confirm the presence of NKCC1 over NKCC2, albeit not from P_7 rats. The negligible signal for *NKCC2* mRNA gives confidence that we were able to associate T4 antibody immunohistochemistry to NKCC1 alone.

The T4 monoclonal antibody used for NKCC immunohistochemistry has been used previously in mammalian tissue for successful tissue immunolocalization of NKCC in rat hippocampus,[17] gerbil inner ear,[18] rabbit parotid and kidney,[19] and human airway smooth muscle.[20] Similarly, T4 resulted in clear CLSM images of NKCC distribution in growth plate sections (Figs. 3 and 4). Quantification of NKCC immunohistochemistry cellular localization (Fig. 5) showed that NKCC was present along the entire growth plate, but with a change in immunolocalization of NKCC from intracellular regions to the cytoplasmic membrane with transition from PZCs to HZCs. Localization of NKCC to the cell membrane is essential for its involvement in HZC volume increase.

While not of primary concern to the role of HZC volume increase, the intracellular localization of NKCC in PZCs is intriguing. PZC NKCC appeared to be adjacent to the nucleus, suggesting an association with endoplasmic reticulum and/or the Golgi apparatus. This could represent the synthesis of NKCC pools ready for translocation to the plasma membrane for future cell volume increases. Such a redistribution of the cotransporter to the cell surface is a mechanism for NKCC upregulation in other cell types.[21] Similar differences in NKCC distribution between PZCs and HZCs are also observed with human cytomegalovirus infection of a fibroblast cell line.[22] Infection inhibits translocation of NKCC to the plasma membrane, resulting in similar perinuclear distribution as shown here, with abolition of cell NKCC activity.

The tissue distribution and cellular localization of NKCC were consistent with its role in HZC volume increase, but it is the bumetanide inhibition of NKCC that provides direct evidence for a role in bone lengthening. The precise bumetanide dose required to inhibit bone lengthening is difficult to determine because in situ the cells would experience less than that added to the culture medium, but it may be similar to the bumetanide concentration required for maximal inhibition of NKCC in isolated cells ($\leq$20 μM). Conversely, the maximum concentration of bumetanide used (200 μM) would ensure that in situ chondrocytes were not exposed to levels associated with nonspecific inhibition of bicarbonate exchanger,[12] chloride channels,[13] and potassium chloride cotransport.[14]

Approximately 80% of bone lengthening has been attributed to HZC volume increase.[1] Therefore, the inhibition of metatarsal longitudinal growth by bumetanide accounts for less than half, if one assumes that NKCC inhibition by bumetanide was limited to HZCs. PZC cell division contributes to approximately 10% of bone lengthening[1] and may be inhibited by bumetanide.[23–25] However, NKCC distribution suggests only low levels of NKCC in the cytoplasmic membrane of PZCs, and histologic analysis (Fig. 2) of bumetanide-treated metatarsals does suggest that inhibition was restricted to HZCs.

The partial inhibition of bone lengthening by bumetanide would suggest the presence of other mechanisms to drive HZC volume increase. Inorganic ion transporters also known to be involved in RVI may be implicated, such as increased activity of sodium hydrogen exchange (NHE), anion exchange (AE), and sodium chloride cotransport (NCC) or decreased activity of ion-transport proteins known to bring about a decrease in cell volume, including potassium-driven transporters and the Na^+/K^+ pump.[6] Of all these membrane proteins, microarray analysis highlighted AE3 (Slc4a3) alone as changing expression between proliferative and hypertrophic zones, with an approximately 14-fold increase (absolute expression values of 217 to 3122) compared with no change for AE1 (Slc4a1; 255 to 216, −1.18-fold change) or AE2 (Slc4a2; 105 to 109, 1.04-fold change). Metatarsal culture experiments in the presence of 100 μM bumetanide and the AE inhibitor DIDS (0 to 1 mM) resulted in a dose-dependent inhibition of bone lengthening greater than bumetanide alone (Fig. 6), inhibiting bone lengthening by a maximum of 80% compared with control bones.

Growth plate chondrocyte AE3 would appear to be a candidate for driving the major portion of growth plate chondrocyte volume increase; however, a number of concerns with this hypothesis exist. First, DIDS is a relatively nonspecific inhibitor of carrier-mediated anion transport.[26] Indeed, in HZ growth plate chondrocytes, DIDS has been shown to completely abolish diastrophic dysplasia sulfate transport (DTDST)–mediated sulfate

uptake critical for proteoglycan synthesis.[27] Second, AE must be coupled with other transport proteins to elicit a volume-regulatory increase, typically sodium hydrogen exchange,[6] but these transport proteins show no increase in mRNA expression between PZCs and HZCs. Finally, we cannot be certain that DIDS inhibition of anion transport does not exert its inhibition of bone lengthening through modulation of intracellular pH. Unlike NKCC, with its specific inhibitors (ie, bumetanide and furosemide), the role of AE3 cannot be ascertained because it has no analogous specific inhibitors, but its role clearly warrants further investigation.

The putative presence of transporters other than NKCC1 and/or redundancy in the system to drive HZC volume increase may explain the reduced size of *NKCC1* knockout mice over the first 2 weeks, a period of maximal growth rate,[16] but their ability to recover to the size of wild-type animals as they reach maturity.[28] This ability of *NKCC1* knockouts to recover may explain why there are limited reports of skeletal growth retardation in children exposed to loop diuretics (eg, bumetanide and furosemide). Reduced bone growth also may go unreported owing to the conditions that required prescription of loop diuretics. Pediatric furosemide therapy is used in the treatment of chronic lung disease, nephritic syndrome, renal failure, congestive heart failure, and hydrocephalus fluid shunts (see ref. [29]), conditions that might be expected to result in poor growth outcome and therefore not subsequently associated with loop diuretics.

A study of four children prescribed the NKCC inhibitor furosemide[30] described bone demineralization, but no mention was made of reduced longitudinal bone growth. However, anecdotal clinical reports led to a study by Koo and colleagues,[31] who subjected 4-day-old rats to furosemide for 24 days and observed a significant reduction in tibial length that was not associated with abnormal calcium, sodium, magnesium, potassium, or parathyroid hormone in plasma or bone. This suggested that bone growth and not subsequent demineralization was responsible. Although no explanation was provided for the bone growth retardation observed, the present findings could implicate direct NKCC1 inhibition of HZCs in vivo.

If NKCC plays the major role of HZC volume increase, it would be expected to be under the same hormonal control that regulates bone growth. NKCC has been shown to be regulated by hormones in other tissues.[32] Future work is required to elucidate this, as well as to study NKCC1 regulation through control of protein synthesis, translocation to the cytoplasmic membrane, and activation through phosphorylation/dephosphorylation events[22,33,34] to provide an insight into the control of HZC volume increase mediated by NKCC1. The regulated activation of NKCC1 within the mammalian growth plate also could provide an ideal model for the study of general NKCC1 physiology.

In summary, we hypothesised that NKCC activity may play a role in the coordinated volume increase seen in HZCs of the growth plate. Using multiple methodologies, we have provided evidence for the role of NKCC1 in growth plate HZC volume increase: the inhibition of bone lengthening (through reduction in HZ height) with the NKCC-specific inhibitor bumetanide, appropriate cellular localization of NKCC in HZCs to the cytoplasmic membrane, and an increase of *NKCC1* mRNA in HZCs with negligible *NKCC2* signal. The involvement of NKCC in bone lengthening warrants further investigation, with special attention to the detrimental therapeutic effects possible with NKCC1 inhibitors (loop diuretics) in children.

Disclosures

All the authors state that they have no conflicts of interest.

Acknowledgments

We would like to thank Mr Jason Horton for his invaluable help with the RT-PCR, Dr Michael Cousin for the donation of some biologic samples, and Dr Peter Flatman for the generous gift of the T4 anti-NKCC antibody. This work was supported by the BBSRC (BB/C513985/1 Grant to ACH) and the NIH/NCI (2R01CA083892 Grant to TAD). MYL was supported by Universiti Putra Malaysia (UPM) and Ministry of Higher Education Malaysia under the SLAB scholarship.

References

1. Wilsman NJ, Farnum CE, Leiferman EM, Fry M, Barreto C. Differential growth by growth plates as a function of multiple parameters of chondrocytic kinetics. J Orthop Res. 1996;14:927–936.
2. Bush PG, Parisinos CA, Hall AC. The osmotic sensitivity of rat growth plate chondrocytes in situ: clarifying the mechanisms of hypertrophy. J Cell Physiol. 2008;214:621–629.
3. Buckwalter JA, Mower D, Ungar R, Schaeffer J, Ginsberg B. Morphometric analysis of chondrocyte hypertrophy. J Bone Joint Surg. 1986;68A:243–255.
4. Haussinger D, Roth E, Lang F, Gerok W. Cellular hydration state: an important determinant of protein catabolism in health and disease. Lancet. 1993;341:1330–1332.
5. Farnum CE, Lee R, O'Hara K, Urban JPG. Volume increase in growth plate chondrocytes during hypertrophy: the contribution of organic osmolytes. Bone. 2002;30:574–581.
6. Lang F, Busch GL, Ritter M, et al. Functional significance of cell volume regulatory mechanisms. Physiol. Rev. 1998;78:247–306.
7. Russell JM. Sodium-potassium-chloride cotransport. Physiol. Rev. 2000;80:211–276.
8. Xu JC, Lytle C, Zhu TT, Payne JA, Benz E Jr, Forbush B 3rd. Molecular cloning and functional expression of the bumetanide-sensitive Na-K-Cl cotransporter. Proc Natl Acad Sci U S A. 1994;91:2201–2205.
9. Gamba G, Miyanoshita A, Lombardi M, et al. Molecular cloning, primary structure, and characterization of two members of the mammalian electroneutral sodium-(potassium)-chloride cotransporter family expressed in kidney. J Biol Chem. 1994;269:17713–17722.
10. Payne JA, Forbush B 3rd. Alternatively spliced isoforms of the putative renal Na-K-Cl cotransporter are differentially distributed within the rabbit kidney. Proc Natl Acad Sci U S A. 1994;91:4544–4548.
11. Wang Y, Middleton F, Horton JA, Reichel L, Farnum CE, Damron TA. Microarray analysis of proliferative and hypertrophic growth plate zones identifies differentiation markers and signal pathways. Bone. 2004;35:1273–1293.
12. Jennings ML. Kinetics and mechanism of anion transport in red blood cells. Annu Rev Physiol. 1985;47:519–533.
13. Evans MG, Marty A, Tan YP, Trautmann A. Blockage of Ca-activated Cl conductance by furosemide in rat lacrimal glands. Pflugers Arch. 1986;406:65–68.
14. Lauf PK, Bauer J, Adragna NC, et al. Erythrocyte K-Cl cotransport: properties and regulation. Am J Physiol. 1992;263:C917–932.

15. Zraly CB, Middleton FA, Dingwall AK. Hormone-response genes are direct in vivo regulatory targets of Brahma (SWI/SNF) complex function. J Biol Chem. 2006;281:35305–35315.
16. Wilsman NJ, Bernardini ES, Leiferman E, Noonan K, Farnum CE. Age and pattern of the onset of differential growth among growth plates in rats. J Orthop Res. 2008.
17. Marty S, Wehrle R, Alvarez-Leefmans FJ, Gasnier B, Sotelo C. Postnatal maturation of Na^+, K^+, $2Cl^-$ cotransporter expression and inhibitory synaptogenesis in the rat hippocampus: an immunocytochemical analysis. Eur J Neurosci. 2002;15:233–245.
18. Crouch JJ, Sakaguchi N, Lytle C, Schulte BA. Immunohistochemical localization of the Na-K-Cl co-transporter (NKCC1) in the gerbil inner ear. J Histochem Cytochem. 1997;45:773–778.
19. Lytle C, Xu JC, Biemesderfer D, Forbush B 3rd. Distribution and diversity of Na-K-Cl cotransport proteins: a study with monoclonal antibodies. Am J Physiol. 1995;269:C1496–1505.
20. Iwamoto LM, Nakamura KT, Wada RK. Immunolocalization of a Na-K-2Cl cotransporter in human tracheobronchial smooth muscle. J Appl Physiol. 2003;94:1596–1601.
21. D'Andrea-Winslow L, Strohmeier GR, Rossi B, Hofman P. Identification of a sea urchin Na(+)/K(+)/2Cl(-) cotransporter (NKCC): microfilament-dependent surface expression is mediated by hypotonic shock and cyclic AMP. J Exp Biol. 2001;204:147–156.
22. Maglova LM, Crowe WE, Russell JM. Perinuclear localization of Na-K-Cl-cotransporter protein after human cytomegalovirus infection. Am J Physiol Cell Physiol. 2004;286:C1324–1334.
23. Iwamoto LM, Fujiwara N, Nakamura KT, Wada RK. Na-K-2Cl cotransporter inhibition impairs human lung cellular proliferation. Am J Physiol Lung Cell Mol Physiol. 2004;287:L510–514.
24. Shiozaki A, Miyazaki H, Niisato N, et al. Furosemide, a blocker of Na^+/K^+/2Cl- cotransporter, diminishes proliferation of poorly differentiated human gastric cancer cells by affecting G0/G1 state. J Physiol Sci. 2006;56:401–406.
25. Panet R, Atlan H. Stimulation of bumetanide-sensitive Na^+/K^+/Cl- cotransport by different mitogens in synchronized human skin fibroblasts is essential for cell proliferation. J Cell Biol. 1991;114:337–342.
26. Kidd JF, Thorn P. Intracellular Ca^{2+} and Cl- channel activation in secretory cells. Annu Rev Physiol. 2000;62:493–513.
27. Satoh H, Susaki M, Shukunami C, Iyama K, Negoro T, Hiraki Y. Functional analysis of diastrophic dysplasia sulfate transporter. Its involvement in growth retardation of chondrocytes mediated by sulfated proteoglycans. J Biol Chem. 1998;273:12307–12315.
28. Pace AJ, Lee E, Athirakul K, Coffman TM, O'Brien DA, Koller BH. Failure of spermatogenesis in mouse lines deficient in the Na(+)-K(+)-2Cl(-) cotransporter. J Clin Invest. 2000;105:441–450.
29. Prandota J. Clinical pharmacology of furosemide in children: a supplement. Am J Ther. 2001;8:275–289.
30. Venkataraman PS, Han BK, Tsang RC, Daugherty CC. Secondary hyperparathyroidism and bone disease in infants receiving long-term furosemide therapy. Am J Dis Child. 1983;137:1157–1161.
31. Koo WW, Guan ZP, Tsang RC, Laskarzewski P, Neumann V. Growth failure and decreased bone mineral of newborn rats with chronic furosemide therapy. Pediatr Res. 1986;20:74–78.
32. Kiilerich P, Kristiansen K, Madsen SS. Cortisol regulation of ion transporter mRNA in Atlantic salmon gill and the effect of salinity on the signaling pathway. J Endocrinol. 2007;194:417–427.
33. Flatman PW. Regulation of Na-K-2Cl cotransport by phosphorylation and protein-protein interactions. Biochim Biophys Acta. 2002;1566:140–151.
34. D'Andrea L, Lytle C, Matthews JB, Hofman P, Forbush B 3rd, Madara JL. Na:K:2Cl cotransporter (NKCC) of intestinal epithelial cells. Surface expression in response to cAMP. J Biol Chem. 1996;271:28969–28976.

A CELL SHRINKAGE ARTEFACT IN GROWTH PLATE CHONDROCYTES WITH COMMON FIXATIVE SOLUTIONS: IMPORTANCE OF FIXATIVE OSMOLARITY FOR MAINTAINING MORPHOLOGY

Mohamad Y. Loqman[1], Peter G. Bush[2], Colin Farquharson[3], and Andrew C. Hall[1]

[1]Centre for Integrative Physiology, School of Biomedical Sciences, George Square, University of Edinburgh, Edinburgh EH8 9XD, Scotland, UK
[2]School of Pharmacy and Biomolecular Sciences, University of Brighton, Lewes Road, Brighton, BN2 4GJ, England, UK
[3]The Roslin Institute, R(D)SVS, Developmental Biology, University of Edinburgh, Roslin EH25 9PS, Scotland, UK

Abstract

The remarkable increase in chondrocyte volume is a major determinant in the longitudinal growth of mammalian bones. To permit a detailed morphological study of hypertrophic chondrocytes using standard histological techniques, the preservation of normal chondrocyte morphology is essential. We noticed that during fixation of growth plates with conventional fixative solutions, there was a marked morphological (shrinkage) artifact, and we postulated that this arose from the hyper-osmotic nature of these solutions. To test this, we fixed proximal tibia growth plates of 7-day-old rat bones in either (a) paraformaldehyde (PFA; 4%), (b) glutaraldehyde (GA; 2%) with PFA (2%) with ruthenium hexamine trichloride (RHT; 0.7%), (c) GA (2%) with RHT (0.7%), or (d) GA (1.3%) with RHT (0.5%) and osmolarity adjusted to a 'physiological' level of ~280mOsm. Using conventional histological methods, confocal microscopy, and image analysis on fluorescently-labelled fixed and living chondrocytes, we then quantified the extent of cell shrinkage and volume change. Our data showed that the high osmolarity of conventional fixatives caused a shrinkage artefact to chondrocytes. This was particularly evident when whole bones were fixed, but could be markedly reduced if bones were sagittally bisected prior to fixation. The shrinkage artefact could be avoided by adjusting the osmolarity of the fixatives to the osmotic pressure of normal extracellular fluids (~280mOsm). These results emphasize the importance of fixative osmolarity, in order to accurately preserve the normal volume/morphology of cells within tissues.

Keywords: Shrinkage, artefact, osmolarity, glutaraldehyde, para-formaldehyde, growth plate.

*Address for correspondence:
Andrew C. Hall
Centre for Integrative Physiology
School of Biomedical Sciences
University of Edinburgh
Hugh Robson Building
George Square, Edinburgh EH8 9XD
Scotland, United Kingdom
Telephone Number: + 44 (0)131 650 3263
FAX Number: + 44 (0)131 650 2872
E-mail: a.hall@ed.ac.uk

Introduction

The accurate study of the morphology of living cells as they appear within tissues is difficult but fundamental for an understanding of normal cell biology, and the changes that occur in disease states. Accordingly a vast amount of research has been performed on chemically-fixed cells and tissues. The intention has been to retain the fine morphology and constituents of living in situ cells so that they can be studied without the complications of deleterious changes to cell metabolism and loss of viability during the investigation (see Hopwood, 1985). In addition, tissue fixation should protect against cell autolysis, attack by bacteria, and changes to cell volume and shape especially during subsequent preparative treatment (Baker, 1960) when tissue dehydration is frequently performed. Thus, fixative solutions should serve to stabilize the specimen and protect it from rigorous physical tissue processing and staining as required for study (Hopwood, 1969). Our particular research emphasis has been on the cellular mechanisms underlying the structure and function of the mammalian growth plate. There has been extensive study on chemically-fixed growth plates, and particular interest in the remarkable increase in chondrocyte volume which is a major determinant of bone growth (Breur *et al*., 1991). The large volumes of growth plate chondrocytes (typically ranging from 1,000 to 10,000μm^3; Bush *et al*., 2008) potentially makes them extremely sensitive to osmotic artefacts during fixation.

Para-formaldehyde (PFA) and glutaraldehyde (GA) and their combinations have long been used as fixative solutions (Fox *et al*., 1985; Hopwood, 1969) to retain the properties of cells and tissues (Kiernan, 1999; Renshaw, 2007). Perhaps the most widely used fixative for histology and histopathology is 10% neutral buffered formalin however this is not usually used for studies on the growth plate. Examples of more conventional aldehyde preparations used for this tissue are (a) 4% (w/v) PFA (Fox *et al*., 1985; Hosoya *et al*., 2005; solution A, Table 1) which has the same formaldehyde concentration (4%) as 10% Formalin (Kiernan, 1999), (b) 2% (w/v) GA & RHT (ruthenium hexamine trichloride) combined with 2% (w/v) PFA (Farnum *et al*., 2002; solution B, Table 1) and (c) 2% GA (w/v) with 0.7% (w/v) RHT (Hunziker *et al*., 1983; solution C see Table 1). Although the fixative properties have been widely known, less appreciated is the fact that the osmolarity of these solutions is markedly greater than that of typical physiological extracellular

solutions (Table 1). The osmolarity of the fixative solutions and their effects on cell and tissue morphology have received relatively little attention recently – indeed often appear ignored – despite the fact that there are studies in the literature highlighting this issue. For example, Schultz and Karlsson (1965) observed that hypertonic fixative solutions perfused into the central nervous system caused cellular shrinkage and increased extracellular spaces, whereas isotonic (300-320mOsm) and hypotonic fixatives could result in cell swelling. Mathieu *et al*. (1978) have reported the importance of both the % of GA and the molarity of the vehicle used for the fixative solution for the preservation of lung tissue. Even with these early studies, there are recent examples of investigators using hyper-osmolar fixative solutions (Farnum *et al*., 2002; Hosoya *et al*., 2005) but little if any comment on the morphology of the fixed cells which frequently appear shrunken/distorted (Erben, 1997; Kouri *et al*., 1996; Ross and Reith, 1985; Sanchez *et al*., 2000; Van der Eerden *et al*., 2000) and little or no attempt at quantification of the shrinkage artefact. We wished therefore (a) to re-visit this issue and emphasize the importance of osmotic correction to fixative solutions in order to retain cell morphology and (b) provide quantitative data on the extent of cell shrinkage and specifically report on the influence of fixative osmolarity on connective tissue cells.

During preliminary experiments attempting to optimize the fixation protocols for mammalian growth plates, we noticed that for the same standard fixative, the appearance of hypertrophic zone cells in histological sections from whole bones were markedly different compared to those from sagittally sectioned bones. The morphology of the cells in the whole bone fixed samples appeared considerably mis-shapen and shrunken, whereas in the bisected bone, morphology was relatively normal. From our previous studies on the shape/volume of chondrocytes exposed to osmotic challenge (Bush and Hall, 2001) we suspected that an artefact of the relatively high osmotic pressure of the fixative solutions might account for the abnormal chondrocyte morphology.

Thus, in the present study, we further examined using standard and modified fixative solutions, these shrinkage artefacts. By quantifying the osmotic shrinkage effect on hypertrophic growth plate chondrocytes, the data confirmed our preliminary observations that whole bones were particularly sensitive compared to those sagittally bisected prior to fixation. We also demonstrate that adjusting the fixative solution to an osmolarity close to that of typical extracellular solutions (approx. 280mOsm; solution D, Table 1) abolishes this artefact.

Materials and Methods

Biochemicals and solutions

Unless otherwise stated, all biochemicals and solutions were purchased from Sigma-Aldrich (Poole, U.K.) RHT was purchased from Polysciences Inc. (Warrington, PA, U.S.A.). Glutaraldehyde was of a grade suitable for electron microscopy. Paraformaldehyde solution was prepared from paraformaldehyde powder (purity of ≥95%). The fluorescent cytoplasmic labelling dye, chloromethylfluorescein diacetate CMFDA (CellTracker™ Green) and calcein AM were obtained from Invitrogen (Paisley, U.K.) and the mounting medium, FluorSave™ was purchased from Calbiochem (Nottingham, U.K.) Sodium cacodylate buffer was prepared by dissolving sodium cacodylate trihydrate powder (assay, approx. 98%) in distilled water, and the pH was corrected to 7.4 by addition of HCl.

Animals and growth plate preparation

Sprague-Dawley rats (7-day-old; P7) were humanely killed for other experiments following U.K. Home Office guidelines. The tibia of each hind limb with intact proximal growth plate cartilage was dissected and temporarily placed in medium (phosphate buffered saline; PBS; approx. 293mOsm) containing alpha modified essential medium (α-MEM; 7.5% v/v; Invitrogen) and bovine serum albumin V (1mM), prior to fixation.

For the preparation of samples for histology, 2 tibia from each animal were used and placed in fixative solutions of differing composition as follows: (a) conventional fixative solutions (Table 1), (b) fixatives with GA concentration maintained constant, but with various osmolarities similar to those used for conventional fixative solutions (Table 2), and (c) fixatives with various concentrations of GA but with osmolarity maintained at approx. 550mOsm (Table 3). The growth plates were fixed for 24hrs at room temperature for subsequent paraffin-

Table 1. Composition of fixative solutions used in the study.

Solution ID	Fixative solution	Cacodylate buffer (mM)	pH	Osmolarity (mOsm)	References
A	PFA 4%	None	7.11	1148 ± 2	Hosoya *et al*., 2005
B	PFA 2% + GA 2% + RHT 0.7%	100	7.06	1135 ± 32	Farnum *et al*., 2002
C	GA 2% + RHT 0.7%	50	6.72	420 ± 20	Hunziker *et al*., 1983
D	GA 1.3% + RHT 0.5%	30	5.67	270 ± 10	(present study)

Fixative solutions were prepared as described in the references cited which reported the morphology of growth plate chondrocytes following fixation. For solution A, distilled water was used instead of cacodylate buffer. Fixative solution D was prepared by diluting solution C with distilled water. [Concentrations are given as % (v/v) for GA= glutaraldehyde and PFA= paraformaldehyde, and as % (w/v) for RHT= ruthenium hexamine trichloride].

Table 2. Modified fixative solutions with constant concentrations of GA and RHT, but with osmolarity varied using NaCl.

Solution ID	Fixative Solution	Cacodylate buffer (mM) pH 7.4	pH	Osmolarity (mOsm)
280	0.7% RHT + 1% GA	50	6.76	273 ± 13
480	0.7% RHT + 1% GA	50	6.60	467 ± 28
640	0.7% RHT + 1% GA	50	6.55	637 ± 20
1200	0.7% RHT + 1% GA	50	6.49	1141 ± 116

Fixative solutions were prepared with the constituents at the concentrations indicated (see Materials and Methods), with the osmolarities and pH of the resulting solutions as shown. Concentrations are given as % (w/v) for RHT, and % (v/v) for GA. Data expressed as means ± S.E.M. from at least 3 independent determinations.

Table 3. Modified fixative solutions with varying GA concentration, but with similar final osmolarity.

Solution ID	Fixatives	Glutaraldehyde concentration (%)	Cacodylate buffer (mM), pH 7.4	pH	Osmolarity (mOsm)
0.5GA	0.7% RHT + GA	0.5	50	6.81	543 ± 1
1GA	0.7% RHT + GA	1.0	50	6.73	542 ± 4
2GA	0.7% RHT + GA	2.0	50	6.72	556 ± 18
4GA	0.7% RHT + GA	4.0	50	6.35	577 ± 11

Fixative solutions were prepared with the constituents including different GA concentrations (% v/v) as indicated (see Materials and Methods), with the osmolarities of the resulting solutions as shown. Concentrations of RHT are given as % (v/v). Data expressed as means ± S.E.M from at least 3 independent determinations.

embedding for histological sectioning. For group (a) three intact tibias and 3 bisected tibias were fixed in each fixative solution, whereas in group (b) and (c), three and five intact tibias were used in each fixative solution respectively.

For the preparation of growth plates for the analysis of *in situ* growth plate chondrocyte (GPC) volume, tibias from eight P7 rat pups were grouped into: (i) five bones maintained intact, and (ii) ten bones that were bisected sagittally. Bones were incubated with either CMFDA-green for 60mins (if the bones were subsequently fixed) or calcein AM (for non-fixed bones). Then, all bones from group (i) and four bones from group (ii) were fixed in solution A. Three bones from group (ii) were fixed in osmotically-corrected fixative solution (solution D, Table 1). When appropriate, bones were fixed for 24hrs at room temperature. The remaining 3 bones from group (ii) were maintained unfixed for *in situ* living cell imaging. The osmolarity of all solutions was determined using a freezing point micro-osmometer (Model 3300, Vitech Scientific Ltd., Partridge Green, U.K.) with solid NaCl or distilled water added to adjust the osmolarity to the required range. The pH of all solutions was measured at room temperature using a SevenEasy™ pH meter (Mettler Toledo, UK) with the pH of fixative solutions altered by adding either HCl or NaOH.

Histology of the growth plate

Bones were embedded in paraffin wax using a standard procedure (Kiernan, 1999) and tissue sections (10μm) cut using a microtome (Reichert-Jung Microtome 2050 Supercut, Arnsberg, Germany). The sections were then mounted on poly-l-lysine-coated microscope slides (Polysine™, VWR International, Leicestershire, UK) and dried overnight. After de-paraffinisation with xylene and rehydration with a series of ethanol solutions (100%, 90%, 75%), the sections were stained with 0.1% (w/v) Toluidine blue O in PBS buffer (pH 5.5; 30secs at room temperature) using the technique adapted from Bancroft and Cook (1994). The sections were then rinsed briefly in distilled water and allowed to air dry prior to mounting in FluorSave™ with cover slips.

Measurement of growth plate chondrocyte shrinkage

Histological sections of fixed hypertrophic GPC stained with 0.1% Toluidine blue O were observed under an x63 (oil-immersion) objective lens. Several histological views of chondrocytes within sections S5 and S6 of the hypertrophic zone (see details in the section *'In situ* volume measurement' (below), and Figure 1(A)) were randomly selected and the images recorded using a mounted digital camera (Coolpix 4500, Nikon, Tokyo, Japan) with Coolpix MDC2 Relay lens (MXA 2900, Nikon). The captured images were then transferred to a computer for further image analysis. Java-based scientific image processing software (ImageJ, NIH, Bethesda, MD, U.S.A.) was then used to measure the cell shrinkage from the images of the histological sections.

In order to determine the extent of chondrocyte shrinkage it was necessary to identify the area of individual chondrocytes and that of their lacuna – i.e., the 'cavity' in which the cell resided. It was in fact relatively straightforward to do this as the outermost edge of the cell area stained distinctly with Toluidine blue O, and the perimeter of the corresponding lacuna was identified as the edge of the extracellular matrix that demarcated the border between the stained area of the matrix and the 'space' of the lacuna which was relatively unstained. It was noted that the area of the lacuna could only be observed if there was cell shrinkage. For each group of treatments, 4 fields of view from each growth plate section were selected and up to 11 cells and their corresponding lacunae randomly taken for area measurement. The area of each

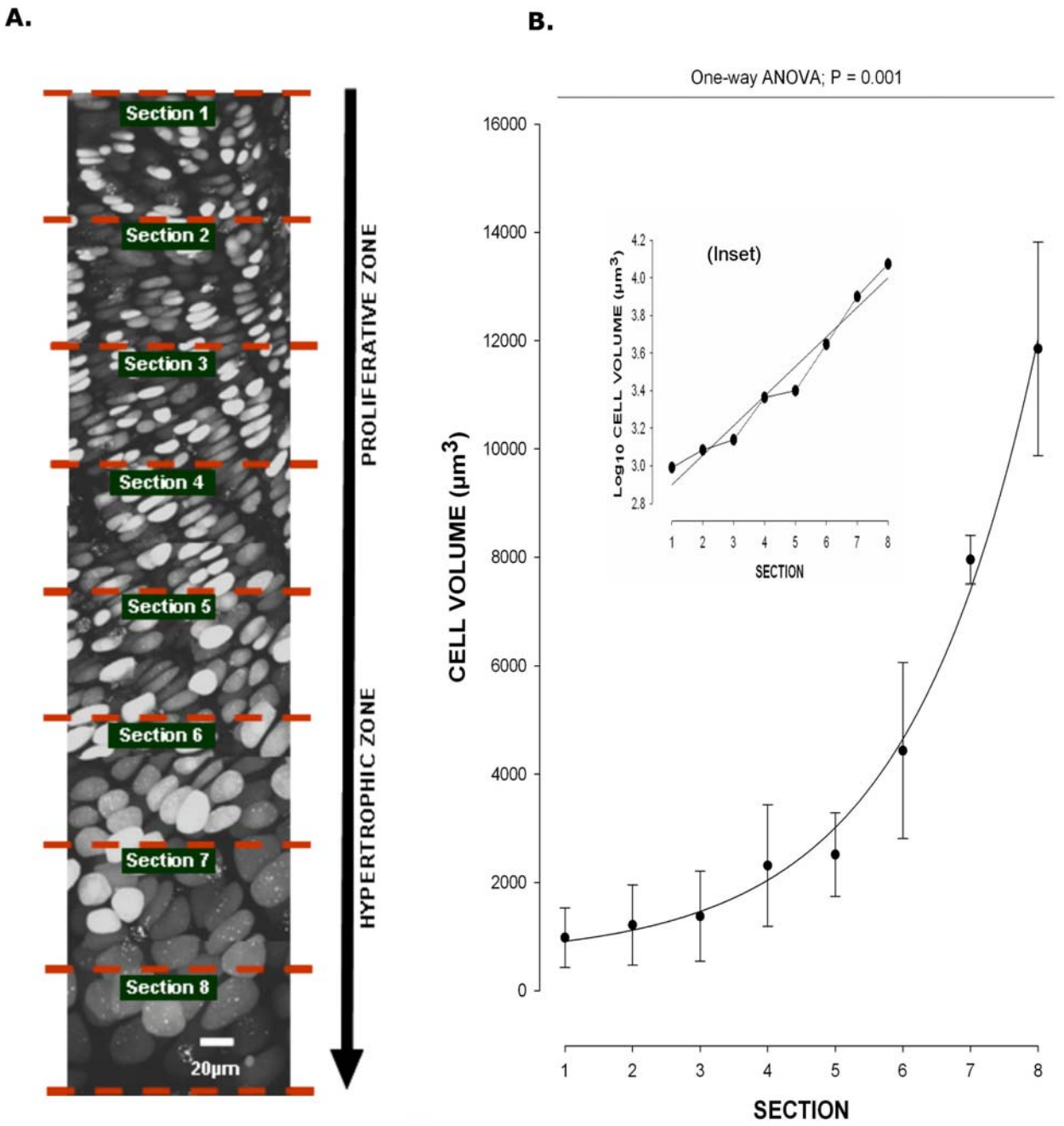

Fig. 1. Overview of the rat growth plate, and division of *in situ* living rat chondrocytes (GPC) into sections from proliferative to hypertrophic zones. Living chondrocytes in a bisected proximal tibia of a 7-day-old rat pup were labelled with calcein AM, and sequential CLSM images taken with a x63 water-dipping objective (see Materials and Methods). Panel **(A)** demonstrates the projected image of a section of the growth plate showing the increase in chondrocyte volume from proliferative to hypertrophic zone. The zones were divided into eight equal sections (labelled S1-S8) from early proliferative zone to late hypertrophic zone. Panel **(B)** shows the changes in the volume along the growth plate sections as measured using Volocity® software on living *in situ* growth plate chondrocyte images captured with CLSM. Also shown is an inset where the same data points were transformed to $\log_{10}$. (Data shown are means ± S.E.M. or S.D. as appropriate, with n = 2 for S1-S4 and S7-S8, and n = 3 for S5-S6; and at least N=15 cells measured at each section).

cell and that of its associated lacuna were selected by outlining their perimeters using the freehand selection tool (see Fig. 2A, panel a). The total area of the cell and its lacuna were then determined using the 'analyze' and 'measure' toolbar in the software. Cell shrinkage was calculated as {100 – [(cell area/lacuna area) x 100]} and expressed as a percentage of the initial volume (see Fig. 2A, panel a). When the cell and its corresponding lacuna shared the same perimeter, the value of cell shrinkage was zero as defined above.

Confocal laser scanning microscopy (CLSM)

An upright Zeiss Axioskop LSM 510 (Carl Zeiss Ltd., Welwyn Garden City, Herts., U.K.) CLSM was used to acquire fluorescent images of *in situ* hypertrophic growth plate chondrocytes. Cells were visualized using a Plan-

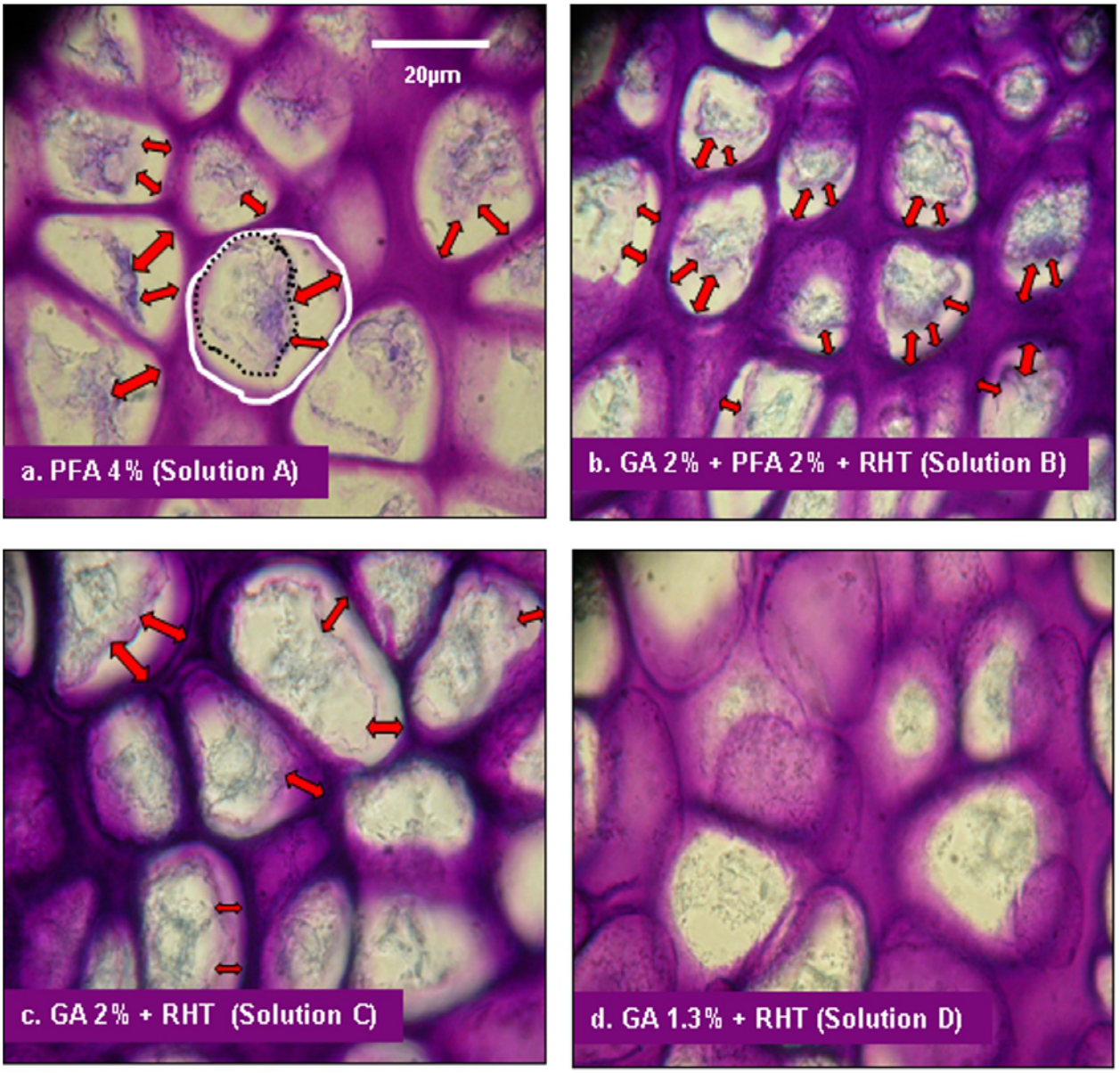

Fig. 2A. Conventional fixatives cause considerable shrinkage of hypertrophic growth plate chondrocytes when applied to whole (intact) bones. Intact proximal tibias of 7-day-old rat pups were fixed using various standard fixative solutions (Table 1) and sections prepared and stained with 0.1% Toluidine blue O (see Materials and Methods). The method used to calculate the extent of chondrocyte shrinkage was illustrated in **Panel (a)**. The thick white line was drawn free-hand around the perimeter of the lacuna and the black broken line drawn around the membrane edge of its resident chondrocyte (see details in Materials and Methods). The gap between the cells and the border of the lacuna is illustrated by double headed arrows. Cell shrinkage was observed in all conventional fixatives **(panels a - c)** but not when the osmolarity of the fixative was adjusted to a 'physiological' osmolarity **(panel d)**. For pooled data see Figure 3. The scale bar of 20µm in this and the following Figure applied to all panels.

Neofluar x10/0.3 numerical aperture (NA) dry objective for a low power overview and an Achroplan x 63/0.95 NA ceramic water-dipping lens for high power views. Intracellular CMFDA was excited using an Argon laser (Ex = 488nm) and emitted fluorescence (Em = 517nm) detected using a 500-550nm band pass filter. The confocal detection pinhole was set at 1.00 Airy Unit. Laser power and detector sensitivity were adjusted to provide optimum image quality. The scanning speed was typically 0.6Hz with 2 frame integration of a 512 x 512 pixel image, with serial 1 µm z-step optical sections (see Bush and Hall, 2001; Bush *et al*., 2007 for further details).

***In situ* volume measurement**

Whole growth plates imaged from the proliferative to hypertrophic zones were divided into eight equal parts and labeled S1 to S8 (Fig. 1A). This was done so that a comparative analysis could be made between corresponding sections from different individuals irrespective of variations in section cutting angle (Bush *et al*., 2008). Since the greatest number of hypertrophic cells that was consistently found to be intact was in S5 and S6, the *in situ* growth plate cell volume analysis was performed only at these sections. Chondrocytes in S7-S8 often appeared to be in poor condition, possibly as a result of

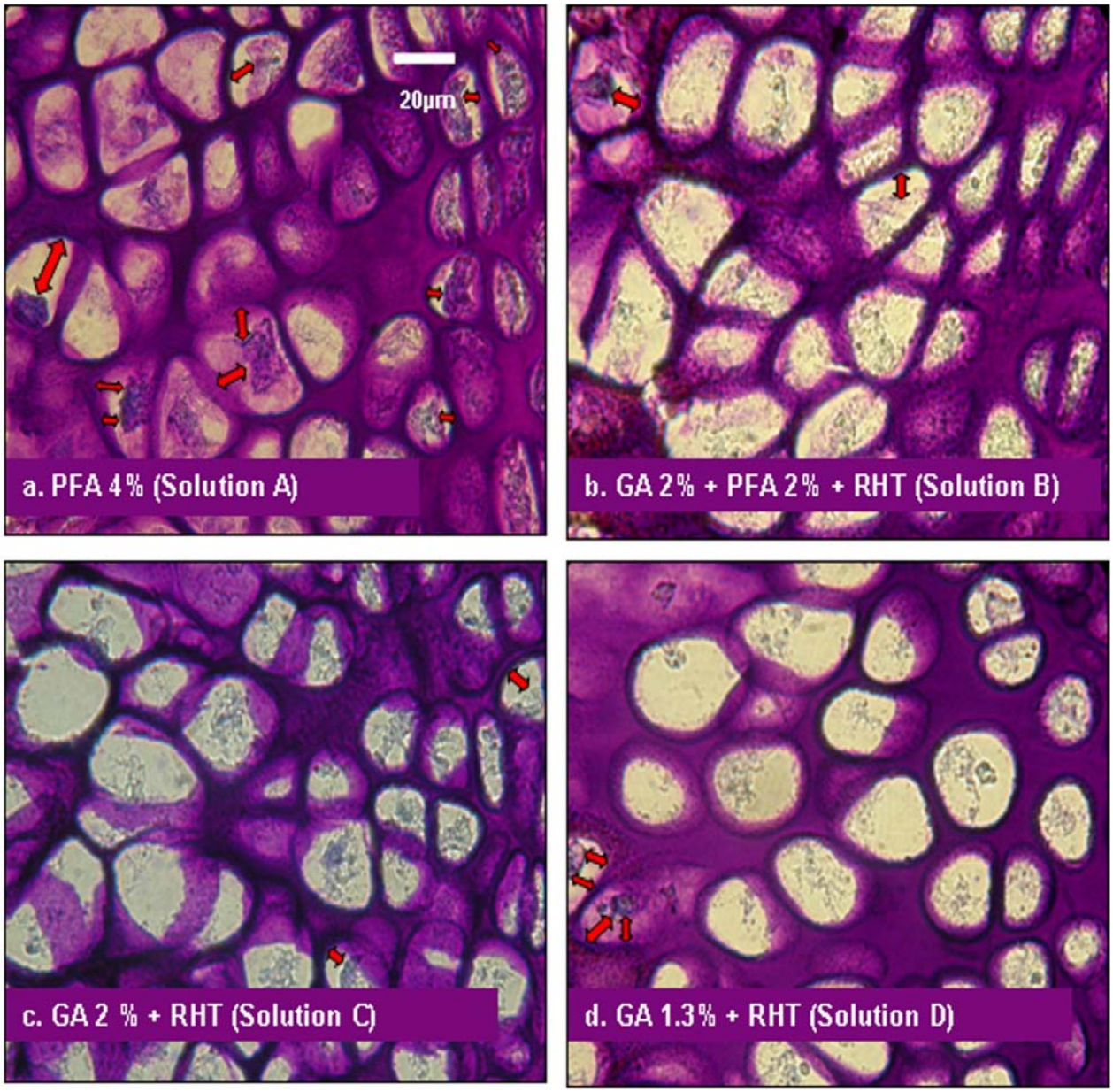

Fig. 2B. Reduced cell shrinkage in GPC of bones sagittally-bisected before fixation. Bisected sections prepared and stained with 0.1% Toluidine blue O (see Materials and Methods). With these bisected bones the extent of cell shrinkage was markedly less compared to the intact bones (Fig. 2A) and shrunken chondrocytes were only occasionally observed as illustrated by the double headed arrows **(panel a)**. The morphology of chondrocytes within the three other fixative solutions **(panels b to d)** was relatively normal (see pooled data in Fig. 3).

cutting trauma during the preparation of the tissue (Huntley *et al*., 2005). Volume analysis was performed using high performance 3D imaging software (Volocity®, Improvision, Coventry, U.K.) on scanned CLSM images using the calibrated cell volume method as previously described (Bush and Hall, 2001).

Statistical analysis

Data were expressed as means ± standard error of the mean (S.E.M), obtained from a minimum of 3 separate animals (n), and (N) chondrocytes at each condition with the data shown as (n[N]). Statistical significance was evaluated using two-tailed Student's unpaired *t*-tests, or ANOVA tests as appropriate, with the *P* value considered significant when $P<0.05$. Statistical tests were performed using Microsoft Office Excel (Microsoft, Redmond, WA, U.S.A.) or SigmaPlot® statistical software (Systat Software, Chicago, IL, U.S.A.).

Results

Volume and morphology of rat growth plate chondrocytes (GPC)

Initially, to determine live cell volumes and the morphology of *in situ*, unfixed chondrocytes, we labelled *in situ* growth plate chondrocytes with calcein as shown (Fig. 1). Imaging of the fluorescently-labelled *in situ* living growth plate chondrocytes demonstrated a clear increase in the size of GPC from the proliferative through to hypertrophic zones (Fig. 1a). Chondrocytes within the proliferative zone (between the reserve and hypertrophic zone) appeared

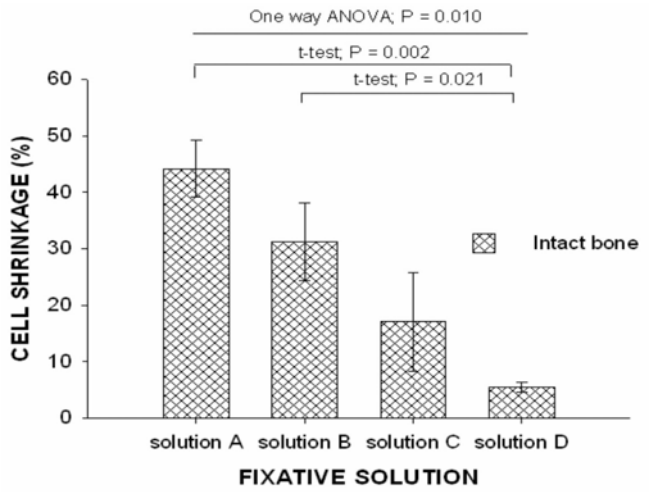

Fig. 3A. Growth plate chondrocyte shrinkage in histological sections from intact bones fixed in four different solutions. Cell shrinkage of *in situ* chondrocytes fixed in solutions A, B, C or D (for composition see Table 1) in intact tibias from 7 day-old rats were measured as described (see Materials and Methods). Data in this and the subsequent Figure were from at least (3[44]) for each condition. In this and the following Figure, *P* values for unpaired Student's *t*-tests are shown. (Data are given as means ± S.E.M.).

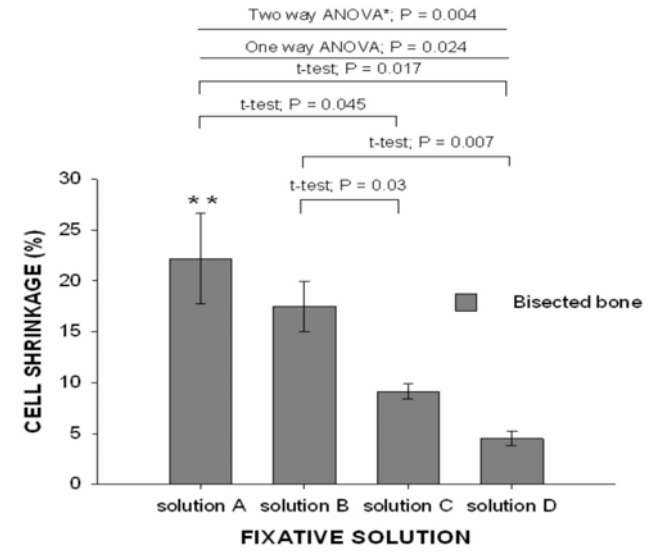

Fig. 3B. Growth plate chondrocyte shrinkage in histological sections from bisected bones fixed in four different solutions. Cell shrinkage of *in situ* chondrocytes fixed in solutions A, B, C or D (Table 1) in sagittally-bisected tibias from 7 day-old rats were measured as described (see Materials and Methods). A single asterisk (*) denoted a significant difference when the two-way ANOVA tested the trend of cell shrinkage between intact and bisected bones in various fixative solutions. A double asterisk (**) denoted a significant difference compared to the intact bone fixed in solution A (Student's unpaired *t*-test).

ellipsoidal and usually arranged in columns of at least three to eight cells. In the hypertrophic zone (between the proliferative zone and the zone of calcification) the cells were larger and frequently more rounded although there were cells with a height greater than the cell's width (Buckwalter *et al*., 1985; Farnum and Wilsman, 1986).

In accordance with the visual appearance of chondrocytes along the growth plate, the quantified volume of *in situ* cells increased although it was clearly not a linear process as there was a relatively poor fit to a linear regression (correlation coefficient $r^2 = 0.793$). The volume increase was initially gradual through to S5, but then became more rapid from S5-S8 similar to an exponential growth relationship (Fig. 1b). When the volume data were transformed to $\log_{10}$ and plotted semi-logarithmically (see inset to Fig. 1b) there was a much better fit to the data ($r^2 = 0.955$) supporting the notion of a logarithmic increase in chondrocyte volume associated with hypertrophy. In the present study we focused on chondrocytes within these latter sections of the growth plate. Although the shrinkage artefact was apparent in the smaller cells, it was very difficult to quantify the phenomenon using our imaging methods (see Materials and Methods). This was because the distinction between the perimeter of the lacuna and the cell edges of smaller (shrunken) cells was difficult to determine accurately, resulting in large variations. Therefore, we decided to study the phenomenon only on chondrocytes in the hypertrophic zone to ensure accurate measurements, and the cells within S5-S6 were chosen because an adequate number of intact cells from these segments could consistently be observed.

Measurement of cell shrinkage

The accuracy of the method used for assessing chondrocyte shrinkage in histological sections as described in Materials & Methods (Fig. 2A panel a) was initially determined by measuring the area of GPC cells that had distinct and well-defined perimeters. The cell measurement was made independently using the free-hand selection tool on the same cell twice and the difference between the two readings compared. The mean difference between the two measurements was 2.7±1.9 % (mean ± standard deviation (S.D.), for 11 cells) indicating the measurement method had an appropriate level of accuracy.

Morphology of growth plate chondrocytes fixed using conventional solutions

An ideal fixative should successfully preserve tissue for subsequent staining procedures, but it is important to accurately retain the original morphology of the living cells in the tissue, free from artefacts occurring during the fixation process. To demonstrate the morphology of GPC

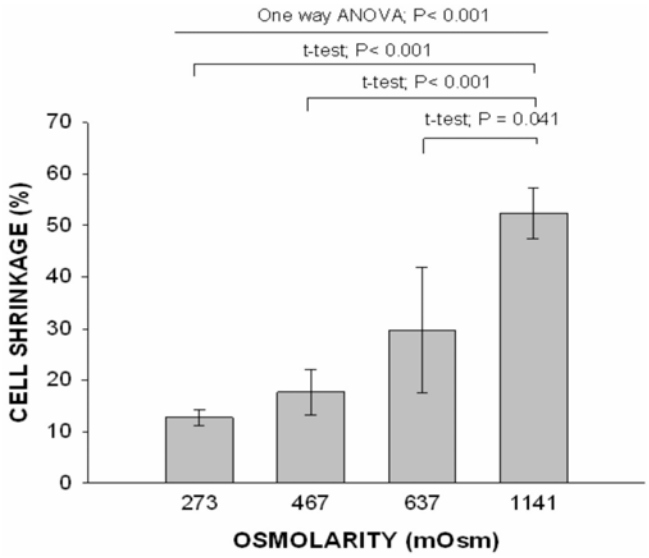

Fig. 4A. Chondrocyte shrinkage increased with elevated osmolarity of the fixative solution. Whole bones were fixed in solutions composed of 1% GA and 0.7% RHT, with osmolarity varied over the range 273 to 1141 mOsm by the addition of NaCl (see Table 2). Shrinkage of GPC was determined as described (see Materials and Methods, and Fig. 2A panel a). Data were from at least (3[44]) for each condition and are presented as means ± S.E.M.

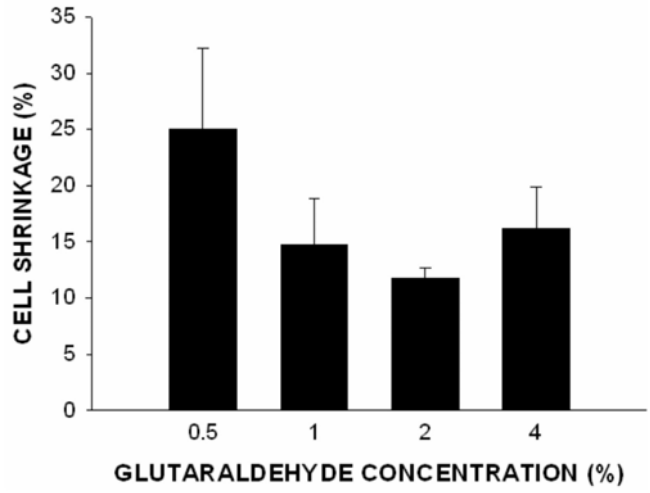

Fig. 4B. There was no difference in cell shrinkage with an increase of fixative concentration if osmolarity was kept constant. Whole bones were fixed in fixative solutions with the GA concentration varied over the range 0.5 to 4%, but with the osmolarity maintained constant at ~550 mOsm (see Table 3 for composition of solutions). Shrinkage of GPC was determined as described (see Materials and Methods, and Fig. 2A panel a). There was no significant difference between any pairs of data (Student's unpaired *t*-test). Data were from at least (5[44]) for each condition and presented as means ± S.E.M.

fixed with conventional fixatives (Farnum *et al*., 2002; Hosoya *et al*., 2005; Hunziker *et al*., 1983), we used three standard and widely-used solutions (Table 1). These fixative solutions were all hyper-osmotic (Table 1), and therefore for comparison an iso-osmotic fixative with osmolarity adjusted to close to that of typical extracellular physiological solutions (280mOsm; Table 1), was also included.

In whole (non-bisected) bone samples, fixed and processed as described for histology (see Materials and Methods), there was a clear cell shrinkage artefact observed in tissue fixed with the three conventional fixatives (solutions A, B & C; Table 1; Fig. 2A panels a-c)). Among the three fixatives, chondrocyte shrinkage assessed visually was most marked for solutions A and B and least for solution C (Fig. 2A(c)). When osmotically corrected solution D (~280mOsm) was used, we observed no apparent cell shrinkage (Fig. 2A panel d). Quantitatively, solution A caused the highest cell shrinkage (44 ± 3 % (3[44])), followed by tissue fixed in solution B (31 ± 4% (3[44]), then cells in solution C 17 ± 5% (3[44]) and finally for the osmotically-corrected fixative solution D, there was no significant change in cell volume (5.5 ± 0.8% (3[44])). When analysing the extent of the shrinkage from solutions A to D (lowering osmolarity, Table 1), there was a significantly decreasing trend (one-way ANOVA test; P=0.010) however only the shrinkage for cells in solutions A and B were significantly different (unpaired Student's *t*-test, P<0.05) from the osmotically-corrected fixative solution D. Note that although shrunken cells were routinely observed microscopically in cells fixed in solution C (Fig. 2A panel c) the pooled data did not show a significant difference and this was mainly because of the range in the magnitude of the shrinkage effect.

In bisected bones (Fig. 2B), microscopic inspection showed clearly that the extent of the chondrocyte shrinking artefact was considerably reduced with the four fixatives when compared to the cells within fixed whole bones (Fig. 2A panels a-d). When the shrinkage was quantified (Fig. 3B), the same decreasing trend in cell shrinkage with the four fixatives was also observed and the trend significant over the whole range (one-way ANOVA test; P=0.024). The absolute level of shrinkage and the trend with decreasing osmolarity, was less compared to the data for intact bones (Fig. 3A). When the data sets for intact and bisected bones over the range of fixatives were compared using a two-way ANOVA, the difference was significant (P=0.004). In solution A cell shrinkage in bisected bones was 22 ± 2.6%, which was significantly less than the shrinkage of chondrocytes fixed in intact tibias (P=0.030). Fixative solution B caused 17 ± 1.4% (3[44]) shrinkage whereas solution C caused 9 ± 0.4% (3[44]) cell shrinkage

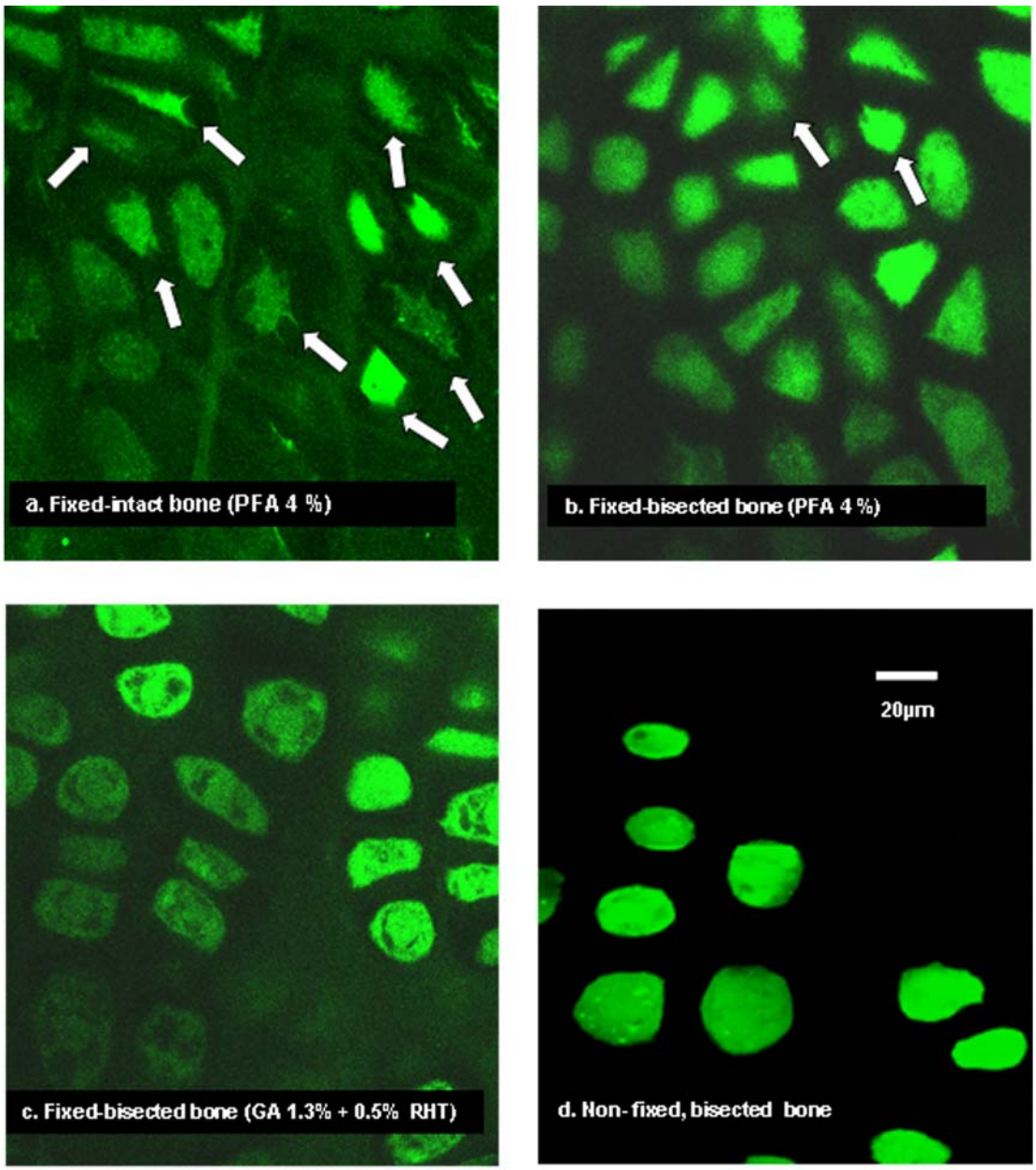

Fig. 5. Reduced volume and altered morphology of *in situ* GPC fixed within intact bone compared to those within bisected bones. **Panels (a-c)** showed the typical appearance of fluorescently (CMFDA-green)-labelled chondrocytes within intact **(panel a)** or bisected **(panels b, c)** bones, and fixed under the various conditions indicated. The shrinkage of some cells was observed in the fixed *in situ* cells (examples indicated with white arrows, **panels a**, **b**) but not in the osmotically-corrected fixative solution D **(panel c). Panel (d)** shows the appearance of unfixed (i.e., living) in situ hypertrophic GPCs labelled with calcein. All images were taken by CLSM using a x63 water-dipping objective. Cell volume measurements were performed as described (see Materials and Methods) with pooled data given in Table 4. Details of the composition of fixative solutions are given in Table 1. Scale bar = 20mm.

and these values were less than for intact bones but did not reach the level of significance ($P>0.05$). Cell shrinkage in the iso-osmotic fixative solution D for GPC in bisected bones was only 4 ± 0.4% (3[44]; Fig. 3) and this was not significantly different from the data in intact bones (see above). These results showed that the shrinkage artefact was considerably reduced if the bones were bisected prior to fixation, and with osmotic correction, there was no significant shrinkage artefact of GPC in either intact or bisected bones.

As noted in Table 1, the pH of the fixatives varied over the range 5.67 to 7.11, which was the result of different types and concentration of fixative agents and buffer concentration. We conducted a further experiment to examine whether pH contributed significantly to the quality of tissue preservation. We tested two pH values (i.e., 5.6 and 7.2) using the same fixative solution (solution D) to fix two groups of growth plate tissue from proximal tibia of P7 rats (n=3). Using the same method to quantify the cell shrinkage as described previously, the result showed that at pH 5.7 there was 8 ± 0.6 % (mean ± S.E.M.) cell shrinkage, whereas at pH 7.2 there was 7 ± 1.5 % of cell shrinkage. These were not significantly different ($P<0.05$) and so we concluded that pH over this range had a

negligible effect on cell shrinkage compared to the osmolarity of the fixative solutions.

Fixation of GPC using different concentrations and osmolarities of glutaraldehyde (GA) solution

To test whether the osmolarity or concentration of fixative was responsible for the shrinkage artefact, whole bones were immersed in solutions with varying osmolarity (273-1141mOsm) and standard fixative concentrations (GA 1%, RHT 0.7%; Table 2), or in solutions varying fixative concentration (GA 0.5-4%) whilst maintaining osmolarity relatively constant (555± 8mOsm; Table 3). At the lowest osmolarity (273 ± 13 mOsm), cell shrinkage was minimal (13 ± 0.6% (3[44])), but as it was raised, there was a progressive and significant increase (ANOVA, $P<0.001$) in the extent of cell shrinkage (Fig. 4(A)). At the highest osmolarity studied (1141mOsm) cell shrinkage was 52 ± 1.6% (3[44]) and significantly greater (unpaired Student's *t*-test, $P<0.001$ for both) than the shrinkage observed in 273 and 467 mOsm solutions. When the GA concentration was varied over the range 0.5 to 4%, but with the osmolarity of all solutions maintained constant, the shrinkage of GPC fixed in intact bones with 1%, 2% and 4% GA was 15 ± 2.4%, 12 ± 0.5%, and 16 ± 2.1% respectively, and not significantly different ($P>0.05$; data from at least (5[44]); Fig. 4B). It was notable that GA at 0.5% showed an apparent slightly higher cell shrinkage (25 ± 4.1% (5[44])) compared to 1% GA, but this was not significantly different from the lowest cell shrinkage produced by GA at 2% ($P>0.05$). The morphology of a noticeable number of these cells was abnormal, suggesting that they were not properly fixed, and thus it was possible that the cells were susceptible to the post-fixation dehydration protocols (Mohamad Yusof Loqman, unpublished observations). Taken together, these data suggest that the shrinkage and morphological changes of GPC fixed using standard solutions could be accounted for by the osmolarity of the fixative solutions and not by the concentration of the fixative.

***In situ* growth plate chondrocyte volume following fixation with solution A in intact and bisected bones**

The volume of *in situ* GPC within intact or sagittally-bisected bones and fixed under various conditions was also assessed using another method. Solution A was chosen as it had the highest osmolarity among the different conventional fixative solutions used in the present study, resulted in the greatest shrinkage artefact (which was easily measured), and has been used previously in the study of growth plate chondrocytes (see Table 1). Images of fluorescently-labelled *in situ* chondrocytes taken by CLSM showed the majority of cells with abnormal shrunken morphology in intact bone fixed with this solution (Fig. 5a). When the bone was sagittally bisected and then fixed using the same solution, the proportion of shrunken chondrocytes was markedly less (Fig. 5b), and similarly when these bones were fixed in the osmotically-corrected solution (solution D, Table 1) there were almost no shrunken cells observed (Fig. 5c) with the cells appearing morphologically normal. The volume of GPC fixed in the intact bone had a significantly reduced cell volume of almost two and half-fold less compared to the cells in the bisected bone (Table 4; unpaired *t*-test: $P = 0.016$, n=5). For comparison, GPC volume of living non-fixed bone and of bisected bones fixed in solution D were not significantly different from the GPC volume of bisected bone fixed in solution A (unpaired *t*-tests, $P>0.05$). However, the volume of GPC fixed in solution A showed no significant decrease compared to the volume of GPCs fixed in solution D and non-fixed GPC as expected due to cell shrinkage, as shown previously (Figure 3B). The reason for this was not immediately obvious, although it should be noted that the errors associated with the measurement of *in situ* GPC volume were relatively large (Table 4). In summary, the reduction in cell volume was significantly greater for GPC within intact bones compared to bisected bones when fixed in a conventional fixative solution (Table 4).

Discussion

This study demonstrated that the osmolarity of fixative solutions was of critical importance for maintaining the normal morphology of *in situ* hypertrophic chondrocytes within the mammalian growth plate following chemical fixation. The shrinkage artefact evident when using conventional fixatives, was abolished when the osmolarity of the medium was reduced to close to that of normal physiological solutions or markedly reduced when the bones were sagittally bisected prior to fixation. These results raise important issues in relation to the accurate preservation of cell morphology by these widely-used chemical fixative solutions.

The first point to consider is the identification of a fixative concentration that ensured proper fixation of the

Table 4. Reduction of *in situ* GPC volume in fixed intact bones compared to bisected bones.

Nature of the bone specimen	Fixatives	*In situ* GPC volume (μm^3)
Intact	PFA 4% (solution A)	1698 ± 166*
Bisected	PFA 4% (solution A)	4064 ± 571
Bisected	GA 1.3% + RHT 0.5% (solution D)	3389 ± 659
Bisected	No fixative	3411 ± 1148

CMFDA-labelled *in situ* chondrocytes were fixed under the conditions shown (see Figure 5), their volume determined as described (see Materials and Methods) and the pooled data presented. Data (as means ± S.E.M.) are from n = 5 animals with 5-29 chondrocytes measured from each animal. *Denotes a significant difference ($P<0.05$; Student's unpaired *t*-test) between the data for the intact bone and each of the data sets for the bisected bone sections.

cells/tissue without the osmolarity being too high to cause a shrinkage artefact and our data suggest that solution D was optimal (Table 1; Fig. 3). This osmolarity would be close to that normally present in physiological extracellular solutions meaning that the osmolarity of the cells within the extracellular matrix of the growth plate would similarly be optimal for normal chondrocyte morphology. (Note however that the exact extracellular osmolarity around the GPC will most likely be higher due to the presence of glycosaminoglycans present in the extracellular matrix (Urban *et al*., 1993)). A lower concentration of GA (0.5%) produced what appeared to be a shrinkage artefact (Fig. 4B) but although individual shrunken cells were present on visual examination, statistical analysis of pooled data showed this was not significant. However we would caution against using such a low concentration as the fine appearance of the cells suggested that there were cells that were not properly fixed, resulting in morphological changes/distortions during post-fixation protocols (Mohamad Yusof Loqman, unpublished observations). Previous studies have, however, successfully utilized low fixative concentrations. For example Maunsbach (1966) investigating the kidney and Hopwood (1967) studying the brain noted that GA was an effective fixative down to 0.25% (Hopwood, 1967; Maunsbach, 1966). It is possible that low fixative concentrations could be used successfully in these studies because of the different physical nature of hard tissues compared to soft tissues, as in the latter the diffusion rate and thus penetration of the fixative would be expected to be considerably greater. Our findings were in general agreement with a previous report that identified the importance of fixative osmolarity to produce correct soft tissue preservation. Mathieu *et al*., (1978) reported both the GA percentage and molarity of the fixative vehicle were of importance for the preservation of lung tissue. In this study, they noted the shrinkage was induced by the osmolarity of buffer and fixative combined, as evidenced by shape changes of erythrocytes in capillaries and small vessels of the trachea, and a reduction in the air-blood tissue barrier of the trachea with different fixative osmolarities. Higher fixative concentrations (e.g. 2-4% GA) could of course be used for some applications where cell shrinkage is not a concern (e.g. for tissue perfusion fixation (Santoreneos *et al*., 1998) or biomaterial fixation (Nuss *et al*., 2006)), but clearly the results from the present study emphasize the importance of researchers being aware of the potential for an osmotic shrinkage artefact to cell shape.

In the present study we included RHT (ruthenium hexamine trichloride) in most of the fixative solutions (Table 1). Hunziker *et al*., (1982) have proposed that this cationic dye stabilized the GPC plasma membrane within the lacuna by establishing electrostatic cross-linkage between anionic components within the plasma membrane and the proteoglycans of the pericellular matrix which surrounds chondrocytes. They suggested that this could prevent the rupture or detachment of the plasma membrane from the pericellular matrix when conventional aldehyde solutions were used simultaneously (Hunziker *et al*., 1982, 1992) (Fixative solutions B and C; Table 1). In our hands however, the presence of RHT could not prevent the shrinkage artefact (see Fig. 3). Thus, although the % shrinkage was not significantly different from the osmotically-corrected fixative solution (solution D) it was still clearly greater than the solution B & C. In addition, we routinely observed abnormal/shrunken cells (Fig. 2A panels b and c) as also observed in the original Hunziker *et al*. (1983) study. Therefore, although it is possible that RHT does protect against the shrinkage effect to some extent by stabilizing the cell membrane against the pericellular matrix, we feel that osmotic correction is the preferred procedure to eliminate the artefact (Fig. 3) and the presence of any abnormal cells (Fig. 2A panel d).

The nature of the chemical fixative is also an issue of importance as there is not one fixative suitable for all applications. For example, GA has been associated with antigen masking due to its excessive and aggressive cross-linking of proteins, and is therefore normally considered unsuitable for tissues intended for immunochemical staining (Renshaw, 2007). GA is usually used as a mixture with PFA termed Karnovsky's fixative (Karnovsky, 1965) so as to take advantage of the latter which has rapid tissue penetration although the fixation rate is not as rapid as that of GA (Kiernan, 1999). Our view is that PFA (4%) alone, probably gives the best compromise between good cytological preservation and immunolocalization, while at the same time maintaining antigen masking to a minimum. However, as it is a fixative solution with high osmolarity (Table 1), tissues should be bisected beforehand to maximize rapid fixative access to limit undesirable cell shrinkage artefacts although it should be noted that they were still clearly apparent (Fig. 2B panel a) and still significant (~20% shrinkage, Fig. 3). We note that although 10% neutral buffered formalin is rarely used in growth plate studies, it is a widely used fixative for routine histology and histopathology (Renshaw, 2007). However it should be noted that its osmolarity (measured at approx. 1700mOsm; Mohamad Yusof Loqman, unpublished observations) is even higher than the fixatives used here and thus we would expect that the artefactual shrinkage would be even more marked than reported for solution A (4% PFA).

The finding that the shrinkage artefact was significantly reduced in bisected compared to whole bones, strongly suggested that the rate of penetration of the fixative compared to the osmotic changes to chondrocytes resulting from the high osmolarity of the fixative solutions are important. In the whole bone, the large shrinkage artefact suggested that osmotically-induced cell shrinkage occurred before the tissue was fixed. Thus when the bone was placed in the fixative solution, water movement out of the bones to the hyper-osmolar fixative solution occurred rapidly, and before the fixative fully penetrated the bone/cartilage matrix to fix the cells throughout the sample. Dempster (1960) has shown that fixatives obeyed the diffusion laws, that is, the depth penetrated (d) was proportional to the square root of time and the coefficient of diffusibility of the fixative, which was specific for each fixative. As the diffusion is directly proportional to the concentration gradient based on Fick's Law (Mehrer, 2007), the diffusibility of the fixative molecules (PFA, FA, GA) through the extracellular matrix of the tissue will undoubtedly be less than that for water molecules because

of their different molecular shape and molecular weight. Thus, the diffusibility of the fixatives will be markedly less than that of water, leading to a greater shrinkage effect in thicker and denser tissues such as bone/cartilage, compared to 'soft' tissues such as brain and kidney. For thick tissues where preservation of cell morphology deep in the tissue is of importance, osmotic adjustment with lower fixation concentrations and longer fixation times would be advisable. Most workers set the fixation period using conventional fixatives of between 1- 4 hrs, or even longer (Hopwood, 1969). The optimum time will depend on several factors including the physical properties of the tissue (e.g. bone/cartilage *vs*. brain) concentration of the fixative and thickness of tissue sections. Higher fixative concentration requires shorter fixation times (Monis *et al*., 1965) whereas thicker blocks and harder tissues will necessitate longer fixation times as the penetration of the fixative will be slower.

Our results demonstrated that the shrinkage artefact could also be significantly reduced – although not abolished – when the bone was bisected before being fixed in standard (high osmolarity) fixative solutions (Fig. 3). Bone bisection would markedly reduce the physical obstacles and diffusional distances thereby providing a more direct and far more rapid exposure of the GPC that were being visualized to the fixative solutions. The rate of fixation would thus be much more rapid compared to GPC within intact bone, although the fact that the shrinkage artefact was still present indicated that despite the increased access provided to the fixative, significant cell shrinkage still occurred before the tissue was effectively fixed (Fig. 3). However, the drawback with bone bisection as a manoeuvre to reduce the fixation artefact would be that it could cause physical trauma/death to the cells at the cut edge (Huntley *et al*., 2005) and unless care was taken with imaging protocols by optically sectioning deeper into the tissue, the damaged surface cells would be the ones that are visualized. Bone bisection would also release internal (physiological) pressures within the bone and result in the loss/damage to matrix constituents (loss of proteoglycans, damage to the collagenous network, altered ionic/osmotic environment) potentially leading to changes to the *in vivo* properties (volume/morphology) of chondrocytes prior to fixation (Guilak and Mow, 2000).

Our measurements of cell shrinkage by a histological method (Fig. 2A,B; Fig. 3) were supported to some extent by volume analysis of fluorescently-labelled living *in situ* GPC images taken by CLSM (Fig.5 and Table 4). Although the latter technique was more time-consuming, it served as a useful additional and direct measure of cell volume to confirm the cell shrinkage due to hyper-osmolar fixatives. The results from this method clearly showed the reduction in the cell volume of chondrocytes fixed with PFA (4%) in intact bone compared to bisected bone (Table 4). We would have expected that in parallel with the histological shrinkage measurements (Fig. 3A, B), the volume of cells within the bisected bone samples would not have been reduced in the PFA solution to the same extent as cells fixed with the osmotically-corrected fixative solution. At present we do not have an explanation for this finding, but note that we did not find the volume method was as sensitive for detecting the chondrocyte shrinkage compared to the histological method.

Both of these approaches provided us with more accurate quantitative measurements of the cell shrinkage artefact, compared to previous indirect methods e.g. counting the number of cell nuclei per unit area of tissue (Fox *et al*., 1985). Previous studies had suggested fixation artefacts arose from subsequent steps in tissue processing e.g. during ethanol-induced dehydration and embedding (Hopwood, 1969). However our data suggested that before it was possible to determine these secondary artefacts resulting from further preparation of tissue for histological analysis, it was essential that as far as possible the fixed tissue was close to its native state by abolishing the osmotic shrinkage artefact reported here.

In summary, our study demonstrated that the high osmolarity of conventional fixatives caused a shrinkage artefact to chondrocytes within the hypertrophic zone of the mammalian growth plate. This was particularly noticeable when whole bones were fixed, but was still present when the bones were bisected prior to fixation. This problem could be avoided by adjusting the osmolarity of the fixatives to the osmotic pressure of normal extracellular fluids (~280mOsm). In conclusion, in order to preserve the normal volume/morphology of cells within tissue samples, careful consideration should be given to the osmotic pressure of the fixative solution.

Acknowledgements

This work was supported by Universiti Putra Malaysia (UPM) and Ministry of Higher Education Malaysia under the SLAB scholarship (Scheme of Academic Training for Bumiputera) for Mohamad Yusof Loqman. Additional funding was provided by the Biotechnology and Biological Sciences Research Council (BB/C513985/1) and Wellcome Trust (075753/Z/04/Z). CF was supported by funding from the Institute Strategic Programme Grant from the Biotechnology and Biological Sciences Research Council, UK. We also thank Dr Michael Cousin for the donation of some biological samples.

References

Baker JK (1960) Cytological Technique: The Principles Underlying Routine Methods. Methuen, London.

Bancroft JD, Cook HC (1994) Manual of Histological Techniques and Their Diagnostic Application. Churchill Livingstone, Edinburgh.

Breur GJ, VanEnkevort BA, Farnum CE, Wilsman NJ (1991) Linear relationship between the volume of hypertrophic chondrocytes and the rate of longitudinal bone growth in growth plates. J Orthop Res **9**: 348-359

Buckwalter JA, Mower D, Schafer J, Ungar R, Ginsberg B, Moore K (1985) Growth-plate-chondrocyte profiles and their orientation. J Bone Joint Surg [Am] **67A**: 942-955.

Buckwalter JA, Mower D, Ungar R, Schaeffer J, Ginsberg B (1986) Morphometric analysis of chondrocyte hypertrophy. J Bone Joint Surg [Am] **68A**: 243-255.

Bush PG, Hall AC (2001) The osmotic sensitivity of isolated and *in situ* bovine articular chondrocytes. J Orthop Res **19**: 768-778.

Bush PG, Wokosin DL, Hall AC (2007) Two-versus one photon excitation laser scanning microscopy: Critical importance of excitation wavelength. Front Biosci **12**: 2646-2657.

Bush PG, Parisinos CA, Hall AC (2008) The osmotic sensitivity of *in situ* rat growth plate chondrocytes: clarifying the mechanism of hypertrophy. J Cell Physiol **214**: 621-629.

Dempster WT (1960) Rates of penetration of fixing fluids. J Amer Anat **107**: 59-72.

Erben RG (1997) Embedding of bone samples in methylmethacrylate: An improved method suitable for bone histomorphometry, histochemistry, and immunohistochemistry. J Histochem Cytochem **45**: 307-313.

Farnum CE, Lee R, O'Hara K, Urban JPG (2002) Volume increase in growth plate chondrocytes during hypertrophy: The contribution of organic osmolytes. Bone **30**: 574-581.

Farnum CE, Wilsman NJ (1986) *In situ* localization of lectin-binding glycoconjugates in the matrix of growth-plate cartilage. Am J Anat **176**: 65-82.

Fox CH, Johnson FB, Whiting J, Roller PP (1985) Formaldehyde fixation. J Histochem Cytochem **33**: 845-853.

Guilak F, Mow VC (2000) The mechanical environment of the chondrocyte: A biphasic finite element model of cell-matrix interactions in articular cartilage. J Biomech **33**: 1663-1673.

Hopwood D (1967) The behaviour of various glutaraldehydes on Sephadex G-10 and some implications for fixation. Histochemie **11**: 289-295.

Hopwood D (1969) Fixatives and fixation: a review. Histochem J **1**: 323-360.

Hopwood D (1985) Cells and tissue fixation 1972-1982. Histochem J **17**: 389-442.

Hosoya A, Hoshi K, Sahara N, Ninomiya T, Akahane S, Kawamoto T, Ozawa H (2005) Effects of fixation and decalcification on the immunohistochemical localization of bone matrix proteins in fresh-frozen bone sections. Histochem Cell Biol **123**: 639-646.

Huntley JS, Bush PG, McBirnie JM, Simpson AH, Hall AC (2005) Chondrocyte death associated with human femoral osteochondral harvest as performed for mosaicplasty. J Bone Joint Surg [Am] **87A**: 351-360.

Hunziker EB, Herrmann W, Schenck RK (1982) Improved cartilage fixation by ruthenium trichloride (RHT). A prerequisite for morphometry in growth cartilage. J Ultrstruct Res **81**: 1-12.

Hunziker EB, Herrmann W, Schenk RK (1983) Ruthenium hexamine trichloride (RHT)-mediated interaction between plasmalemmal components and pericellular matrix proteoglycans is responsible for the preservation of chondrocytic plasma membranes *in situ* during cartilage fixation. J Histochem Cytochem **31**: 717-727.

Hunziker EB, Ludi A, Hermann W (1992) Preservation of cartilage matrix proteoglycans using cationic dyes chemically related to ruthenium hexamine trichloride. J Histochem Cytochem **40**: 909-917.

Karnovsky MJ (1965) A formaldehyde-glutaraldehyde fixative of high osmolality for use in electron microscopy. J Cell Biol **27**: 137A-138A.

Kiernan JA (1999) Histological and Histochemical Methods: Theory and Practice. Butterworth-Heinemann, Oxford.

Kouri JB, Jimenez SA, Quintero M, Chico A (1996) Ultrastructural study of chondrocytes from fibrillated and non-fibrillated human osteoarthritic cartilage. Osteoarthr Cartil **4**: 111-125.

Lee K, Lanske B, Karaplis AC, Deeds JD, Kohno H, Nissenson RA, Kronenberg HM, Segre GV (1996) Parathyroid hormone-related peptide delays terminal differentiation of chondrocytes during endochondral bone development. Endocrinology **137**: 5109-5118

Mathieu O, Claassen H, Weibel ER (1978) Differential effect of glutaraldehyde and buffer osmolarity on cell dimensions: A study on lung tissue. J Ultrastruct Res **63**: 20-34.

Maunsbach AB (1966) The influence of different fixatives and fixation methods on the ultrastructure of rat kidney proximal tubule. II. Effects of varying osmolality ionic strength, buffer system and fixative concentration of glutaraldehyde solutions. J Ultrastruct Res **15**: 283-309.

Mehrer H (2007) Diffusion in Solids: Fundamentals, Methods, Materials, Diffusion-Controlled Process. Springer, Berlin-London.

Monis B, Wasserkrug H, Seligman AM (1965) Comparison of fixatives and substrates for aminopeptidase. J Histochem Cytochem **13**: 503-509.

Nuss KMR, Auer JA, Alois Boos A, Rechenberg BV (2006) An animal model in sheep for biocompatibility testing of biomaterials in cancellous bones. BMC Musculoskelet Disord **7**: 67.

Renshaw S (2007) Immunochemical staining. In Renshaw S (ed). Immunohistochemistry. Scion Publishing Limited, Oxfordshire. pp 45-56.

Ross MH, Reith EJ (1985) Histology: A Text and Atlas. Harper & Row Publishers, JB Lippincott Company, New York.

Sanchez CP, Kuizon BD, Abdella PA, Juppner H, Salusky IB, Goodman WG (2000) Impaired growth, delayed ossification, and reduced osteoclastic activity in the growth plate of calcium-supplemented rats with renal failure. Endocrinology **141**:1536-1544.

Santoreneos S, Stoodley MA, Jones NR, Brown CJ (1998). A technique for *in vivo* vascular perfusion fixation of the sheep central nervous system. J Neurosci Meth **79**: 195–199.

Schultz RL, Karlsson U (1965) Fixation of the central nervous system for electron microscopy by aldehyde perfusion. II Effect of osmolarity, pH of perfusate and fixative concentration. J Ultrastr Res **12**: 187-206.

Urban JPG, Hall AC, Gehl KA (1993) Regulation of matrix synthesis rates by the ionic and osmotic environment of articular chondrocytes. J Cell Physiol **154**: 262-270.

Van der Eerden BCJ, Karperien M, Gevers EF, Lowik CWGM, Wit JA (2000) Expression of Indian Hedgehog, parathyroid hormone-related protein, and their receptors in the postnatal growth plate of the rat: evidence for a locally acting growth restraining feedback loop after birth. J Bone Miner Res **15**: 1045-1055.

Discussion with Reviewer

Reviewer I: 10% Neutral Buffered Formalin is probably the most widely used fixative for routine histology and histopathology. Was this fixative tested at all? Did the authors simply concentrate on fixatives considered specific for growth plates?

Authors: While 10% Neutral Buffered Formalin (also referred to as 4% formaldehyde (Renshaw, 2007)) is widely used for processing tissues for routine histology, its use in growth plate tissue fixation is rather uncommon compared to other conventional fixatives as tested in the present study. Accordingly we have not focussed on this fixative. We note that the osmolarity of the 10% neutral phosphate buffered formaldehyde solution measured in our laboratory was ~1700mOsm, and thus much higher than the osmolarity of the fixatives used in the present investigation. We would expect that the artefactual shrinkage produced by this fixative would be much more marked, and have included a comment on the use of this commonly used fixative compared to the other fixatives used in our study.

Appendix

Appendix 1

Skeletal anatomy of a rat. Some of the anatomical features of a growing rat (>3wks) as observed in the whole-body dorso-ventral view of radiograph (inset). After Hughes and Tanner (1970).

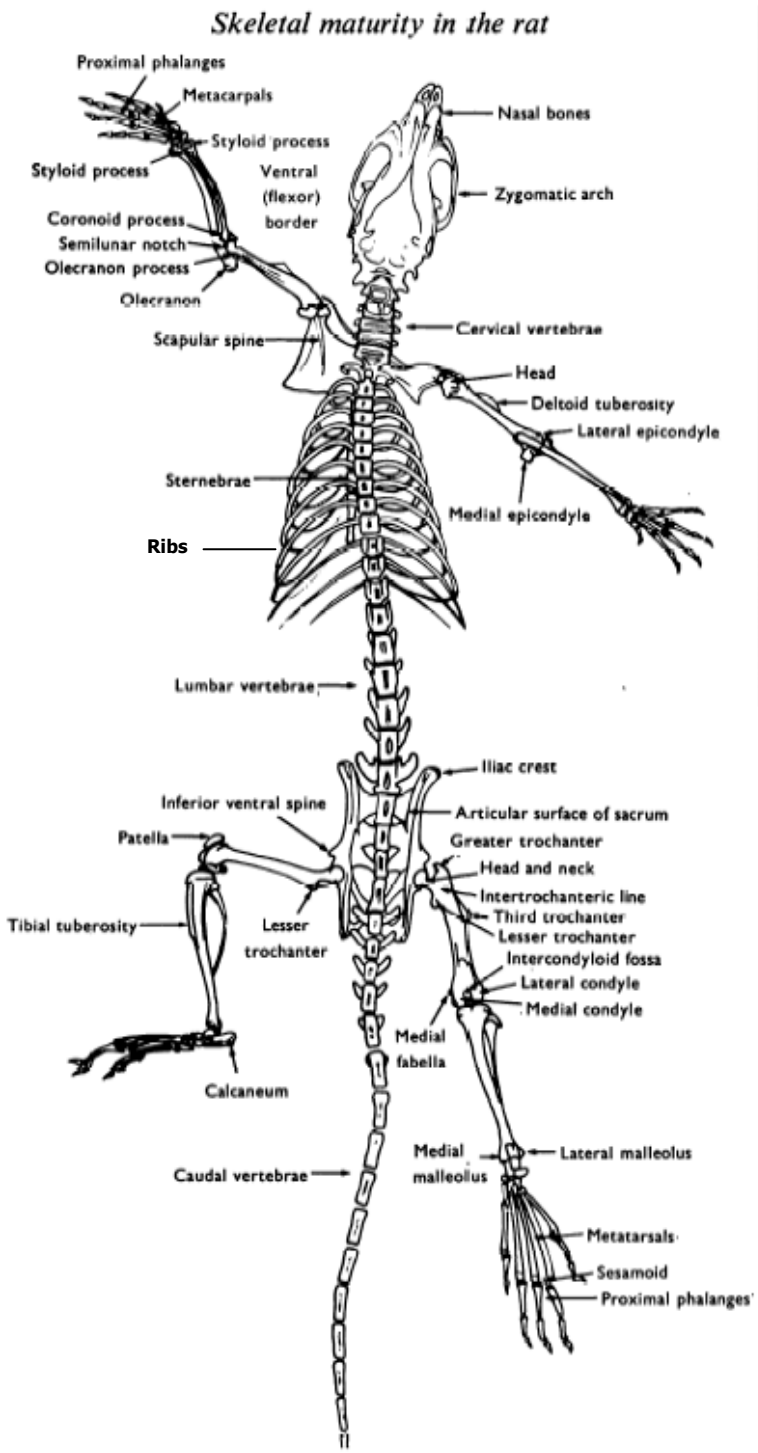

Appendix 2

Equipments

Automatic pipettor	Swiftpet, HTL
Balances	BP210D, Sartorius Analytical Plus, Ohaus
Confocal laser scanning microscope (CLSM)	Zeiss Axioskop LSM 510, Carl Zeiss Ltd., Welwyn Garden City, Herts., U.K.
Cryanoacrylate super glue	Loctite®, Cheshire, U.K.
Culture dish	Cellstar®, Greiner Bio One, U.K.
Coolpix MDC2 relay lens	MXA 2900, Nikon, Japan
Digital camera	Leica DFC 490, Peterbrough, U.K. Coolpix 4500, Nikon, Japan COHU, San Diego, California
Digital Eyepiece Camera	DCM 35 350K, Brunel Microscopes, U.K.
Dissecting stereomicroscope	Wild M3, Switzerland
Fume hood	Clean Air Ltd., Bolton
Humidity chamber	Magnetic Immuno Staining Tray, MIST, Cellpath, Hempstead

Incubator	37° C: Biohit
Inverted microscope	Eclipse T300, Nikon, Surrey, U.K.
Microbiological safety cabinet (Class II)	Bio 2+, Envair Ltd., Lancahire
Micro computed tomography (Micro-CT) scanner	SkyScan 1172 instrument, Kontich, Belgium
Micro-osmometer	Model 3300, Vitech Scientific Ltd., Partridge Green, U.K.
Microwave	XB2316, Durabrand
Microscope	Leica DMR, Peterbrough, U.K. Labophot 2, Nikon
Microtome	Reichert-Jung Microtome 2050 Supercut, Arnsberg, Germany
Poly-l-lysine-coated microscope slides	Polysine™, VWR International, Leicestershire, UK
pH meter	SevenEasy™ , Mettler Toledo, U.K.
Pipettes	Pipetman, Gilson
Pixel Digital Eyepiece Camera	DCM 35 350K, Brunel Microscopes, U.K.
Refigeration	4°C: Bosch

	-20°C: Bosch
Scalpel blade (No.11)	Swan-Morton, Sheffield, U.K.
Stirrer	Magnetic Stirrer Hotplate, Stuart Scientific PC-353, Corning Stirer
Vortex	Whirlmixer™, Fisons